MECHANICS OF IMPACT PILE DRIVING

BY

JERRY FRANK PAROLA
B.S., University of Illinois, 1962
M.S., University of Illinois, 1963

THESIS

Submitted in partial fulfillment of the requirements
For the degree of Doctor of Philosophy in Civil Engineering
in the Graduate College of the
University of Illinois at Urbana-Champaign, 1970

Urbana, Illinois

MECHANICS OF IMPACT PILE DRIVING

Jerry Frank Parola, Ph.D.
Department of Civil Engineering
University of Illinois, 1970

Impact pile driving was studied by utilizing longitudinal wave propagation theory as an analytical tool. Field data from pile driving jobs was used to establish the validity and usefulness of the analytical techniques developed herein.

The theoretical treatment of the dynamics of impact pile driving included an analysis of both the force generated at the head of the pile and the response of the pile tip to a generated force pulse. A model consisting of a hammer system operating on the head of an infinitely long pile was used to determine both the pile force pulse and the transmitted energy. The model was used to make a dimensionless parameter study of the factors influencing force and energy. The driver system consisted of concentrated masses for both the ram and the drivehead and an energy absorbing spring (both linear and nonlinear) for the hammer cushion.

Soil and pile responses were investigated with respect to an arbitrary force pulse in order to assess the variables controlling pile penetration and load capacity. Special emphasis is placed on soil and pile response at the pile tip; the soil model includes viscous damping, mass and an elastic-plastic spring.

Characteristics of the hammer-pile-soil system as a whole are summarized. Theoretical results using wave propagation theory are compared with both case histories and commonly used dynamic formulas. Correlation of wave analyses and field case histories are used to support the conclusion that wave propagation theory is the proper theoretical tool for pile driving analysis.

ACKNOWLEDGMENTS

The writer would like to acknowledge Professor M. T. Davisson for his suggestions and guidance during the analysis of the data. Professor V. J. McDonald and Mr. J. Sterner are acknowledged for their effort and guidance offered during the programming and use of the analog computer.

Acknowledgment is also extended to members of the writer's committee, Professors R. B. Peck and A. R. Robinson, for their suggestions during the preparation of this manuscript.

TABLE OF CONTENTS

CHAPTER Page

LIST OF TABLES

LIST OF FIGURES

Figure Page

NOTATION

Symbol		Units
$\bar{A}$	dimensionless impedance coefficient	1
A	cross-sectional area of pile	L^2
A_c	cross-sectional area of concrete pile	L^2
A_p	effective area of piston	L^2
A_s	cross-sectional area of steel pile	L^2
A_w	cross-sectional area of wood pile	L^2
a	area of cushion	L^2
	acceleration	L/T^2
$\bar{B}$	dimensionless weight coefficient	1
C_1	recoverable deformation of drivehead and pile head	L
C_2	recoverable deformation of pile	L
C_3	recoverable deformation of soil	L
C_4	slope of a regression line (dimensionless)	1
C_5	intercept of a regression line	F
C(m,t)	deformation of spring (m) at time interval (t)	L
C_E	pile energy coefficient	1
C_R	ram displacement coefficient	1
C_{F1}	pile force coefficient	1
C_{F2}	peak pile force coefficient	1
C_{F3}	peak pile force coefficient	FT/L
C_P	pile head displacement coefficient	1

Symbol		Units
c_1	arbitrary coefficients	1
c_2	arbitrary coefficients	1
c_o	viscous damping at soil tip	FT/L
c	velocity of wave propagation	L/T
D(m,t)	displacement of mass (m) at time interval (t)	L
D'(m,t)	plastic displacement of soil spring (m) at time interval (t)	L
E_t	transmitted energy to the pile	LF
E_i	kinetic hammer energy at ram impact	LF
E_c	secant modulus of hammer cushion	F/L^2
E_r	rated hammer energy	LF
E_R	reflected energy at pile tip	FL
E_T	transmitted energy at soil tip	FL
E_I	incident energy of pile force pulse	FL
E	pile modulus of elasticity	F/L^2
e	coefficient of restitution	1
$\bar{e}$	temporary set representing losses	L
e_f	hammer efficiency	%
e_t	transmission efficiency	%
$\bar{F}(t)$	force pulse input into top of pile	F
F(m,t)	force in internal spring (m) at time interval (t)	F
$\bar{F}$	force applied by theoretical steam or air pressure required at hammer	F

Symbol		Units
F	pile force	F
F_p	peak pile force	F
F_R	reflected pile force pulse	F
F_I	incident pile force pulse	F
f	arbitrary functions representing force waves	1
g	arbitrary functions representing force waves	1
	acceleration of gravity	L/T^2
h	height of ram fall, ram stroke	L
I_R	impedance ratio	1
J	viscous damping factor for soil	T/L
J_s	viscous damping factor for soil along the pile's length	T/L
J_{pt}	viscous damping factor for soil tip	T/L
J'	modified viscous damping factor for soil	T/L
$K(m)$	pile spring stiffness of mass (m)	F/L
$K'(m)$	soil spring stiffness for mass (m)	F/L
k	elastic cushion spring stiffness	F/L
k_ℓ	loading stiffness of bilinear hammer cushion	F/L
k_u	unloading stiffness of bilinear hammer cushion	F/L
k_p	equivalent linear loading stiffness for peak pile force	F/L
k_{t_d}	equivalent linear loading stiffness for time duration	F/L
k_c	equivalent linear loading stiffness for recommended secant modulus	F/L

Symbol		Units
k_s	soil spring stiffness at pile tip	F/L
ΔL	segment length	L
ℓ	cushion stack length	L
L	length of pile	L
$\bar{L}$	length of pile, measured from head to center of driving resistance	L
M	pile mass	FT^2/L
m_1	ram mass	FT^2/L
m_2	drivehead mass	FT^2/L
m	soil mass at pile tip	FT^2/L
	mass number as used in Smith's lumped mass-spring model	1
N	power of instantaneous pile velocity	1
n	coefficient of restitution	1
p	mean pressure of steam or air	F/L^2
Q	soil quake	L
Q_s	quake for soil along the pile's length	L
Q_{pt}	quake at soil tip	L
R_u	static ultimate soil resistance and pile capacity	F
R_p	load carried by pile point resistance	F
R_f	load carried by pile friction	F
R	ultimate soil resistance at pile tip	F
$\bar{R}(t)$	total soil resistance with respect to time (t)	F
$\bar{R}_o$	static ultimate soil resistance as determined by Tomko	F

Symbol		Units
$R(m,t)$	total soil resistance on mass (m)	F
R_{static}	static soil resistance	F
$R_{dynamic}$	dynamic soil resistance	F
r	roots of an equation	1
s	net set per hammer blow	L
T	psuedo ram period	T
t	real time	T
	time interval number as used in Smith's lumped mass-spring model	1
t_1	selected time duration of force pulse	T
t_d	approximate time pulse duration	T
t_o	time when velocity at top of pile is zero	T
Δt	time interval	T
u	longitudinal displacement of bar in x direction	L
V	particle velocity in pile	L/T
V_R	reflected particle velocity in pile	L/T
V_I	incident particle velocity in pile	L/T
V_o	ram impact velocity	L/T
$\bar{V}$	velocity of rigid body pile	L/T
$V(m,t)$	velocity of mass (m) at time interval (t)	L/T
W	soil weight at pile tip	F
W_1	ram weight	F
W_2	drivehead weight	F

Symbol		Units
$W(m)$	weight of mass (m)	F
W_p	weight of pile	F
X_1	*ram co-ordinate in nondimensional expressions*	L
$\dot{X}_1$	first derivative of ram co-ordinate in nondimensional expressions	L
$\ddot{X}_1$	second derivative of ram co-ordinate in nondimensional expressions	L
X_2	drivehead co-ordinate in nondimensional expressions	L
$\dot{X}_2$	first derivative of drivehead co-ordinate in nondimensional expressions	L
$\ddot{X}_2$	second derivative of drivehead co-ordinate in nondimensional expressions	L
x	pile tip displacement	L
x_1	ram co-ordinate	L
$\dot{x}_1$	ram velocity	L/T
$\ddot{x}_1$	ram acceleration	L/T^2
x_2	drivehead co-ordinate	L
$\dot{x}_2$	drivehead velocity	L/T
$\ddot{x}_2$	*drivehead acceleration*	L/T^2
x_3	pile head co-ordinate	L
z	dimensionless time	1
δ	maximum free-tip pile displacement	L
δ_s	maximum free-tip displacement for a sine pulse	L
ρ	pile mass per unit volume	FT^2/L^4
ρcA	pile impedance	FT/L

CHAPTER 1

INTRODUCTION

1.1 Scope

The purpose of this dissertation is to investigate analytically the mechanics of impact pile driving with the goals of increasing the ability of the engineer to design a pile foundation and aiding the contractor in proper selection of equipment. These goals will be accomplished by considering the behavior of single piles.

The design of all pile foundations depends upon load capacity and settlement criteria as well as feasibility of installation. Therefore, the ultimate goal is a general understanding of pile-soil interaction during installation and the interaction of superstructure, piles and soil after construction. With the exception of a few isolated instances, group behavior has been physically difficult and financially impossible to investigate in detail. As a consequence, an understanding of single-pile behavior plus theory, model studies and judgment regarding the relationship between a single pile and a pile group must be relied on in order to produce an acceptable design.

The dynamics of driving piles with impact hammers is investigated by considering both the force pulse generated at the head of the pile and the response of the pile tip to a generated force pulse. It is possible to obtain significant results by studying incident waves only at both the pile head and pile tip; an analytical model using an infinitely long pile serves to eliminate reflected waves from the far end.

A model consisting of a hammer system operating on the head of an infinitely long pile is utilized for determining both the pile force pulse and the transmitted energy. The driver system consists of concentrated masses for the ram and drivehead and an energy absorbing spring (both linear and nonlinear) for the hammer cushion.

Next, soil and pile response is investigated with respect to an arbitrary force pulse in order to determine the characteristics of pile penetration and load capacity. Special emphasis is placed on soil and pile response at the pile tip; the soil model includes viscous damping, mass, and an elastic-plastic spring.

The characteristics of the hammer-pile-soil system as a whole are described after the elements of the mechanics of impact pile driving are studied. Theoretical results using wave propagation theory are compared with both case histories and commonly used dynamic formulas. Correlations of wave equation analyses and field case histories are used to investigate the validity and usefulness of the wave propagation concept as the proper theoretical framework for pile driving analysis.

The mechanics of pile driving deserves investigation for the enlightenment of both foundation engineers and pile contractors. The foundation engineer is concerned with the performance of a pile foundation. In an effort to predict pile performance, the engineer has allocated to pile drivers a rather unique dual role, that of a driving tool and that of a measuring instrument. Although the pile driver's primary role is pile installation, the pile driver is also used as a measuring instrument, i.e. the resistance to penetration in terms of hammer blows per inch is used as a measure of the pile's ability to support load.

Of course, the engineer must be able to predict similarities and differences between pile behavior during driving and under static load in order to make the pile driver an effective measuring tool.

With an understanding of the mechanics of pile driving in conjunction with experience, the pile contractor can install the optimum pile foundation, i.e. the one with the lowest cost providing the desired foundation performance. The cost of the pile foundation includes not only the amount of pile material needed, but also the driving expense which involves driving time, pile damage, and replacing damaged or inadequate piles. The pile driving contractor should be able to choose the proper equipment along with the pile that, as well as being in accordance with the technical specifications, can be installed in the most expeditious and economical manner.

The foundation engineer must also have a working knowledge of pile installation in order to write satisfactory and rational specifications. With an understanding of the mechanics of pile driving, the engineer can avoid unnecessary restrictions in the specifications to prevent a cost burden on the pile contract. The restrictions in the specifications can include limitations on hammer size, pile type and pile dimensions.

1.2 Impact Pile Driving

One of the oldest and simplest methods of driving a pile is by the use of a drop hammer. Drop hammers, now rarely used, were prevalent before the twentieth century. The disadvantage of the drop weight technique is the long driving time because of the time consumed be-

tween blows to raise the ram by power winching. In order to achieve an increase in pile penetration rates, hammer development has been directed toward applying the driving energy at a faster rate. A faster energy rate is associated with a larger number of hammer blows supplied in a period of time (blow rate).

The desire for faster driving rates led to the single-acting steam hammer. The Vulcan single-acting steam hammer introduced in 1887 (Vulcan Iron Works, 1927) is the forerunner of modern impact hammers. Instead of being raised by a power winch, the ram is lifted by steam pressure which is regulated to apply an upward force on a piston connected to the ram. The valving mechanism exhausts steam at the top of stroke and allows the ram to fall by gravity through a stroke h before impact. A schematic of both the drop and single-acting hammers is presented in Figure 1.1a. The major components of the pile hammer are the ram, hammer cushion and drive head. The ram with an impact velocity, V_o, imparts the energy and force pulse to the pile through the hammer cushion and drive head.

Several years after development of the single-acting hammer, double-acting and differential hammers were introduced to increase the blow rate. Hammers of these types not only use pressure to lift the ram but also increase the downward acceleration of the ram by adding force to the gravity force (Figure 1.1b). Differential and double-acting hammers commonly have half the stroke and twice the blow rate of the comparable single-acting hammer.

With the development of portable air compressors, the substitution of air pressure for steam pressure has now become common practice. The

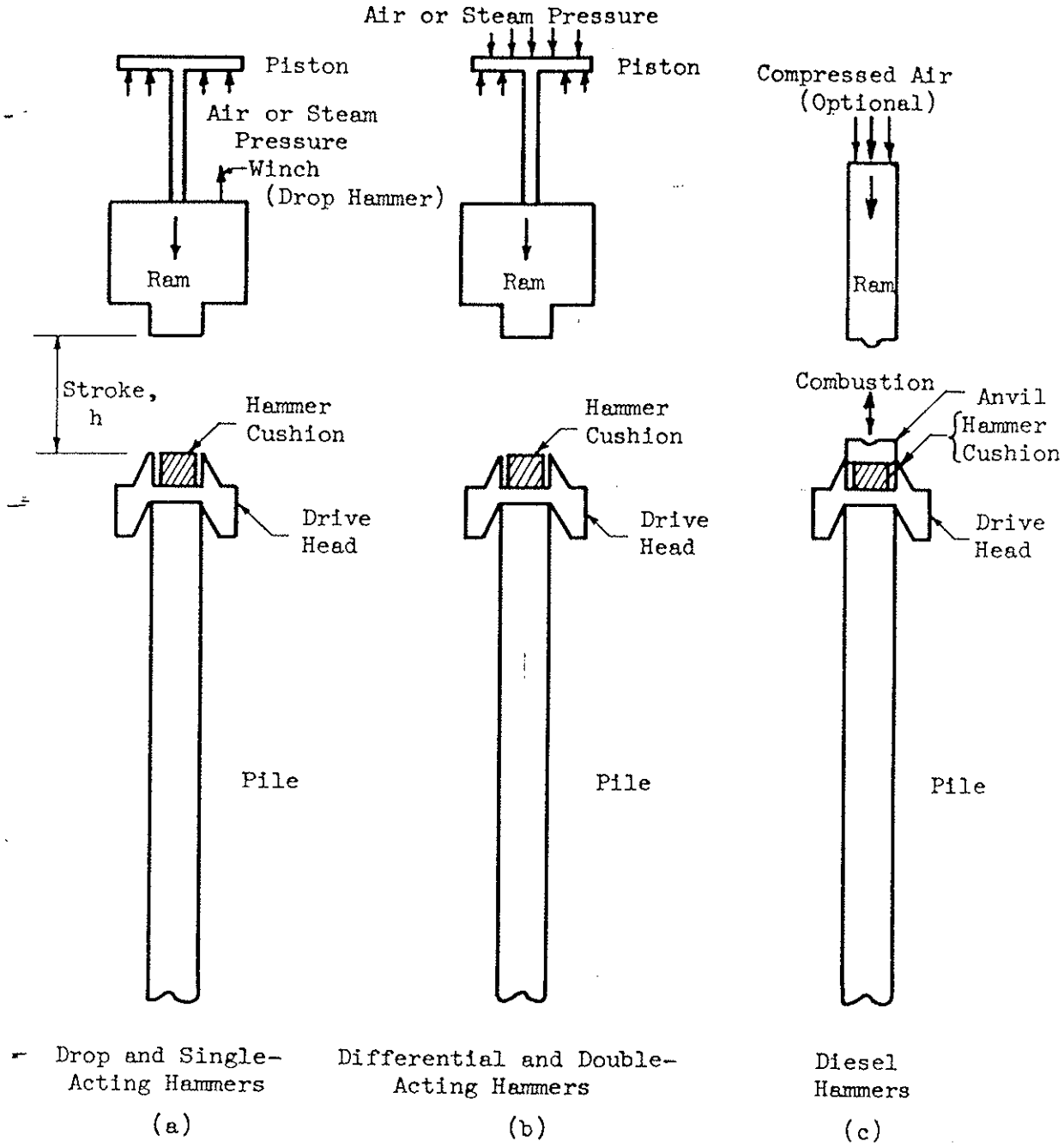

Figure 1.1 SCHEMATIC DIAGRAMS OF IMPACT PILE DRIVERS

use of air pressure is accomplished without change in the hammer mechanism because operating pressures of both air and steam are commonly 100 to 120 psi. Recently, a hydraulically powered differential hammer has become operational with the ports sized to be consistent with fluid pressures of 3000 to 5000 psi.

The most recent development in impact hammers is the diesel powered driver introduced in Germany prior to World War II. The integrally powered diesel hammer is currently popular because it requires less equipment and manpower than steam or air hammers. The diesel hammer utilizes the combustion of diesel fuel to lift the ram. The hammer ram serves as the piston, compressing air on the downward stroke after the intake valve is closed. The atomized diesel oil explodes upon the rise in temperature of the compressed air which results from the ram drop. Impact of the ram on the anvil is approximately simultaneous with combustion of the diesel oil; therefore, the force driving the anvil is a combination of combustion and impact (Figure 1.1c). The combustion force also drives the ram upwards to the top of its stroke. The diesel hammer can be open-ended at the cylinder top or closed-ended with an air chamber (bounce chamber). On the up stroke, air is compressed in the bounce chamber and thus shortens the stroke and increases the blow rate.

Vibratory pile drivers are also in common use, but they are not impact hammers. They produce a combination of axial oscillations and static thrust as discussed by Smart (1969).

Impact hammers are normally rated or sized according to the equivalent potential energy available at the top of their stroke.

Energy ratings for drop or single-acting hammers are readily defined, e.g. $E_r = W_1 h$ where E_r is the rated hammer energy, W_1 is ram weight and h is the stroke (height of ram fall). However, energy ratings for double-acting or differential hammers must also account for the effect of the downward thrust in addition to gravity, e.g. $E_r = W_1 h + \bar{F}h$ where $\bar{F}$ is the force applied by the theoretical steam or air pressure required at the hammer.

Diesel hammer ratings are complicated by the unknown effectiveness of the combustion force and the variability of the ram stroke under field conditions; therefore, confusion exists regarding the rating of diesel hammers. Rated energy for open-end diesel hammers is determined by the maximum ram drop. For closed-end diesels, the ratings are established from the equivalent stroke which is the actual stroke plus an equivalent increment of stroke based on the energy stored in the bounce chamber.

The common range in rated energies per blow for impact drivers is from 5,000 ft-lbs to 120,000 ft-lbs; the most common values lie between 15,000 ft-lbs and 40,000 ft-lbs. For offshore driving, there is a need for larger hammer sizes than are now available. Commonly used impact hammers have blow rates varying from 40 to 200 blows per minute whereas that for drop hammers is 5 to 20 blows per minute. Single-acting and open-end diesel hammers commonly operate at 40-60 blows/minute and differential, double-acting and closed-end diesel hammers at 80-120 blows/minute. Pile-driver data for the hammers currently available in the United States are given in Table 1.1.

Table 1.1

IMPACT PILE-DRIVER DATA

Rated Energy, ft-lb	Make of Hammer	Size	Type	Blows per min	Stroke at Rated Energy in.	Weight Striking Parts, lb	Total Weight, lb	Length of Hammer	Air Cfm	A.S.M.E. Boiler H.P.	Steam or Air, psi	Size of Hose, in.	$\sqrt{E_r \times W_1}$ Rating $(ft\text{-}lbs^2)^{1/2}$
					Energy over 100,000 ft-lb								
180,000	Vulcan	060	Single-act.	62	36	60,000	121,000	18'6"	4626	740	130	(2)4	103,900
130,000	McKiernan-Terry	S-40	Single-act.	55	39	40,000	96,000	16'0"	--	375	150	4	72,100
120,000	Vulcan	040	Single-act.	60	36	40,000	87,500	17'11"	3400	535	120	(2)3	69,300
113,478	Super-Vulcan	400C	Differential	100	16 1/2	40,000	83,000	16'9"	4659	700	150	5	67,400
					Energy 50,000 to 100,000 ft-lb								
97,500	McKiernan-Terry	S-30	Single-act.	60	39	30,000	86,000	16'0"	--	280	113	4	54,000
79,600	Kobe	K42	Diesel	45-60	98	9,200	22,000	14'6"	--	--	--	--	27,100
60,000	Vulcan	020	Single-act.	60	36	20,000	39,000	15'0"	1756	278	120	3	34,600
60,000	McKiernan-Terry	S20	Single-act.	60	36	20,000	38,650	18'5"	1720	280	150	3	34,600
56,500	Kobe	K32	Diesel	45-60	98	7,060	15,400	13'7"	--	--	--	--	20,000
50,200	Super-Vulcan	200C	Differential	98	15 1/2	20,000	39,050	13'2"	1746	260	142	3	31,700
					Energy 30,000 to 50,000 ft-lb								
48,750	Vulcan	016	Single-act.	60	36	16,250	30,250	14'6"	1290	210	110	3	28,100
46,750	Raymond	0000	Single-act.	46	39	15,000	23,000	--	--	85	140	2 1/2	27,000
44,500	Kobe	K22	Diesel	45-60	98	4,850	10,600	13'4"	--	--	--	--	14,700
42,000	Vulcan	014	Single-act.	60	36	14,000	27,500	14'6"	1282	200	110	3	24,200
40,600	Raymond	000	Single-act.	50	39	12,500	21,000	15'7"	--	70	135	2 1/2	22,500
39,800	Delmag	D-22	Diesel	42-60	n/a	4,850	10,054	12'10 1/2"	--	--	--	--	13,900
37,500	McKiernan-Terry	S14	Single-act.	60	32	14,000	31,600	14'10"	1260	190	100	3	23,000
36,000	Super-Vulcan	140C	Differential	103	15 1/2	14,000	27,984	12'3"	1425	211	140	3	22,000
32,500	McKiernan-Terry	S10	Single-act.	55	39	10,000	22,200	14'1"	1000	140	80	2 1/2	18,000
32,500	Vulcan	010	Single-act.	50	39	10,000	18,750	15'0"	1002	157	105	2 1/2	18,000
32,500	Raymond	00	Single-act.	50	39	10,000	18,500	15'0"	--	55	125	2	18,000
32,000	McKiernan-Terry	DE-40	Diesel	48	96	4,000	11,275	15'0"	--	--	--	--	11,300
30,225	Vulcan	08	Single-act.	50	39	9,300	16,765	15'0"	1020	--	100	2 1/2	16,800
					Energy 20,000 to 30,000 ft-lb								
26,300	Link-Belt	520	Diesel	80-84	43 1/6	5,070	12,545	18'6"	--	--	--	--	11,500
26,000	McKiernan-Terry	C-8	Double-act.	77-85	20	8,000	18,750	9'9"	875	110	100	2 1/2	14,400
26,000	Vulcan	08	Single-act.	50	39	8,000	16,750	15'0"	880	127	80	2 1/2	14,000
26,000	McKiernan-Terry	S8	Single-act.	55	39	8,000	18,100	14'4"	850	119	80	2 1/2	14,400
24,450	Super-Vulcan	80C	Differential	111	16 1/2	8,000	17,885	11'4"	1245	180	120	2 1/2	14,000
24,450	Vulcan	8M	Differential	111	n/a	8,000	18,400	10'6"	1245	180	120	2 1/2	14,000
24,370	Vulcan	0	Single-act.	50	39	7,500	16,250	15'0"	841	--	80	2 1/2	13,500
24,000	McKiernan-Terry	C-826	Double-act.	85-95	18	8,000	17,750	12'2"	875	120	125	2 1/2	13,900
22,600	Delmag	D-12	Diesel	42-60	n/a	2,750	5,440	12'7 3/4"	--	--	--	--	7,900
22,400	McKiernan-Terry	DE-30	Diesel	48	96	2,800	9,075	15'0"	--	--	--	--	7,900
24,400	Kobe	K13	Diesel	45-60	98	2,870	6,400	12'8"	--	--	--	--	8,400
					Energy 10,000 to 20,000 ft-lb								
19,875	Union	0	Double-act.	110	24	3,000	14,500	10'1"	800	--	125	2	6,360
19,850	McKiernan-Terry	11B3	Double-act.	95	19	5,000	14,500	11'1"	900	126	100	2 1/2	9,780
19,500	Vulcan	06	Single-act.	60	36	6,500	11,200	13'0"	625	94	100	2	11,200
19,200	Super-Vulcan	65C	Differential	117	15 1/2	6,500	14,886	12'1"	991	152	150	2	11,200
18,250	Link-Belt	440	Diesel	86-90	36 7/8	4,000	10,300	14'6 1/4"	--	--	--	--	8,540
16,250	McKiernan-Terry	S5	Single-act.	60	39	5,000	12,375	13'3"	600	84	80	2	9,000
16,000	McKiernan-Terry	DE-20	Diesel	48	96	2,000	6,325	13'3"	--	--	--	--	5,660
16,000	McKiernan-Terry	C5	Compound	110	18	5,000	11,880	8'9"	585	56	100	2 1/2	8,940
15,100	Super-Vulcan	50C	Differential	120	15 1/2	5,000	11,782	10'2"	880	125	120	2	8,690
15,100	Vulcan	5M	Differential	120	15 1/2	5,000	12,900	9'4"	880	125	120	2	8,690
15,000	Vulcan	1	Single-act.	60	36	5,000	10,100	13'0"	565	81	80	2	8,660
15,000	Link-Belt	312	Diesel	100-105	30 7/8	3,857	10,375	10'0"	--	--	--	--	7,610
13,100	McKiernan-Terry	10B3	Double-act.	105	19	3,000	10,850	9'4"	750	104	100	2 1/2	6,270
12,725	Union	1	Double-act.	125	21	1,600	10,000	8'2"	600	--	100	1 1/2	4,530
					Energy 5,000 to 10,000 ft-lb								
9,040	Delmag	D5	Diesel	42-60	n/a	1,100	2,401	11'2 1/2"	--	--	--	--	3,150
9,000	McKiernan-Terry	C-3	Double-act.	130-140	16	3,000	8,500	7'9 1/2"	450	60	100	2	5,200
9,000	McKiernan-Terry	S3	Single-act.	65	36	3,000	8,800	12'4"	400	57	80	1 1/2	5,200
8,800	McKiernan-Terry	DE-10	Diesel	48	96	11,000	3,518	12'2"	--	--	--	--	3,110
8,750	McKiernan-Terry	9B3	Double-act.	145	17	1,600	7,000	8'2"	600	85	100	2	3,740
8,280	Union	1 1/2A	Double-act.	135	18	1,500	9,200	8'4"	450	--	100	1 1/2	3,520
8,100	Link-Belt	180	Diesel	90-95	37 5/8	1,725	4,550	11'3"	--	--	--	--	3,740
7,260	Vulcan	2	Single-act.	70	29 3/4	3,000	7,100	12'0"	336	49	80	1 1/2	4,670
7,260	Super-Vulcan	30C	Differential	133	12 1/2	3,000	7,036	8'11"	488	70	120	1 1/2	4,670
7,260	Vulcan	3M	Differential	133	n/a	3,000	8,490	7'11"	488	70	120	1 1/2	4,670
6,500	Link-Belt	105	Diesel	90-98	35 1/4	1,445	3,885	10'3"	--	--	--	--	3,070
					Energy Under 5,000 ft-lb								
4,900	Vulcan	DGH900	Differential	238	10	900	5,000	6'9"	580	75	78	1 1/2	1,900
3,600	Union	3	Double-act.	160	14	700	4,700	6'4"	300	--	100	1 1/4	1,600
3,600	McKiernan-Terry	7	Double-act.	225	9 1/2	800	5,000	6'1"	450	63	100	1 1/2	1,700
445	Union	6	Double-act.	340	7	100	910	3'10"	75	--	100	3/4	210
386	Vulcan	DGH100A	Differential	303	6	100	786	4'2"	74	8	60	1	200
356	McKiernan-Terry	3	Double-act.	400	5 3/4	68	675	4'10"	110	--	100	1	150
320	Union	7A	Double-act.	400	6	80	540	3'7"	70	--	100	3/4	160

E_r = rated striking energy in foot-pounds; W_1 = weight of striking parts in pounds.

Note: Ram weights of drop hammers vary from 500 to 10,000 lbs with variable strokes therefore variable energy.

Rated hammer energy is only an index to hammer capability. The actual energy available at impact is more indicative of hammer capability than rated energy; the energy at impact is less than the rated energy because of mechanical losses due to friction, pre-admission of steam or air, etc. The hammer kinetic energy at impact may be expressed as $E_i = \frac{1}{2}\frac{W_1}{g} V_o^2$, where V_o is the ram velocity at impact and g is the acceleration of gravity. The ratio of energy at impact to rated energy is defined as hammer efficiency, i.e. $e_f = \frac{E_i}{E_r} \times 100\%$. Some widely accepted but undocumented hammer efficiencies are given by Chellis (1961) as follows:

Hammer Type	Hammer Efficiency, e_f, %
Drop	
Trigger Release	100
Winch	75
Single-Acting	75 to 85
Double and Differential Acting	75 to 85
Diesel	100

The dynamic response of ram, anvil, hammer cushion, drive head and pile determines how much of the energy available at impact is transmitted to the pile. The efficiency of transmission may be defined as $e_t = \frac{E_t}{E_i} \times 100\%$ where E_t is the energy transmitted to the pile. A few field measurements and calculations indicate transmission efficiencies of 50 to 90 percent should be common.

A typical force pulse delivered to the pile head by an impact hammer is shown in Figure 1.2a. Durations of 20 to 50 milliseconds are common with pile peak forces in the range of 100 to 1000 kips. As noted

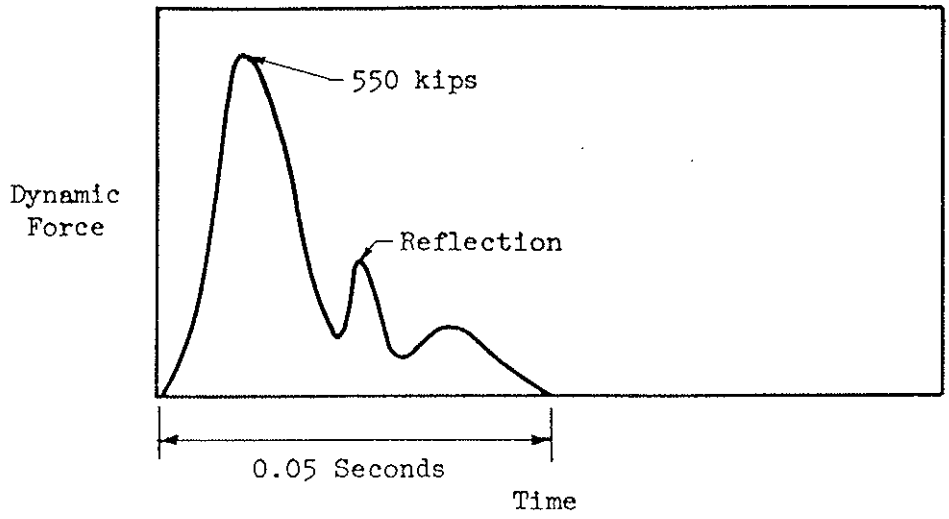

(a) Single Hammer Blow

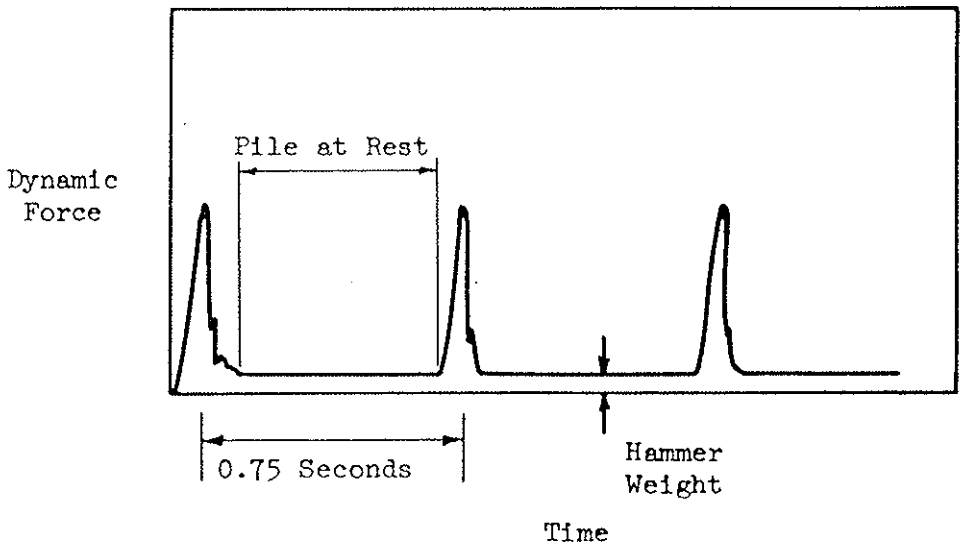

(b) Several Hammer Blows

Figure 1.2 TYPICAL FORCE INPUT
TO PILE HEAD

in Figure 1.2b, pile oscillations are damped very quickly and one hammer blow has no effect on succeeding blows; therefore, the mechanics of impact pile driving may be investigated with respect to the events associated with a single impact. Blow rates of 300-600 blows/minute would be required before piles with typical lengths could be kept in steady motion making it necessary to analyze a sequence of blows.

For a given hammer-pile-soil system, maximizing the energy transmitted to the pile is the first step towards maximizing pile penetration per blow. However, the transmitted energy must also be in an acceptable form (force pulse shape) in order to maximize pile penetration. For example, consider the point bearing pile shown in Figure 1.3a and the generated force pulse versus ultimate tip resistance R as shown in Figure 1.3b. Pile penetration will occur when the pile peak force generated by the impact hammer exceeds the ultimate soil resistance at the pile tip. In fact, if the tip resistance is rigid-plastic, penetration will occur as long as the peak force exceeds 0.5 R, as will be shown later. If the peak force is less than 0.5 R, then only enough soil resistance is mobilized to counteract the pile force and no net movement of the pile point results even if the transmitted pile energy has been maximized.

For the friction pile (Figure 1.3c), the pile force pulse is attenuated with depth by the soil resistance along the pile's length. Because of attenuation, very low peak force may reach the pile tip; however, no force is necessary to overcome the tip resistance.

Pile penetration is controlled by the magnitude and duration of the generated force in the pile with respect to the response of the soil.

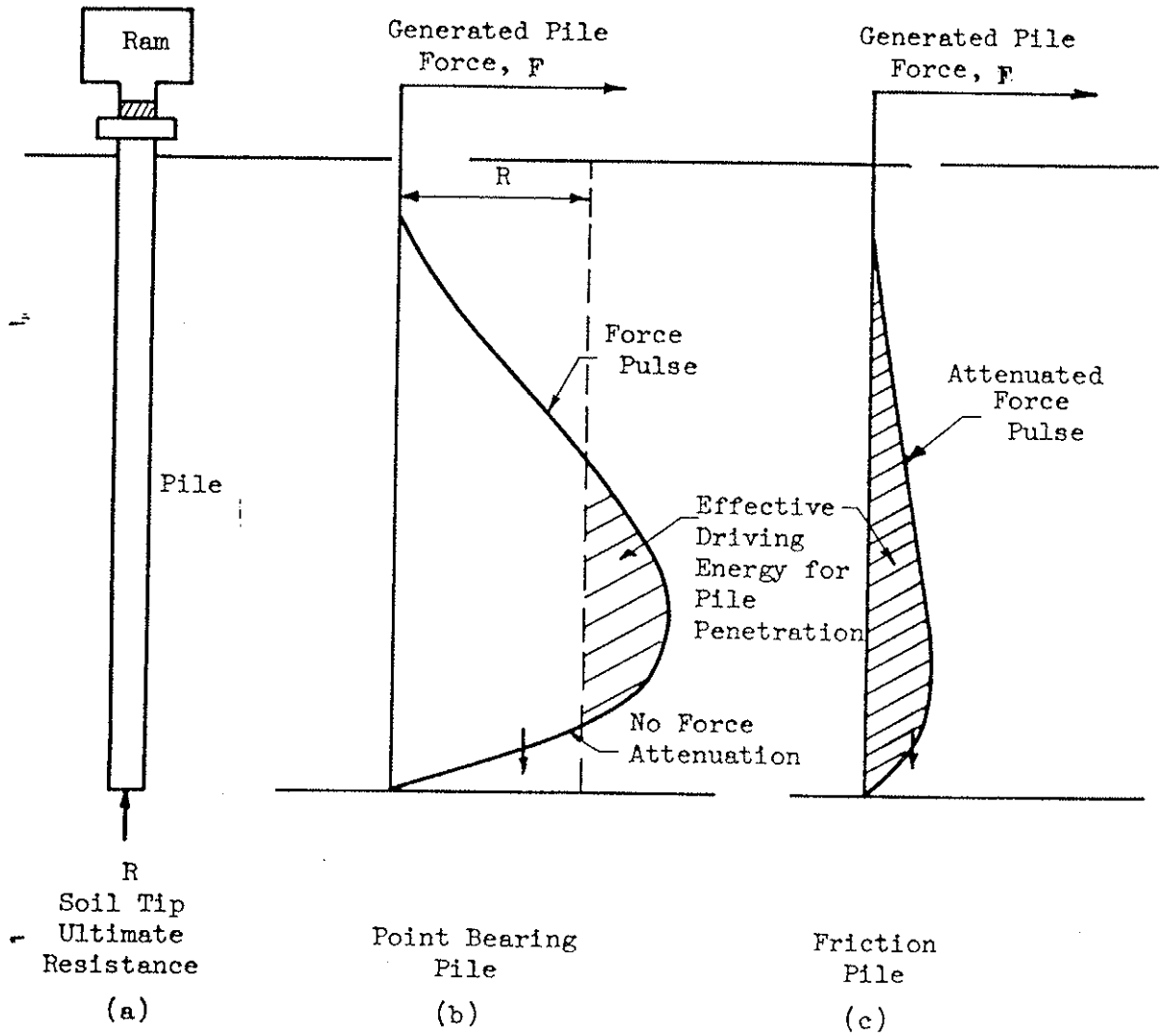

Figure 1.3 EFFECT OF PILE FORCE PULSE ON PILE PENETRATION

The ram-cushion-drive head-pile system controls the force pulse generated in the pile head. Therefore, a pile hammer may be considered to be a force pulse generator.

1.3 Single-Pile Analysis

Current methods of analyzing a single pile can be grouped in two general categories, namely, static and dynamic. A review of these analytical methods is given in Appendix A; only a brief summary of the concepts is presented here.

A static analysis of pile point bearing and skin friction is rather limited in scope because information is obtained with respect to load capacity only. No information is obtained on driving characteristics. However, a static analysis is a valuable tool for determination of driving characteristics when used in conjunction with a dynamic analysis, as will be shown later.

A dynamic analysis is the proper tool to investigate the mechanics of impact pile driving. However, there are three methods of analysis that differ in concept: (1) Dynamic energy formulae based on simple energy considerations, probably the oldest method of pile analysis; (2) Wave equation analysis based on one-dimensional wave propagation; (3) A method utilizing measured force and acceleration at the pile head. In all cases, dynamic analyses are used to predict static load capacity.

In order to use a dynamic analysis to predict static load capacity, a knowledge of the relationship between static and dynamic soil resistance is necessary. Dynamic versus static behavior is complex and

can be determined only qualitatively. Correlation studies of dynamic and static soil resistance are difficult because of the infinite variety of soil profiles as well as the variety of single soil properties. Additional complicating factors that affect soil properties are the pile shape, pile volume and method of pile installation. The experience and judgment of the engineer in selecting appropriate soil data input for dynamic analysis are critical to the success of the analysis.

Several examples of soil type will help illustrate the soil behavior encountered. For dense and submerged cohesionless soils, either fine or coarse-grained, dynamic resistance may greatly exceed static resistance (Yang, 1956 and Yang, 1970) because of temporary negative pore pressures due to rapid dilation of the soil structure. The opposite effect is observed in loose cohesionless soils where pile driving causes temporary positive pore pressures which reduce soil resistance. Consequently, the dissipation of excess pore pressures results in a gain or loss of strength with time after driving. For dense soils, dynamic resistance is greater than static resistance, whereas dynamic resistance is less than static for loose soils. Pile driving disturbance of cohesive soils produces the same effect as in loose cohesionless soil, namely, lower dynamic soil resistance than subsequent static soil resistance.

In this thesis, special emphasis is placed on the wave equation analysis of pile driving, although other methods are also discussed in Appendix A. Recent investigations have shown that analyses involving impact and wave transmission theory represent the best techniques now available. The wave equation analysis provides a theoretical framework

within which all practical pile driving experience can be properly assessed. The investigations reported in this thesis are based on the theory of wave propagation and the behavior of single piles driven with pure impact hammers. Diesel hammers are considered beyond the scope of this dissertation.

1.4 Purposes

Generally, the purpose of this dissertation is to investigate analytically the mechanics of pile driving. More specifically, this dissertation covers:

1. The parameters controlling the force pulse delivered to the head of a pile, both with respect to maximizing energy transmission and maximizing pile penetration (Chapter 2).
2. Soil resistance parameters governing pile penetration (Chapter 3).
3. Characteristics of pile hammer, pile and soil resistance affecting pile driving behavior, namely, pile penetration and capacity (Chapter 4).
4. A comparison of results from wave transmission theory with case histories and also with commonly used dynamic formulas (Chapter 4).

The foregoing purposes are accomplished by independent idealized studies of the parameters controlling the generated force pulse in the pile head and the soil resistance parameters at the pile tip. The behavior of

the hammer-pile-soil system as a whole is then summarized and explained using both the idealized theoretical studies and the wave equation analysis; case histories are used to support the summary. The wave equation analysis is a numerical technique applied to a lumped mass-spring model; it is an analysis of the entire system, but it does not facilitate an understanding of the controlling parameters. It will be shown that the idealized studies in Chapters 2 and 3 lead directly to pile design and hammer selection criteria.

CHAPTER 2

THE PILE HAMMER AS A FORCE GENERATOR

2.1 Introduction

The objective of this chapter is to investigate the effects of the various parameters controlling the force pulse delivered to the pile head, with respect both to maximizing energy transmission and maximizing pile penetration. The shape of the generated force pulse and the energy in the pile head are the decisive factors for overcoming soil resistance and achieving maximum pile penetration (net set per hammer blow). A procedure will be developed for matching the driving equipment and pile so as to impart maximum energy to the pile head; however, as maximum transmitted energy alone does not guarantee the best hammer-pile combination for maximizing pile penetration, the shape of the force pulse is also given consideration.

In order to establish a basis for investigating driving equipment, only the generated force pulse will be considered; no extraneous effects will be included. The effects of wave reflections will be considered in the following chapter after the basis of the generated force pulse is established.

The model of the force generator used herein is shown in Figure 2.1. The driving mechanism consists of point masses for the ram and drivehead, whereas the hammer cushion is assumed massless. Several different approximations are made regarding the stress-strain characteristics, including linear elastic, linear inelastic and nonlinear inelastic.

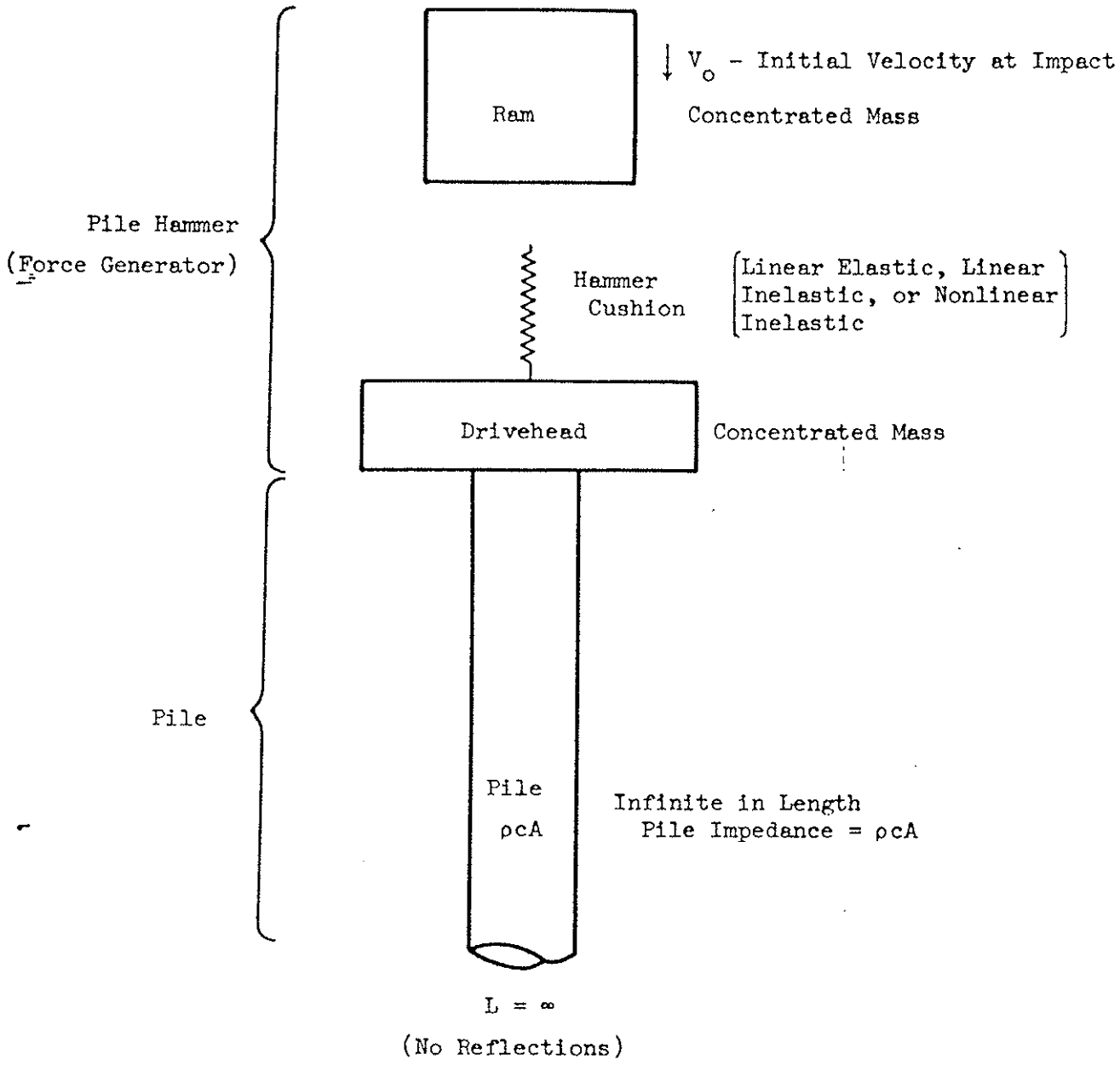

Figure 2.1 MODEL OF FORCE GENERATOR

The ram and drivehead are for practical purposes infinitely stiff compared to the hammer cushion; therefore, the assumption of lumped masses is justifiable. The force generator operates on the head of an infinitely long pile which is considered to have distributed mass and elasticity. It will be shown that pile force is a linear function of particle velocity. The ratio of pile force to the induced velocity in the pile is the mechanical impedance of the pile (Kolsky, 1963). The pile force can be written:

$$F = (\rho c A)V \qquad (2.1)$$

where F = force in the pile

V = particle velocity in pile

ρcA = pile characteristic impedance hereafter referred to as pile impedance

ρ = pile mass per unit volume

$c = \sqrt{E/\rho}$, velocity of wave propagation

A = cross-sectional area of pile

E = pile modulus of elasticity

Equation 2.1 can be readily derived from the classical one-dimensional equation of wave propagation (Timoshenko and Goodier, 1951).

The model of the infinitely long pile (Figure 2.1) can be used to investigate the force pulse and energy transmitted to the pile head without consideration of reflected force waves from the pile tip. The effect of pile tip response on the generated force pulse will be presented in the following chapter.

The input parameters of the force generator include the ram and drivehead weight, load-deformation relationship of hammer cushion, im-

pedance of the pile and initial velocity of ram at impact. Ram impact velocity is a function of rated hammer energy and hammer efficiency and normally ranges from 9 to 15 ft/sec for typical hammers.

Experience has shown that a hammer cushion is required to protect the hammer from damage; however, the inclusion of a cushion also affects the force pulse shape and energy transmitted to the pile. Housel (1965) showed the effect of a cushion on the generated force pulse. As shown in Figure 2.2, the peak force and pulse shape are grossly affected by cushion material.

Wood, one of the first materials to be used as a cushion, is in common use today. Recently, alternating thin discs of aluminum and micarta have become prominent. Other types of cushion materials such as wire rope, asbestos, etc. are employed in practice; however, the aluminum-micarta and wood cushions represent common limits in load-deformation characteristics. The aluminum-micarta assembly is a stiff spring, whereas the wood cushion corresponds to a soft spring.

The spring constants for various types of cushion blocks are obtained from test results. A typical shape of the dynamic load-deformation curve for a cushion is shown in Figure 2.3a. The difficulty encountered in solving analytically for the real load-deformation characteristics warrants the use of an idealized load-deformation curve (bilinear) as shown in Figure 2.3b. The idealized shape can be readily used where a loading stiffness, k_ℓ, can be based on typical values of secant moduli and the unloading stiffness, k_u, can be based on typical values of the coefficient of restitution, e (See Figure 2.3). The unloading curve is followed after the peak load is generated; the unloading slope is related

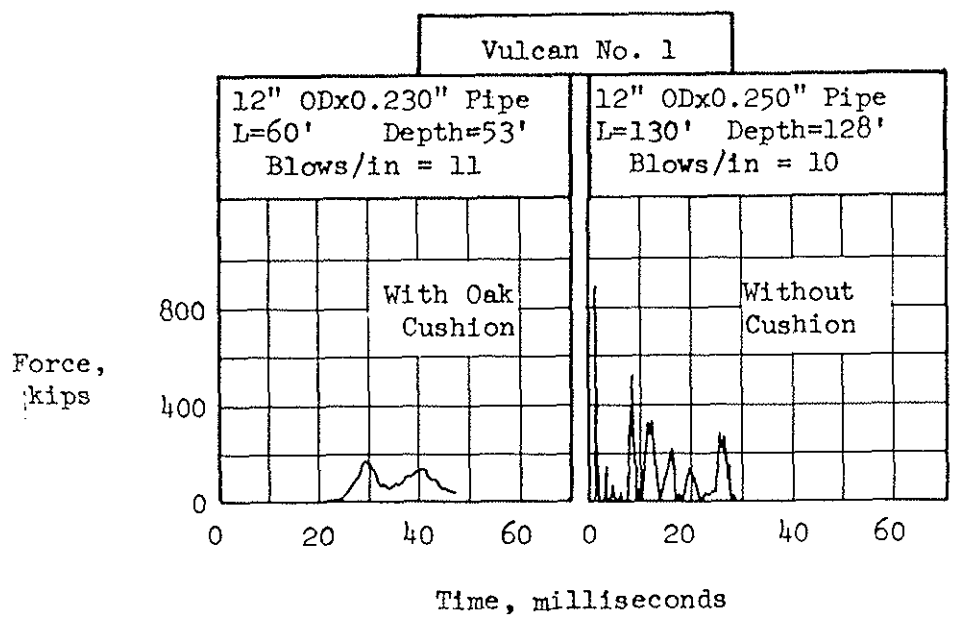

After Housel (1965)

Figure 2.2 PILE FORCE PULSE WITH AND WITHOUT HAMMER CUSHION

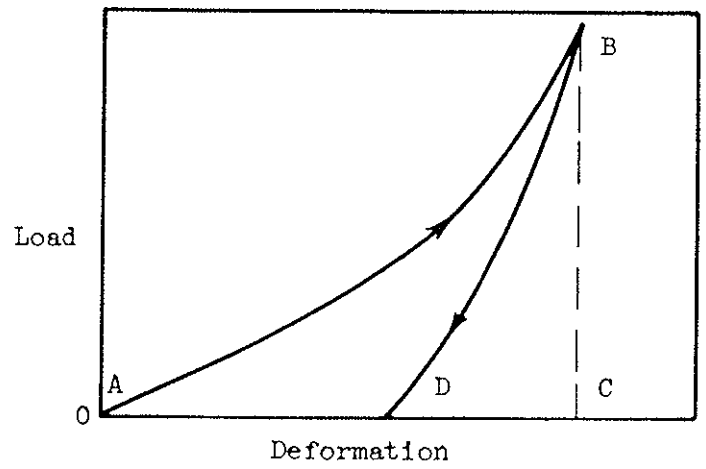

a) Real Curve

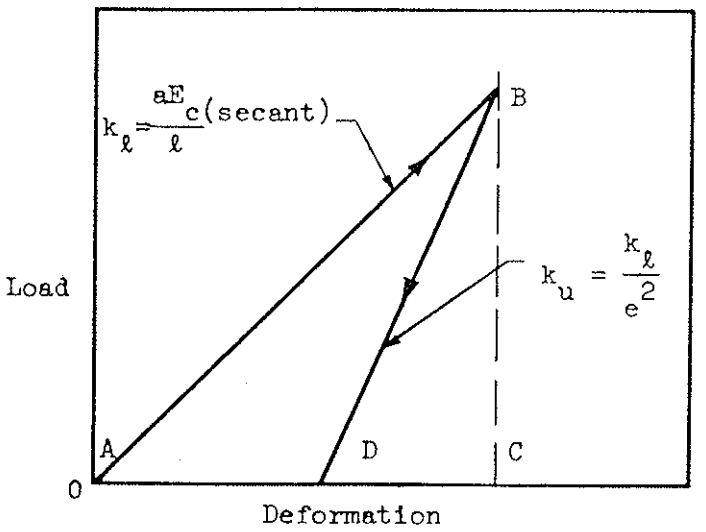

b) Idealized Curve

Note:

e = Coefficient of Restitution

$e = \sqrt{\frac{\text{Area BCD}}{\text{Area ABC}}}$

Figure 2.3 DYNAMIC LOAD-DEFORMATION RELATIONSHIPS FOR HAMMER CUSHION

to the loading slope and coefficient of restitution, i.e. $k_u = \frac{k_\ell}{e^2}$. The coefficient of restitution accounts for the energy loss in the cushion material.

The force generator will be investigated in terms of three types of behavior for the hammer cushion: 1) linear elastic, referred to herein as linear, 2) linear inelastic, referred to as bilinear, and 3) nonlinear inelastic, referred to as nonlinear. A comparison of common soft (wood) and stiff (aluminum-micarta) nonlinear and inelastic cushions for typical pile hammers will be made. The range of cross sectional pile properties will be represented by the variable pile impedance, ρcA.

2.2 Basic Equations

The basic differential equations governing the force generator-pile system are developed on the basis of the model shown in Figure 2.4a. The hammer ram and drivehead possess weights W_1 and W_2 and masses m_1 and m_2, respectively. At the instant the ram impacts the hammer cushion, with initial velocity V_o, x_1 is considered to be zero. The hammer cushion is initially treated as a massless elastic spring with stiffness k; the spring is considered to act in compression only. The drivehead co-ordinate x_2 is considered zero at the instant of impact as is co-ordinate x_3 describing motion of the pile head. It will be shown that the infinitely long pile behaves in the model as a dashpot; therefore, $x_2 = x_3$ and x_3 may be eliminated.

Forces acting on the ram and drivehead are shown in Figure 2.4b. Only gravity, acceleration and spring forces act on the ram. Similar

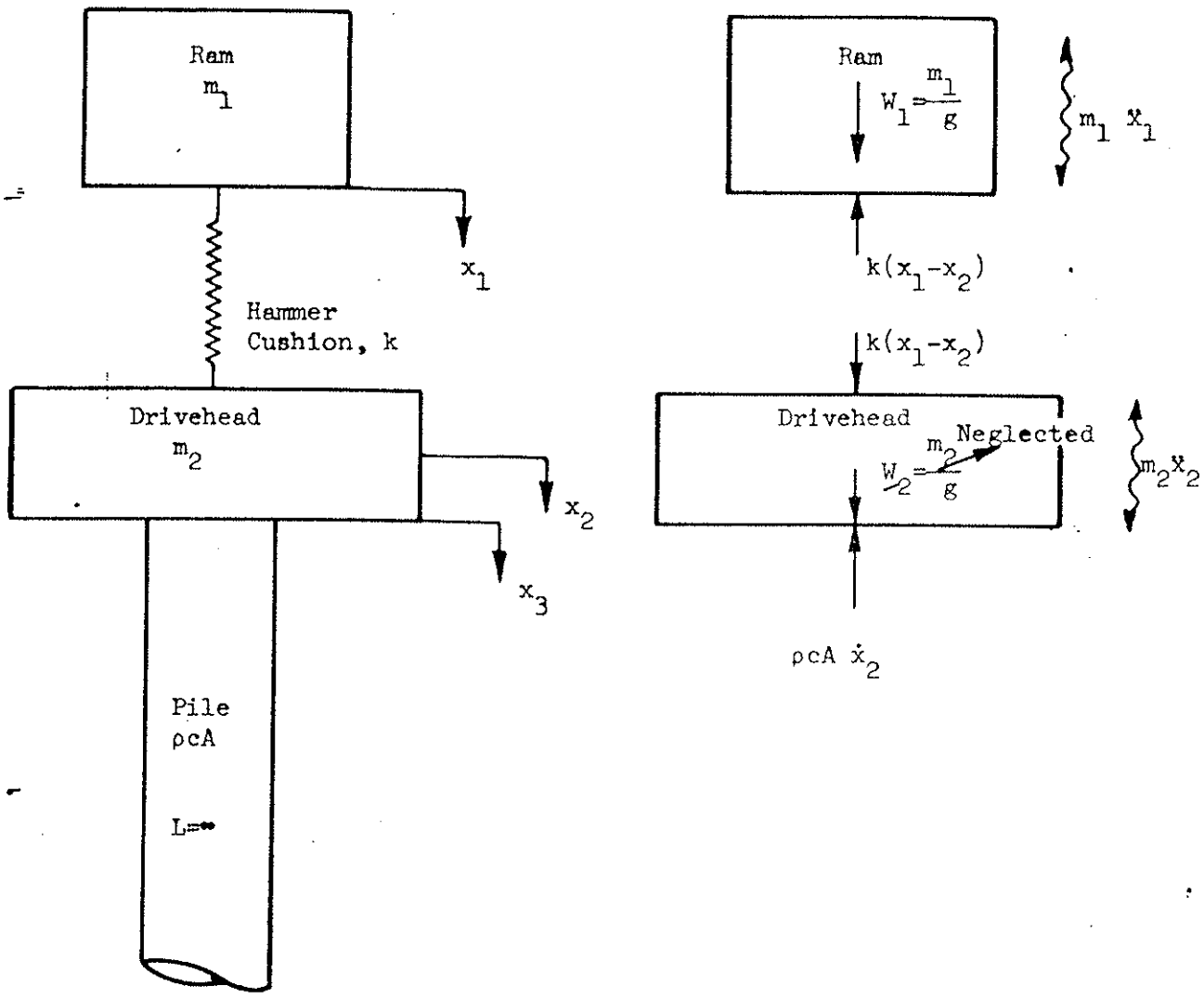

(a) Model

(b) Free Body Diagrams

Figure 2.4 FREE-BODY DIAGRAM OF FORCE GENERATOR MODEL

forces act on the drivehead in addition to the pile force, $\rho cA\dot{x}_2$. Because the pile is infinitely long no reflections enter into the analysis; therefore, force on the pile head is controlled only by pile head velocity, $\dot{x}_2$, which in turn is controlled only by the force generator. The drivehead weight is a small force relative to the forces under discussion and causes unnecessary complications in the analysis; therefore, it has been discarded. Thus, the resulting equations of equilibrium become:

$$\begin{aligned} m_1\ddot{x}_1 + k(x_1-x_2) - m_1 g &= 0 \\ m_2\ddot{x}_2 + \rho cA\,\dot{x}_2 - k(x_1-x_2) &= 0 \end{aligned} \tag{2.2}$$

Initial conditions are $x_1 = x_2 = \dot{x}_2 = 0$, and $\dot{x}_1 = V_o$. The equations are solved under the condition that $k(x_1-x_2)$ cannot be negative (no tension in the hammer cushion).

Equation 2.2 can be expressed in dimensionless form; this has been accomplished by utilizing the following definitions:

$$T = \sqrt{\frac{m_1}{k}} \text{ and } z = \frac{t}{T}$$

where T is the psuedo period of the ram on the cushion and z is dimensionless time. Substitution of these definitions into Equation 2.2, and rearranging yields the following expressions:

$$\begin{aligned} \ddot{X}_1 + (X_1-X_2) - gT^2 &= 0 \\ \ddot{X}_2 + \bar{A}\dot{X}_2 - \bar{B}(X_1-X_2) &= 0 \end{aligned} \tag{2.3}$$

where $X = x$, $\dot{X} = \frac{dx}{dz}$, $\ddot{X} = \frac{d^2x}{dz^2}$, $\bar{A} = \frac{\rho cA}{\sqrt{m_1 k}}$, $\bar{B} = \frac{W_1}{W_2}$ or $\frac{m_1}{m_2}$. The initial conditions become: $X_1 = X_2 = \dot{X}_2 = 0$, and $\dot{X}_1 = V_o T$.

Equation 2.3 has been solved using an electronic analog computer; details of the computer program are given in Appendix B. Only the solutions involving linear and bilinear hammer cushions can effectively utilize the nondimensional form. For nonlinear cushions, the nondimensional equations were used to solve a particular case.

It is noted that if the hammer cushion stiffness is made a function of (X_1-X_2) for purposes of representing nonlinear cushion behavior, it is possible to substitute the function directly into Equation 2.3 because no operations are performed on the functions. Arbitrarily assumed functions are used to represent the actual load-deformation relationships of nonlinear cushions.

2.3 Linear Cushion

Introduction

The study of the linear hammer cushion will be used to investigate hammer-pile parameters controlling both maximum energy and the force pulse shape transmitted to the pile. Initially, maximum transmitted energy to the pile will be investigated which involves the impedance match of hammer and pile. Then, the generated pile force shape will be investigated and related to the impedance match of hammer and pile.

For the investigation of pile force pulse and energy the $\bar{B}$ coefficient, relating ram weight to drivehead weight as shown in Equation 2.3, was selected to cover the range of the practical limits of driving

equipment. The $\bar{B}$ coefficients investigated are 1, 3, 5, 10 and 20; coefficients between 3 and 10 are typical for driving equipment and 5 is a reasonable average value. The $\bar{A}$ coefficient, relating pile impedance and hammer impedance as shown in Equation 2.3, was varied for a particular value of $\bar{B}$ to include very high and low pile impedances with respect to the driving equipment. The term hammer impedance is defined herein as the quantity $\sqrt{m_1 k}$ for purposes of discussion even though this quantity may not precisely describe the real impedance of the hammer.

To facilitate the use of the parameter study results for all types of common pile materials, the pile is designated simply by its characteristic impedance, ρcA. A tabulation of pile impedance for steel, concrete and wood piles and the corresponding dimensions are shown in Table 2.1. The pile impedances listed in Table 2.1 correspond to typical pile dimensions and are referred to in the presentation of the results. It should be noted that the low pile impedances correspond to light-wall pipe or wood piles, whereas the high impedances correspond to heavy-wall pipe (mandrels), concrete or H-piles.

Pile Energy

Energy transmitted to the pile head can be qualitatively considered in terms of the ram and drivehead motion as shown in Figure 2.5. First, maximum energy can be delivered to the pile when the pile impedance is matched with respect to the hammer impedance; the ram and drivehead motion continues downward to maximum displacement and remains at that location (Figure 2.5b). When the pile impedance is higher than the matched impedance (high pile impedance with respect to the hammer impedance), the ram motion continues downward to a maximum displacement and

Table 2.1

TABULATION OF PILE IMPEDANCES AND PILE TYPES

Pile Impedance ρcA lbs-sec/in.	Steel* Area in.^{2}	Pile Material Concrete* Area in.^{2}	Concrete* Diameter in.	Concrete* Width in.	Wood* Area in.^{2}	Wood* Diameter in.
725	5(Thin Wall Pipe)	23.5	5.5	4.8	82	10.2
1450	10	47	7.8	6.9	164	14.5
2900	20	94	11.0	9.7	328	20.4
5800	40 (Mandrel)	188	15.5	13.7	656	29.0
8700	60	282	18.0	16.8	984	--

*The following material properties were used to determine pile dimensions from impedances. Subscripts (s = steel, c = concrete, w = wood) are used.

Steel $E_s = 29 \times 10^6$ psi $\quad \rho_s = 15.2 \frac{\text{lbs-sec}^2}{\text{ft}^4}$

$c_s = \sqrt{E_s/\rho_s} = 16{,}600$ ft/sec $\quad (\rho c)_s = 145 \frac{\text{lbs-sec}}{\text{in.}} / \text{in.}^2$

Concrete $E_c = 4.25 \times 10^6$ psi $\quad \rho_c = 4.65 \frac{\text{lbs-sec}^2}{\text{ft}^4}$

$c_c = \sqrt{E_c/\rho_c} = 11{,}500$ ft/sec $\quad (\rho c)_c = 30.9 \frac{\text{lbs-sec}}{\text{in.}} / \text{in.}^2$

Wood $E_w = 1.3 \times 10^6$ psi $\quad \rho_w = 1.24 \frac{\text{lbs-sec}^2}{\text{ft}^4}$

$c_w = \sqrt{E_w/\rho_w} = 12{,}300$ ft/sec $\quad (\rho c)_w = 8.84 \frac{\text{lbs-sec}}{\text{in.}} / \text{in.}^2$

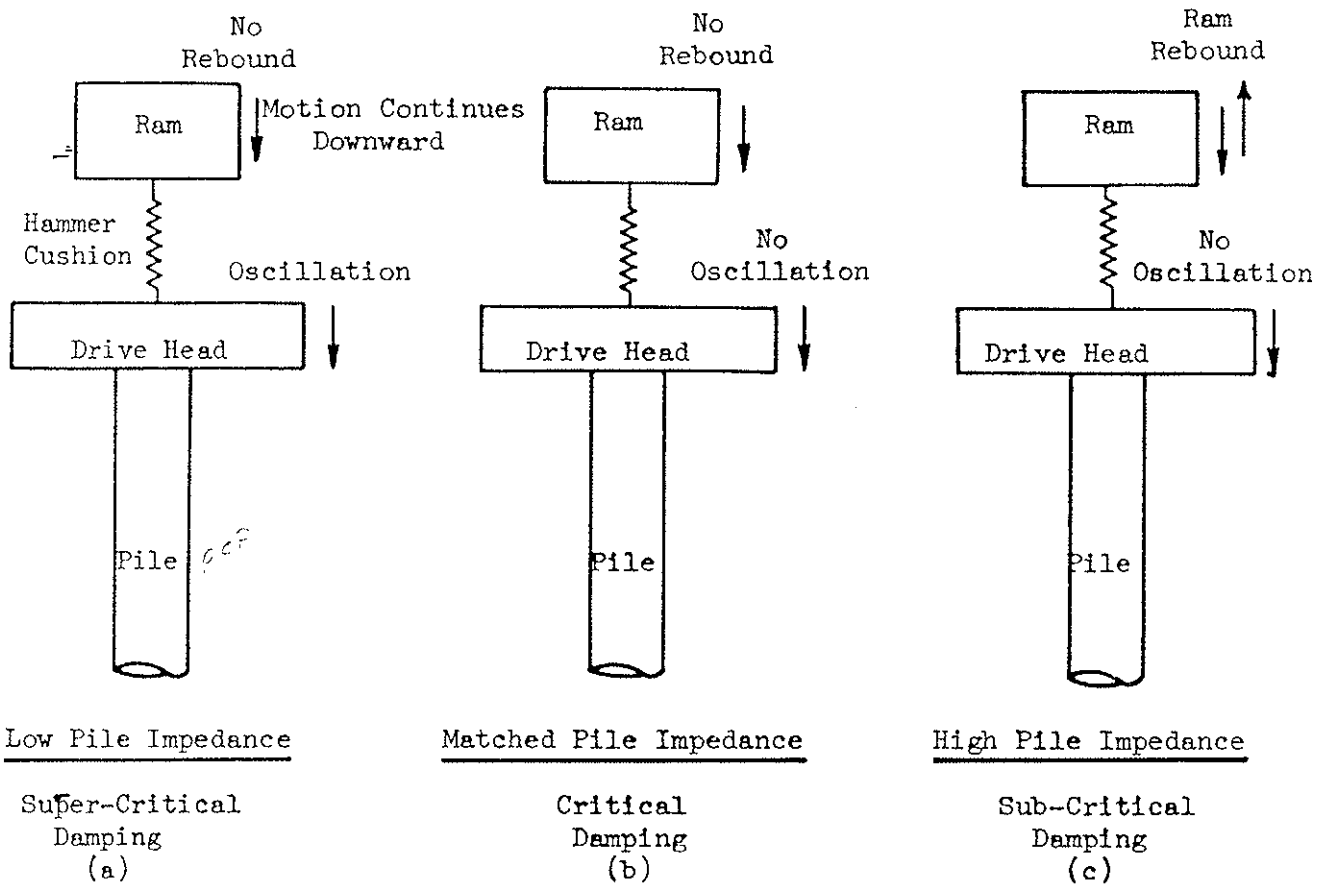

Low Pile Impedance

Super-Critical
Damping
(a)

Matched Pile Impedance

Critical
Damping
(b)

High Pile Impedance

Sub-Critical
Damping
(c)

Figure 2.5 SCHEMATIC OF PILE-HAMMER RESPONSE

rebounds while the drivehead motion is downward as shown in Figure 2.5c. For this case when the ram rebounds, some of the initial kinetic energy is lost in the rebound; therefore, the energy transmitted to the pile is less than the impact energy of the driver system.

For low pile impedance with respect to the matched pile impedance the ram and drivehead motion continues downward; however, the drivehead is driven downward at a faster rate than the ram motion (Figure 2.5a). The ram continues downward as the drivehead slows again and produces another ram blow, whereupon the drivehead oscillatory motion is repeated. With time, the energy is fully transmitted to the pile; however, the rate at which energy is transmitted decreases with decreasing pile impedance. The interference of hammer operations in returning the ram for another stroke can prevent the energy from being fully transmitted to the pile for the condition of low pile impedance.

The hammer and pile response for $\bar{B} = 5$ and a linear elastic cushion can be used to illustrate further the preceding qualitative discussion. The response of pile energy, ram displacement, pile displacement and pile force versus dimensionless time, z, is shown in Figure 2.6. The energy, displacements and force are expressed in terms of coefficients: C_E = pile energy coefficient, C_R = ram displacement coefficient, C_P = pile head displacement coefficient, and C_{F1} = pile force coefficient. The procedure for converting the hammer and pile response into real quantities is explained in Appendix B. The individual curves are represented by $\bar{A}$ coefficients relating pile impedance and hammer impedance, i.e. $\bar{A} = \rho c A \bar{B}/\sqrt{m_1 k'}$. The hammer and pile response shown in Figure 2.6 illustrates the behavior for low, matched and high pile impedance relative to hammer impedance.

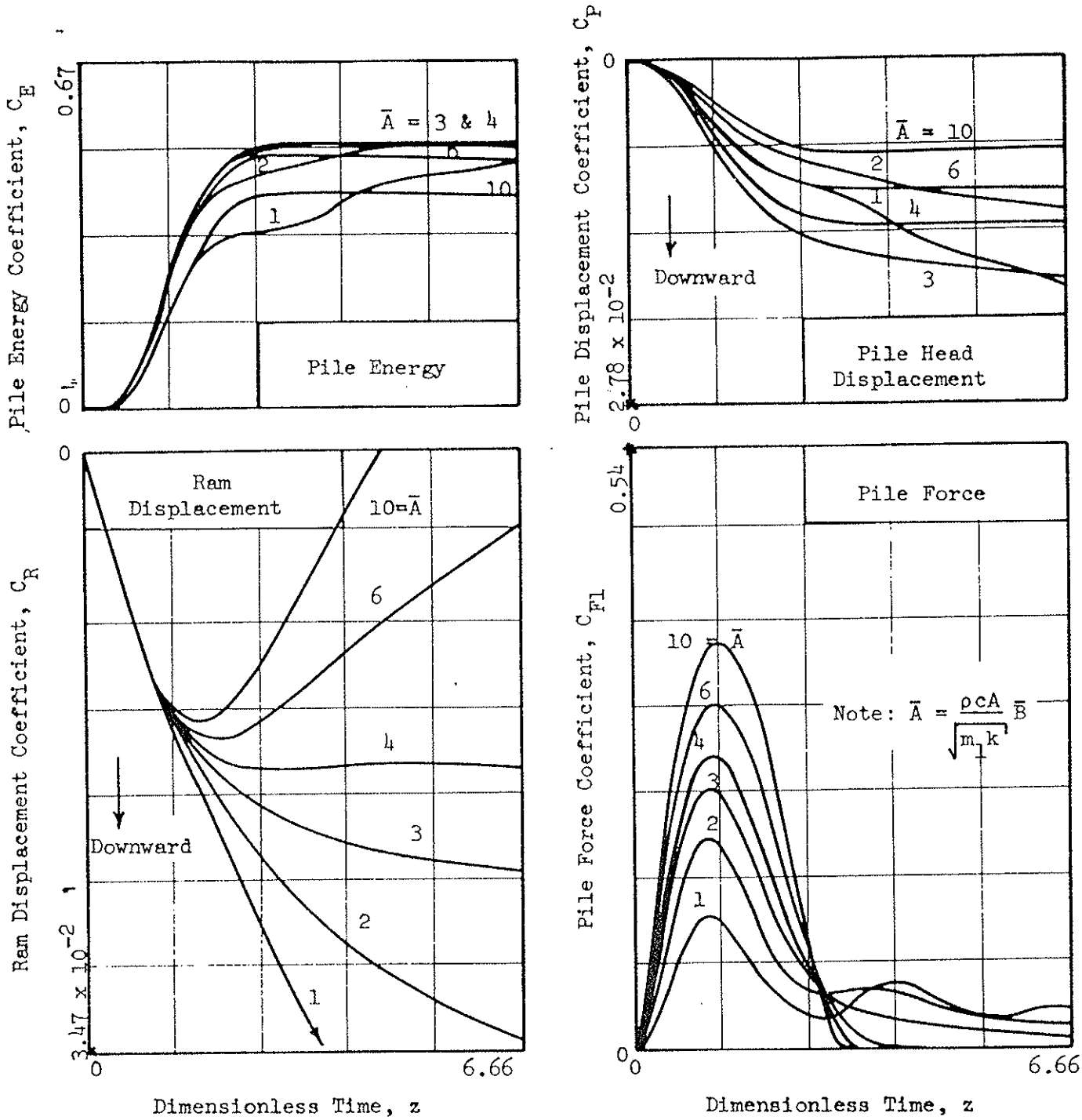

$\bar{B}$ = Ram Weight W_1/Drivehead Weight W_2

Figure 2.6 PILE AND HAMMER RESPONSE FOR $\bar{B}$ = 5 AND LINEAR CUSHION

The representative plot of pile energy shown in Figure 2.6 shows that when $\bar{A}$ is 4 a good impedance match of hammer and pile exists. The ram and pile displacements occur as expected. In the case of energy loss due to ram rebound as shown for $\bar{A}$ = 10 (pile impedance greater than matched impedance), the pile energy is lower than for the impedance match condition of $\bar{A}$ = 4.

An example of low pile impedance with respect to the matched impedance is shown in Figure 2.6 by the curve for $\bar{A}$ = 1. The rate of energy transmitted to the pile is less than that for the matched conditions and the drivehead motion is oscillatory. The pile force pulse also shows a change in pulse shape as compared to the condition of $\bar{A}$ = 4 and 10. It is noted in Figure 2.6 that there is a range in $\bar{A}$ coefficients that represent essentially a match between pile and hammer with respect to energy. The energy was determined at a time approximately equal to four times the pseudo period of the ram.

The most efficient pile-hammer combinations for energy transmission were determined from the analog computer studies of hammer and pile response for each $\bar{B}$ coefficient is shown in the range band in Figure 2.7 in terms of an impedance ratio; the impedance ratio is simply the ratio of the $\bar{A}$ to $\bar{B}$ coefficient, or $I_R = \bar{A}/\bar{B} = \frac{\rho c A}{\sqrt{m_1 k}}$. The range band for the matched pile impedance represents an efficiency of energy transmission of 90 percent or more. The impedance ratio for matched pile impedance decreases with an increase in the ratio of ram weight to drivehead weight.

Above the impedance match condition shown in Figure 2.7, the pile impedance is high relative to hammer impedance with energy losses

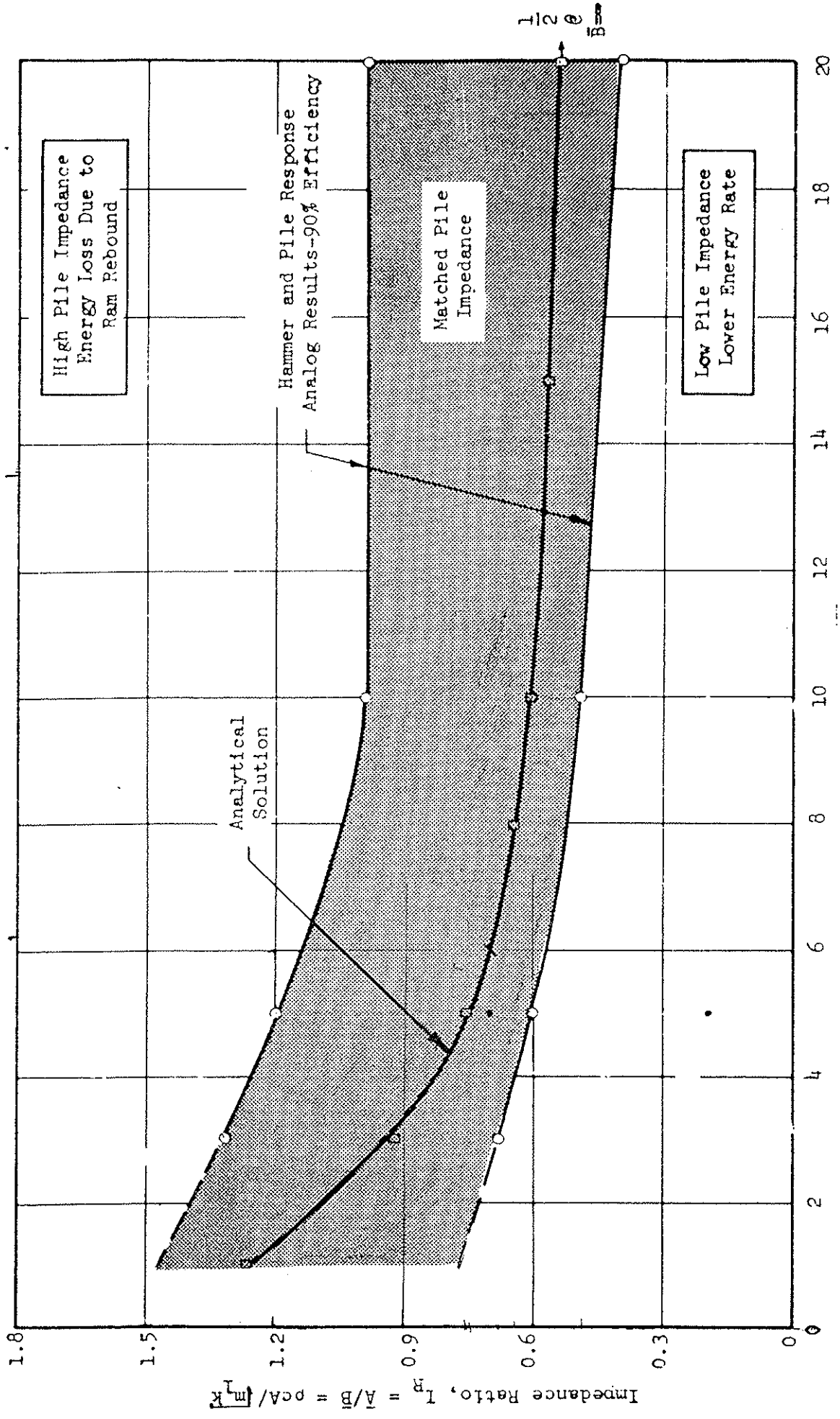

Figure 2.7 IMPEDANCE RATIO FOR PILE-HAMMER SYSTEM

due to ram rebound; therefore, as previously discussed, this is not an efficient energy system. Below the matched condition, the pile impedance is low relative to hammer impedance and the rate of energy transmission is lowered. A low rate of energy transmission is not the only disadvantage of the low pile impedance condition; possible hammer damage caused by driving the drivehead out from beneath the ram should be considered. Consideration of hammer damage suggests that it is better to be on the high side of the impedance ratio than the low side.

In general, the practical range of impedance ratio for matched pile impedance is 0.60 to 1.10 for typical ratios of ram to drivehead weight ($\bar{B}$ = 3 to 10). This means that for an optimum pile-hammer combination with respect to maximum energy transmitted to the pile, the pile impedance (ρcA) is related to the hammer impedance ($\sqrt{m_1 k}$) by:

$$\rho cA = [0.60 \text{ to } 1.10] \sqrt{m_1 k} \qquad (2.4)$$

A closed form solution was attempted in order to define the conditions of maximum energy transmitted to the pile for the force function generator described herein. The homogeneous solution of Equation 2.3 may be written in the form of

$$X_1 = c_1 e^{rz} \quad \text{and} \quad X_2 = c_2 e^{rz}$$

where c_1 and c_2 are arbitrary coefficients and r represents the roots of a quartic indicial equation. Three conditions can be determined from the roots of the indicial equation:

$$4(I_R)^4 - I_R^2 - \frac{20I_R^2}{\bar{B}} + \frac{8I_R^2}{\bar{B}^2} + \frac{4}{\bar{B}^4}(\bar{B}+1)^3 > 0 \quad \text{One real and two imag. roots Subcritically damped} \qquad (2.5)$$

$$4(I_R)^4 - I_R^2 - \frac{20I_R^2}{\bar{B}} + \frac{8I_R^2}{\bar{B}^2} + \frac{4}{\bar{B}^4}(\bar{B}+1)^3 = 0 \quad \text{3 real roots 2 equal Critically damped} \qquad (2.6)$$

$$4(I_R)^4 - I_R^2 - \frac{20I_R^2}{\bar{B}} + \frac{8I_R^2}{\bar{B}^2} + \frac{4}{\bar{B}^4}(\bar{B}+1)^3 < 0 \quad \text{3 real roots unequal Supercritically damped} \qquad (2.7)$$

The conditions of Equations 2.5, 2.6 and 2.7 imply the ram motion to be oscillatory or deadbeat. With a high pile impedance with respect to the hammer impedance the ram motion is oscillatory and ram rebound occurs; therefore, this condition of motion is commonly defined as a subcritical damping. The transition of ram motion from subcritical to supercritical damping is the critically damped condition.

For the critically damped system or pile-hammer match, the impedance ratio of Equation 2.6 can be determined for particular values of the $\bar{B}$ coefficient. The relationship between the impedance ratio and $\bar{B}$ coefficient for the analytical solution is shown in Figure 2.7; the analytical curve falls within the matched pile impedance zone as determined from the analog computer results. The impedance ratios of the critically damped system for $\bar{B} \geq 8$ are real values and the maximum value was selected. For the special condition where the drivehead weight approaches zero, i.e. $\bar{B} = \infty$, the impedance ratio for the critically damped pile-hammer system equals 0.5. This value is a lower bound for the pile-hammer match. For cases where $\bar{B} < 8$, the calculated impedance ratios were imaginary values; therefore, the minimum point of Equation 2.6 with respect to impedance ratio was selected as the criti-

cal condition. A full explanation of the analytical interpretation of this minimum point criterion is beyond the scope of this presentation.

Pile Force

Introduction. The generated pile force with respect to peak value, force shape, and duration will be discussed relative to the impedance match of the pile and hammer, i.e. high pile impedance, matched impedance and low pile impedance. The hammer variables, such as ram velocity, ram and drivehead weight, and cushion properties will be investigated with respect to the pile impedances given in Table 2.1.

In order to facilitate the discussion of pile force, the generated pile forces will be summarized for $\bar{B}$ coefficients of 3, 5, 10 and 20 as shown in Figure 2.8. The force pulse generated for different $\bar{A}$ coefficients is expressed in terms of the pile force coefficient, C_{F1}, and dimensionless time, z. Real time can be easily determined by the expression, $t = zT$; however, the pile force is a function of several variables as shown in the expression below:

$$F = \frac{\rho c A\, V_o}{\bar{A}} [C_{F1}] \qquad (2.8)$$

Equation 2.8 shows that the pile force is directly proportional to the force coefficient and inversely proportional to the $\bar{A}$ coefficient. The inverse proportionality of the $\bar{A}$ coefficient does not alter the shape and magnitude of an individual force curve for a particular $\bar{A}$ coefficient, but it causes an apparent misrepresentation of the relative magnitude of the force curves for different $\bar{A}$ values. For in-

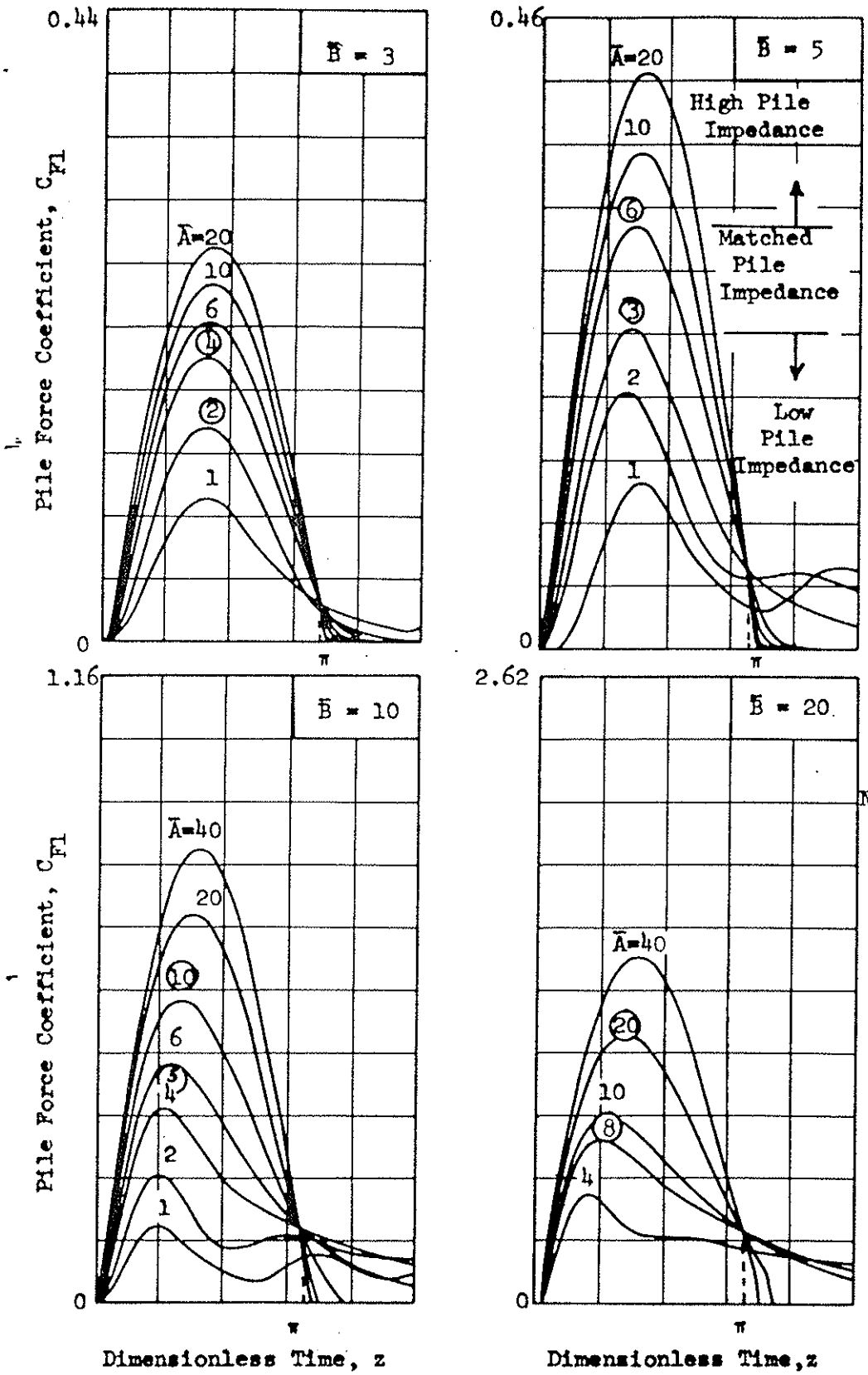

Note:
1. Circled Ā Coeff. represents the "Matched Pile Impedance"

Figure 2.8 GENERATED PILE FORCE SUMMARY FOR LINEAR CUSHION

stance, the low value of the $\bar{A}$ coefficient has a larger peak pile force than the higher $\bar{A}$ coefficient value for a given pile impedance and ram velocity. The reason for the apparent discrepancy is that the $\bar{A}$ coefficient increases at a faster rate than the pile force coefficient, C_{F1}, decreases.

For $\bar{B}$ = 5, Figure 2.8, the $\bar{A}$ value of 1 represents a low pile impedance relative to the hammer impedance; therefore, the pile is driven out from under the ram resulting in oscillatory and damped pile forces. With an increase in the $\bar{A}$ coefficient to 3 or 6, the impedances of hammer and pile match and the force pulse is approaching the shape of a damped sinusoidal wave. With larger $\bar{A}$ coefficients such as 20 or 40, the pile impedance is larger than the hammer impedance; therefore, the ram is rebounding and the force pulse is approaching the shape of a sine wave. The presentation of the pile forces as shown in Figure 2.8 will be used to aid the discussion of generated pile force with respect to peak, shape and duration.

Peak Force. The peak pile force can be summarized for $\bar{B}$-coefficients of 3, 5, 10 and 20 as shown in Figure 2.9. The peak pile force, F_p, is related to the pile and hammer characteristics by the following:

$$F_p = [\sqrt{m_1 k}\, V_o][C_{F2}] \text{ or } [\frac{\rho c A}{I_R} V_o][C_{F2}] \qquad (2.9)$$

where C_{F2} is the peak pile force coefficient. Equation 2.9 and Figure 2.9 can be used to determine peak pile force for a particular pile.

With reference to Figure 2.9, the $\bar{B}$ coefficient has a negligible effect on the peak pile force for a given hammer and pile; therefore, generated peak pile forces are nearly independent of drivehead weight.

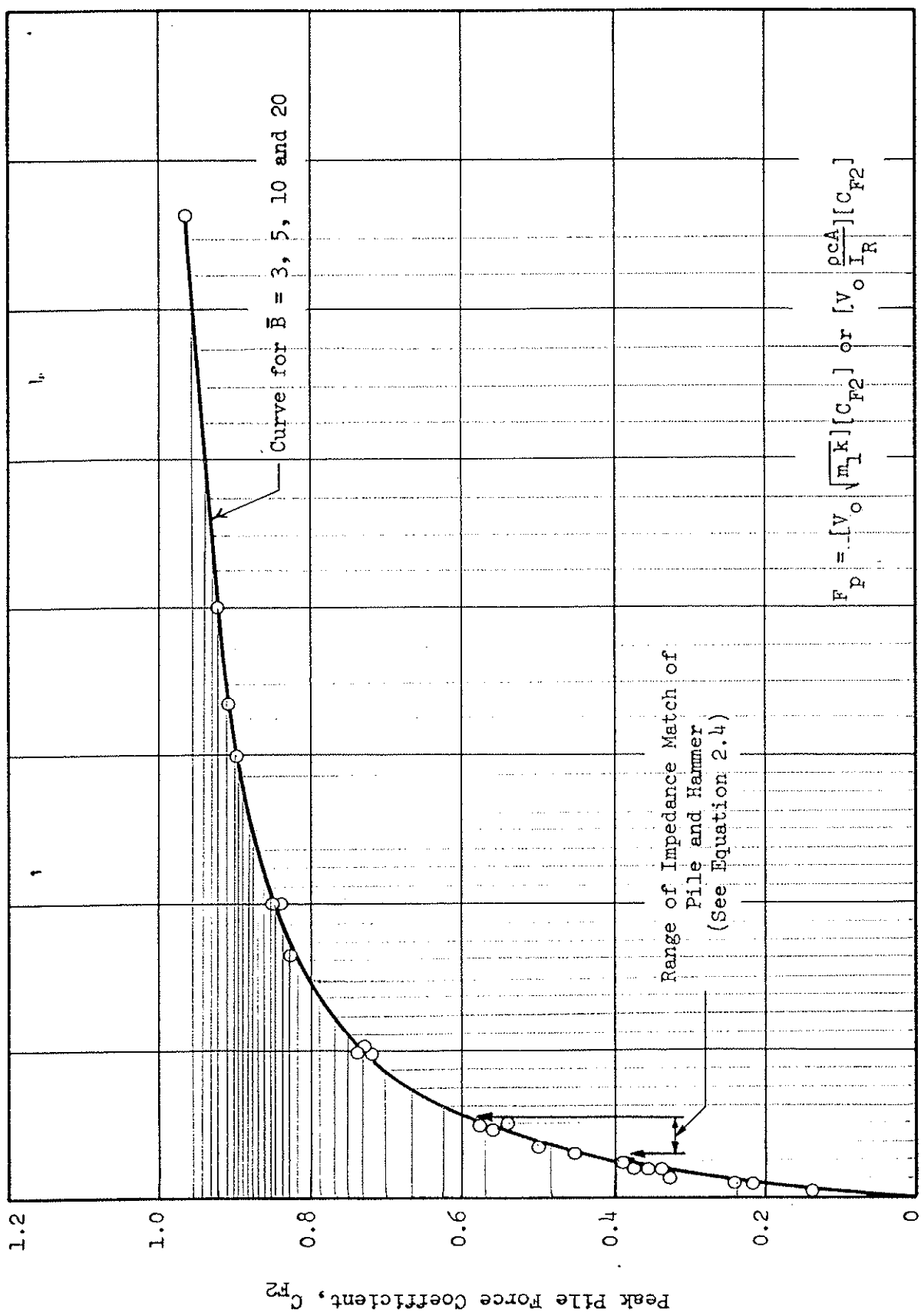

Figure 2.9 PEAK PILE FORCE VERSUS IMPEDANCE RATIO

The relationship between peak pile force and impedance ratio (Equation 2.9 and Figure 2.9) can be used to determine the peak force for a particular pile impedance, ram weight and cushion stiffness. To exemplify the interrelationship of parameters, particular values of pile impedance were selected and peak forces were determined for common ram weights and cushion stiffnesses as shown in Figure 2.10. Since the effect of drivehead weight on peak force is negligible, a common $\bar{B}$ coefficient of 5 was used to obtain ther results shown in Figure 2.10. The pile impedances selected represent a range of typical pile sections varying from light weight (thin-walled pipe) to heavy weight (mandrel or H-piles) as tabulated in Table 2.1. In terms of pile impedance, the steel piles can easily account for the full range of impedances investigated, namely 725 to 8700 $\frac{\text{lbs. sec.}}{\text{in.}}$. Wood piles fall in the impedance range of thin-walled pipe, whereas concrete sections correspond to the higher impedance range of steel piles.

Peak pile force may be determined by the following expression:

$$F_p = [C_{F3}][V_o \text{ ft/sec}] \qquad (2.10)$$

where F_p is a peak force in kips, C_{F3} is a peak pile force coefficient (Figure 2.10) which has units of kip-seconds/foot, and V_o is ram velocity at impact in feet/second.

With reference to Figure 2.10, the peak pile force generally increases with increases in ram velocity, cushion stiffness, ram weight and pile impedance. The ram velocity is directly proportional to the peak pile force as shown in Equation 2.10. The velocity at

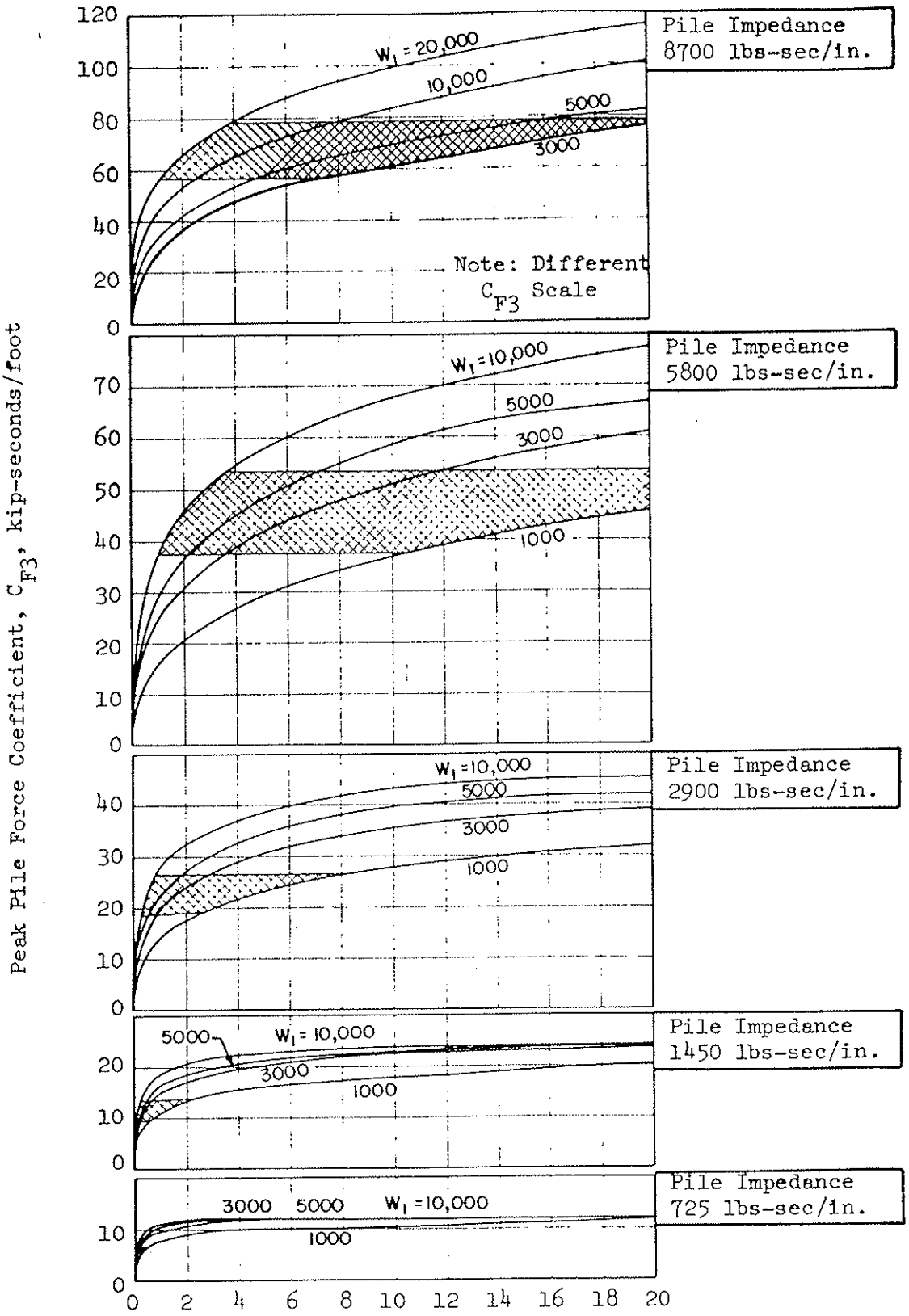

Note: $F_P = [C_{F3}][V_0$ ft/sec] kips

Cross-hatching represents zone of impedance match of pile and hammer.

Figure 2.10 RELATIONSHIP OF PEAK PILE FORCE WITH HAMMER CHARACTERISTICS AND PILE IMPEDANCES

impact, and therefore the peak force, can be related to the height of ram fall and hammer efficiency for a free-fall drop as shown below:

$$V_o = 8.03\sqrt{\frac{e_f}{100}\,h} \qquad (2.11)$$

where V_o is expressed in feet/second and h is in feet. Equation 2.11 can be expressed graphically as shown in Figure 2.11 for the practical range of hammer efficiency from 30 to 100 percent. The drop height, h, is the actual fall distance of the ram for a single-acting hammer. For a double-acting or differential hammer, the drop height h is the equivalent height with consideration of the downward acceleration added by air or steam pressure.

The effect of ram weight and cushion stiffness for particular pile impedances is shown in Figure 2.10. In general, the peak force increases with an increase in both cushion stiffness and ram weight for a given pile impedance; however, there are limiting conditions beyond which the peak forces do not increase. With respect to the limitations of hammer cushion, the peak force becomes independent of cushion stiffness beyond an upper limiting stiffness, defined herein as the upper limit of effective cushion stiffness. For the limitations of the ram weight, peak force becomes independent of ram weight for low pile impedances (See Figure 2.10).

In order to clarify the meaning of the upper limit of effective cushion stiffness, consider the pile impedance of 725 $\frac{\text{lbs-sec}}{\text{in}}$ as shown in Figure 2.10. For the ram weight of 10,000 lbs, the peak force increases with cushion stiffness up to a stiffness of approximately

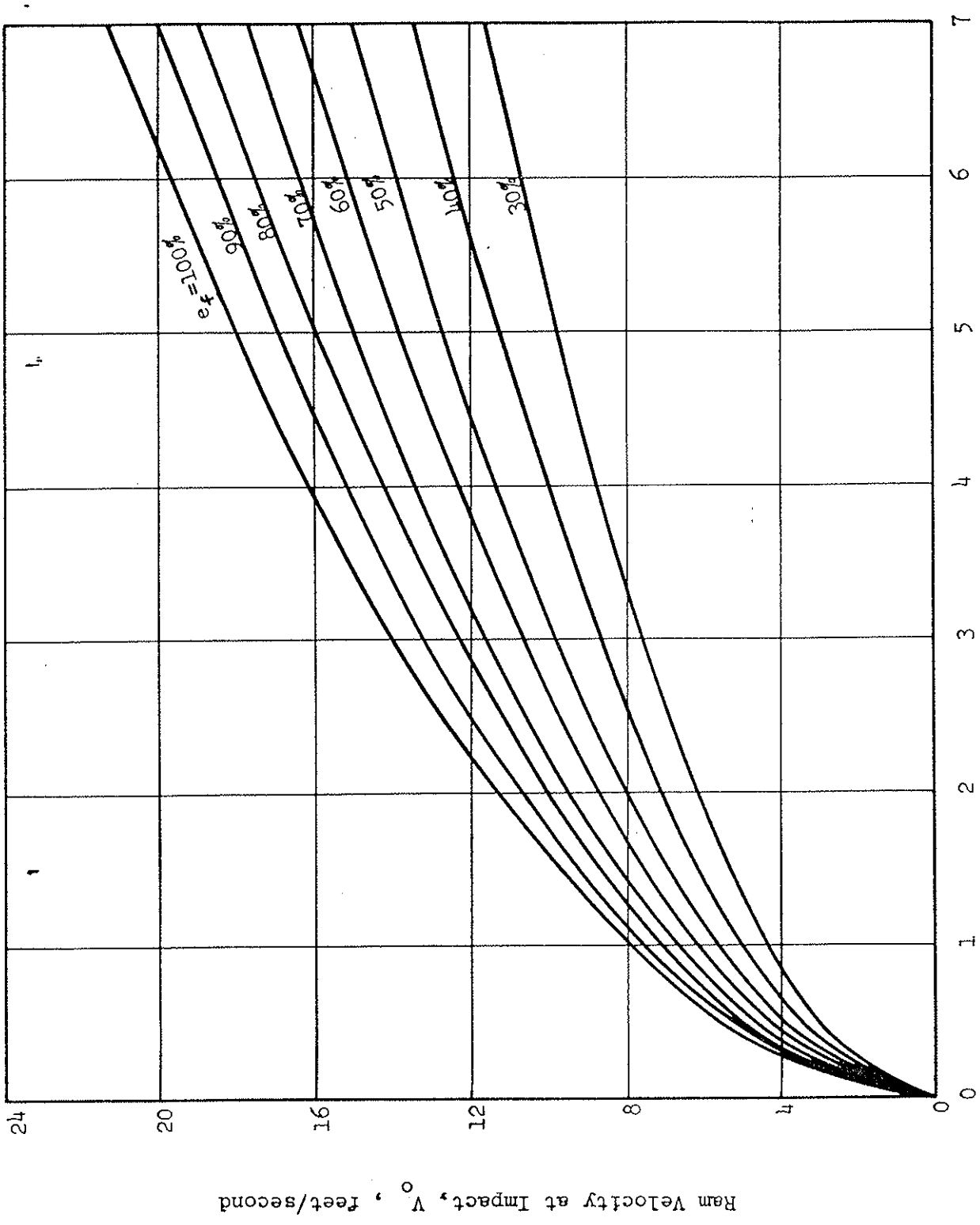

Figure 2.11 RAM VELOCITY AT IMPACT

1×10^6 lbs/in., and thereafter is independent of stiffness. The stiffness of 1×10^6 lbs/in. therefore, represents the upper limit of effective stiffness. For the light ram (1000 lbs), the upper limit of effective stiffness is approximately 4×10^6 lbs/in. With reference to pile impedances greater than 725 $\frac{\text{lbs-sec}}{\text{in.}}$, peak pile force becomes independent of cushion stiffness at higher stiffness levels. For instance, the upper limit of effective cushion stiffness increases with an increase in pile impedance as shown below:

Pile Impedance lbs-sec/in.	Range in Ram Weights lbs.	Approximate Upper Limit of Effective Cushion Stiffness
725	10,000 - 1,000	1 to 4 $\times 10^6$ lbs/in.
1450	10,000 - 1,000	4 to 8 $\times 10^6$
2900	10,000 - 1,000	8 to 12 $\times 10^6$
5800	20,000 - 1,000	12 to 16 $\times 10^6$
8700	20,000 - 3,000	16 to 20 $\times 10^6$

It should be noted that the lower cushion stiffness corresponds to the heavier ram weight and the higher stiffness corresponds to the lighter ram.

The impedance match of hammer and pile for maximum energy transmission can be superimposed on the results of Figure 2.10. For a given pile impedance and ram weight, cushion stiffness can be determined for the impedance match of the hammer and pile; this is shown cross-hatched in Figure 2.10. For comparison, the range in cushion stiffnesses for the impedance match condition will be tabulated along with the approximate upper limit of cushion stiffness for maximum pile peak force as

shown in Table 2.2. The cushion stiffness at which the upper limit of peak pile force occurs is considerably larger than that for the impedance match condition. As pile impedance increases, the cushion stiffness for efficient energy transmission approaches that for the approximate limit of peak pile force. The cushion stiffness at which the approximate peak pile force is first attained corresponds to an energy transmission efficiency of approximately 80%.

The effect of ram weight can be represented by a relationship between pile impedance and peak pile force as shown in Figure 2.12. The peak force, expressed in terms of the impact velocity, V_o, was arbitrarily determined at a cushion stiffness of 20×10^6 lbs/in. As shown in Figure 2.12, the peak force is independent of ram weight at low pile impedances; however, the ram weight becomes more significant with respect to the generated peak force as the pile impedance increases.

Figure 2.12 is also representative of the effect of pile impedance on the generated peak force. Peak pile force increases with an increase in pile impedance. For low values of pile impedance, the generated peak force approaches a direct proportion to the increase in pile impedance, i.e. a 50% increase in pile impedance will produce a 50% increase in peak force. For high pile impedances, peak pile force increases at a rate less than the increase in pile impedance. The proportional relationship between peak force and pile impedance is superimposed on Figure 2.12 in order to evaluate the lack of proportionality at high pile impedances. With the proportional relationship line as reference, it is seen that the proportionality between peak force and pile impedance decreases with an increase in pile impedance. Also, the propor-

Table 2.2

A COMPARISON OF CUSHION STIFFNESSES
FOR IMPEDANCE MATCH AND LIMIT OF
PEAK PILE FORCE

Pile Impedance, lbs.-sec/in.	Ram Weights lbs.	Hammer Cushion Stiffness, k, x 10^6 lbs/in.		Percent Change in Pile Force from Matched to Limit Condition
		Impedance Match	Approximate Limit of Peak Force	
725	10,000-3,000	0.02 to 0.2	1 to 2	100%
	1,000	0.2 to 0.6	4	82%
1450	10,000-3,000	0.1 to 0.7	4 to 6	96-82%
	1,000	0.7 to 2.2	8	52%
2900	10,000-3,000	0.3 to 3.0	8 to 10	87-50%
	1,000	2.7 to 9.0	12	33%
5800	20,000-3,000	0.5 to 12.0	12 to 14	78-23% Below Match Condition
	1,000	10.7 to 36.0	16	
8700	20,000-3,000	1.2 to 27.0	16 to 20	69-Below Match

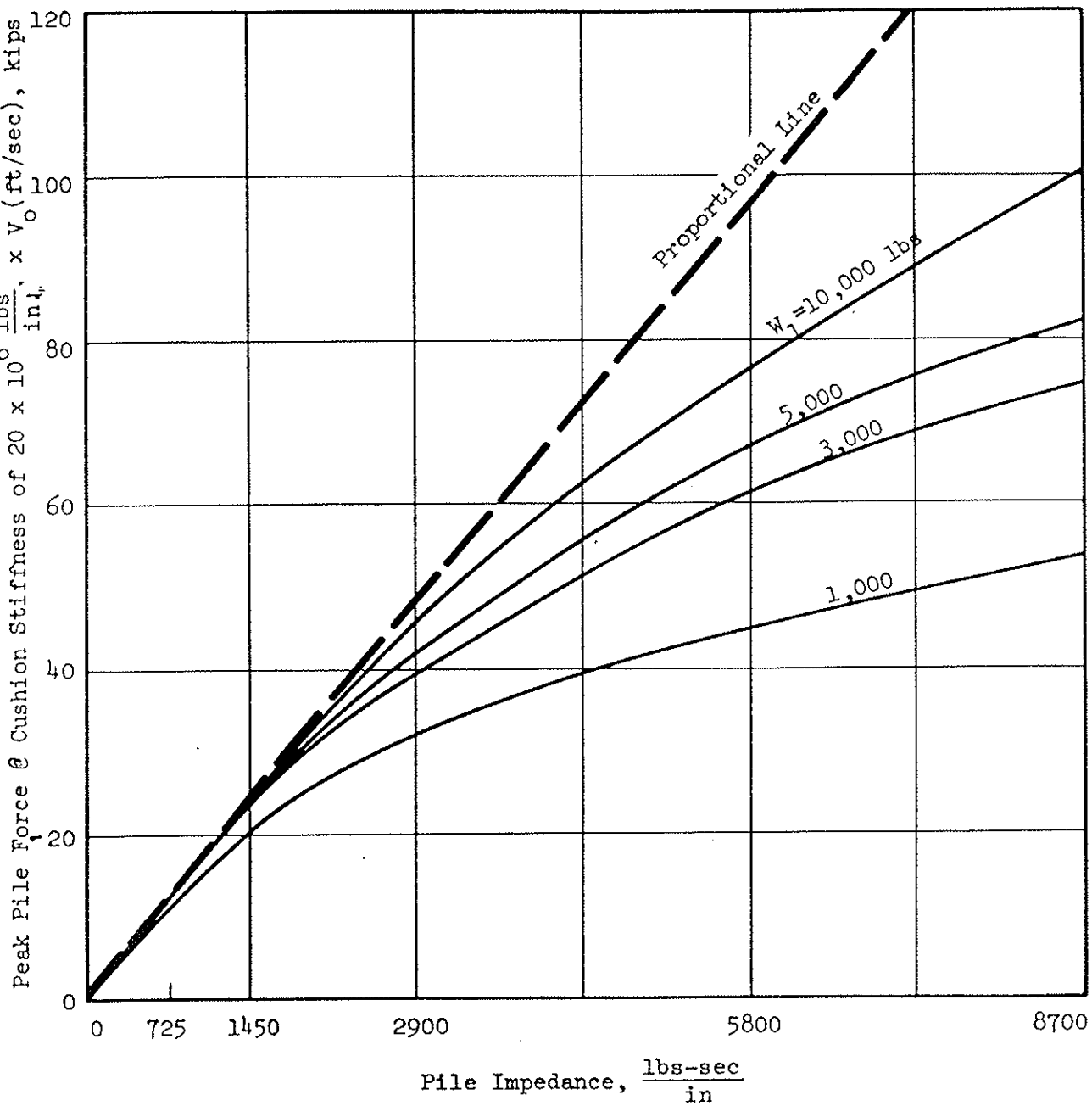

Figure 2.12 PEAK PILE FORCE VERSUS PILE IMPEDANCE FOR DIFFERENT RAM WEIGHTS

tionality decreases with a decrease in ram weight. For high pile impedances, a typical lower limit of proportionality may be 60%, i.e. a 50% increase in pile impedance will produce a 30% increase in peak force.

Shape and Duration. The effect of pile and hammer parameters on the generated pile force shape and duration will now be considered.

Although the drivehead weight has a negligible effect on the peak pile force, the shape of the force pulse is noticeably affected. For the conditions of high pile impedance (high $\bar{A}$ values) as shown in Figure 2.8, the force pulses for all $\bar{B}$ coefficients are nearly sinusoidal and the pulse durations are nearly equal. As pile impedance approaches the matched condition, the pulse becomes skewed and approaches a damped sinusoidal shape. In addition, duration of pulse is larger as the $\bar{B}$ coefficient increases (or drivehead weight decreases). The skewed trend is also prevalent for the low pile impedance condition (lower than impedance match) and the force becomes oscillatory.

For the force pulse curves shown in Figure 2.8, it can be seen that the force curves intersect at a value of dimensionless time (z) approximately equal to π; this is not true for low impedance ratios where oscillations occur. This point of intersection can be used as a guide to the duration of the force pulse. For typical $\bar{B}$ coefficients of 3 to 10, the duration of the force pulse can be represented by the intersection point for all conditions of impedance ratio, $\bar{A}/\bar{B}$; however, oscillations of the force pulse occur within the range of this intersection for low impedance ratios.

If the dimensionless duration is converted into real time for the intersection point, then real duration, t_d, will be:

$$t_d = zT = \pi\sqrt{\frac{m_1}{k}} \qquad (2.12)$$

It is of interest to note that t_d in Equation 2.12 is equivalent to one-half the real period of the ram and cushion, i.e. $2\pi\sqrt{\frac{m_1}{k}}$.

The duration given in Equation 2.12 is directly proportional to the square root of the ram weight and inversely proportional to the square root of the cushion stiffness. This means that by increasing the ram mass by a factor of 2, the pulse length is increased by a factor of $\sqrt{2}$, or 1.41. Also, an increase in stiffness by a factor of 2 produces a decrease in pulse length by a factor of $\sqrt{2}$, or 1.41.

The duration as a function of hammer and pile characteristics is graphically shown in Figure 2.13. The pile impedances of Table 2.1 are superimposed on the hammer characteristics for matched conditions. It is seen that for a given ram weight, the duration decreases with an increase in pile impedance. Duration is approximately the inverse proportionality to pile impedance, i.e. a 50% increase in pile impedance results in an approximate 50% decrease in time duration. It should be noted that the aforementioned duration for low pile impedance relative to hammer impedance does not include the total length of force pulse with all the damped oscillating peaks, but only gives approximately the duration of the first oscillatory pulse cycle.

The force pulse shape and the duration are independent of the ram velocity at impact for a linear cushion.

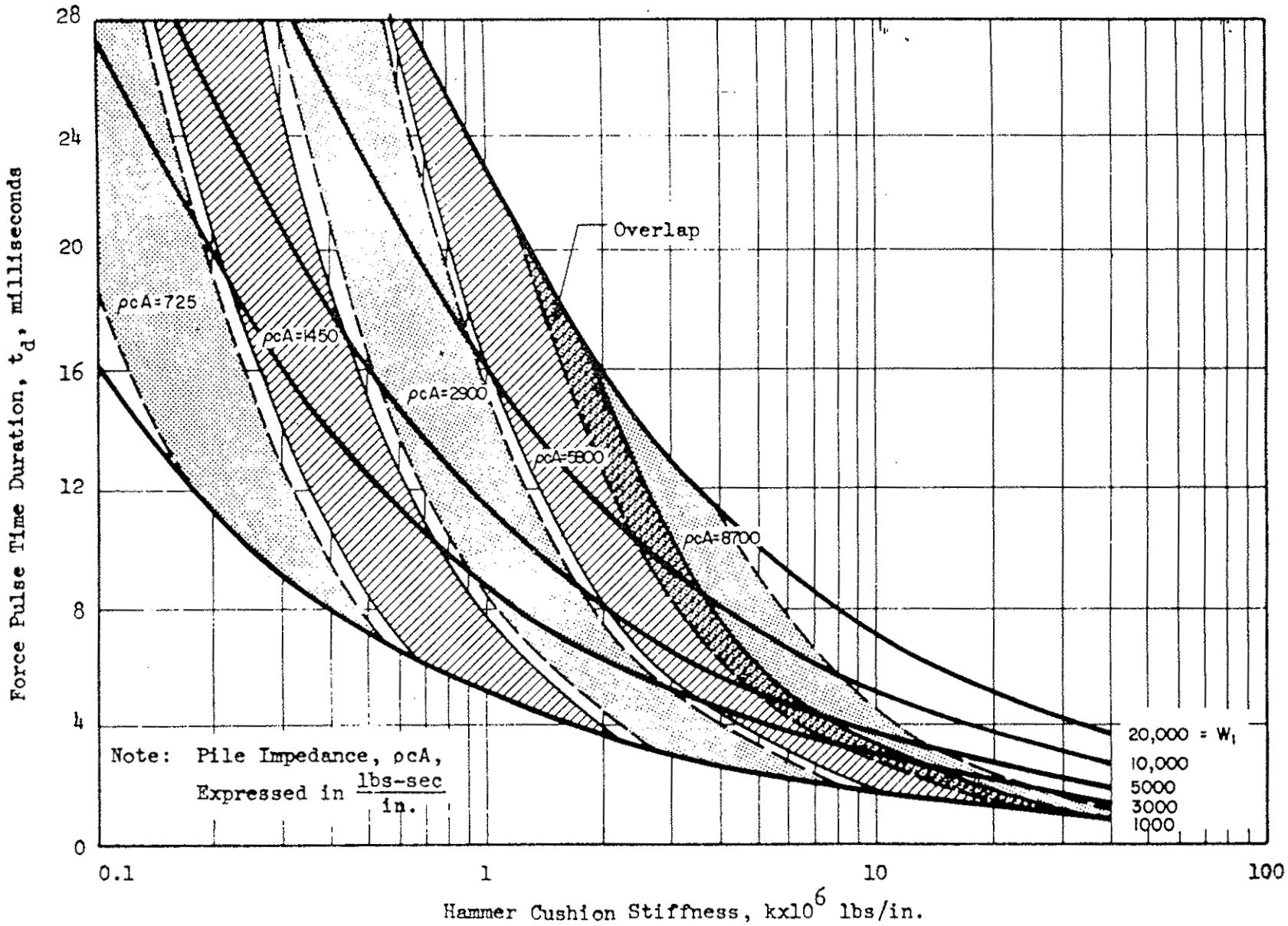

Figure 2.13 TIME DURATION OF FORCE PULSE AS A FUNCTION OF HAMMER AND PILE CHARACTERISTICS

2.4 Bilinear Cushion

Pile Energy

The effect of energy loss in a bilinear cushion will now be investigated. First, it should be pointed out that inelastic behavior does not invalidate the concept of impedance match of hammer and pile; however, inelastic behavior is associated with energy losses within the cushion. The effect of the coefficient of restitution on the percentage of energy loss in the hammer cushion is shown in Table 2.3 for $\bar{B}$ coefficients of 3, 5 and 20; $\bar{B} = 5$ is a typical ram to drivehead weight ratio. The coefficients of restitution were varied between 1/3 and 1 (e - 1 is linear elastic), whereas pile impedance was varied from low to high relative to the hammer.

With reference to Table 2.3, it can be seen that the energy loss increases as the coefficient of restitution decreases. As the $\bar{B}$ coefficient increases, the energy loss with respect to a particular coefficient of restitution decreases for the impedance match and low pile impedance condition. For the high pile impedance condition, the energy loss for a particular coefficient of restitution is independent of $\bar{B}$. For typical values of $\bar{B}$ the energy loss in the cushion for coefficients of restitution of 1 to 3/4, which correspond to stiffer cushions such as aluminum-micarta, varies from 0 to 20%. For coefficients of restitution of 1/2 to 1/3, which correspond to soft cushions such as wood, the energy loss in the cushion, varies from 20 to 40%.

Table 2.3

ENERGY LOSS OF BILINEAR CUSHION

$\bar{B} = 3$

Coefficient of Restitution*	Percentage of Energy Loss in Cushion High Pile Impedance $\bar{A} = 10$	Matched Impedance $\bar{A} = 3$	Low Pile Impedance $\bar{A} = 1$
e = 1	0	0	0
e = 3/4	13	16	21
e = 1/2	27	30	36
e = 1/3	36	37	45

$\bar{B} = 5$

Coefficient of Restitution*	Percentage of Energy Loss in Cushion High Pile Impedance $\bar{A} = 10$	Matched Impedance $\bar{A} = 4$	Low Pile Impedance $\bar{A} = 1$
e = 1	0	0	0
e = 3/4	13	14	12
e = 1/2	27	23	25
e = 1/3	37	27	40

$\bar{B} = 20$

Coefficient of Restitution*	Percentage of Energy Loss in Cushion High Pile Impedance $\bar{A} = 40$	Matched Impedance $\bar{A} = 15$	Low Pile Impedance $\bar{A} = 4$
e = 1	0	0	0
e = 3/4	12	10	9
e = 1/2	25	18	-
e = 1/3	34	21	17

* See Figure 2.3

Pile Force

The effect of a bilinear cushion will be investigated with respect to peak pile force, force shape and duration. The variables are the same considered in the discussion of energy losses.

Inelastic behavior of the cushion has three distinct effects on the generated force pulse, namely: 1) it lowers the peak force only for the low pile impedance conditions, 2) it attenuates the duration of the force pulse, and 3) it causes possible minor oscillation of the force pulse for the matched and high pile impedance conditions. The effects of varying the coefficient of restitution for $\bar{B} = 5$ are considered typical; the results are presented in Figure 2.14.

The effect of an inelastic cushion on peak pile force is tabulated in Table 2.4 for different $\bar{B}$ coefficients and the various coefficients of restitution considered herein. The peak pile force is expressed as a percentage of the peak force generated with an elastic cushion ($e = 1$). It is noted in Table 2.4 that peak pile force is independent of the degree of inelastic behavior for the impedance match and high pile impedance conditions. However, the peak force decreases with an increase in inelastic behavior (lower coefficient of restitution) for the low pile impedance condition.

With reference to Figure 2.14, it can be seen that a decrease in the coefficient of restitution results in a decrease in duration of the force pulse. In Table 2.4, the duration is expressed in dimensionless time (z) which is directly proportional to real time. The dimensionless duration of the force pulse is arbitrarily selected at a value of 10%

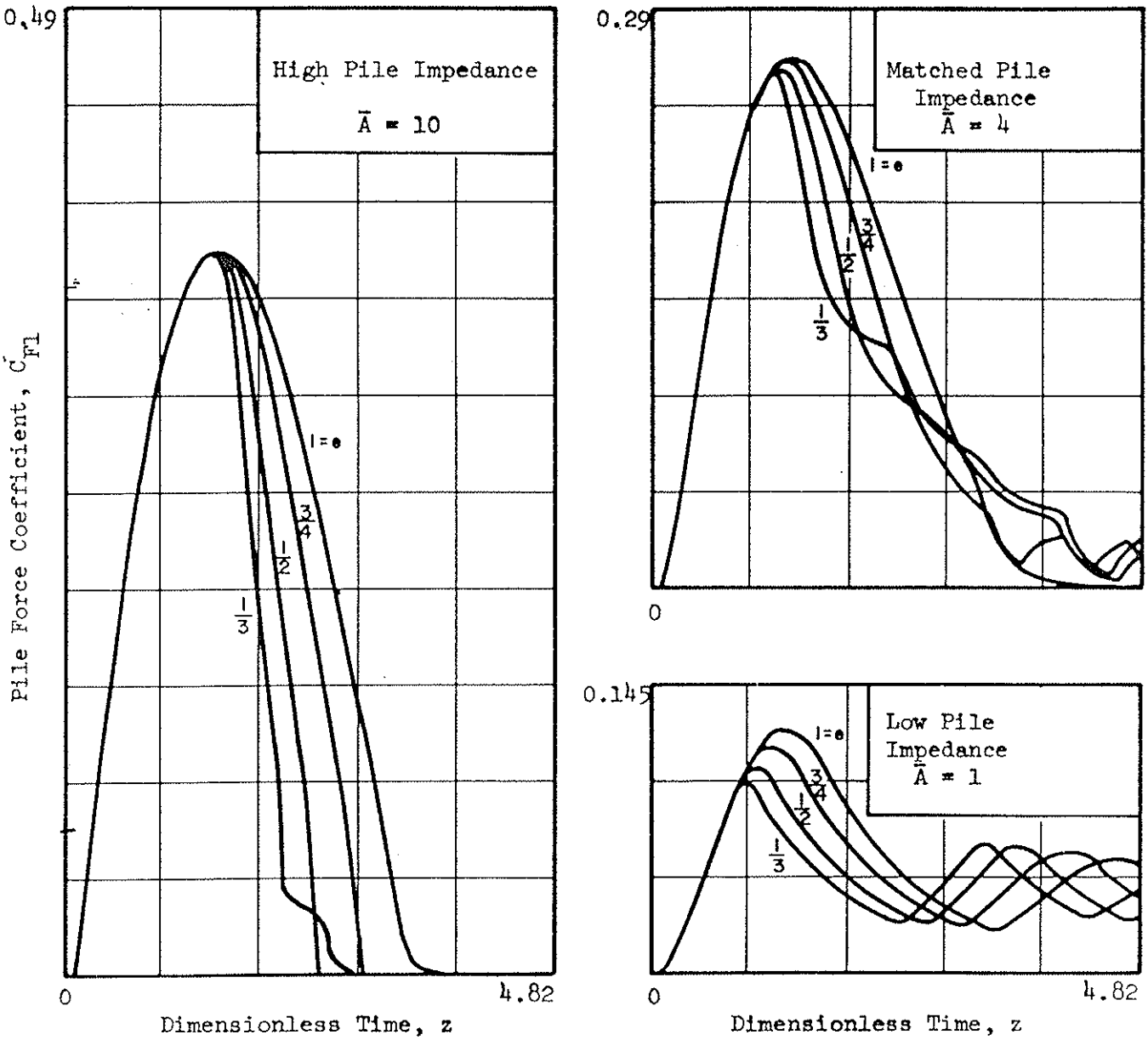

$\bar{B}$ = 5

Figure 2.14 EFFECT OF BILINEAR CUSHION ON PILE FORCE

Table 2.4

EFFECT OF BILINEAR CUSHION ON PEAK PILE FORCE AND PULSE DURATION

$\bar{B} = 3$

Coefficient of Restitution	Percentage of Peak Pile Force Generated with an Elastic Cushion			Dimensionless Time Pulse Duration**		
	High Pile Impedance $\bar{A} = 10$	Impedance Match $\bar{A} = 3$	Low Pile Impedance $\bar{A} = 1$	High Pile Impedance $\bar{A} = 10$	Impedance Match $\bar{A} = 3$	Low Pile Impedance $\bar{A} = 1$
e=1(elastic)	100	100	100	3.2	3.3	4.2*
e=3/4	100	99	94	2.8	2.9	3.9*
e=1/2	100	97	86	2.6	3.9*	3.3*
e=1/3	100	96	81	2.1	3.5*	2.9*

$\bar{B} = 5$

Coefficient of Restitution	Percentage of Peak Pile Force Generated with an Elastic Cushion			Dimensionless Time Pulse Duration**		
	High Pile Impedance $\bar{A} = 10$	Impedance Match $\bar{A} = 4$	Low Pile Impedance $\bar{A} = 1$	High Pile Impedance $\bar{A} = 10$	Impedance Match $\bar{A} = 4$	Low Pile Impedance $\bar{A} = 1$
e=1(elastic)	100	100	100	3.2	3.3	>6
e=3/4	100	99	93	2.8	3.3*	>6
e=1/2	100	96	85	2.5	3.9*	>6
e=1/3	100	94	80	2.5*	4.0*	>6

$\bar{B} = 20$

Coefficient of Restitution	Percentage of Peak Pile Force Generated with an Elastic Cushion			Dimensionless Time Pulse Duration**		
	High Pile Impedance $\bar{A} = 40$	Impedance Match $\bar{A} = 15$	Low Pile Impedance $\bar{A} = 4$	High Pile Impedance $\bar{A} = 40$	Impedance Match $\bar{A} = 15$	Low Pile Impedance $\bar{A} = 4$
e=1(elastic)	100	100	100	3.2	3.6	>5.0*
e=3/4	100	100	--	2.9	3.6	--
e=1/2	100	100	--	2.5	3.8*	--
e=1/3	100	100	90	2.4	4.0*	>5.0*

*Denotes oscillating force pulse. **Dimensionless time taken at a load 10% of peak.

of the peak force. For a given pile impedance, duration decreases with an increase in the degree of inelasticity (decrease in coefficient of restitution) except for the special case of force pulse oscillations at the impedance match condition.

Small oscillations of the pile force for the impedance match condition ($\bar{A} = 4$) and low coefficients of restitution, as shown in Figure 2.14, indicate discontinuity in oscillatory behavior. It is believed that a relay in the analog computer system was responding erratically only during unloading of the cushion; therefore, discontinuity of the force pulse exists. In order to verify the results of this bilinear study, the linear cushion study was compared with the bilinear study for coefficients of restitution equal to unity (elastic case). The comparison showed no difference in the generated force pulse; therefore, the general conclusions based on the bilinear study are assumed to be unaffected by the discontinuity in the force pulse oscillations. It should be noted that the discontinuities occur long after the initial peak force.

2.5 Nonlinear Cushion

Scope

The importance of the hammer cushion in determining peak pile force and duration was demonstrated in the preceding sections. This section will further exemplify the effect of the hammer cushion by comparing the behavior associated with typical soft and hard nonlinear cushions, namely, pine plywood and aluminum-micarta. The effect of soft and hard nonlinear cushions will be investigated in two parts; 1) com-

parison of generated pile force peak, shape and duration, 2) comparison of linear and nonlinear cushion behavior.

Nonlinear cushions were investigated for typical hammer sizes, i.e. Vulcan 2 to Vulcan 010, and normal ram velocities ranging from 9 to 15 ft/sec. The hammer and cushion details investigated are tabulated in Table 2.5. A drivehead weight of 1000 lbs was selected as typical for the hammer range studied.

Load-deformation characteristics for pine plywood cushions were taken from the investigation by Hirsch, et al. (1966) as shown in Figure 2.15a. This relationship can be approximated by a series of straight lines as shown in Figure 2.15b to obtain the assumed load-deformation characteristics utilized herein (Appendix B). The unloading slope is related to the coefficient of restitution (e = 0.27 for the pine plywood cushion). Similar approximate curves for other hammer sizes are shown in Figure 2.16.

The load-deformation relationship for the aluminum-micarta cushion was obtained from a static test. The static properties for typical cushion materials agreed remarkably well with those determined under impact loads (Hirsch, et al. 1966). Both the real and assumed load-deformation characteristics are shown in Figure 2.17 and the approximate loading curves for the hammer sizes considered herein are presented in Figure 2.18. The aluminum-micarta cushion approaches an elastic cushion with a coefficient of restitution of 0.95.

Before discussing the effects of pine plywood and aluminum-micarta cushions, their load-deformation relationships are compared for

Table 2.5

TABULATION OF PROBLEMS INVESTIGATED FOR NONLINEAR CUSHIONS

Problem No.	Hammer Type	Ram Wt. lbs.	Drivehead Wt. lbs.	$\bar{B}$ Coeff.	Ram Velocity V_o, ft/sec	Hammer Cushion Type	Hammer Cushion Size	Cushion Data Used
1	Vulcan 010	10,000	1,000	10	9	Pine Plywood	13 1/2" ϕ - 10" Ht.	3/4" Pine Plywood
2	Vulcan 010	10,000	1,000	10	12	Pine Plywood	13 1/2" ϕ - 10" Ht.	9" ϕ - 9" Ht.
3	Vulcan 010	10,000	1,000	10	15	Pine Plywood	13 1/2" ϕ - 10" Ht.	Dynamic Blow No. 80 e = 0.27
4	Vulcan 08	8,000	1,000	8	9	Pine Plywood	13 1/2" ϕ - 10" Ht.	
5	Vulcan 08	8,000	1,000	8	12	Pine Plywood	13 1/2" ϕ - 10" Ht.	
6	Vulcan 08	8,000	1,000	8	15	Pine Plywood	13 1/2" ϕ - 10" Ht.	
7	Vulcan 06	6,500	1,000	6.5	9	Pine Plywood	11" ϕ - 8" Ht.	Dynamic Test (Hirsch et al., 1966)
8	Vulcan 06	6,500	1,000	6.5	12	Pine Plywood	11" ϕ - 8" Ht.	
9	Vulcan 06	6,500	1,000	6.5	15	Pine Plywood	11" ϕ - 8" Ht.	
10	Vulcan 1	5,000	1,000	5	9	Pine Plywood	11" ϕ - 8" Ht.	
11	Vulcan 1	5,000	1,000	5	12	Pine Plywood	11" ϕ - 8" Ht.	
12	Vulcan 1	5,000	1,000	5	15	Pine Plywood	11" ϕ - 8" Ht.	
13	Vulcan 2	3,000	1,000	3	9	Pine Plywood	10" ϕ - 8" Ht.	
14	Vulcan 2	3,000	1,000	3	12	Pine Plywood	10" ϕ - 8" Ht.	
15	Vulcan 2	3,000	1,000	3	15	Pine Plywood	10" ϕ - 8" Ht.	
16	Vulcan 010	10,000	1,000	10	9	Aluminum-Micarta	13 1/2" ϕ - 10" Ht.	Aluminum-Micarta 13.4" ϕ 4" ϕ Concentric Holes 7.3" Ht. 1 1/16" Micarta Disc 1/2" Alum. Disc e = 0.95
17	Vulcan 010	10,000	1,000	10	12	Aluminum-Micarta	13 1/2" ϕ - 10" Ht.	
18	Vulcan 010	10,000	1,000	10	15	Aluminum-Micarta	13 1/2" ϕ - 10" Ht.	
19	Vulcan 08	8,000	1,000	8	9	Aluminum-Micarta	13 1/2" ϕ - 10" Ht.	
20	Vulcan 08	8,000	1,000	8	12	Aluminum-Micarta	13 1/2" ϕ - 10" Ht.	
21	Vulcan 08	8,000	1,000	8	15	Aluminum-Micarta	13 1/2" ϕ - 10" Ht.	
22	Vulcan 06	6,500	1,000	6.5	9	Aluminum-Micarta	11" ϕ - 8" Ht.	
23	Vulcan 06	6,500	1,000	6.5	12	Aluminum-Micarta	11" ϕ - 8" Ht.	
24	Vulcan 06	6,500	1,000	6.5	15	Aluminum-Micarta	11" ϕ - 8" Ht.	Static Test
25	Vulcan 1	5,000	1,000	5	9	Aluminum-Micarta	11" ϕ - 8" Ht.	
26	Vulcan 1	5,000	1,000	5	12	Aluminum-Micarta	11" ϕ - 8" Ht.	
27	Vulcan 1	5,000	1,000	5	15	Aluminum-Micarta	11" ϕ - 8" Ht.	

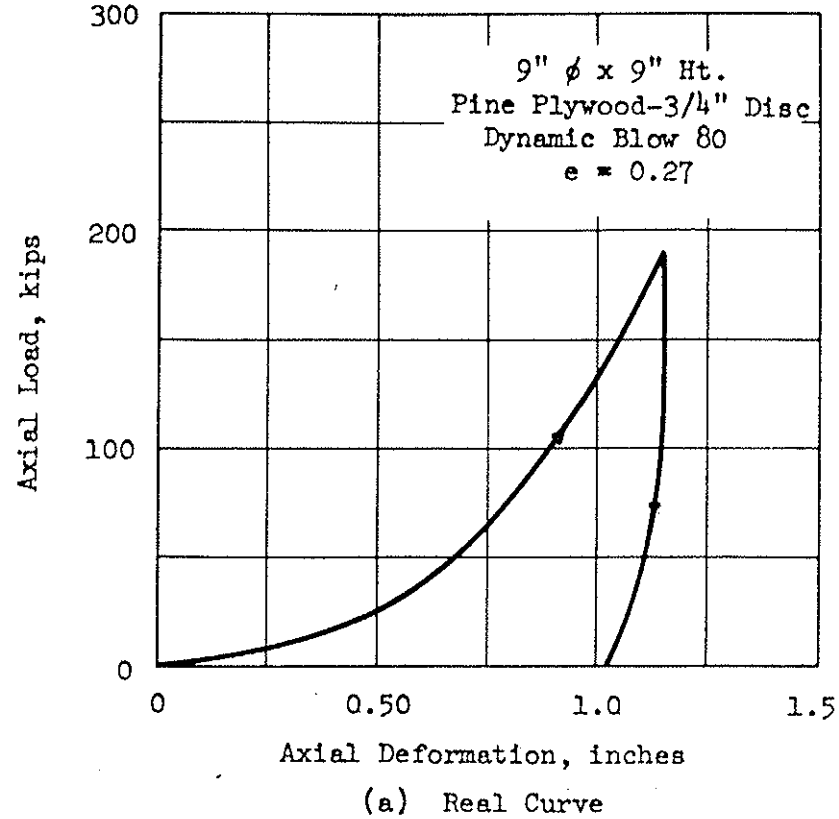

(a) Real Curve

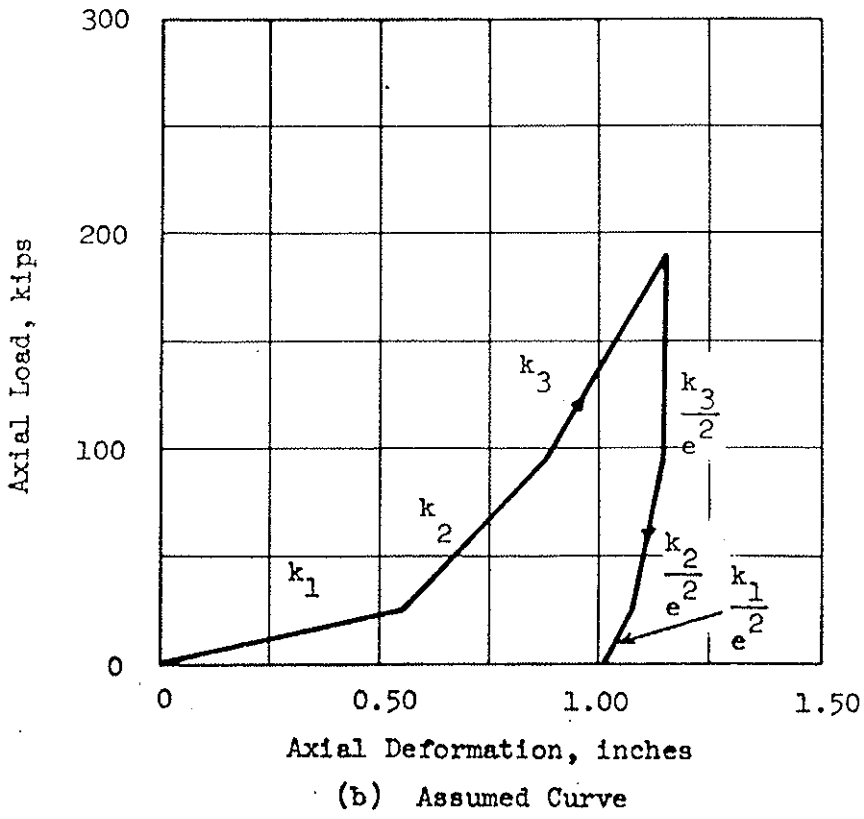

(b) Assumed Curve

Figure 2.15 REAL AND ASSUMED CURVES FOR PINE PLYWOOD CUSHION

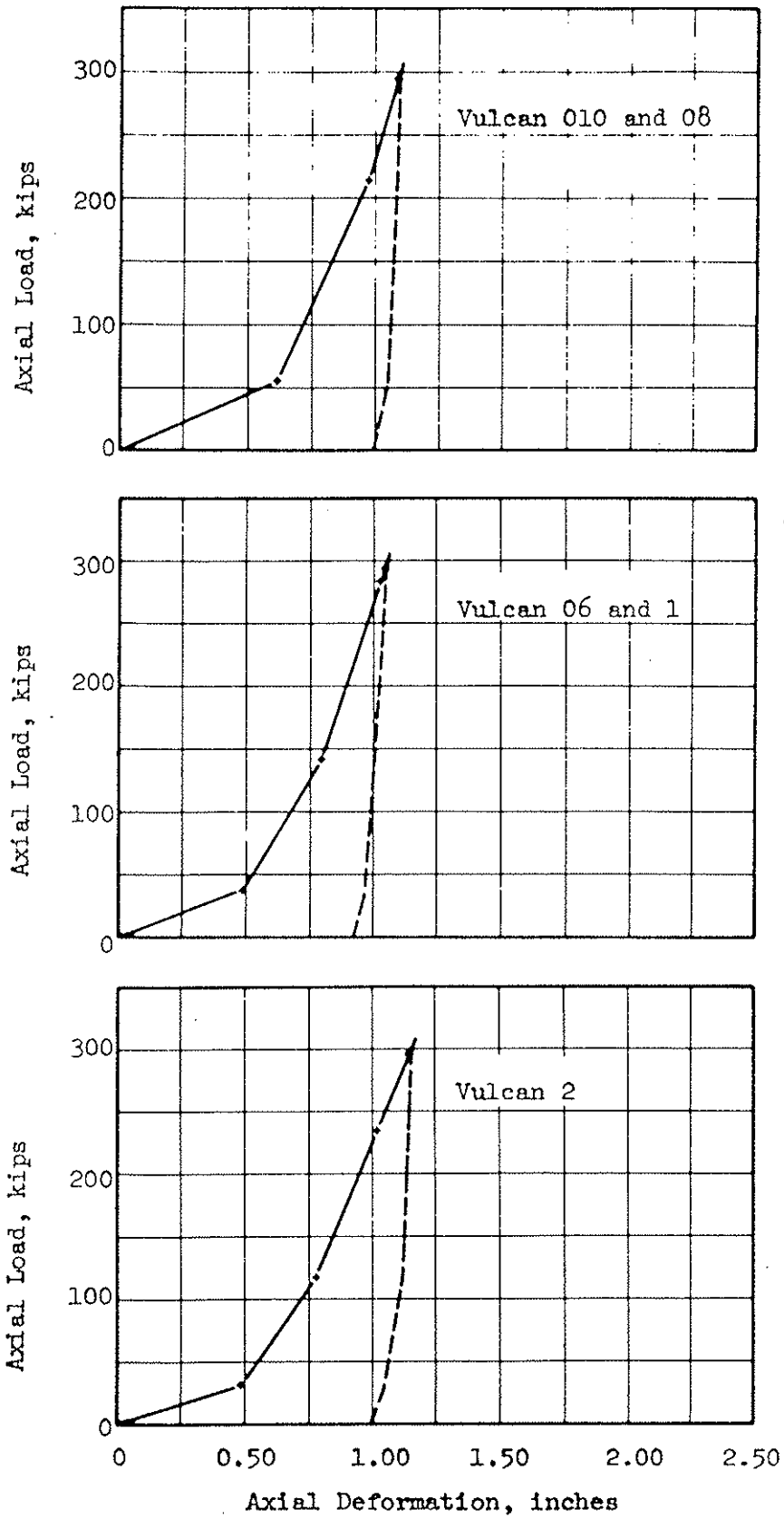

Figure 2.16 ASSUMED PINE PLYWOOD CUSHIONS FOR DIFFERENT HAMMERS

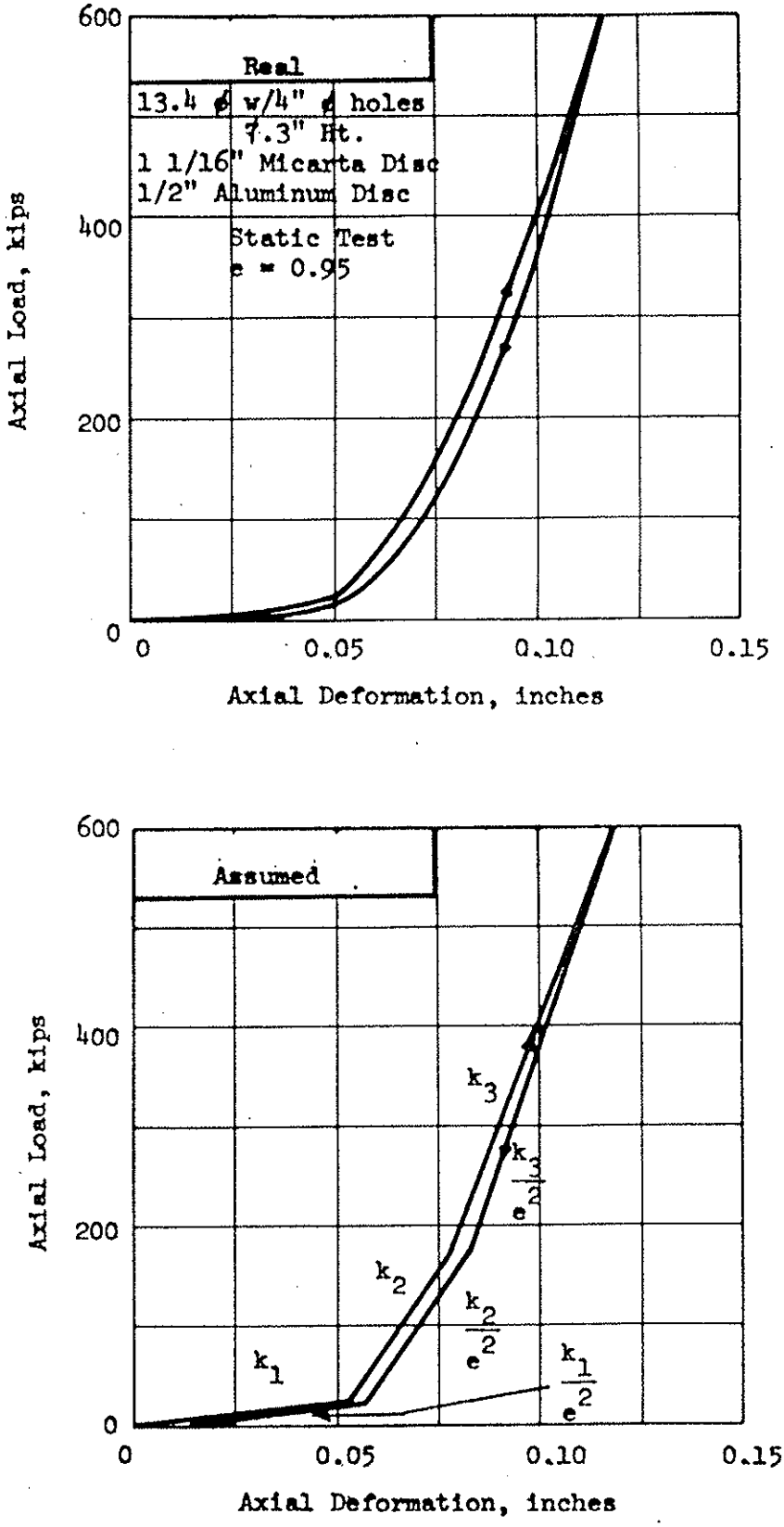

Figure 2.17 REAL AND ASSUMED CURVES FOR ALUMINUM-MICARTA CUSHION

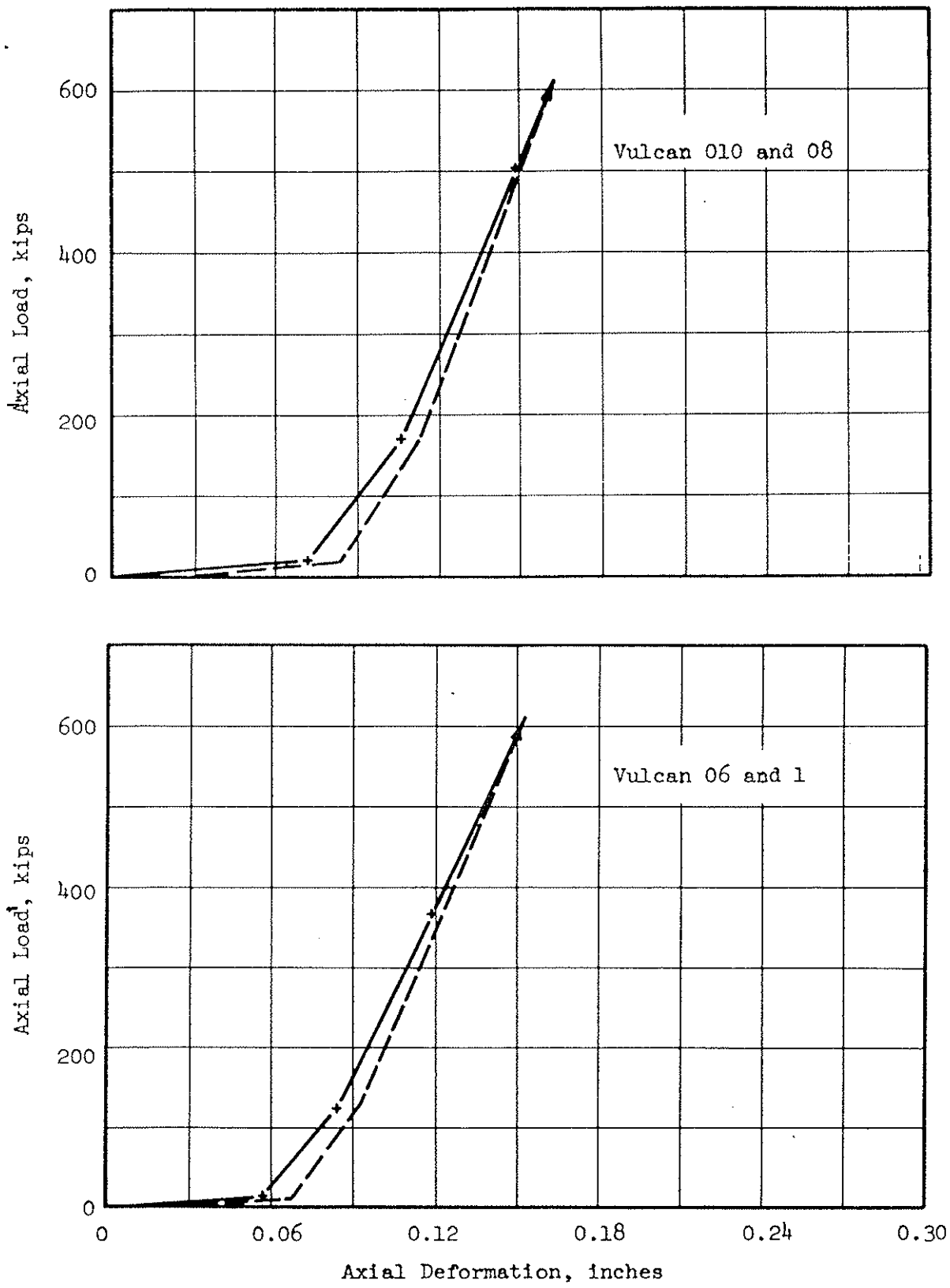

Figure 2.18 ASSUMED ALUMINUM-MICARTA CUSHIONS FOR DIFFERENT HAMMERS

a Vulcan No. 1 hammer (Figure 2.19). The comparison shows the marked difference in stiffness between the cushions as well as the difference in the degree of inelasticity. These cushions represent the range of properties normally encountered in practice.

Pile Force

Peak Force. The peak pile force was investigated for values of impact velocity equal to 9, 12 and 15 ft/sec, which represents a typical range in velocities. For comparison, the tabulated impact velocities for several hammers along with the associated efficiencies are given below:

Hammer	Drop Height, ft.	Impact Velocity, V_o, ft./sec. e_f = 100%	e_f = 75%	e_f = 50%
Vulcan 010	3.25	14.4	12.5	10.2
Vulcan 08	3.25	14.4	12.5	10.2
Vulcan 06	3.00	13.8	12.0	9.8
Vulcan 1	3.00	13.8	12.0	9.8
Vulcan 2	2.50	12.7	11.0	9.0

Pile peak forces vary linearly with impact velocity; therefore, the peak forces can also represent typical values of hammer efficiency for the different hammers tabulated above. Pile peak force versus pile impedance relationships for different hammers with pine plywood and aluminum-micarta cushions are shown in Figure 2.20. The relationships between pile force and impedance are expressed in terms of the useful range of hammer efficiencies, namely, 50 and 100%. Because peak force

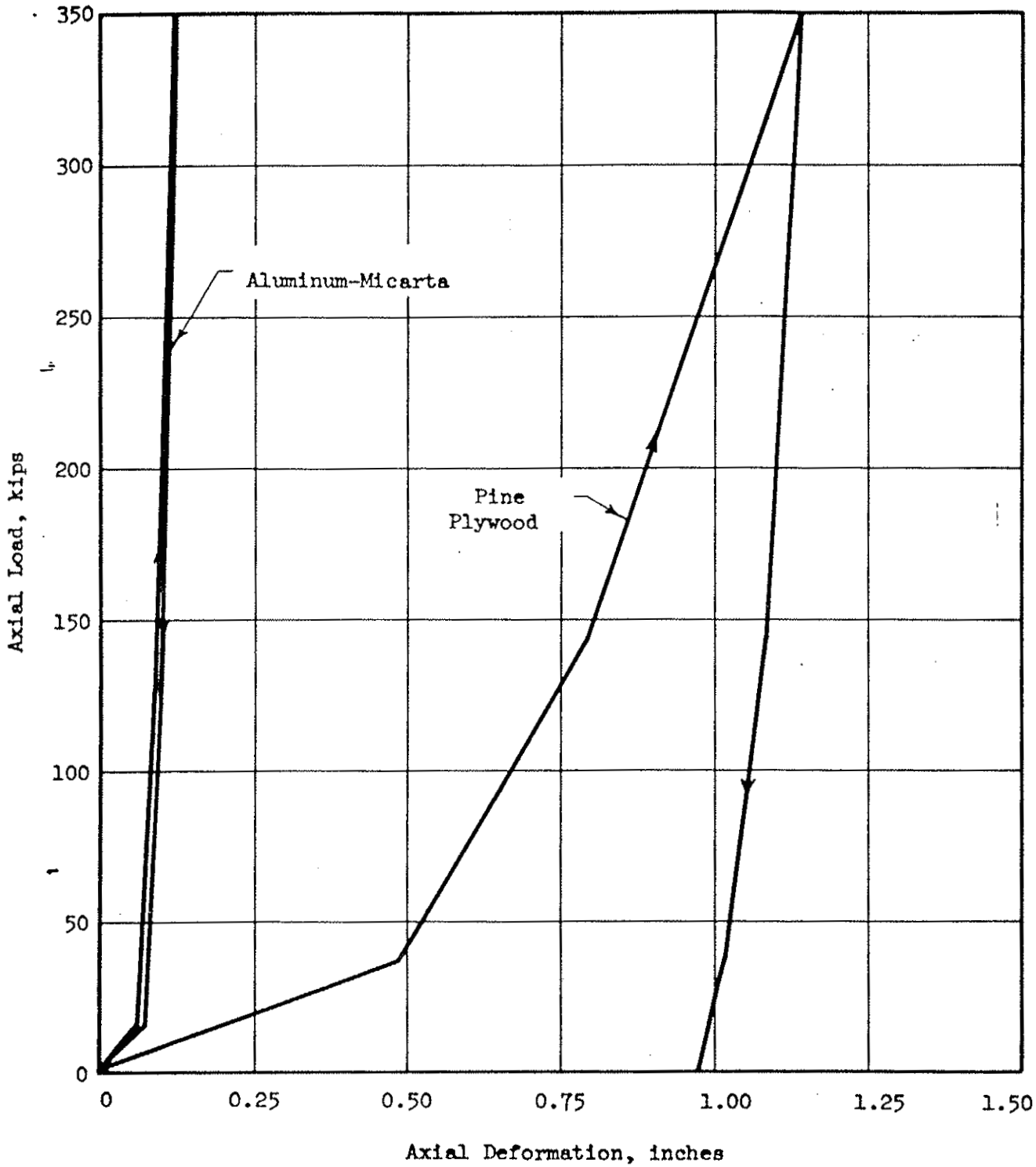

Figure 2.19 COMPARISON OF PINE PLYWOOD AND ALUMINUM-MICARTA CUSHIONS FOR VULCAN NO. 1 HAMMER

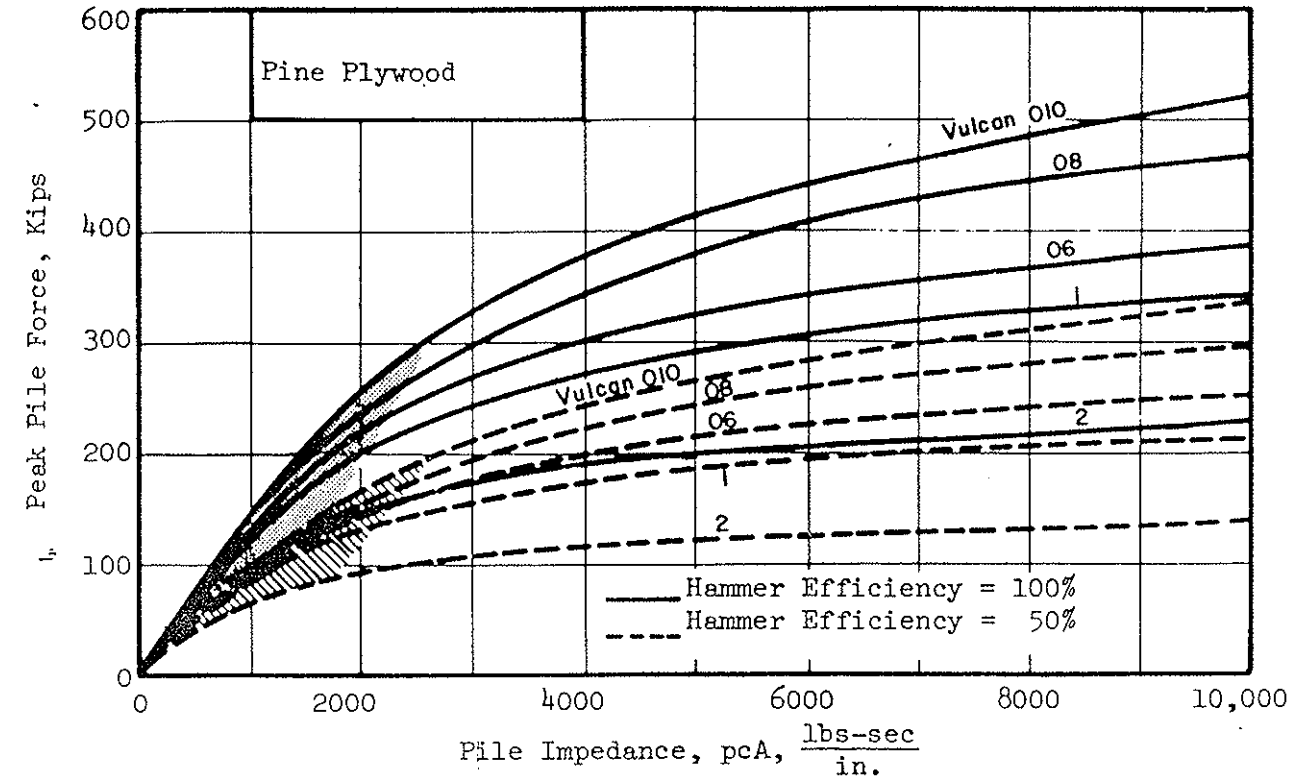

Note: 1. Shaded areas represent maximum energy transmission
2. Assume 1000 lbs. drivehead for all hammers.

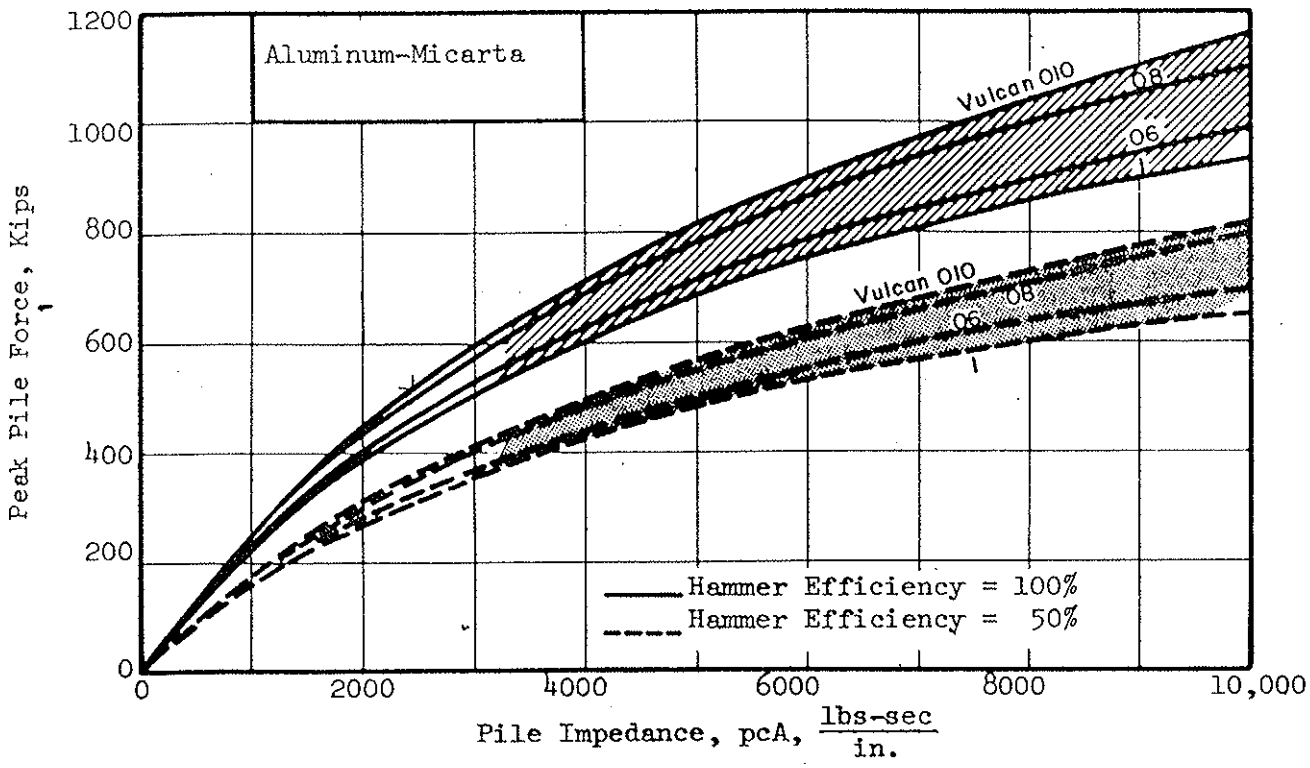

Figure 2.20 PEAK PILE FORCE FOR PINE PLYWOOD AND ALUMINUM-MICARTA CUSHIONS

and impact velocity are linearly related, peak force for other efficiencies can be readily determined by interpolation in terms of the square root of hammer efficiency ($\sqrt{e_f}$).

With reference to Figure 2.20, it is shown that for a given hammer and efficiency the peak force increases with an increase in pile impedance for both cushion materials. However, the increase is more pronounced for the aluminum-micarta (hard) than for the pine plywood (soft) as the pile impedance approaches high values. Also, the peak force generated in the pile with the aluminum-micarta cushion is approximately double that generated with the pine plywood cushion.

The optimum pile-hammer match for maximum energy transmitted to the pile head is superimposed on Figure 2.20. It is seen, as expected, that the best match for the softer cushion (pine plywood) is the low pile impedance range of 600 to 2600 lbs-sec/in. (equivalent steel area of 4 to 18 in.^{2}). The harder cushion (aluminum-micarta) is matched with high pile impedances, or equivalent steel areas of approximately 20 to 80 in.^{2}.

Shape and Duration. The pile force shape and duration is also affected by differences in cushion material. Force pulses generated by a Vulcan hammer for the aluminum-micarta and pine plywood cushions are compared in Figure 2.21 in terms of the pile force coefficient, C_{F1}. The Vulcan 1 hammer with different cushion materials and an impact velocity of 12 ft/sec (e_f = 74.5%) was chosen as representative of typical hammer behavior.

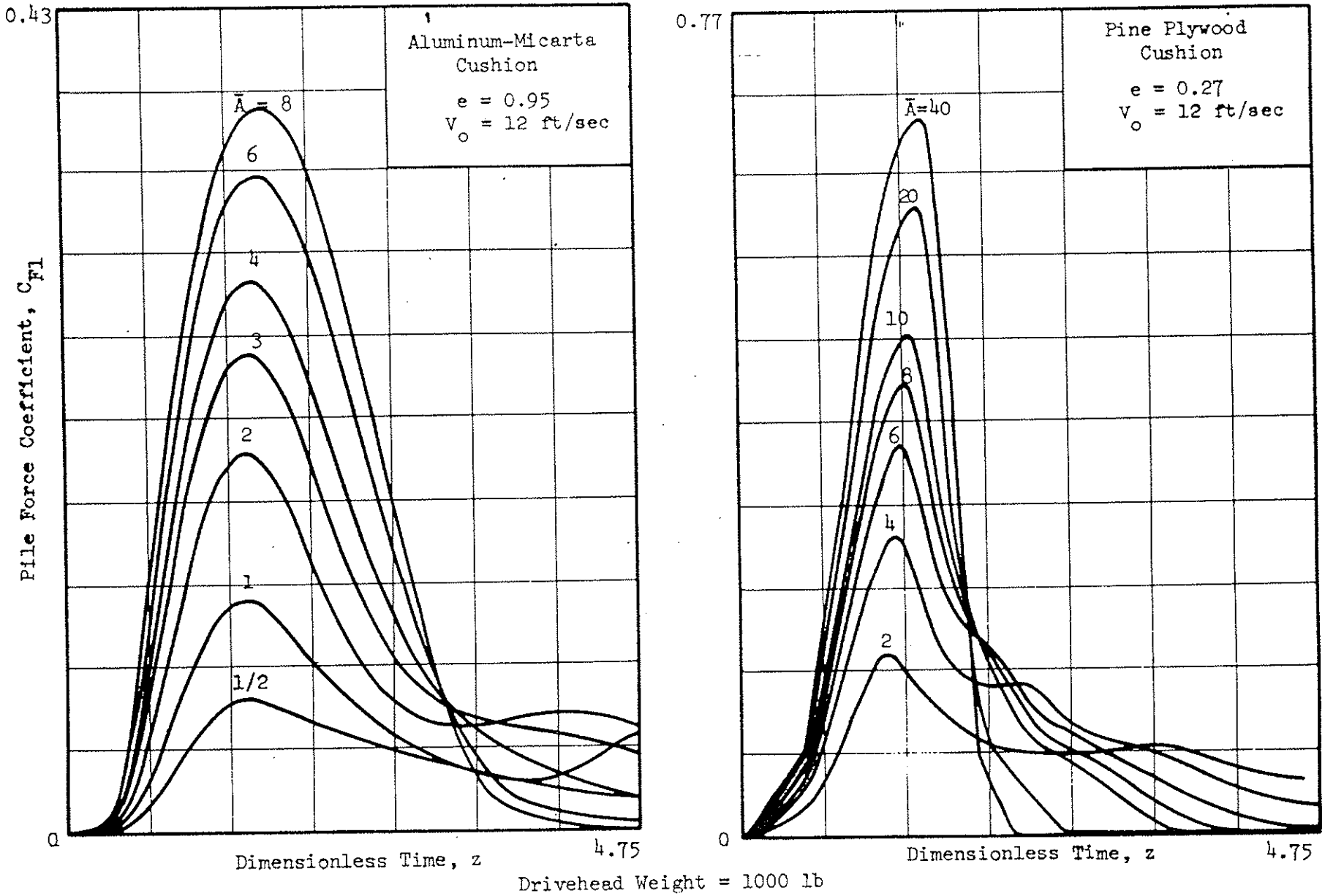

Figure 2.21 GENERATED FORCE PULSE FOR VULCAN NO. 1 HAMMER WITH ALUMINUM-MICARTA OR PINE PLYWOOD CUSHION

For the range in velocities investigated, 9 to 15 ft/sec, there was a decrease in duration associated with the higher velocities; however, the variation was less than 10%. The pulse shape is associated with the cushion load-deformation characteristics. If the cushion loading curve is gradual and the unloading is abrupt, then the force pulse loading and unloading pattern is analogous in behavior. Comparison of the force pulses in Figure 2.21 shows the more gradual loading and more abrupt unloading of the pine plywood as opposed to the aluminum-micarta cushion. The abrupt unloading pattern is caused by increased cushion stiffness upon unloading associated with the low coefficient of restitution of the pine plywood cushion (e = 0.27) as compared to the aluminum-micarta cushion (e = 0.95). The abrupt unloading of the pine plywood cushion causes force pulse oscillations near the impedance match condition of hammer and pile. This oscillatory force behavior for conditions of impedance match and low coefficients of restitution also occurred in the bilinear study.

The pulse duration for the soft cushion (pine plywood) as compared to the hard cushion (aluminum-micarta) is larger by a factor of 3 to 5. The real duration at 10% of peak force is tabulated below for the Vulcan No. 1 hammer and various pile impedances.

	Pulse Duration at 10% of Peak, milliseconds						
	High Pile Impedance				Matched Pile Impedance		Low Pile Impedance
Vulcan 1	$\bar{A}$ = 40	$\bar{A}$ = 20	$\bar{A}$ = 10	$\bar{A}$ = 8	$\bar{A}$ = 6	$\bar{A}$ = 4	$\bar{A}$ = 2
Pine Plywood	16	18	24	27	29	36	50
Alum.-Micarta	5	5	5	6	6	7	12

For the impedance match of hammer and pile, the duration of the pulse for the pine plywood cushion is approximately 5 times longer than that for the aluminum-micarta cushion. The relationship is similar for other hammers as shown below:

	Impedance Match Conditions Only Time Pulse Duration at 10% Peak	
	Pine Plywood	Aluminum-Micarta
Vulcan 2	25-35 ms	--
Vulcan 1 - Vulcan 010	30-50 ms	6-12 ms

The longer duration corresponds to the hammer with the heaviest ram (Vulcan 010).

The pronounced differences in behavior between a typical soft cushion (pine plywood) and a typical hard cushion (aluminum-micarta) point to the importance of the hammer cushion in pile driving. Pine and aluminum-micarta were chosen to encompass the potential range in behavior of the generated force pulse. As a practical consideration, the hammer cushion can be readily changed. Thus, cushion stiffnesses can be chosen so as to attain the desired pile-hammer impedance match

or generated pile force pulse leading to maximum pile penetration per blow.

Equivalent Linear Cushion

Introduction. In this section, nonlinear and linear cushion behavior are compared with respect to generated pile force pulse, i.e. peak force and duration, for purposes of developing a method of representing nonlinear cushions with equivalent linear cushions. The nonlinear cushions considered are pine plywood and aluminum-micarta. The comparisons of cushion behavior are made with respect to a range in hammer sizes, using the Vulcan 1 and Vulcan 010 hammers with a drivehead weight of 1000 lbs and an impact velocity of 12 ft/sec (e_f = 74.5%).

Peak Force. First, equivalent linear cushions are selected that lead to the same generated peak pile force. The equivalent linear cushion stiffness refers to the loading stiffness only. As shown in the bilinear cushion study, the unloading stiffness has a negligible effect on the generated peak force except for the condition of very low pile impedances and low coefficients of restitution for the cushion. Even for extreme conditions, the unloading stiffness affects the peak force by less than 20%.

Equivalent linear stiffnesses for a range of pile impedances and the pine plywood and aluminum-micarta cushions of the Vulcan 1 and 010 hammers are tabulated in Table 2.6. The equivalent linear cushion stiffness increases with an increase in pile impedance for both hammers and both cushion types. It should be noted that all equivalent stiffnesses are bounded by the lowest (k_1) and highest (k_3) loading stiffnesses

Table 2.6

EQUIVALENT LINEAR CUSHION FOR PEAK PILE FORCE

Vulcan 1

Impedance Condition	Pile Impedance,* $\frac{\text{lbs-sec}}{\text{in.}}$	Area of Steel in.^2	Equivalent Linear Cushion: Pine Plywood $k_p \times 10^6$ lbs/in.	Pine Plywood Percent of k_3	Aluminum-Micarta $k_p \times 10^6$ lbs/in.	Aluminum-Micarta Percent of k_3
Low	725	5	0.13	23	2.0	29
	1450	10	0.27	46	4.1	58
Medium	2900	20	0.41	71	5.6	79
High	5800	40	0.45	78	6.8	95
	8700	60	0.47	81	7.1	100

Note: Assumed nonlinear cushion stiffnesses for Vulcan 1:
Pine Plywood $k_1 = 0.076 \times 10^6$ lbs/in., $k_2 = 0.36 \times 10^6$ lbs/in., $k_3 = 0.58 \times 10^6$ lbs/in.
Aluminum-Micarta $k_1 = 0.26 \times 10^6$ lbs/in., $k_2 = 4.0 \times 10^6$ lbs/in., $k_3 = 7.1 \times 10^6$ lbs/in.

Vulcan 010

Impedance Condition	Pile Impedance,* $\frac{\text{lbs-sec}}{\text{in.}}$	Area of Steel in.^2	Equivalent Linear Cushion: Pine Plywood $k_p \times 10^6$ lbs/in.	Pine Plywood Percent of k_3	Aluminum-Micarta $k_p \times 10^6$ lbs/in.	Aluminum-Micarta Percent of k_3
Low	725	5	0.11	15	1.4	18
	1450	10	0.25	36	4.1	53
Medium	2900	20	0.44	63	5.7	73
High	5800	40	0.51	73	6.4	82
	8700	60	0.52	75	7.1	91

Note: Assumed nonlinear cushion stiffnesses for Vulcan 010:
Pine Plywood $k_1 = 0.092 \times 10^6$ lbs/in., $k_2 = 0.43 \times 10^6$ lbs/in., $k_3 = 0.70 \times 10^6$ lbs/in.
Aluminum-Micarta $k_1 = 0.28 \times 10^6$ lbs/in., $k_2 = 4.4 \times 10^6$ lbs/in., $k_3 = 7.8 \times 10^6$ lbs/in.

*Refer to Table 2.1 for comparison of pile impedances with dimensions of other pile types, concrete and wood.

(Figure 2.15 and 2.17) of the nonlinear cushions (See Table 2.6).

The equivalent linear cushion stiffness is shown in Table 2.6 as a percentage of the highest loading stiffness (k_3). The range of low pile impedances, 725 to 1450 lbs-sec/in., can be covered by a stiffness range of 20 to 60 % for both hammers and cushions investigated; the higher percentage corresponds to the higher pile impedance. The intermediate pile impedance is covered by a range of 60 to 80%, whereas 75 to 100% of the stiffest portion of the nonlinear cushion is required to cover the higher pile impedances. The larger percentages correspond to the stiffer cushion, i.e. aluminum-micarta.

Duration. The durations of the force pulses can be compared in order to obtain an equivalent linear cushion, i.e., one giving the same duration. The effect of the inelastic behavior (hysteresis) of the nonlinear cushion makes the analogy with the linear cushion difficult because of attenuation of the pulse duration caused by inelastic behavior. Therefore, an equivalent linear cushion (linear and elastic) will be related to the nonlinear cushion (nonlinear and elastic) for the determination of durations. It is assumed that inelastic behavior (same coefficient of restitution) for both the bilinear and nonlinear cushions will attenuate the pulse durations in a similar manner.

The pulse duration is based on the point of intersection of the nonlinear and elastic force curves where dimensionless time z approximately equals π; therefore, the real duration is approximated by the relationship, $t_d = \pi\sqrt{\frac{m_1}{k}}$ (same as Equation 2.12). Equivalent linear cushion stiffnesses for the approximated time pulse length for all pile impedances are tabulated below:

	Equivalent Linear Stiffness for Duration, $k \times 10^6$ lbs/in.	
	Pine Plywood Equivalent	Aluminum-Micarta Equivalent
Vulcan 1	0.20	5.0
Vulcan 010	0.40	5.0

It is seen from the above tabulation that the equivalent linear loading stiffness (k_{td}) for the duration corresponds to the linear loading stiffnesses (k_p) for the peak pile force of the low to medium pile impedances (Figure 2.22b). This means that the equivalent linear stiffness is reasonably matched for both peak force and duration with respect to the low to medium pile impedances.

For the very low and the high pile impedances, equivalent linear cushions for duration and peak forces are not equal. For very low pile impedances, the equivalent linear cushion (k_p) for peak pile force represents the actual peak force, but the duration for this equivalent cushion is longer than the actual duration (Figure 2.22a). The equivalent linear cushion (k_{td}) for the duration represents the actual duration; however, the peak force as determined by this equivalent cushion is larger than the actual peak force. For high pile impedances, the opposite effect exists wherein the shorter time pulse is associated with the equivalent cushion (k_p) for the peak force, and the lower peak force is associated with the equivalent cushion (k_{td}) for the duration (Figure 2.22c).

Recommended Secant Modulus. The equivalent linear cushion stiffness can also be obtained from recommended secant moduli values given

k_P = Equivalent Linear Loading Stiffness for Peak Pile Force.

k_{td} = Equivalent Linear Loading Stiffness for Time Duration.

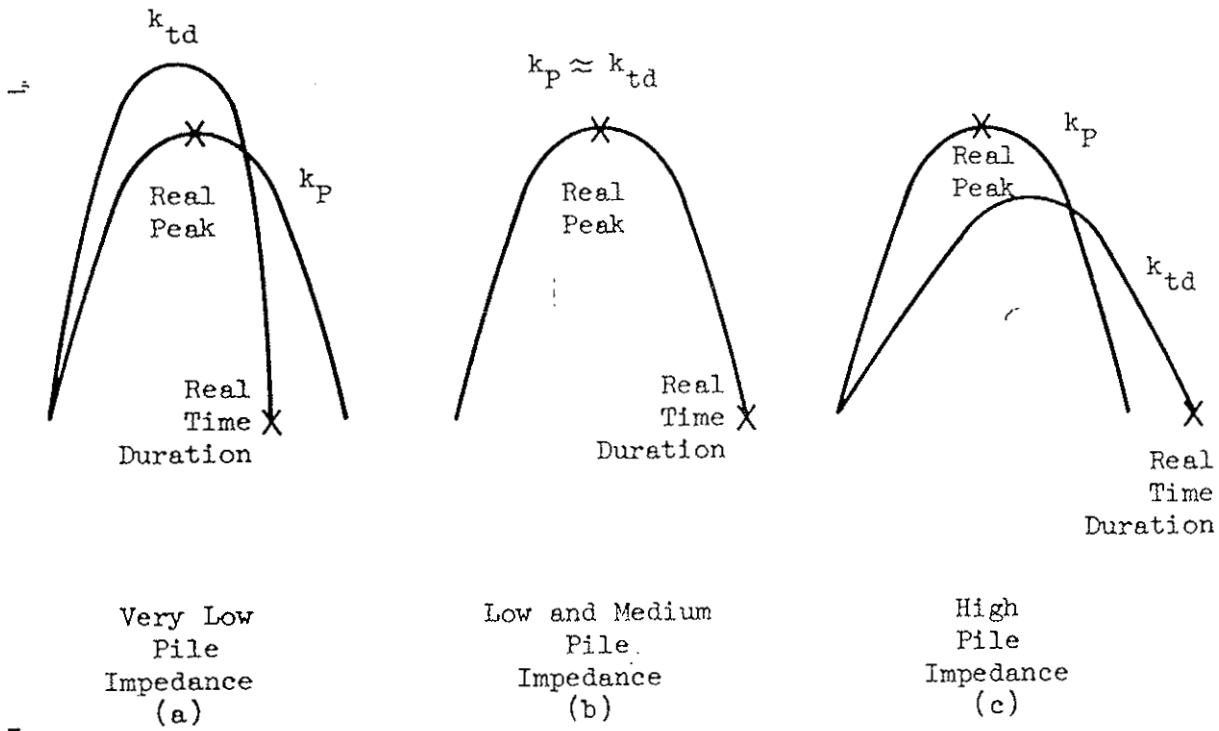

Very Low Pile Impedance (a)

Low and Medium Pile Impedance (b)

High Pile Impedance (c)

Figure 2.22 SCHEMATIC COMPARISON OF EQUIVALENT LINEAR CUSHION STIFFNESS WITH RESPECT TO PEAK PILE FORCE AND TIME DURATION

by Lowery et al. (1969) which are supposed to be valid for predicting both force pulse shape and magnitude. Equivalent linear stiffness values calculated from these recommended secant moduli will be evaluated on the basis of the linear stiffness values determined previously for matching peak pile force and duration. The calculated values of linear loading stiffness (k_c) for the hammers and cushions considered in this section are tabulated below:

	Calculated Linear Cushion Stiffness, $k_c \times 10^6$ lbs/in.	
	Pine Plywood*	Aluminum-Micarta**
Vulcan 1	0.30	5.3
Vulcan 010	0.36	6.4

*E (secant) = 25,000 psi **E (secant) = 450,000 psi

The calculated values of the linear stiffnesses (k_c) correspond to the peak force equivalent cushion (k_p) given earlier for the intermediate range of pile impedances. The duration equivalent cushion (k_{td}) given earlier is in general agreement with the calculated cushion stiffness (k_c).

In general, it appears that the equivalent linear cushions as calculated from recommended secant moduli given by Lowery et al. (See Appendix A) can give values in close agreement with the real behavior of nonlinear cushions with certain exceptions as shown below.

	Very Low Pile Impedance		Low and Medium Pile Impedance		High Pile Impedance	
	Peak	Duration	Peak	Duration	Peak	Duration
Calculated Linear Stiffness, k_c	Too High (15-25%) too high	Match	Match	Match	Too Low (5-15%) too low	Match

For very low impedance, the peak forces or stresses calculated using the secant modulus are larger than the real peak forces or stresses. At the very low pile impedance, the maximum induced stresses are critical because of the susceptibility of the pile to damage. By contrast, for high impedance piles, actual induced stresses are normally low relative to the yield point of the pile material; however, the real peak forces or stresses are larger than the calculated values based on the recommended secant moduli.

CHAPTER 3

PILE AND SOIL RESPONSE

3.1 Introduction

Pile penetration is accomplished only by generating a pile force that will overcome soil resistance at the pile tip. Therefore, emphasis is placed on the pile and soil response at the pile tip. The investigation of the soil and pile tip response includes a study of tip displacement, transmitted and reflected force pulses, and transmitted and reflected energies. In addition, the effect of soil resistance along the pile length (skin friction resistance) will be qualitatively consisidered with respect to attenuation of the generated pile force as it approaches the tip.

The model of pile and soil tip used in this investigation is shown in Figure 3.1. Viscous damping (c_o), an elastic-plastic soil spring (k_s), and a concentrated mass (m) are used to approximate the rheological behavior of the soil under dynamic loading. Therefore, the soil resistance takes into account: 1. elastic deformation, 2. permanent deformation, 3. static resistance, 4. viscous damping-strain rate effect. Without the concentrated mass, the soil model is analogous to the Kelvin-Voigt model and Smith's model (Smith, 1962).

3.2 Dynamic Behavior of Soils

The main obstacle to predicting pile penetration response and static ultimate capacity is simulating the soil mechanism during driving

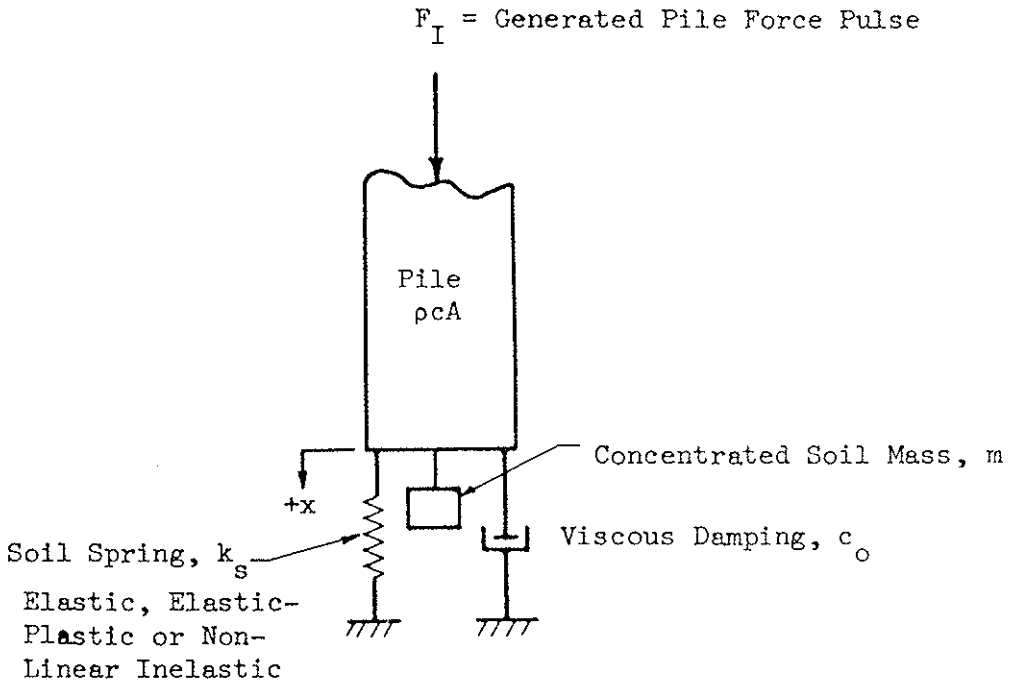

Figure 3.1 PILE AND SOIL TIP MODEL

with the proper dynamic characteristics of the soil. In an attempt to determine the dynamic properties of the soil, a literature search was made for laboratory and field data that might lead to understanding the nature of dynamic soil resistance. The application of lab results such as triaxial unconfined compression, direct shear and model tests should be considered only as indicative of the general nature of dynamic pile driving resistance.

Experimental Results

According to Schimming et al. (1966), a French engineer, A. Collin, first recognized the time-dependent nature of soil strength in 1846. For many years, only static strength and creep problems of soils received attention until the needs of protective structures required a better understanding of dynamic soil behavior. Casagrande and Shannon (1948) initiated a test program to study the effects of the rate of loading on soils such as clays, shales and dense dry sand. The tests results indicated a significant increase in transient strength for cohesive soils and only a slight effect on strength for dry sand. Seed and Lundgren (1954) studied the strain-rate effect on strength and deformation characteristics of saturated sands. Whitman (1957) measured the increase in compressive strengths of cohesive soils. Since 1957, considerable attention has been devoted to dynamic soil properties. A summary of soil dynamic test results is presented in Table 3.1. The summary is divided into two general soil classifications, cohesionless and cohesive.

The review of research shown in Table 3.1 indicates that both the strength and modulus of the soil increase with an increase in strain

Table 3.1

SUMMARY OF DYNAMIC TEST RESULTS

COHESIONLESS SOILS

Source	Type of Test	Confining Pressure, psi,	Rise Time, seconds	Strain Rate Effect: Compressive Strength Ratio*	Strain Rate Effect: Secant Modulus Ratio**	Soil Type
Casagrande & Shannon (1948)	Triaxial	4.2 to 12.8	0.03 to 2100	1.1 to 1.15	1.3	dry dense sand
Seed & Lundgren (1954)	Triaxial	28.4	0.02 to 900	1.15 to 1.40		saturated fine sand
				1.25 to 1.50		saturated coarse sand
Whitman (1957)	Triaxial	15.0	0.005 to 300	1.1 to 1.15		dry dense and loose
		60.0	0.005 to 300	1.1		uniform and well graded sand
Whitman & Healy (1962)	Triaxial	10.0		2.0		saturated dense uniform sand
			0.025 to 5	1.4		saturated loose fine sand
						saturated loose coarse sand
Healy (1962)	Triaxial	5, 10, 20 & 40 psi	0.013 to 4	1.1 to 1.2		fine silty sand
Curry & Sloan (1962)	Small Scale Footing Tests	—	0.008 to 1440	1.25	1.25	dry dense sand
						dry dense & loose sand
Schimming, Haas, & Saxe (1966)	Direct Shear	—	0.001 to 50	1.0		powdered silt powdered Jordan Bluff clay
		30		1.2		saturated med.-dense Ottawa sand
		15	0.001 to static	1.3		saturated med.-dense Arkansas sand
Reeves, Coyle & Hirsch (1967)	Triaxial	15	vary	1.5		saturated med.-dense Victoria fine sand
				2.0 to 2.4		saturated med.-dense Ottawa sand
			0.001 to static	1.5 to 1.7		saturated med.-dense Arkansas sand
Coyle & Gibson (1970)	Triaxial	15	vary	1.6 to 1.8		saturated med.-dense Victoria fine sand

COHESIVE SOILS

Source	Type of Test	Confining Pressure, psi,	Rise Time, seconds	Strain Rate Effect: Compressive Strength Ratio*	Strain Rate Effect: Secant Modulus Ratio**	Soil Type
Casagrande & Shannon (1948)	Unconfined & Triaxial	42.5 & 85	0.01 to 600	1.5 to 2.0	2.0	undisturbed clays & remolded Kaolin clays
Whitman (1957)	Triaxial	30, 42 or 85	0.005 to 300	1.3 to 2.0		varied from a stiff dry clay to plastic clay
Warton & Yoder (1959)	Unconfined	—	0.020 to 60	1.9 to 2.6	1.8 to 4.0	remolded silty clay remolded heavy clay
Whitman, Richardson & Nasim (1962)	Triaxial	60 psi OCR 3.16	0.0015 to 300 @ 1% strain	1.5 to 1.7		saturated loess & heavy clay (normal consolidated & over consolidat
Curry & Sloan (1962)	Small Scale Footing Tests	—	0.008 to 1440	1.2		backswamp medium stiff clay
Kane, Davisson, etc. (1964)	Triaxial	114 & 1010	0.003 to 100	1.5		remolded Goose Lake clay
				1.8 - 2.5		compacted Jordan Bluff clay
Schimming, Haas & Saxe (1966)	Direct Shear	—	0.001 to 50	1.8		compacted Bentonite clay
				1.7		undisturbed Chicago Blue clay
						Goose Lake clay
					2.3	(clayey silt-remolded
Olson & Parola (1967)	Triaxial	1000 & 1000	0.006 to 6000	1.5	(Defined at	close to optimum water content
				1.3	1% strain)	very dry of optimum water content
Gibson & Coyle (1968) Coyle & Gibson (1970)	Unconfined	—	0.001 to 600	1.8 to 2.7		remolded sandy clay organic clay & highly plastic clay (no effect of confining pressures)

*Compressive Strength Ratio = $\frac{\text{Dynamic Strength}}{\text{Static Strength}}$.

**Secant Modulus Ratio = $\frac{\text{Dynamic Modulus}}{\text{Static Modulus}}$. Defined at one-half stress at failure unless otherwise noted.

rate. However, the change in soil properties due to strain rate effect are more pronounced in cohesive soils than in cohesionless soils.

For dry cohesionless soils there is a minimal difference between dynamic and static behavior characteristics. The investigations on saturated cohesionless soils show a variation in strain rate effect from minimal to significant and approaching that of the cohesive soils. This variation can be attributed to the time dependency of excess pore pressures. Whitman and Healy (1962) stated that since the friction angle is essentially independent of time to failure, the strength of sand varies with time to failure when excess pore pressures are time dependent. The time dependency of pore pressures and strain-rate effect are a function of the moisture content, grain size distribution, chemical composition, and density or compactness of the soil material.

The possibility that cavitation may occur in some samples and not in others might explain some of the variation of strain-rate effect in sands (Jones et al., 1966). According to Jones et al., cavitation, developing at the expected reduced pressure of -14 psi in sands, imposes a limit on increases in strength due to strain-rate effect, but this limitation does not apply to clays in which cavitation does not normally occur during shear (Bishop and Blight, 1963).

The strain rate effect of cohesive soils is more definitive than for cohesionless soils. This strain rate effect could be caused by a combination of factors such as a change in the inter-particle mechanism of yield in clay and a change in pore pressures due to nonuniform stress conditions. Whitman (1957) pointed out that the strain-rate effect of cohesive soils is the result of viscous phenomena except when failure occurred by splitting. The dynamic properties of cohesive soils

are dependent upon moisture content or degree of saturation, structural configuration, pore fluid type and degree of consolidation. The moisture content or degree of saturation appears to be the most pertinent soil property. Viscous characteristics are most pronounced above the optimum water content and decrease to a negligible effect at no water content. Also, test results by Schimming et al. (1966) indicated that a pore fluid viscosity radically different than that of water would produce radically different behavior.

The preceding summary of dynamic soil behavior does not permit postulating a failure mechanism during pile driving, but it indicates two basic requirements for the model simulation of dynamic soil behavior, namely: 1) under instantaneous applied load, the soil model should undergo instantaneous deformation and obtain a limiting value of capacity that is equal to or in excess of the static value, 2) the soil model should indicate an increase in soil stiffness with an increase in loading rate. The soil model shown in Figure 3.1 satisfies these two requirements. The soil spring is normally assumed to be elastic-plastic and independent of time of loading whereas viscous damping and soil mass influence the strain rate behavior. The static and dynamic load-deformation characteristics of the soil are shown in Figure 3.2. The strains at failure are shown to be approximately independent of strain-rate; this independence has been proven by the test results previously summarized.

Field Results

Several investigators have attempted to correlate the wave equation analysis using Smith's lumped-mass model (Appendix A) with pile load

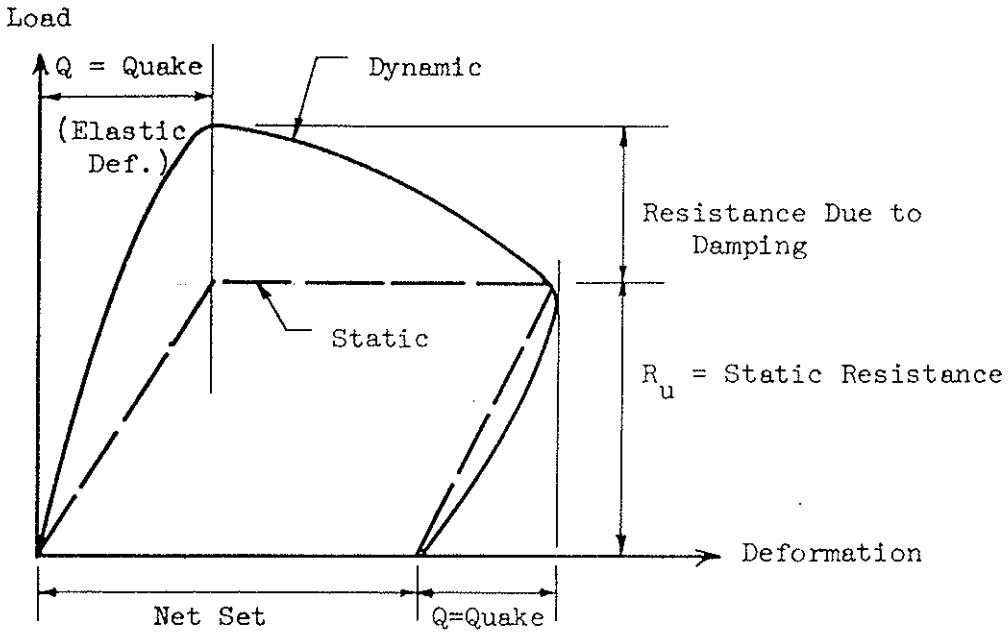

Figure 3.2 LOAD-DEFORMATION CHARACTERISTICS OF SOIL MODEL

tests. In a limited number of studies, attempts were made to determine the dynamic properties of the soil model by trial and error procedures. This section will show the correlation with the field results and consider the results of some model pile tests.

First, however, the soil model used in Smith's wave equation analysis is reviewed. The model is similar to that model shown in Figures 3.1 and 3.2 except that the soil mass is not included. The soil resistance equation proposed by Smith is shown below:

$$R_{dynamic} = R_{static}(1+JV) \qquad (3.1)$$

where $R_{dynamic}$ = dynamic soil resistance, R_{static} = static soil resistance, J is a viscous damping factor and V is the instantaneous velocity of the pile. This means that the real viscous damping constant c_o equals JR_{static}; therefore, the J factor is related not only to velocity but also to static resistance. R_{static} equals $k_s x$ where x is the elastic soil deformation. The yield point deformation is referred to as quake, Q. Smith proposed the same soil model for both the soils at the pile tip and along the sides; however, the soil along the sides could act in tension as well as compression whereas the soil at the tip did not have tension restraint.

On the basis of a limited number of load test data, Smith (1960) proposed the following values for the soil parameters:

$$Q_{side} = Q_{point} = 0.1 \text{ inch}$$

$$J_{point} = 0.15 \text{ sec/ft}$$

$$J_{side} = 1/3\ J_{point} = 0.05 \text{ sec/ft}$$

Side damping was considered to be much less important than damping at the pile point because of the difference in the physical mechanism of the soil failure. The side damping was arbitrarily taken as one-third of the damping at the pile point.

Forehand and Reese (1964) correlated soil parameters used in the wave equation analysis with load test data. Three different types of piles, concrete, steel pipe and steel H-sections, were investigated for both sand and clay soils. Becuase most of the hammer and pile variables could be satisfactorily evaluated, the soil parameters could be varied and correlated with the load test data. Because of lack of knowledge, the side damping factor was assumed to be one-thrid of the point damping in this study. The results of the correlation attempts for piles driven in sand were consistent with Smith's recommended values. The range in values of point and side quake was 0.05 to 0.15 in. and the range in point damping was 0.05 to 0.2 sec/ft. For piles driven into clay, the correlation values of the soil parameters were much wider spread and not in accord with Smith's values. On the assumption that quake lies within the range of 0.1 to 0.2 inches, the range of the damping factors at the point was 0.5 to 1.0 sec/ft for Q = 0.1 in. and 0.3 to 0.5 sec/ft for Q = 0.2 in. These damping factors for clays are greater than Smith's recommended values.

Correlation of the wave equation analysis with field load test data was also performed by Lowery et al. (1968). The pile-driving problems in this study were investigated in three general locations, the Texas Gulf coast, the Arkansas River, and the sites of the Michigan Pile

Load Test programs. Nine different hammers were used to drive prestressed concrete, steel H-sections, fluted-taper and pipe piles with lengths ranging from 30 to 180 feet. The soil conditions varied from sands in the Arkansas River Project (Mansur et al., 1964) to clays in the Michigan Program (Michigan State Highway Commission, 1965) and combinations of sands and clays in the Michigan Program and Texas Gulf Coast. According to this correlation study, the soil quake ranged from 0.05 to 0.2 in. with 0.1 in. being the most typical value for average driving conditions. The soil damping factor, J_{point}, recommended for sands was 0.1 sec/ft; for clays it is 0.3 sec/ft. The soil parameters for the combinations of sand and clay were proportioned relative to the type and amount of material supporting the pile. The side damping factor was assumed one-third of the point damping.

Pile load test results on the Arkansas River Project in medium to fine silty sands below the water table indicated soil quake along the side of the pile equal to 0.1 to 0.2 inches (Coyle and Sulamin, 1967). A study of load transfer of piles in clay indicated that the soil quake along the pile varied with depth; recommended values of quake were equal to 0.15 inches to a depth of 20 feet and 0.07 inches for depths greater than 20 feet (Coyle and Reese, 1966).

Correlation studies between field data and soil model parameters are somewhat limited; however, there are some trends that can be deduced. First, the results for sands seem to be in general agreement with Smith's recommended values of soil parameters. Secondly, the clay properties are more varied and damping factors for clay are higher than

Smith's values; however, the complexity of cohesive soils due to thixotropy and pore pressure effects with respect to time make an analysis during driving very difficult. Because of this complexity wide variations in clay properties are expected. The results of the lab strength tests also agree with these general conclusions.

Dynamic triaxial test results by Coyle and Gibson (1970) indicated that the damping factor (J) as defined by Smith is not a constant for a particular soil but is a function of the loading velocity rate for both sand and clay soils. This study shows the nonlinear relationship between the ratio of dynamic to static resistance and loading velocity, and possibly helps explain some of the variation in the soil parameter studies. For normal loading velocities of 2 to 12 fps, the damping factor for sands varies from 0.1 to 0.4 sec/ft; for clays it ranges from 0.15 to 0.6 sec/ft. The lower damping factors correspond to the higher loading rates. Coyle and Gibson (1970) suggested the following modification of Smith's relationship to obtain a constant value of J':

$$J' = \frac{1}{V^N}\left(\frac{R_{dynamic}}{R_{static}} - 1\right) \qquad (3.2)$$

An acceptable constant, J', for saturated sands is derived if N is 0.20 and for clays if N is 0.18. For the soils investigated, J' ranges from 0.5 to 0.9 for sands, and 0.7 to 1.1 for clays. These soil damping constants are related to common soil properties of both sand and clay.

The soil model chosen herein is representative of soil behavior based on research on dynamic soil properties in both the laboratory and the field. At present, there are definite trends for the soil model

parameters with soil index properties. Of course, the correlation is complicated by the differences in soil behavior during and after pile driving. There is no attempt in this treatment to correlate soil parameters with index properties; however, this study will investigate the effect of the soil parameters with respect to generated force pulses in pile driving.

3.3 Basic Equations

The equations of equilibrium of the pile and soil tip can be written for the soil model as previously described and shown in Figure 3.3. The incident force pulse in the pile describes the velocity (V_I) at a point in the pile as shown below:

$$F_I = \rho c A \, V_I \tag{3.3}$$

where ρcA is pile impedance. Equation 3.3 is similar to Equation 2.1, but subscripts I and R are required to distinguish between incident and reflected waves.

When the incident wave encounters a discontinuity of material and area such as the soil at the pile tip, the incident wave is transmitted to the soil and/or reflected back through the pile. The conditions to be satisfied at the pile and soil interface are the equality of both force and particle velocity (Figure 3.3);

$$\rho c A \, V_I + \rho c A \, V_R = m\ddot{x} + c_o \dot{x} + k_s x \tag{3.4}$$

$$V_I - V_R = \dot{x} \tag{3.5}$$

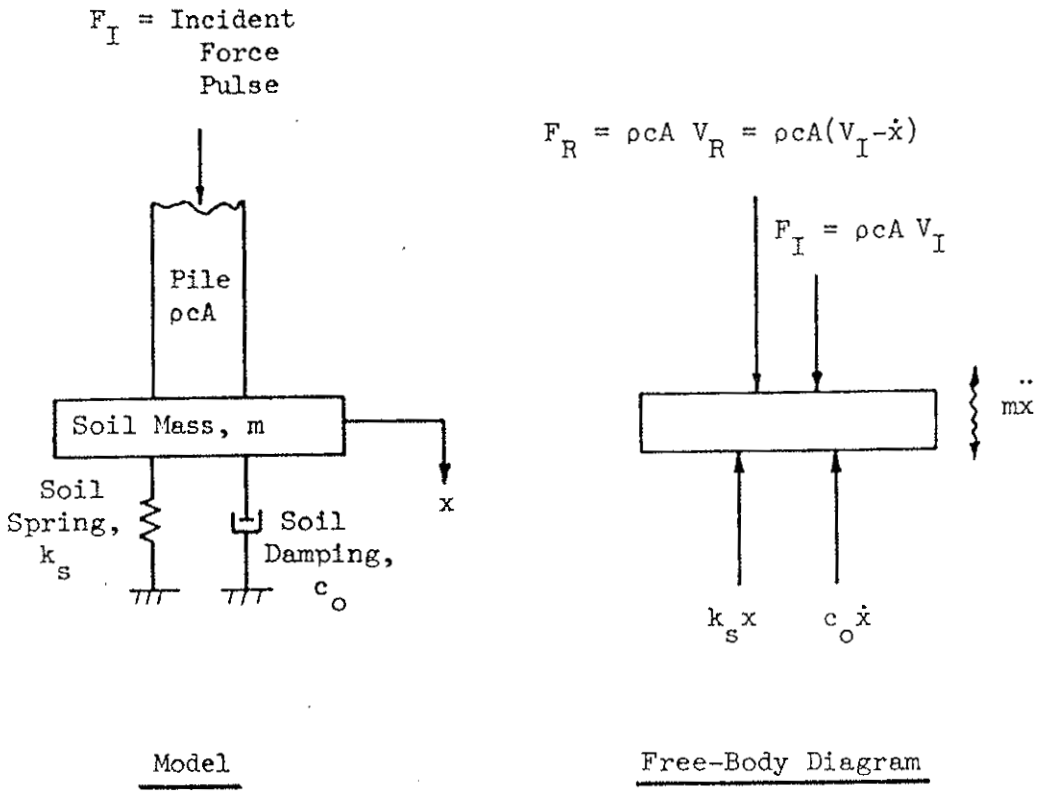

Figure 3.3 FREE-BODY DIAGRAM OF PILE AND SOIL TIP MODEL

where V_I and V_R refer to the pile particle velocity of the incident and reflected waves, m is the soil mass, c_o is the soil damping, and k_s is the soil spring stiffness which can be varied from elastic to nonlinear inelastic.

Simultaneous solution of Equations 3.4 and 3.5 yields the following expression between the incident force pulse and the soil tip response:

$$m\ddot{x} + (c_o + \rho cA)\,\dot{x} + k_s x = 2\,\rho cA\,V_I \qquad (3.6)$$

The solution of Equation 3.6 is used for the determination of tip displacement, transmitted and reflected force pulse, and transmitted and reflected energy. The reflected force pulse can be shown to be

$$F_R = \rho cA\,V_R = \rho cA\,(V_I - \dot{x}) \qquad (3.7)$$

The force reflections depend upon the following cases:

1) If $\dot{x}$ matches V_I, no reflections occur

2) If $\dot{x} < V_I$, compressive reflections occur

3) If $\dot{x} > V_I$, tensile reflections occur.

The transmitted energy, i.e. the energy transmitted to the soil, can be defined in terms of the incident and reflected energy as shown below:

Transmitted Energy (E_T) = Incident Energy (E_I) - Reflected Energy (E_R)

$$E_T = \int_0^t \frac{F_I^2}{\rho c A}\, dt - \int_0^t \frac{F_R^2}{\rho c A}\, dt \qquad (3.8)$$

The solutions of Equations 3.6, 3.7 and 3.8 were obtained with the use of the analog computer as described in Appendix C. Attempts were made to nondimensionalize these euqations; however, the restrictions of the initial and boundary conditions did not permit taking advantage of this approach. Therefore, particular problems were chosen and studied individually.

3.4 Tip Response of Pile and Soil

Introduction

The response of the pile tip was investigated for varying pile impedances, force pulse shapes and energies, and soil parameters. The pile impedances selected are 1000, 3000 and 6000 lbs-sec/in., which represent thin-wall pipe to a heavy-wall pipe, H-piles and mandrels. The impedances and equivalent section sizes for pile types such as steel, concrete and wood are shown in Table 3.2. These three impedances were selected to represent the range of piling in common use. The energy levels were varied from 6250 to 25,000 ft-lbs, which represent the common range of hammer energies after consideration of hammer efficiencies.

The primary wave shape considered in this investigation is the sine wave, which corresponds to the impedance match condition described in Chapter 2. Other wave shapes such as rectangular and triangular are also included in order to determine the effect of wave shape on pile

Table 3.2

PILE IMPEDANCE AND PILE TYPES FOR THE TIP MODEL INVESTIGATION

Pile Impedance, pcA, $\frac{\text{lbs-sec}}{\text{in.}}$	Steel Area, in^2	Concrete			Wood	
		Area, in^2	Diameter, in.	Width (square) in.	Area, in^2	Diameter, in.
1000	6.9 (Thin-wall Pipe)	32.4	6.4	5.7	113	12.0
3000	20.7 (Pipe or H-Pile)	97.2	11.1	9.9	339	20.8
6000	41.4 (Mandrel)	194.4	15.7	13.9	678	29.4

penetration (net set) and capacity. Considering the duration of the force pulse for the matched condition of pile impedance and hammer, as shown in Figure 3.4 and described in Chapter 2, the peak force for the sine wave can be determined from the following relationship:

$$F_{peak} = \sqrt{2 \frac{\rho cA}{t_1} E_I} \tag{3.9}$$

where ρcA is impedance, E_I is the incident energy and t_1 is the duration of the force pulse. The duration t_1 was varied according to the range in hammer weight and cushion stiffness for the matched condition as shown in Figure 3.4; the corresponding peak forces used in this study are referenced by case number as given in Table 3.3. The duration and the corresponding peak force were varied with respect to a particular energy level in order to investigate their effect on pile tip response. These peak forces correspond to the peak values shown in Figure 2.10 (Chapter 2) determined on the basis of a three-foot hammer drop.

It is assumed that the incident force wave can fully develop without interruption from the reflections at the pile head; therefore, the pulse length can be no longer than twice the pile length. The pulse length and corresponding pile length can be defined as follows:

$$\text{Pile Length} \geq \frac{1}{2} \text{ Pulse Length} = \frac{1}{2} \left(\frac{ct_1}{1000}\right) \text{ ft.} \tag{3.10}$$

where c is the velocity of wave propagation and t_1 is the pulse duration in milliseconds. For steel, the velocity of wave propagation is

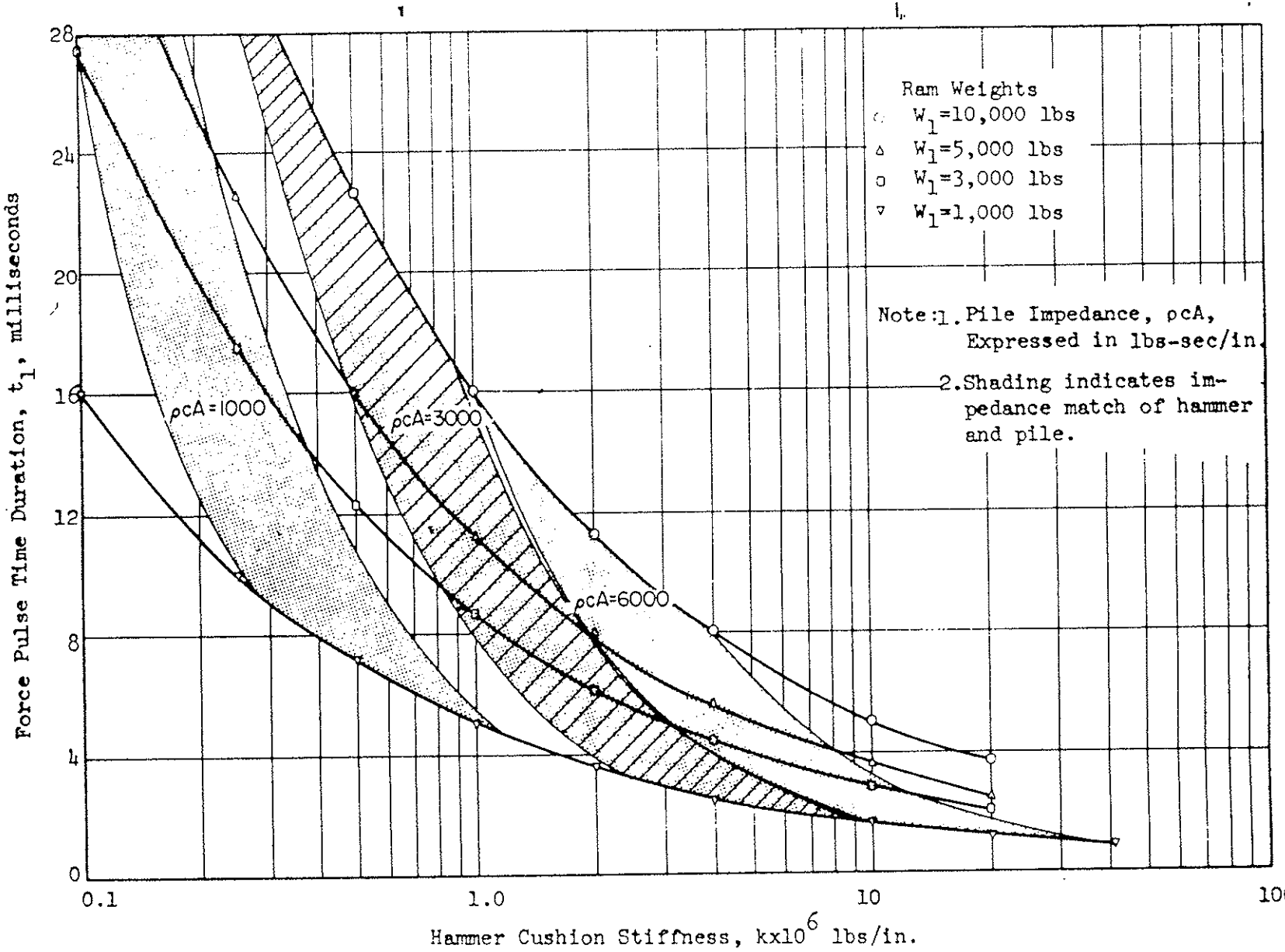

Figure 3.4 TIME DURATION OF PULSE LENGTH

Table 3.3

INCIDENT FORCE PULSE AND ENERGIES FOR TIP MODEL

Pile Impedance ρcA, $\frac{\text{lbs-sec}}{\text{in.}}$	Energy, ft-lbs 6,250	12,500	25,000
1000	Case 1-1 F_p = 141 1/2 kips t_1 = 7 1/2 ms	Case 1-2 F_p = 141 1/2 kips t_1 = 15 ms	Case 1-3 F_p = 141 1/2 kips t_1 = 30 ms
	Case 1-4 F_p = 100 kips t_1 = 15 ms	Case 1-5 F_p = 100 kips t_1 = 30 ms	--
	Case 1-6 F_p = 70.7 kips t_1 = 20 ms	--	--
3000	Case 3-1 F_p = 425 kips t_1 = 2 1/2 ms	Case 3-2 F_p = 425 kips t_1 = 5 ms	Case 3-3 F_p = 425 kips t_1 = 10 ms
	Case 3-A F_p = 300 kips t_1 = 5 ms	Case 3-B F_p = 300 kips t_1 = 10 ms	Case 3-C F_p = 300 kips t_1 = 20 ms
	Case 3-4 F_p = 212 kips t_1 = 10 ms	Case 3-5 F_p = 212 kips t_1 = 20 ms	--
6000	Case 6-1 F_p = 850 kips t_1 = 1 1/4 ms	Case 6-2 F_p = 850 kips t_1 = 2 1/2 ms	Case 6-3 F_p = 850 kips t_1 = 5 ms
	Case 6-4 F_p = 600 kips t_1 = 2 1/2 ms	Case 6-A F_p = 600 kips t_1 = 5 ms	Case 6-B F_p = 600 kips t_1 = 10 ms
	Case 6-5 F_p = 425 kips t_1 = 5 ms	Case 6-6 F_p = 425 kips t_1 = 10 ms	Case 6-7 F_p = 425 kips t_1 = 20 ms

Note:
1. Force pulse is a sine wave with t_1 representing the time duration and F_p representing the peak force.
2. Soil mass (W/g) equals 1/4; equivalent soil weight is 97 lbs.
3. Soil spring is elastic-plastic with a soil quake equal to 0.1 in.
4. Soil damping is varied over a wide range.

about 16,600 ft/sec, whereas for both concrete and wood the propagation velocity is approximately 12,000 ft/sec. The maximum duration of a force pulse was chosen to be 30 milliseconds. Some of the actual durations for low pile impedances coupled with high energy levels exceeded this 30 millisecond criterion (Figure 3.4); they were not included in this study because they represent impractical conditions.

The soil parameters include stiffness, mass and damping. The soil spring commonly employed is elastic-plastic in behavior with the unloading parallel to the loading curve. The soil quake or soil yield point deflection is varied; however, experimental and field results show that a value of 0.1 in. is common. A nonlinear inelastic spring was also investigated for comparison. The soil mass was varied to represent a soil weight (W) of 0 to 386 pounds. The soil damping was varied over a wide range for each parameter study and individual problem. The damping constant c_o was varied from 0 to 20,000 $\frac{\text{lbs-sec}}{\text{in.}}$ for the low pile impedance and from 0 to 50,000 $\frac{\text{lbs-sec}}{\text{in.}}$ for the high pile impedance.

Soil Mass

The influence of soil mass on the dynamic behavior of the pile tip is a function of the pile tip area and the stress distribution. The soil mass is an additional resistance to pile motion or penetration. The soil mass was varied according to typical zones of influence of the stress distributions and investigated with respect to pile impedance. The problems investigated are shown in Table 3.4.

The soil mass restraint is expected to be more influential for low impedance piles than for piles with high impedances; therefore,

Table 3.4

CASES INVESTIGATED FOR SOIL MASS EFFECT

Pile Impedance, ρcA, $\frac{\text{lbs-sec}}{\text{in.}}$	Case	Energy ft-lbs	Peak Force, kips	Time Duration, t_1 ms	Soil Mass, m: W/g, $\frac{\text{lbs-sec}^2}{\text{in.}}$	Soil Mass, m: W, lbs
	1-A	16,680	200	10	1	386
	1-B	16,680	200	10	1/4	97
1000	1-C	16,680	200	10	0	0
	1-2	12,500	141 1/2	15	1	386
	1-7	12,500	141 1/2	15	1/4	97
3000	3-6	12,500	300	10	1	386
	3-B	12,500	300	10	1/4	97
6000	6-8	12,500	600	5	1	386
	6-A	12,500	600	5	1/4	97

Note: 1. Sinusoidal Force Pulse

2. Elastic-Plastic Soil Spring with Quake = 0.1 in.

the soil mass effect was initiated for a pile with low impedance, namely, $1000\frac{\text{lbs-sec}}{\text{in.}}$. This study (Table 3.4) included a sine force pulse with an energy of 16,680 ft-lbs. and soil masses (W/g) of 0, 1/4 and 1, which are equivalent to soil weights, 0, 97 and 386 lbs, respectively. The effect of soil mass on the net set of the pile tip for the above described conditions is negligible as shown in Figure 3.5.

It should be noted that the soil mass was assumed attached to the pile tip. Consequently, the mass undergoes both penetration and rebound. In the real case, the pile can separate from the mass during rebound or during impact when the mass is driven faster than the pile tip motion. However, because the mass had a negligible effect on pile tip penetration (Figure 3.5); it was assumed that the effect of mass is also negligible if the pile tip can separate from the soil mass.

Transmitted energy for the low pile impedance, $1000\frac{\text{lbs-sec}}{\text{in.}}$, was also compared for different mass constants and the differences were found to be negligible. However, the mass caused a delayed response of the net transmitted energy; similar behavior occurred for the reflected force pulse. This delayed response can be seen by comparing the reflected force for the different mass constants (Figure 3.6). As shown in Figure 3.6, the larger soil mass has an instantaneous resistance effect for low damping values and thereby delays the peak reflected tensile force and changes the reflected force shape. With an increase in resistance, e.g. damping (c_o) of 2000 $\frac{\text{lbs-sec}}{\text{in.}}$, the mass effect becomes negligible with respect to the response pattern. The response pattern was shown for no soil spring resistance; however, the behavior characteristics

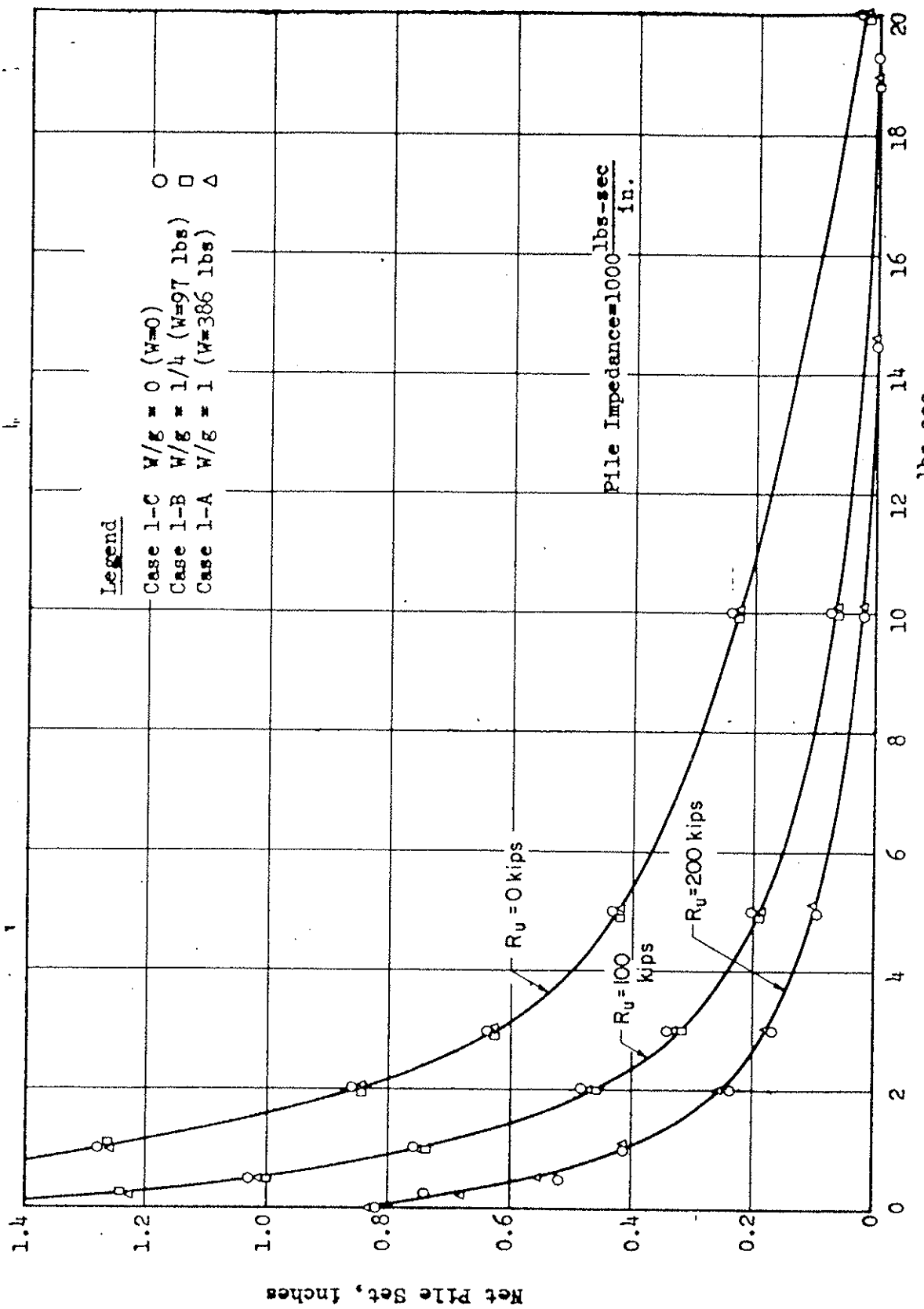

Figure 3.5 EFFECT OF SOIL MASS ON NET TIP DEFORMATION

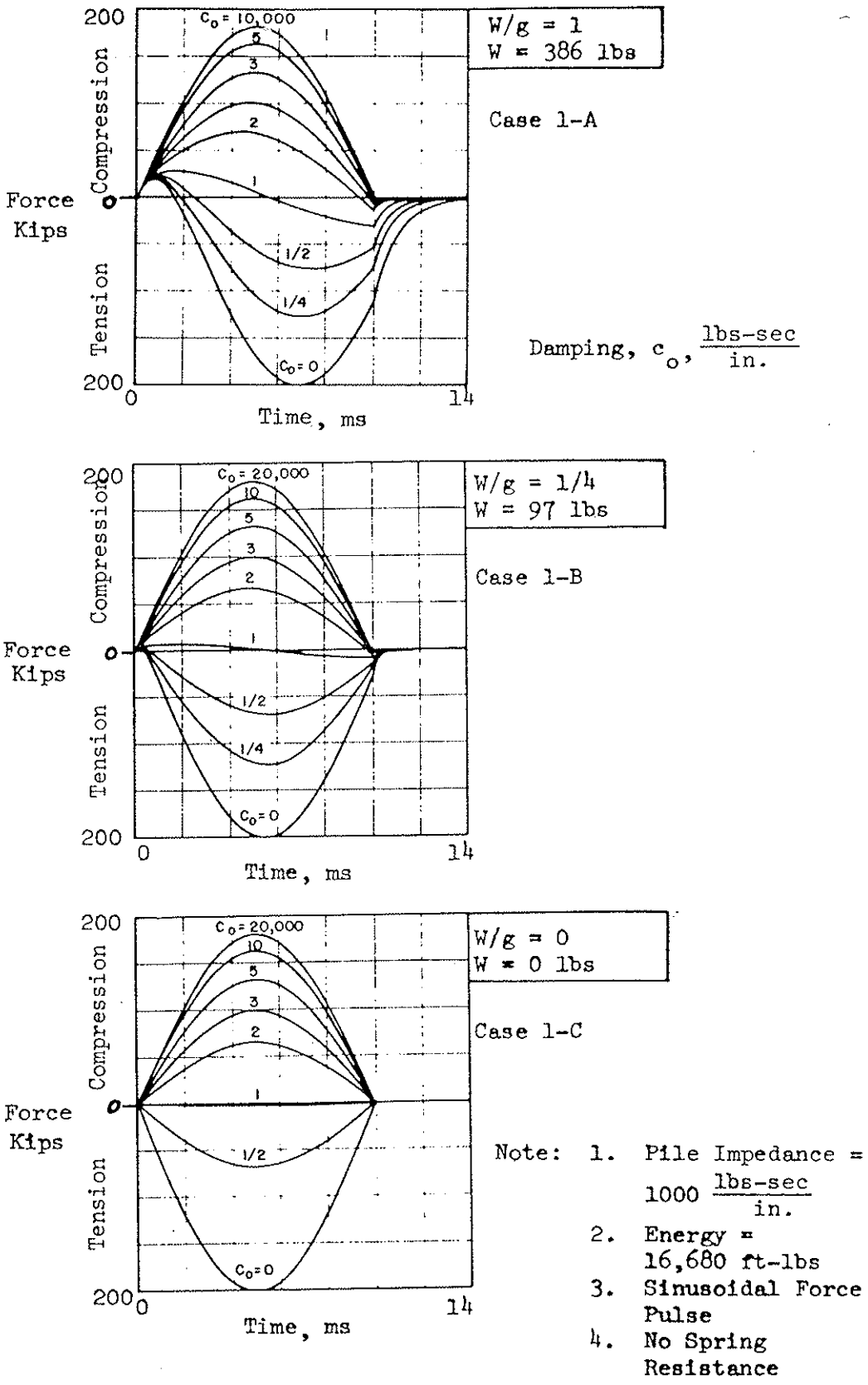

Figure 3.6 COMPARISON OF REFLECTED FORCE PULSE RESPONSE FOR DIFFERENT SOIL MASSES

were the same with different spring forces as evidenced by the negligible effect of soil mass on the net set of pile tip for different soil spring resistances (Figure 3.5). The other cases listed in Table 3.4 resulted in similar conclusions.

Because the range in soil mass investigated did not have a significant effect on pile tip response, a soil mass of 1/4 or an equivalent weight of 97 lbs. was used for the following parameter study as a standard allowance.

Incident Force Pulse

In the most efficient pile driving technique, the incident force pulse is effective against the soil resistance in such a way that maximum penetration (net set) or minimum driving time occurs along with the desired pile performance. The effectiveness of the incident force pulse is investigated by varying the energy, peak force and duration of a sinusoidal wave, and by varying the wave shape.

The effects of a sinusoidal incident force wave with different energies and different durations for the same energy will be investigated. The cases investigated are summarized in Table 3.3; however, the behavior pattern for a pile impedance of 3000 $\frac{\text{lbs-sec}}{\text{in.}}$ is representative of all cases and, hence, is the only data presented. The net set response of the pile tip for different ultimate soil spring resistances (R_u) and energy levels are shown in Figure 3.7. The soil spring is elastic-plastic with a quake value of 0.1 in., and soil damping is varied. It should be noted that for a given soil damping value the net set increases with an increase of input energy providing the peak force is more than one-half of the ultimate spring force.

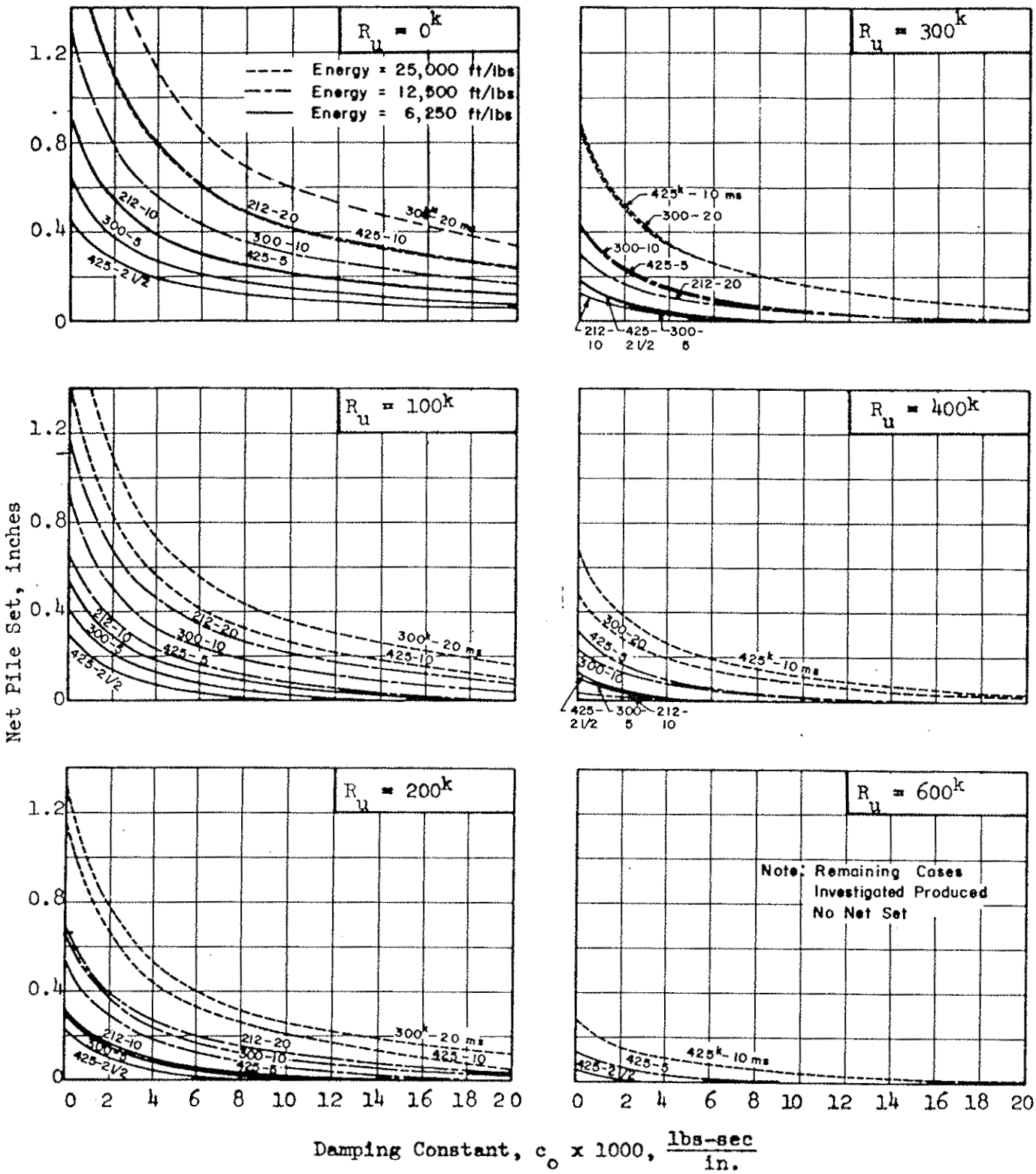

Note: Soil Spring Elastic-Plastic and Quake = 0.1 in.

Figure 3.7 NET SET RESPONSE OF THE PILE TIP FOR PILE IMPEDANCE OF 3000 $\frac{\text{lbs-sec}}{\text{in.}}$

The force pulses with longer durations for a given energy level are more efficient for pile penetration provided the peak pile force is equal to or greater than the ultimate soil spring resistance. For example, compare the conditions where the soil spring ultimate equals 100 and 300 kips as shown in Figure 3.7. The different force pulses working against a soil spring resistance of 100 kips clearly show that maximum net set occurs with an increase in force duration for the same energy level. However, all the peak pile forces considered are greater than the 100 kips. For the condition of 300 kips resistance, the cases wherein the peak forces equal or exceed the spring resistance are more efficient for pile penetration than the longer time pulses with peak forces lower than the ultimate spring resistance. The condition of 400 kips resistance further exemplifies the influence of the generated peak force versus time pulse length. Also, the pile tip deformation is completely elastic if twice the peak pile force is equal to or less than the ultimate spring resistance. Based on the previous example, and the analogous behavior of the other pile impedances investigated, the following conditions can be summarized for a given energy input:

1. For the condition $\frac{F_{(\text{pile peak force})}}{R_{u(\text{soil spring ultimate})}} \to \infty$, maximum pile penetration occurs with no soil resistance.

2. For the condition $\frac{F_{(\text{pile peak force})}}{R_{u(\text{soil spring ultimate})}} > 1$, maximum penetration increases with an increase in duration and is influenced little by the peak force.

3. For the condition $\frac{F_{(\text{pile peak force})}}{R_{u(\text{soil spring ultimate})}} < 1$ and $> 1/2$, maximum pile penetration is primarily dependent on the peak force and is influenced little by the duration.

4. For the condition $\frac{F_{(\text{pile peak force})}}{R_{u(\text{soil spring ultimate})}} \leq 1/2$, no net pile penetration occurs; the deformations are purely elastic.

An investigation was also made of the effect of force pulse shape. The wave shapes--triangular, sine and square--are compared for a constant incident energy of 12,500 ft-lbs and a constant peak force for a particular value of pile impedance; therefore, the duration is different for each wave shape. The triangular pulse is symmetric in shape as shown in Table 3.5. The cases compared for the effect of wave shape are tabulated in Table 3.5; however, the behavior pattern for a pile impedance of 3000 $\frac{\text{lbs-sec}}{\text{in.}}$ is representative of all cases and, hence, is the only data presented. The effect of wave shape on pile penetration is shown in Figure 3.8.

For the pile impedance of 3000 $\frac{\text{lbs-sec}}{\text{in.}}$, the longer pulse (triangular wave) is the most efficient for pile penetration provided the pile peak force is greater than the soil spring resistance as shown in Figure 3.8 for a soil spring ultimate (R_u) equal to 100 kips. This behavior indicates that the efficiency order of the wave shape is triangular (most efficient), sine and square (least efficient) for the condition of the peak pile force greater than R_u. As the peak pile force approaches and becomes less than the soil spring resistance (R_u), the order of efficiency reverses with the square wave being the most effi-

Table 3.5

CASES INVESTIGATED FOR WAVE SHAPE EFFECT

Pile Impedance, ρcA, $\frac{\text{lbs-sec}}{\text{in.}}$	Case	Wave Shape	Energy ft-lbs	Peak Force, kips	Time Duration t_1, ms	Wave
1000	1-13	Spiked	12,500	141 1/2	22 1/2	 141 1/2 kips; 22 1/2 ms
	1-2	Sine	12,500	141 1/2	15	 141 1/2 kips; 15 ms
	1-14	Square	12,500	141 1/2	7 1/2	 141 1/2 kips; 7 1/2 ms
3000	3-12	Spiked	12,500	300	15	 300 kips; 15 ms
	3-B	Sine	12,500	300	10	 300 kips; 10 ms
	3-13	Square	12,500	300	5	 300 kips; 5 ms
6000	6-9	Spiked	12,500	600	7 1/2	 600 kips; 7 1/2 ms
	6-A	Sine	12,500	600	5	 600 kips; 5 ms
	6-10	Square	12,500	600	2 1/2	 600 kips; 2 1/2 ms

Note: 1) Elastic-plastic spring with Quake = 0.1 in.

2) Soil Mass, $W/g = 1/4$

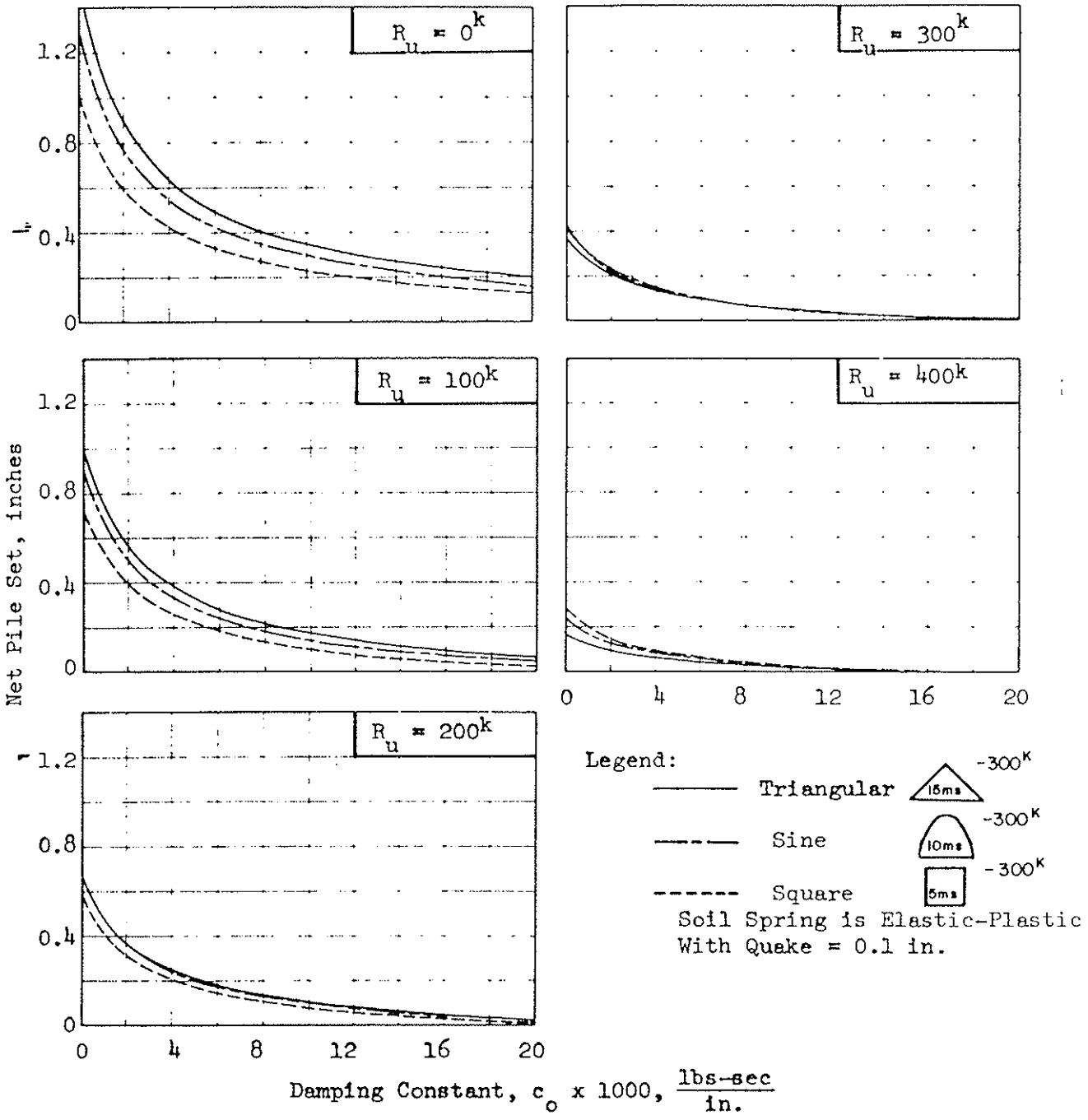

Figure 3.8 EFFECT OF WAVE SHAPE ON PILE PENETRATION FOR PILE IMPEDANCE OF 3000 $\frac{lbs-sec}{in.}$

cient and the triangular wave the least efficient, as shown in Figure 3.8 for the condition of R_u equal to 400 kips. This behavior indicates that duration near the peak pile force is significant for the condition of peak pile force less than the soil spring resistance.

Based on the previous example, and the analogous behavior of the other pile impedances investigated, the following conditions can be summarized for different wave shapes with a particular energy:

1. For the condition of $\frac{F_{(\text{pile peak force})}}{F_{(\text{soil spring ultimate})}} \rightarrow \infty$, maximum pile penetration occurs with no soil resistance.

2. For the condition of $\frac{F_{(\text{pile peak}}}{F_{\text{soil spring ultimate})}} > 1$, maximum pile penetration occurs for the force pulse shape with the longest duration.

3. For the condition of $\frac{F_{(\text{pile peak force})}}{F_{\text{soil spring ultimate})}} < 1$ and $> 1/2$, maximum pile penetration occurs for the force pulse shape with the longest duration near the peak pile force.

4. For the condition of $\frac{F_{(\text{pile peak force})}}{F_{(\text{soil spring ultimate})}} \leq 1/2$, no net pile penetration (only elastic deformation) occurs; therefore, wave shape is not pertinent.

It is believed that the foregoing behavior is generally valid for other wave shapes, pile impedances and energy levels.

Soil Properties

The soil properties are represented by the soil spring, damping and mass resistance. The soil mass effect has been previously discussed and will not be included in this section; however, the effects of both damping and the soil spring on pile tip response will be discussed herein.

Before the numerical results are considered, the response behavior of a pile tip with respect to the soil restraint will be discussed qualitatively. For damping restraint only with no soil spring resistance (free-end condition) the incident compressive wave is reflected as a tensile wave with the same peak force and shape at zero damping, and no transmitted wave exists. As the damping restraint is increased, the reflected wave passes from a tensile to a compressive wave with no reflections occurring when the pile impedance and the damping constant are equal. A compressive wave reflection equal to the incident wave corresponds to a fixed-end condition. The no-reflection condition represents the optimum match between pile and soil for maximizing transmitted energy.

When a soil spring is included along with damping, the damping constant required for maximum energy transmission decreases with increases in spring resistance. Soil damping and the soil spring control both the reflected force wave and transmitted energy. With respect to the efficiency of pile driving, the set (penetration) efficiency is more significant than energy efficiency; however, the concept of transmitted energy efficiency can be used as a reference framework for discussing the behavior characteristics of the pile tip.

The foregoing brief qualitative behavior of pile tip response can best be exemplified by consideration of a particular problem, namely, Case 3-B with a pile impedance of 3000 $\frac{\text{lbs-sec}}{\text{in.}}$. The reflected force wave for this case due to an incident sinusoidal wave is shown in Figure 3.9. The set shown by the curves for a spring force equal to zero clearly shows the transition of tensile to compressive reflection; no reflection occurs at a damping constant of 3000 $\frac{\text{lbs-sec}}{\text{in.}}$ which equals the pile impedance.

With the addition of the elastic-plastic soil spring, the wave shape for low damping values is controlled by the springs, whereas for high damping values the reflected wave is dominated by the damping restraint. The first break in the low damping value reflections as shown in Figure 3.9 (R_u = 100 kips) signifies the beginning of plastic spring behavior, and the cross-point of the reflected waves (Figure 3.9 and R_u = 100 kips) signifies the unloading of the spring. The beginning of the plastic behavior of the soil spring occurs more rapidly with the smaller soil spring resistances (R_u), whereas the unloading condition occurs more rapidly with the higher soil spring resistance (R_u).

It can be seen by the reflected forces (Figure 3.9) that as the soil spring ultimate (R_u) increases the damping constant decreases from 3000 $\frac{\text{lbs-sec}}{\text{in.}}$ to zero for the condition of least reflection; therefore, this condition also applies to the maximum transmitted energy of the soil. The soil damping values at maximum transmitted energy and the corresponding transmitted energy efficiencies (percentage of transmitted to incident energy) have been tabulated for the cases of the

c_o = Damping constant, $\frac{\text{lbs-sec}}{\text{in.}}$

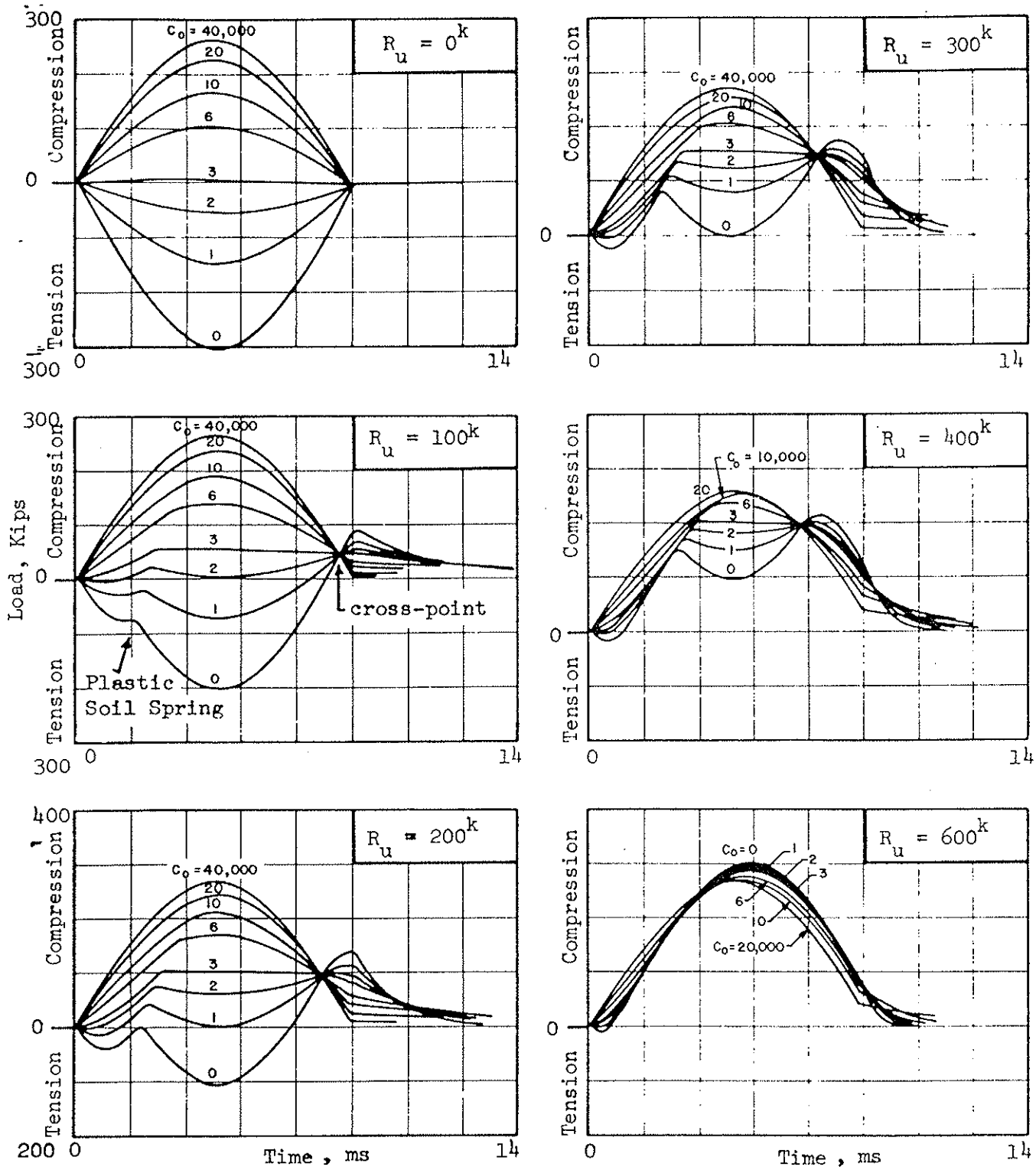

Incident Wave: Sine Wave F_p = 300 kips t_1 = 10ms. E_I = 12,500 ft-lbs

Figure 3.9 REFLECTED FORCE PULSES FOR CASE 3-B WITH PILE IMPEDANCE OF 3000 $\frac{\text{lbs-sec}}{\text{in.}}$

basic parameter study listed in Table 3.3 as well as the Case 3-B presented herein (Table 3.6). As seen from Table 3.6, soil damping values at maximum transmitted energy for different pile impedances and soil spring resistances (R_u) correspond to the general behavior as previously described. The transmitted energy efficiciency has a value of 100% at zero soil spring resistance and reduces to a minimum value of approximately 70% as the soil spring resistance approaches the value of the pile peak force. With a soil spring force in excess of the peak force in the pile, the efficiency of the transmitted energy reduces markedly. This reduction in energy transmission is indicative of the pile penetration, i.e., pile penetration decreases with a decrease in transmitted energy. However, it should be noted that maximum energy transmission does not guarantee maximum pile penetration. Maximum pile penetration is also dependent on the force pulse shape with respect to the soil resistance as described previously.

The relected force pulses shown in Figure 3.9 are representative of the behavior of the other cases studied. The reflected wave corresponds to the incident wave form, i.e. a longer and lower peak incident wave produces a corresponding reflected wave. Also, the reflected wave shape corresponds to the incident wave as shown by the examples used for the triangular and square wave investigation.

The effect of damping on pile penetration is clearly defined by the condition that any additional restraint impedes penetration; therefore, an increase in either the damping constant or spring ultimate reduces the pile tip set for a given problem. This fact is readily

Table 3.6

SOIL DAMPING AT OPTIMUM ENERGY TRANSMISSION

Pile Impedance = 1000 $\frac{\text{lbs/sec}}{\text{in.}}$

Case	Energy Input ft-lbs.	Peak Force, kips	Time Duration, ms.	Damping Value at Maximum Energy Transmission, c_o, lbs-in/sec / Transmitted Energy Efficiency, %			
				$R_u = 0$	$R_u = 50^k$	$R_u = 100^k$	$R_u = 200^k$
1-1	6,250	141 1/2	7 1/2	1000 / 100	1000 & 500 / 93	250 / 92	250 / 46
1-4	6,250	100	15	1000 / 100	500 - 250 / 97	0 / 88	--
1-6	6,250	70.7	30	1000 / 100	250 / 98	0 / 56	
1-2	12,500	141 1/2	15	1000 / 100	500 / 98	250 / 95	0 / 55
1-5	12,500	100	30	1000 / 100	500 / 93	250 / 81	--
1-3	25,000	141 1/2	30	1000 / 100	---	500 / 90	0 / 55

Pile Impedance = 3000 $\frac{\text{lbs/sec}}{\text{in.}}$

Case	Energy Input ft-lbs.	Peak Force, kips	Time Duration, ms	Damping Value at Maximum Energy Transmission, c_o, lbs-in/sec / Transmitted Energy Efficiency, %					
				$R_u = 0^k$	$R_u = 100^k$	$R_u = 200^k$	$R_u = 300^k$	$R_u = 400^k$	$R_u = 600^k$
3-1	6,250	425	2 1/2	3000 / 100	3000 & 2000 / 96	2000 / 90	2000 & 1000 / 83	1000 / 72	6000 / 47
3-A	6,250	300	5	3000 / 100	2000 / 96	1000 / 88	0 / 74	0 / 50	10,000 / 26
3-4	6,250	212	10	3000 / 100	2000 & 1000 / 94	0 / 81	0 / 48	6000 / 16	--
3-2	12,500	425	5	3000 / 100	3000 & 2000 / 98	2000 & 1000 / 93	1000 / 90	0 / 83	0 / 51
3-B	12,500	300	10	3000 / 100	2000 / 97	1000 / 92	0 / 83	0 / 59	20 / 14
3-5	12,500	212	20	3000 / 100	3000 & 1000 / 97	0 / 90	0 / 55	20,000 / 9	--
3-3	25,000	425	10	3000 / 100	3000 & 2000 / 98	2000 & 1000 / 96	1000 / 92	0 / 87	0 / 55
3-C	25,000	300	20	3000 / 100	2000 / 99	1000 / 95	0 / 85	0 / 60	--

Pile Impedance = 6000 $\frac{\text{lbs/sec}}{\text{in.}}$

Case	Energy Input ft-lbs.	Peak Force, kips	Time Duration, ms	Damping Value at Maximum Energy Transmission, c_o, lbs-in/sec / Transmitted Energy Efficiency, %						
				$R_u = 0^k$	$R_u = 100^k$	$R_u = 200^k$	$R_u = 300^k$	$R_u = 400^k$	$R_u = 600^k$	$R_u = 800^k$
6-1	6,250	850	1 1/4	6000 / 100	6000 / 100	6000 / 95	6000 / 90	6000 / 86	6 & 10,000 / 79	6 & 10,000 / 72
6-4	6,250	600	2 1/2	6000 / 100	6000 / 98	6000 / 92	6 & 3000 / 84	6 & 3000 / 78	--	10,000 / 55
6-5	6,250	425	5	6000 / 100	6000 / 99	3000 / 92	3000 / 82	3 & 1000 / 71	10,000 / 44	--
6-2	12,500	850	2 1/2	6000 / 100	6000 / 99	6000 / 95	6 & 3000 / 91	3000 / 89	3000 / 81	3000 / 70
6-A	12,500	600	5	6000 / 100	6000 / 98	3000 / 93	3000 / 92	3 & 1000 / 85	1000 & 0 / 73	0 / 50
6-6	12,500	425	10	6000 / 100	6000 / 99	3000 / 97	1000 / 91	1000 & 0 / 82	0 / 98	--
6-3	25,000	850	5	6000 / 100	6000 / 99	6 & 3000 / 96	3000 / 96	3000 / 95	1000 / 89	1000 & 0 / 81
6-B	25,000	600	10	6000 / 100	6000 / 98	3000 / 97	3000 / 95	1000 / 91	0 / 81	0 / 60
6-7	25,000	425	20	6000 / 100	3000 / 100	3000 / 98	1000 / 94	6 / 87	0 / 53	--

shown in the results of the investigation such as the particular case previously discussed and shown in Figure 3.7.

Soil spring quake and spring force-deflection shape will now be investigated. The cases investigated for the quake and spring shape effect are shown in Table 3.7. The soil quake effect was investigated with respect to an elastic-plastic soil spring and a sine force pulse with an energy level of 12,500 ft. lbs. The range in quake values (0 to 0.40 in.) covered both stiff soils to soft soils. Effects of the soil quake on the net penetration are shown in Figures 3.10, 3.11 and 3.12 for pile impedances of 1000, 3000, and 6000 $\frac{\text{lbs-sec}}{\text{in.}}$, respectively. All plots show a decrease in net penetration with an increase in soil quake. This decrease in net penetration with a softer soil spring can be attributed to the larger elastic strain energy required to reach the yield point, Q.

The problems previously discussed have been associated with an elastic-plastic soil spring; however, the behavior of a different force-deformation shape will also be considered herein. The range of the investigation with respect to the spring force shape is listed in Table 3.7. The incident force pulses and pile impedances are the same as for the quake study. The nonlinear and inelastic spring can be compared to the elastic-plastic spring for the effect of penetration (Figure 3.13); soil quake at the break in spring load-deformation curve was held constant (0.1 in.). The stiffer nonlinear spring increases the soil resistance; therefore, the nonlinear spring will reduce penetration as shown in Figure 3.13. It should be noted that at high damping constants

Table 3.7

CASES ASSOCIATED WITH SOIL SPRING QUAKE
AND SPRING FORCE DEFLECTION SHAPE

EFFECT OF SOIL QUAKE*

Pile Impedance, lbs-sec/in.	Case	Input Energy, ft-lbs	Peak Force, kips	Force Time Duration, ms	Quake, in.
1000	1-10	12,500	141 1/2	15	0.05
	1-2	12,500	141 1/2	15	0.10
	1-11	12,500	141 1/2	15	0.20
	1-12	12,500	141 1/2	15	0.40
3000	3-9	12,500	300	10	0.05
	3-B	12,500	300	10	0.10
	3-10	12,500	300	10	0.20
	3-11	12,500	300	10	0.40
6000	6-11	12,500	600	5	0.05
	6-A	12,500	600	5	0.10
	6-12	12,500	600	5	0.20
	6-13	12,500	600	5	0.40

EFFECT OF SPRING FORCE SHAPE**

Pile Impedance, lbs-sec/in.	Case	Input Energy, ft-lbs	Peak Force, kips	Force Time Duration, ms	Soil Spring Type
1000	1-2	12,500	141 1/2	15	elastic-plastic 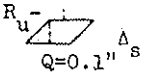
	1-8	12,500	141 1/2	15	nonlinear and inelastic 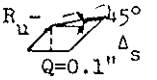
	1-9	12,500	141 1/2	15	elastic 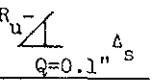
3000	3-B	12,500	300	10	elastic-plastic 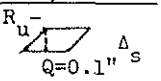
	3-7	12,500	300	10	nonlinear and inelastic 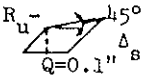
	3-8	12,500	300	10	elastic 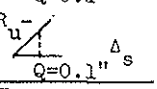
6000	6-A	12,500	600	5	elastic-plastic 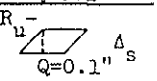
	6-14	12,500	600	5	nonlinear and inelastic 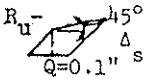
	6-15	12,500	600	5	elastic 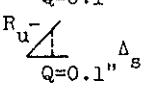

* 1. Elastic-plastic soil spring
2. Sinusoidal force pulse

** Sinusoidal force pulse

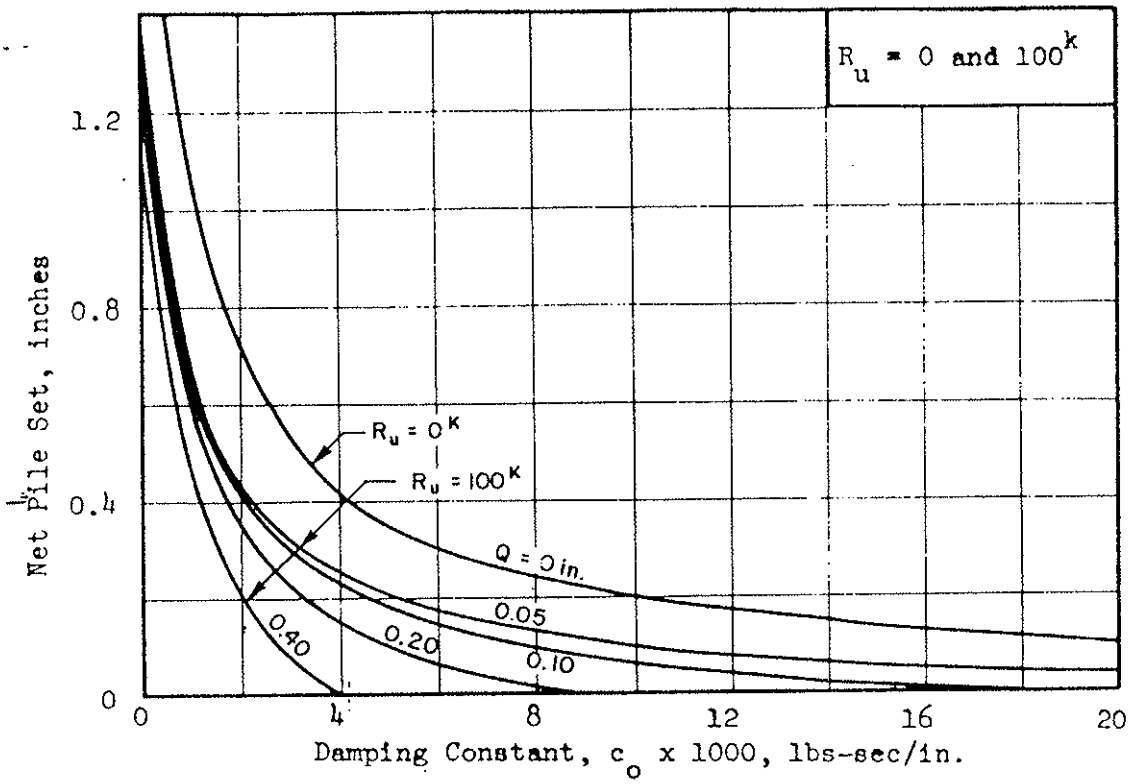

Incident Force Wave: Sine Wave with F_p = 141 1/2 kips and t_1 = 15 ms. E_I = 12,500 ft-lbs

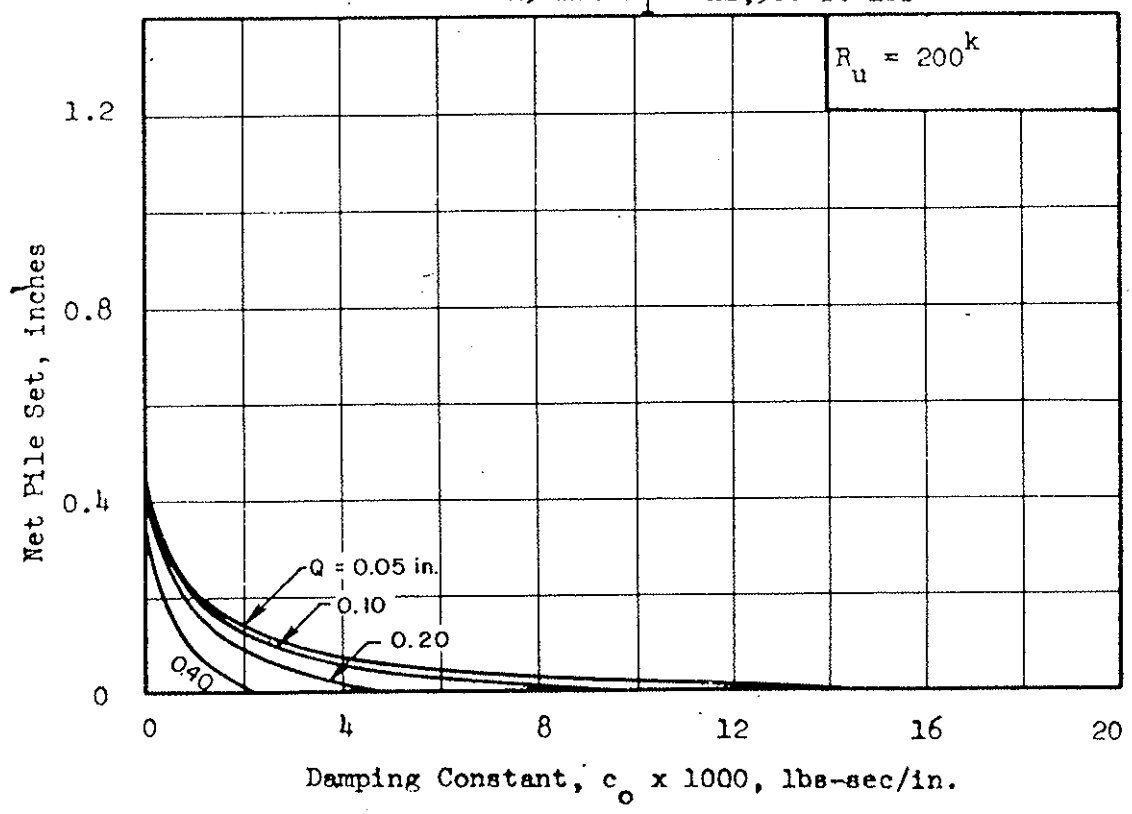

Figure 3.10 EFFECT OF SOIL QUAKE ON PENETRATION FOR PILE IMPEDANCE OF 1000 $\frac{\text{lbs-sec}}{\text{in.}}$

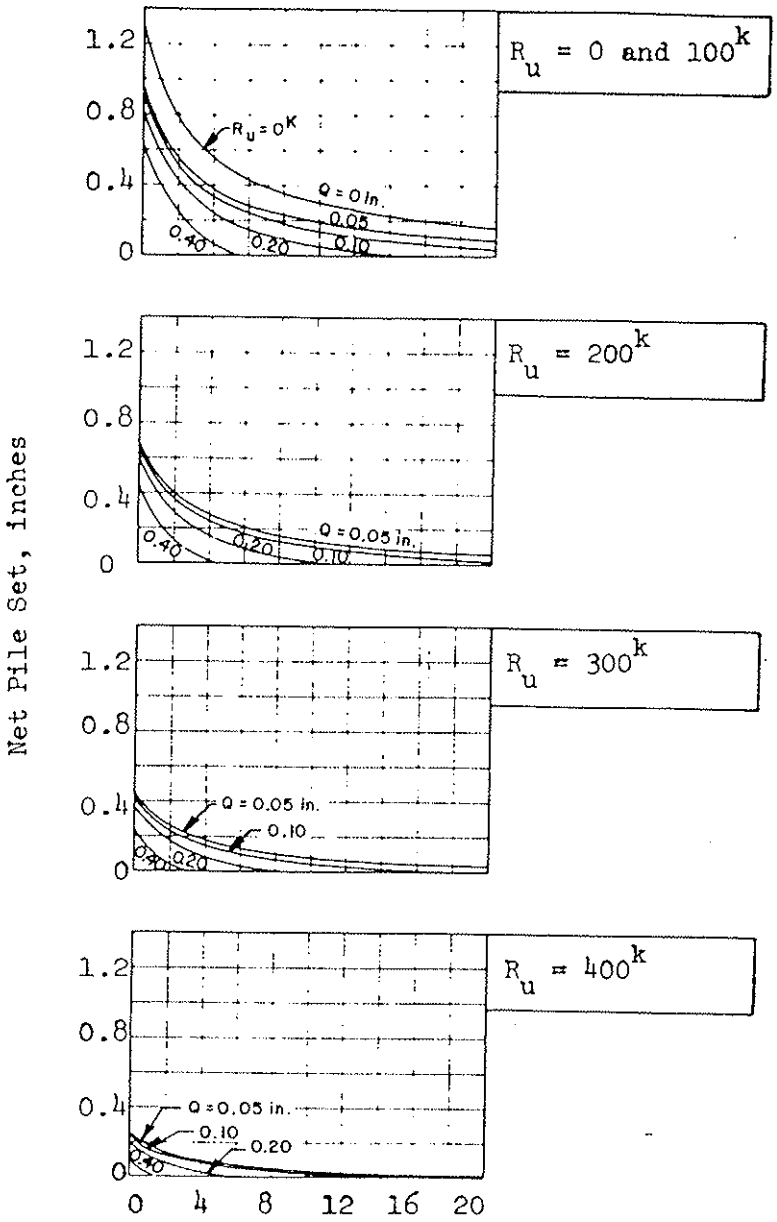

Incident Force Wave: Sine Wave with F_p=300 kips t_1=10 ms. E_I=12,500 ft-lbs

Figure 3.11 EFFECT OF SOIL QUAKE ON PENETRATION FOR PILE IMPEDANCE OF 3000 lbs-sec/in.

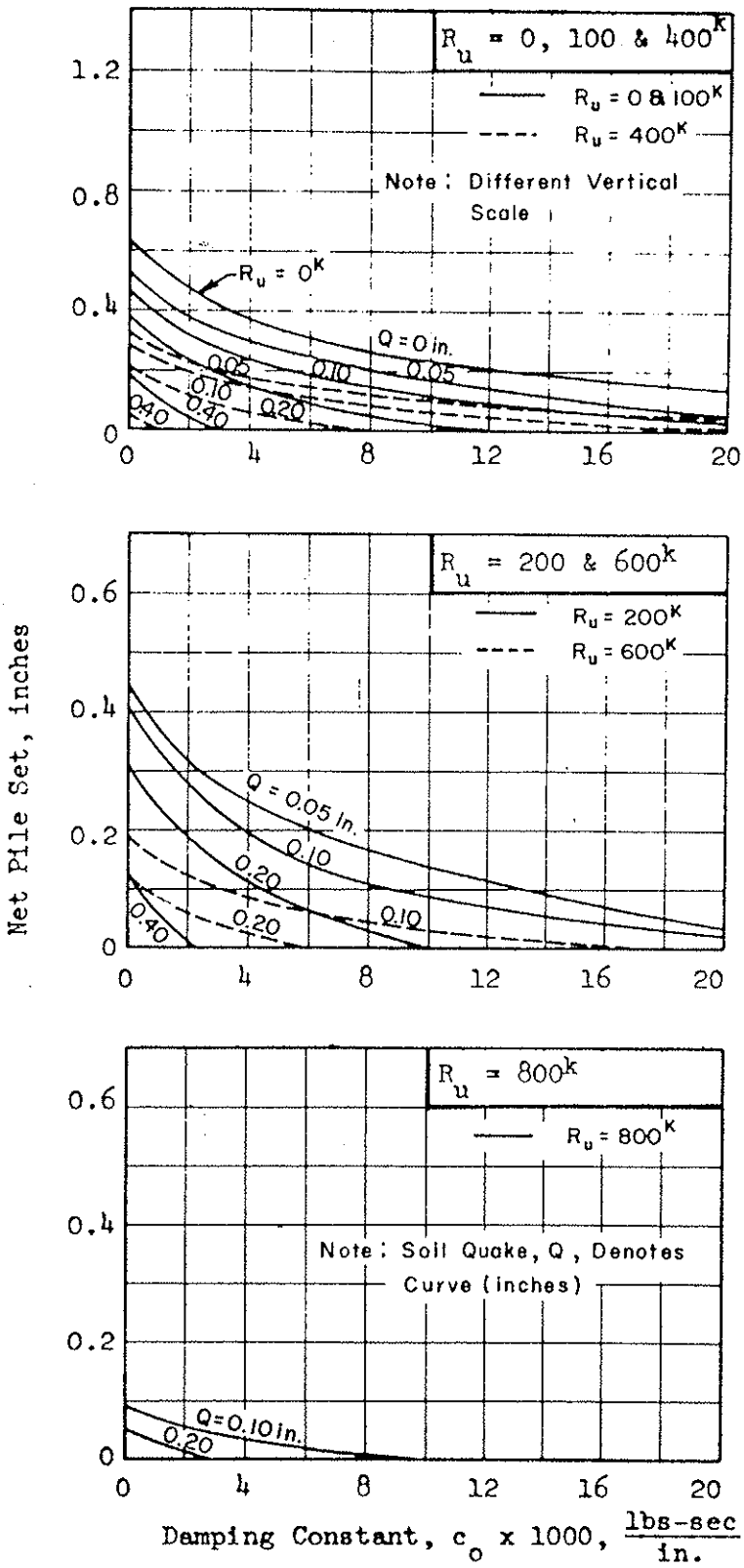

Incident Force Wave: Sine Wave F_p = 600 kips t_1 = 5ms E_I = 12,500 ft-lbs

Figure 3.12 EFFECT OF SOIL QUAKE ON PENETRATION FOR PILE IMPEDANCE OF 6000 lbs-sec/in.

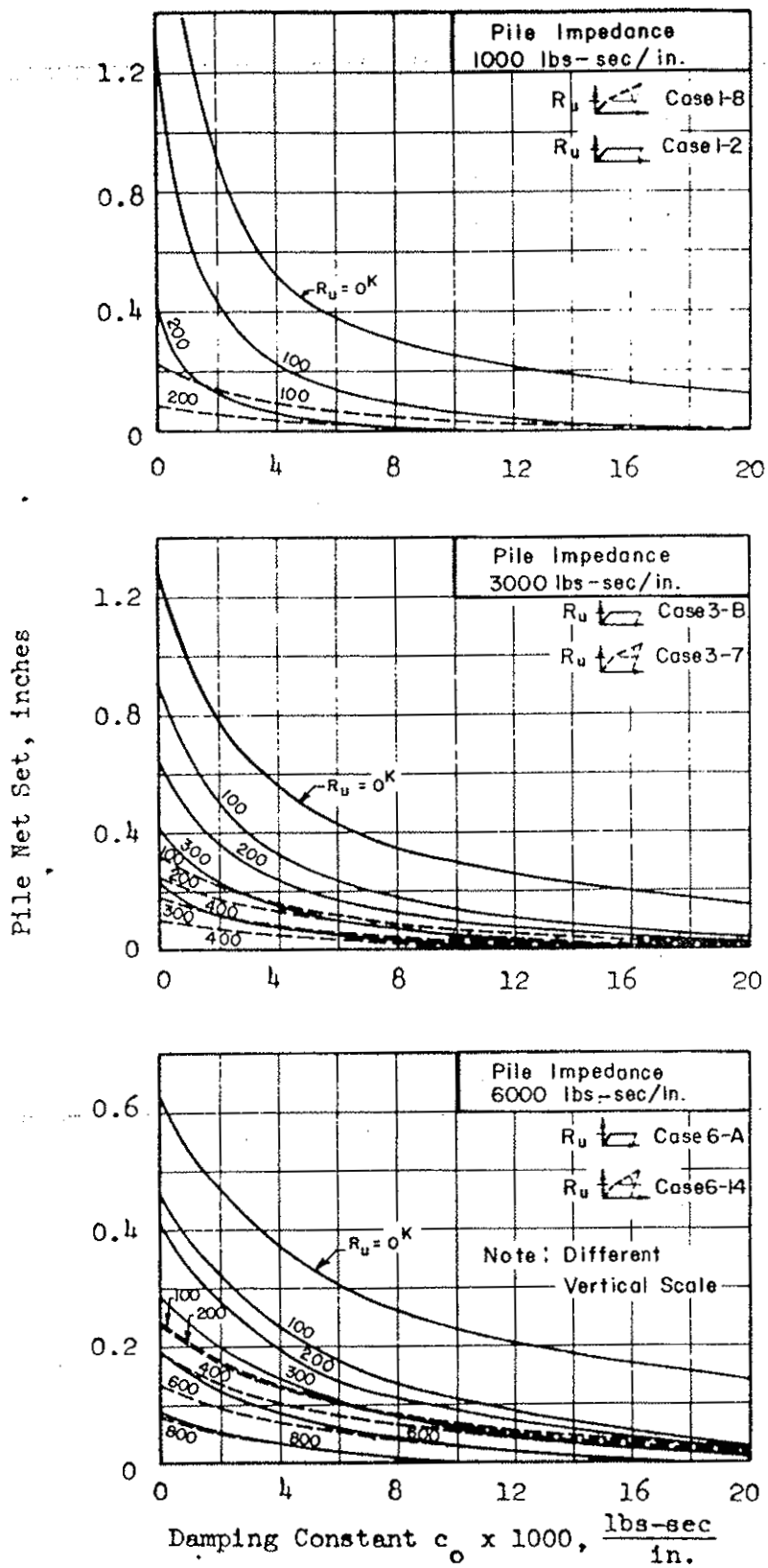

Figure 3.13 EFFECT OF SOIL SPRING FORCE SHAPE ON PILE PENETRATION

penetration is not influenced by the spring force shape. The reflected force also changes little for different spring force shapes with high damping.

This study has indicated the influence on pile penetration of the parameters of the incident force wave with respect to the soil resistance properties. The investigation of pile response was devoted to the pile tip only; the effect of soil resistance along the pile (skin friction) was not included.

3.5 Effect of Soil Resistance Along Pile Length

Introduction

The purpose of this section is to investigate qualitatively the effect of the side soil resistance (skin friction) on the attenuation and shape of the incident force pulse. It is the attenuated force pulse that reaches the pile tip and causes penetration.

In order to study attenuation of the incident force pulse an illustrative problem with selected hammer, pile and soil characteristics will be solved with the use of Smith's lumped-mass and spring model (See Appendix A). The problem shown in Figure 3.14 considers a 150 ft long pile with an impedance of 3000 $\frac{\text{lbs-sec}}{\text{in.}}$ driven with a hammer with an energy delivery at impact of 12,500 ft-lbs. The soil skin friction resistance is considered uniformly distributed along the pile; however, values of the soil resistance parameters will be varied. The soil resistance distribution includes a variation in the relative amounts of total skin friction and point bearing. The soil resistance is repre-

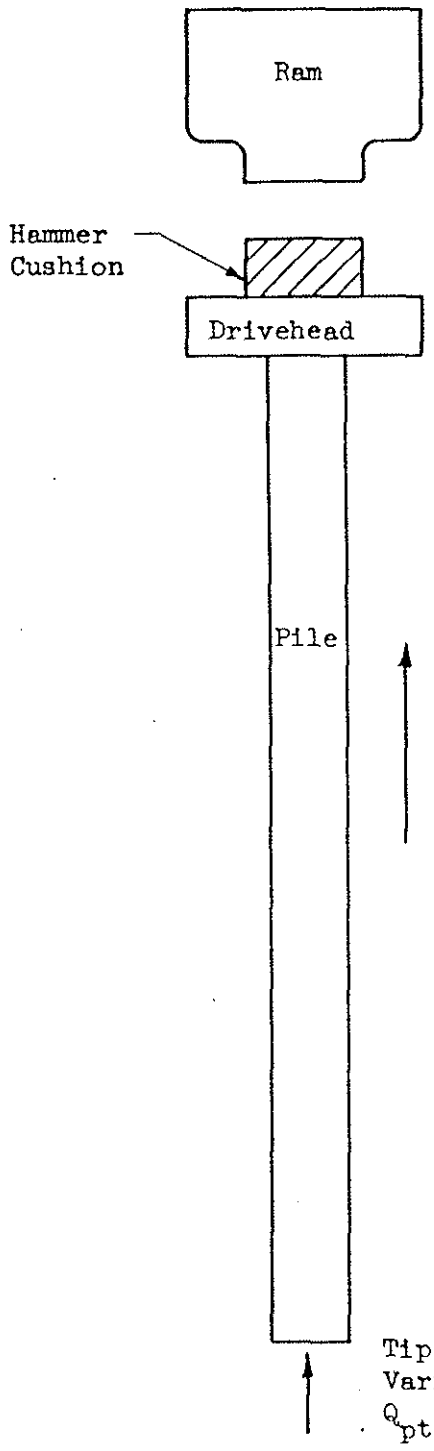

W_1 = 5000 lbs.
Energy at Impact = 12,500 ft-lbs.

$k = 1 \times 10^6$ lbs/in. and e = 1.0
W_2 = 1000 lbs

Side Soil Resistance - Uniform
Varied from 0 to 100%
Q_s = 0.05 to 0.20 in. Normally 0.10 in.
J_s = 0 to 0.15 $\frac{sec}{ft}$ Normally 0.05 $\frac{sec}{ft}$

Pile: Impedance = 3000 $\frac{lbs\text{-}sec}{in.^2}$
Area of Steel = 20.7 $in.^2$
Length = 150 ft

Pile Model: Lumped-Masses and Springs
Segment Length = 5 ft
$\frac{wt}{seg}$ = 353 lbs $K_{seg} = 10 \times 10^6 \frac{lbs}{in.}$

Tip Soil Resistance
Varied from 0 to 100%
Q_{pt} = 0.10 in. J_{pt} = 0.15 sec/ft

Note: Total Soil Resistance Equals 100 kips

Figure 3.14 EXAMPLE PROBLEM FOR THE EFFECT OF SOIL RESISTANCE ALONG PILE

sented by an elastic-plastic spring and damping. Details of the example problem are shown in Figure 3.14.

Distribution of Soil Resistance

The attenuation of the incident force pulse at the pile head was investigated with respect to a range in uniform soil resistance along the pile length of 0% (point-bearing) to 100% (friction) utilizing the soil parameters recommended by Smith (1960). From this study, the generated peak force pulse was attenuated by approximately one-half the total of the side friction load. The total side friction load is probably a limit of attenuation.

The effect of attenuation by frictional soil resistance is not as critical to pile penetration as the effect of the tip resistance because of the physical nature of the soil resistance distribution. Soil resistance along the pile is distributed in parts, i.e. a percentage of resistance at each lumped mass segment; therefore, the effect of the total soil spring resistance for all segments is smaller for a given quake value than if the same resistance occurred at one segment (pile tip).

Also, the tip resistance damping is assumed higher than the side resistance damping because of the physical mechanism of the soil failure; hence, resistance to penetration is greater at the pile tip. Therefore, driving a point bearing pile would be the more difficult (less set per blow) and driving a friction pile would be the less difficult (more set per blow). Other pile driving conditions are intermediate between those of pure friction and point bearing piles.

Soil Parameters

The effect of soil parameters, quake and damping, along the pile length will now be investigated. This soil parameter study makes use of the illustrative problem (Figure 3.14) with a uniform soil skin friction distribution amounting to 50% of total pile load capacity. Soil quake and soil damping along the pile length were varied. The soil properties at the tip were held constant.

In order to compare the effects of soil parameters, the total force response (incident and reflected added together) at the pile tip were compared for the variations in soil parameters. It is assumed that any changes in the soil parameters along the pile would produce a change in the total force response at the pile tip.

The side soil quake was varied between 0.05 and 0.20 in. as shown in Figure 3.15, and the difference in total force response was found to be negligible.

Also shown in Figure 3.15 is the effect of side soil damping, which was varied between limits of 0 and 0.15 sec/ft. The change in response for the side damping is slightly more noticeable than the effect of quake; however, the force pulse is still not particularly sensitive to the side damping term.

The relative percentage of total resistance at the pile tip and along the pile length is significant for evaluation of pile penetration. Pile penetration behavior is not particularly sensitive to soil parameters along the pile length; therefore, these parameters are not of major importance to the evaluation of pile penetration.

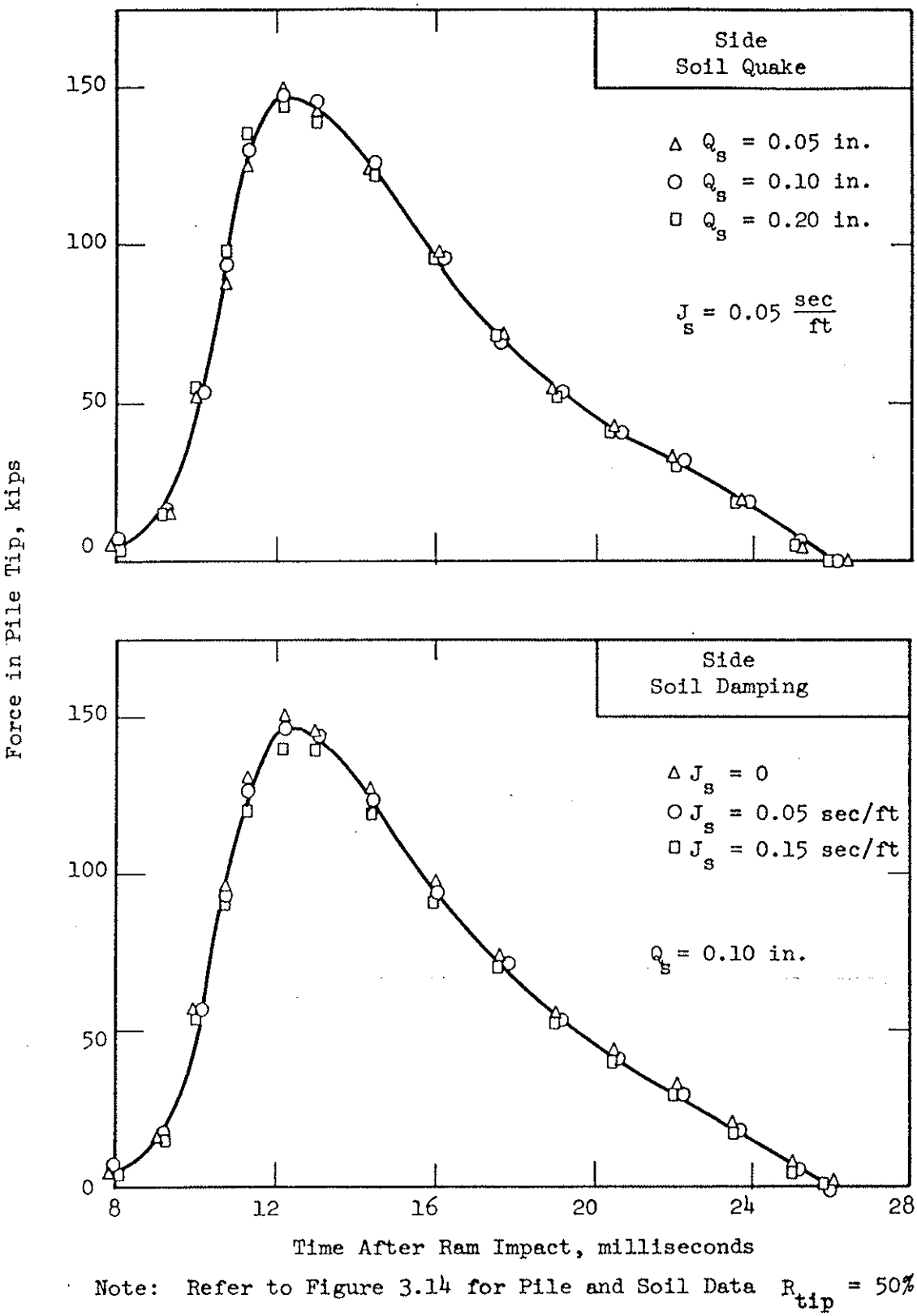

Note: Refer to Figure 3.14 for Pile and Soil Data R_{tip} = 50%

Figure 3.15 EFFECT OF QUAKE AND DAMPING ALONG THE PILE ON PILE TIP FORCE

CHAPTER 4

CHARACTERISTICS OF HAMMER-PILE-SOIL SYSTEM AFFECTING PILE DRIVING BEHAVIOR

4.1 Introduction

The purpose of this chapter is to summarize the effects of the variables affecting pile driving behavior by looking at the hammer-pile-soil system as a whole. The variables of the hammer, pile and soil will be summarized and explained with the use of parameter studies (Chapters 2 and 3) and illustrative examples from field case histories. A corresponding analysis using the wave equation (Smith's lumped mass-spring model) will also be shown for each field case history. Field studies with diesel hammers will be included where the variable under consideration is independent of combustion force uncertainties. Comparison of wave equation analyses with field case histories will illustrate the power of this analytical tool, and lend further validity to the use of wave propagation theory in pile driving. Dynamic energy formulas will be compared to the wave equation analysis, and the limitations of energy formulas will be delineated.

4.2 Pile Hammer

Energy

The pile hammer is an energy source used to generate a force pulse in the pile in order to overcome soil resistance and achieve penetration. The potential energy of the hammer is a function of the ram weight and stroke, or equivalent stroke at impact. Hammer potential energy has two

sources of losses, namely, energy loss during ram fall and loss in transmission through the cushion and drivehead to the pile. Energy losses prior to impact include mechanical losses such as friction, preadmission of steam or air etc., whereas the transmitted energy losses include the inelastic behavior of the hammer cushion and contacts, and ram rebound.

It should be noted that it is not only necessary to transmit energy in order to achieve maximum penetration and load capacity, but it is also necessary that the shape of the generated force-time pulse be proper. In this section transmitted energy will be considered first and the effect of force pulse shape will follow.

Considering transmitted energy only, pile penetration and load capacity increase with an increase in transmitted energy for a given pile provided the peak force generated is greater than one-half the ultimate soil spring resistance at the pile tip. The effect of energy on the response of piles with impedances of 1000, 3000 and 6000 $\frac{\text{lbs-sec}}{\text{in.}}$ (equivalent pile types and sizes are shown in Table 3.2) is shown in Figure 4.1. The pile response is taken from some of the cases investigated in Chapter 3 for a sinusoidal incident wave acting against a viscous damping factor, J_{pt} = 0.15 sec/ft, and soil quake, Q_{pt} = 0.10 in., which are commonly assumed in wave equation analyses. The soil spring is elastic-plastic with a variable ultimate resistance (R_u). The curves on Figure 4.1 were obtained by selecting the pile net set (Chapter 3) for various ultimate spring resistances (R_u), and the damping value related to the J factor; the number of hammer blows per unit set is the reciprocal of pile net set.

As shown in Figure 4.1, pile penetration and capacity increase with an increase in transmitted energy for a given pile impedance. Fur-

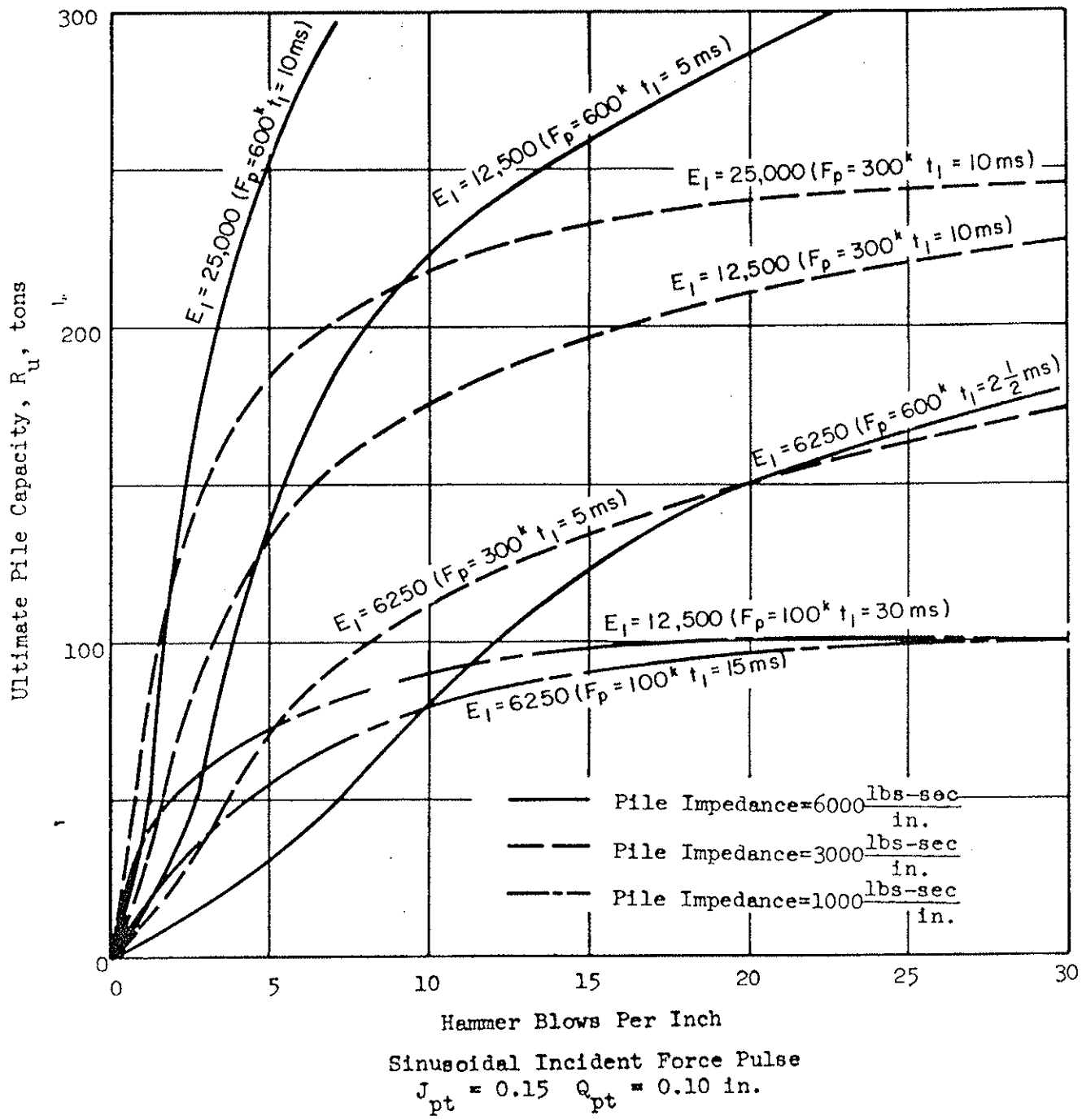

Figure 4.1 EFFECT OF HAMMER ENERGY ON PILE RESPONSE

ther, ultimate pile capacity increases, with an increase in energy, at a greater rate for higher pile impedances.

In order to compare the effect of transmitted energy on pile impedance (Figure 4.1), the ultimate pile resistance was determined at ten blows per inch, which was arbitrarily selected as a practical limit to driving resistance. With the energy input doubled, ultimate pile capacity increased more significantly for the high pile impedance than for the low impedance. For example, the ultimate capacity for the pile impedance of 6000 $\frac{\text{lbs-sec}}{\text{in.}}$ increases approximately 180 percent when the input energy doubles (6250 to 12,500 ft lbs); whereas, the ultimate capacity increases approximately 40 and 15 percent for impedances of 3000 and 1000 $\frac{\text{lbs-sec}}{\text{in.}}$, respectively. Increasing the energy from 12,500 to 25,000 ft lbs increases the ultimate capacity approximately 50 percent for an impedance of 6000 $\frac{\text{lbs-sec}}{\text{in.}}$, and 25 percent for an impedance of 3000 $\frac{\text{lbs-sec}}{\text{in.}}$.

It was noted in Chapter 3 that a finite tip displacement was observed for the condition of zero ultimate pile capacity. This occurred because only one pass of the force pulse was considered. In reality, larger tip displacements would occur because of reflections and translation of the pile; at zero damping the displacement would be infinite (Kolsky, 1963). Therefore, in plots of hammer blows per inch versus ultimate pile capacity, as shown in Figure 4.1, the curve starts at the origin. This also explains the reverse curvature near the origin.

The pile tip model (Chapter 3) is used to investigate the effect of the first cycle of the force pulse. Displacement of the pile tip with a free-end condition due to the incident and reflected pulse can be readily determined by the expression:

$$\delta = 2 \frac{\text{Impulse}}{\rho c A} \qquad (4.1)$$

where δ is the maximum free-tip displacement. For the sine force pulses used in Figure 4.1, the displacement of the free-end tip can be written:

$$\delta_s = \frac{4\ F_p t_1}{\pi\ \rho c A} \tag{4.2}$$

where δ_s is the maximum free-tip displacement, F_p is peak force and t_1 is pulse duration.

As seen from Equation 4.2, the tip displacement for the high pile impedance is smaller than for low pile impedance. Longer durations associated with lower pile impedances cause a larger net set, or a smaller number of hammer blows. Therefore, more reverse curvature near the origin is noted for high pile impedance than low pile impedance. The calculated tip displacements (Equation 4.2) matched the displacements determined in Chapter 3 (Equation 3.6).

The effect of energy losses such as mechanical and transmitted is important to the pile response. The determination of the mechanical losses and the corresponding energy at impact were previously discussed. More information is needed on hammer efficiencies for the purpose of improving input data to wave equation analyses.

The transmitted energy is a function of the impedance ratio, $I_R = \frac{\rho c A}{\sqrt{m_1 k}}$, and the coefficient of restitution of the hammer cushion. For normal drivehead weights the condition of maximum energy transmission occurs when I_R equals 0.6 to 1.1. For high impedance ratios, transmitted energy is reduced because of ram rebound, whereas the low impedance ratio causes a slower rate of energy transmission. Energy losses increase with a decrease in the coefficient of restitution of the cushion material. Coefficients of restitution ranging from 1 to 3/4 (equivalent to an aluminum-micarta cushion) yield energy losses of 0 to 20%, respectively,

whereas coefficients of 1/2 to 1/3 (equivalent to a wood cushion) yield energy losses of 20 to 40%, respectively.

Lost energy can not drive piles, but losses can be minimized by ensuring proper hammer operation and proper match of the hammer and pile. The hammer cushion plays a vital role in energy transfer; an ideal cushion would have a coefficient of restitution equal to unity (no hysteresis). All present cushion materials exhibit hysteresis; soft materials such as wood lead to the highest energy losses. A more efficient low-stiffness cushion than wood could be obtained by the use of a longer aluminum-micarta stack, or possibly by the use of other materials.

Field Study 1. This field investigation exemplifies the improvement of driving efficiency with greater hammer energy. Of course, this greater hammer energy should not cause pile damage.

The soil profile consists of 10 ft of alluvium, dense sand and gravel, underlain by a very dense sand with thin layers of silty clay. The piles were 14BP89, 90 ft long. Some were driven with a Vulcan 08 and some with a Vulcan 014 hammer. Both hammers had a standard aluminum-micarta cushion. Test drives with the two hammers were made 15 ft apart. The driving records are shown in Figure 4.2. The Vulcan 014 hammer has a rated energy approximately 60% greater than the Vulcan 08, and the driving records indicate an improved driving efficiency for the Vulcan 014 approximately proportional to the difference in the rated energies.

Results of a wave equation analysis shown in Figure 4.2 are in accord with the driving records and the effects of greater input energy. On the basis of the final driving resistance at an elevation of 206 ft, the wave equation analysis predicts a capacity of 250 tons for the pile driven with the Vulcan 014 hammer and 210 tons for the pile driven with

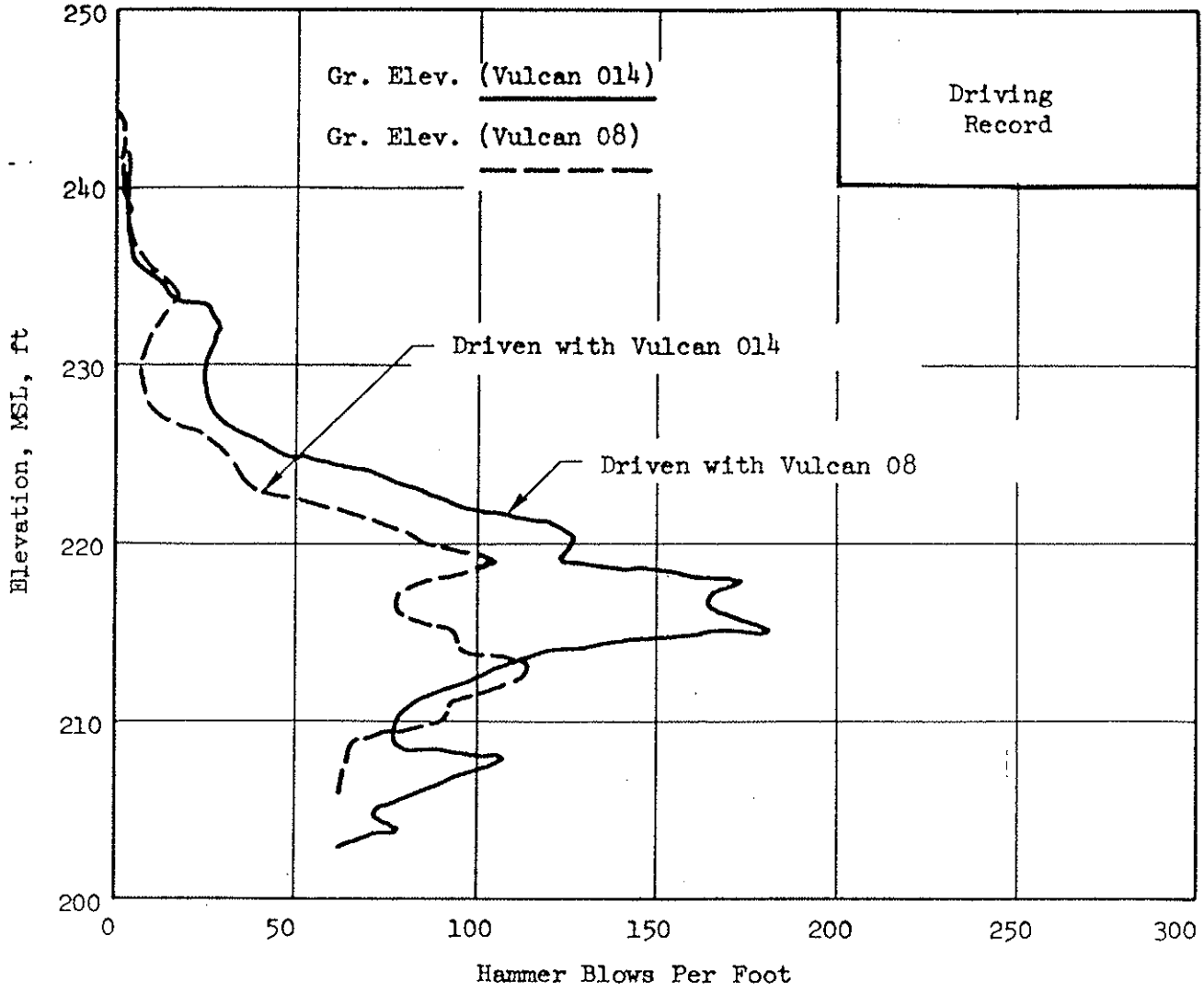

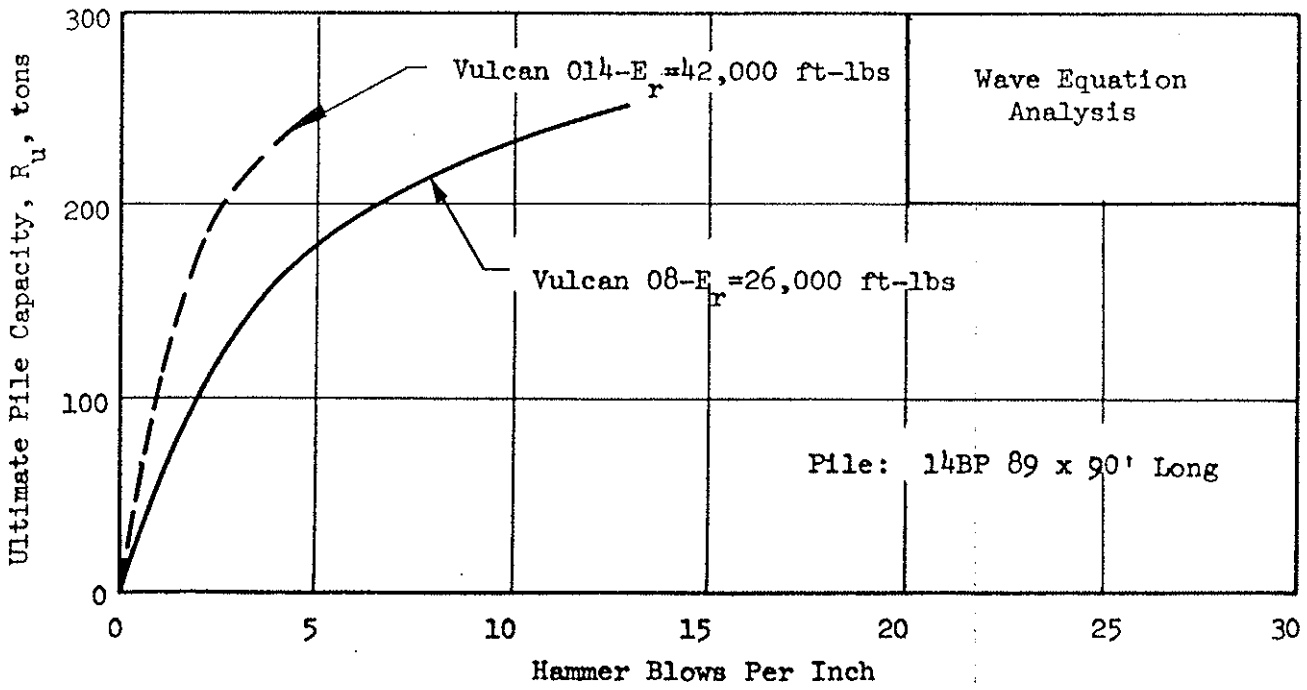

Figure 4.2 FIELD STUDY 1-EFFECT OF INPUT ENERGY ON PILE RESPONSE

the Vulcan 08. (This discrepancy may be accounted for by variations in soil profile; no load tests were performed.) Thus, the wave equation analysis has the ability to treat properly major changes in the variables.

Generated Force Pulse

Energy is not the only consideration for the determination of pile driving behavior; the form of the generated force pulse can be variable for a given energy input. The relative shape of the force pulse, whether a high peak value with short duration or a low peak with long duration, has an important influence in overcoming the soil resistance and achieving pile penetration.

As determined in the parameter study of Chapter 3, the force pulse with a longer duration for a given energy level is more efficient for penetration (more set per blow) when the peak pile force is equal to or greater than the soil spring resistance. When the peak pile force is less than the soil spring resistance, penetration efficiency is larger for the largest peak forces; duration is not critical in this case. The penetration will be completely elastic when the peak force is equal to or less than one-half the soil spring resistance.

The behavior pattern of a point bearing pile driven with various force pulses is illustrated by the example in Figure 4.3. This example assumes a pile impedance of 3000 $\frac{\text{lbs-sec}}{\text{in.}}$ and an energy level of 12,500 ft-lbs. The generated force pulse with the longer pulse length and smaller peak force is more efficient for driving at low soil spring resistances; however, maximum pile capacity can be obtained with the larger peak force. This example points out the improvement in driving efficiency with high peak forces at high soil resistances.

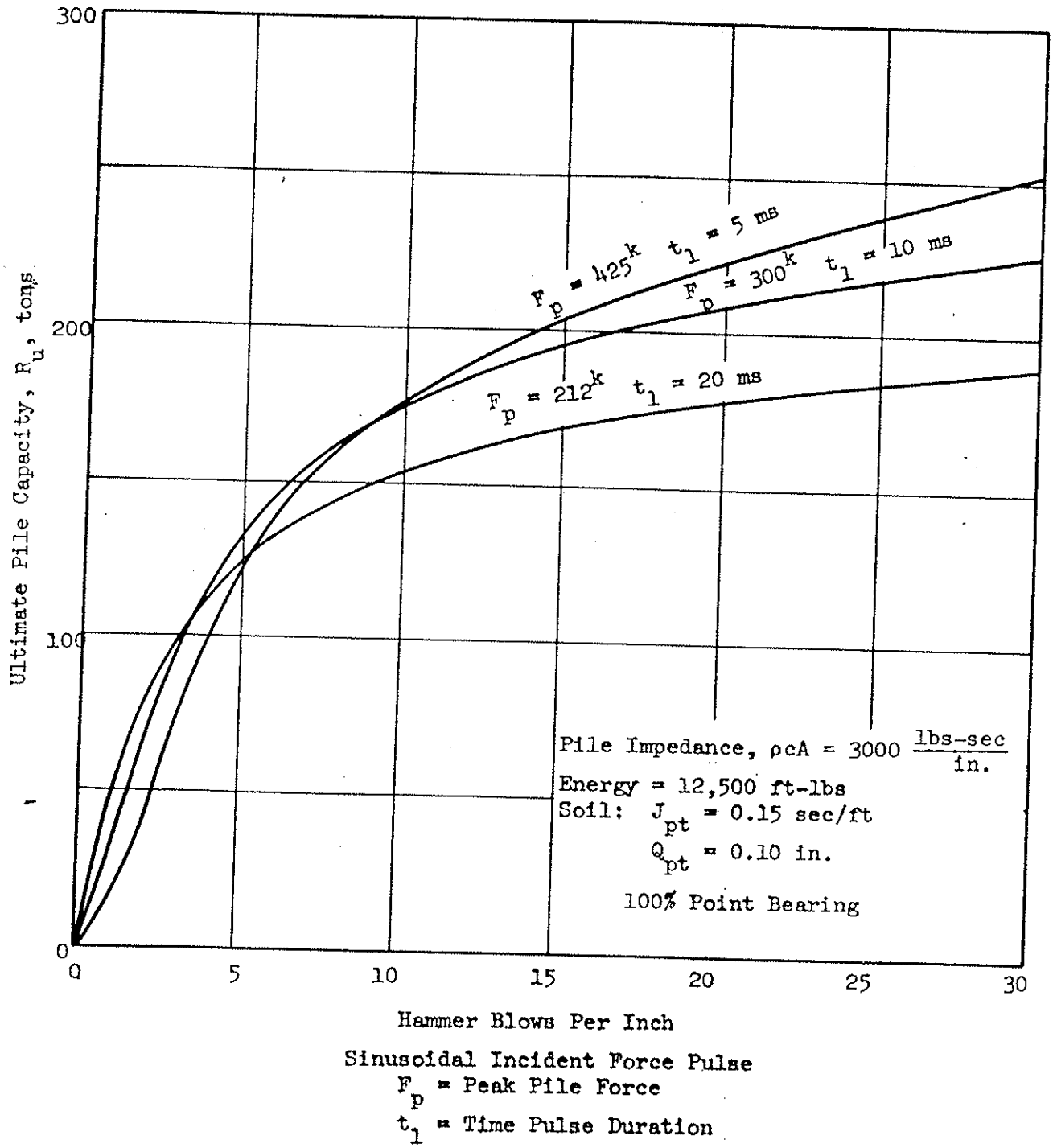

Figure 4.3 EFFECT OF GENERATED FORCE PULSE ON PILE RESPONSE FOR A GIVEN ENERGY LEVEL

An extreme example of the foregoing behavior pattern is shown in Figure 4.4 for a pile impedance of 6000 $\frac{\text{lbs-sec}}{\text{in.}}$ and an energy of 6,250 ft-lbs. This example typifies the behavior pattern when the input energy is too low for practical driving. At driving resistances beyond the practical limit (10 to 20 blows/inch), efficiency is higher for the force pulse with the longer duration. However, the pulse with the higher peak force still becomes the most efficient, eventually, but only at extremely high driving resistances. Thus, as a general rule, for easy driving the pulse length is important, whereas for hard driving the peak force is important for driving efficiency provided sufficient input energy is available.

The force pulse can be varied by varying hammer parameters (see Chapter 2). Energy at impact can be written in the following form:

$$\text{Energy @ Impact} = \frac{1}{2} m_1 V_o^2 \qquad (4.3)$$

where m_1 is ram mass and V_o is the ram velocity at impact. For the same input energy, an increase in ram mass by a factor α results in a decrease in ram velocity by a factor $1/\sqrt{\alpha}$; therefore, both ram weight and velocity are variables that should be investigated in relation to the generated pile force pulse. Ram velocity is directly proportional to pile peak force provided the pile behaves elastically; however, the duration of the pulse is independent of ram velocity (Chapter 2).

The ram weight affects both peak force and pulse duration. The pulse length can be approximated by the expression $t_d = \pi\sqrt{\frac{m_1}{k}}$, Equation 2.17, therefore, an increase in ram weight by a factor of 2 causes an increase in pulse length by a factor of 1.41. For the same height of fall or impact velocity the heavier ram increases the peak pile force

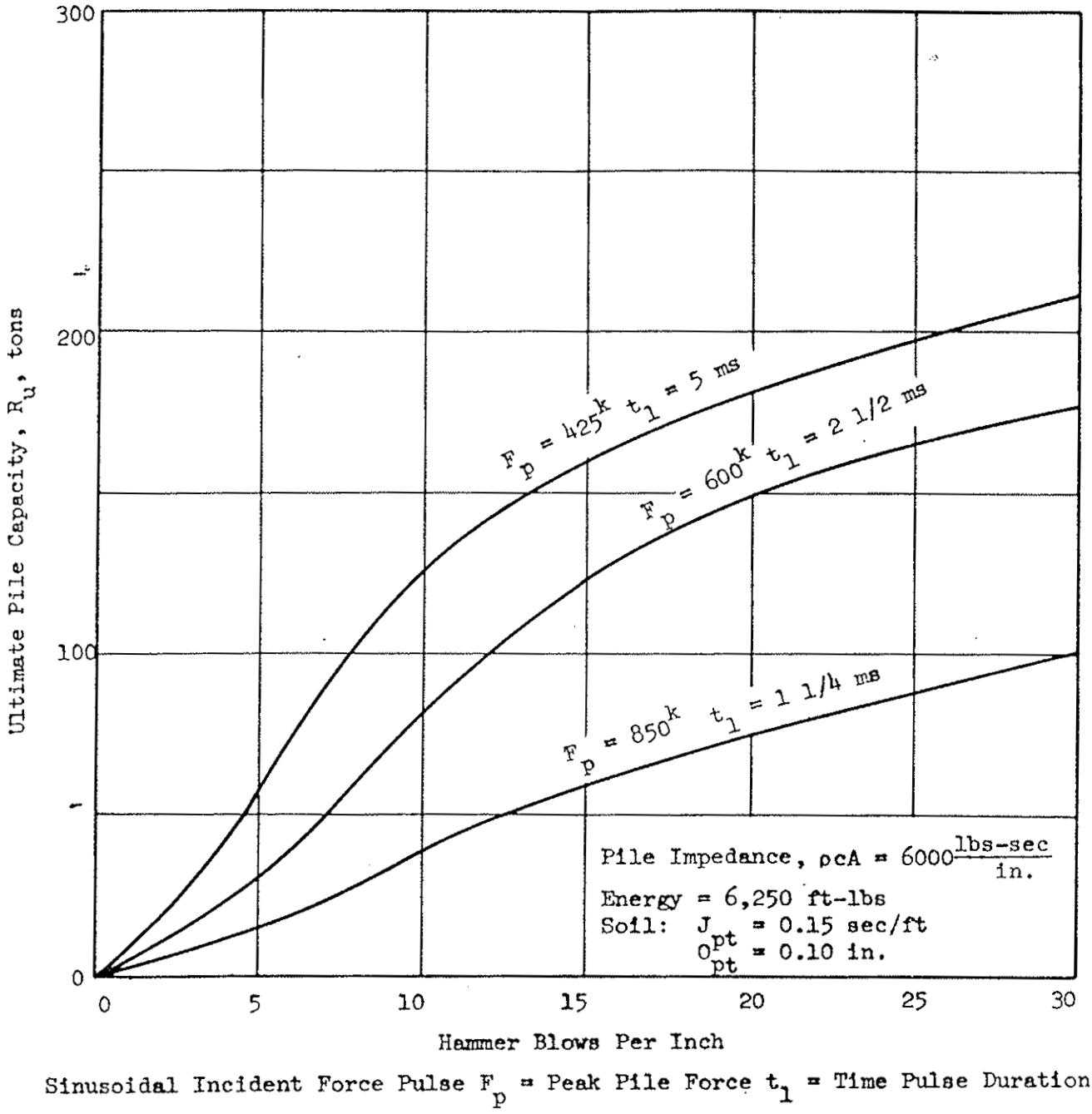

Figure 4.4 LACK OF PILE ENERGY TO PRODUCE EFFICIENT DRIVING FOR HIGH PILE PEAK FORCES

(Figure 2.10); however, this increase in peak force is minimized at low pile impedance. For example, consider the study of the nonlinear and inelastic cushions (Chapter 2) for the Vulcan 1 and Vulcan 010 hammers with ram weights of 5,000 and 10,000 lbs, respectively. The peak force increases approximately 10% with the increase in ram weight at a low pile impedance of 725 $\frac{\text{lbs-sec}}{\text{in.}}$. At a high impedance of 8700 $\frac{\text{lbs-sec}}{\text{in.}}$, the peak pile force increases approximately 25%.

The hammer cushion is a transmitting element; however, the cushion properties can be readily changed in order to shape the force pulse as well as to achieve an impedance match of pile and hammer. As a practical matter, the hammer cushion is one of the most important items in pile driving because it can be easily changed in order to achieve the desired driving force pulse. An increase in cushion stiffness causes an increase in pile peak force; however, there is a limit beyond which peak force is not significantly improved (Figure 2.10). This stiffness limit increases as the pile impedance increases, and decreases with an increase in ram weight (See Table 2.2).

The pulse length is inversely proportional to the square root of the cushion stiffness as shown in Equation 2.12. This means that an increase in cushion stiffness by a factor of 2 decreases the pulse length by a value of 1.41. Also, inelastic behavior of the cushion causes a decrease in pulse duration; this trend increases with an increase in degree of cushion inelasticity (Table 2.3). The effect of cushion inelasticity on peak force is minimal except for the condition of low pile impedance and coefficients of restitution less than 0.5.

For typical drivehead weights, equal to 1/3 to 1/10 of ram weight, the peak force is approximately independent of drivehead weight; however,

the pulse duration is larger with a decrease in drivehead weight for the matched and low pile impedance conditions.

Field Study 2. This field investigation points out the importance of shaping the generated force pulse with respect to a given hammer energy input. In this case history, the change in the force pulse was accomplished by changing the hammer cushion material.

A pile job was being successfully accomplished with precast concrete piles (design load of 75 bons) driven with a Link Belt 520 hammer. The 50 ft concrete piles had a 16 in. square butt and 10 in. square tip and were driven into 10 to 20 ft of silty clay underlain by silty sand and gravels. Two pile load tests were performed and the desired ultimate capacity of 150 tons obtained at an embedded length of 50 ft. The Link Belt 520 hammer with a standard aluminum-micarta cushion plus a pile cushion consisting of a 2 inch oak block with rubber belting drove each pile in 15 to 20 minutes. However, the Link Belt hammer broke down and was replaced with a Vulcan 1 hammer.

Pile driving was continued with the Vulcan 1 hammer and a standard wood cushion (oak) during repair of the Link Belt hammer. Driving was accomplished to the desired penetration depth of 50 ft; however, the driving time, on the order of 60 to 80 minutes, was excessive. Upon changing to an aluminum-micarta cushion assembly, the driving time decreased 30 to 40 minutes per pile. The results of the wave equation analysis for the Vulcan 1 hammer with aluminum-micarta cushion assembly and a wood cushion assembly are shown in Figure 4.5. The wave equation analysis readily shows the effect of the different cushion materials. The stiffer cushion (aluminum-micarta) results in higher generated peak forces as well as higher efficiency of energy transmission to the pile;

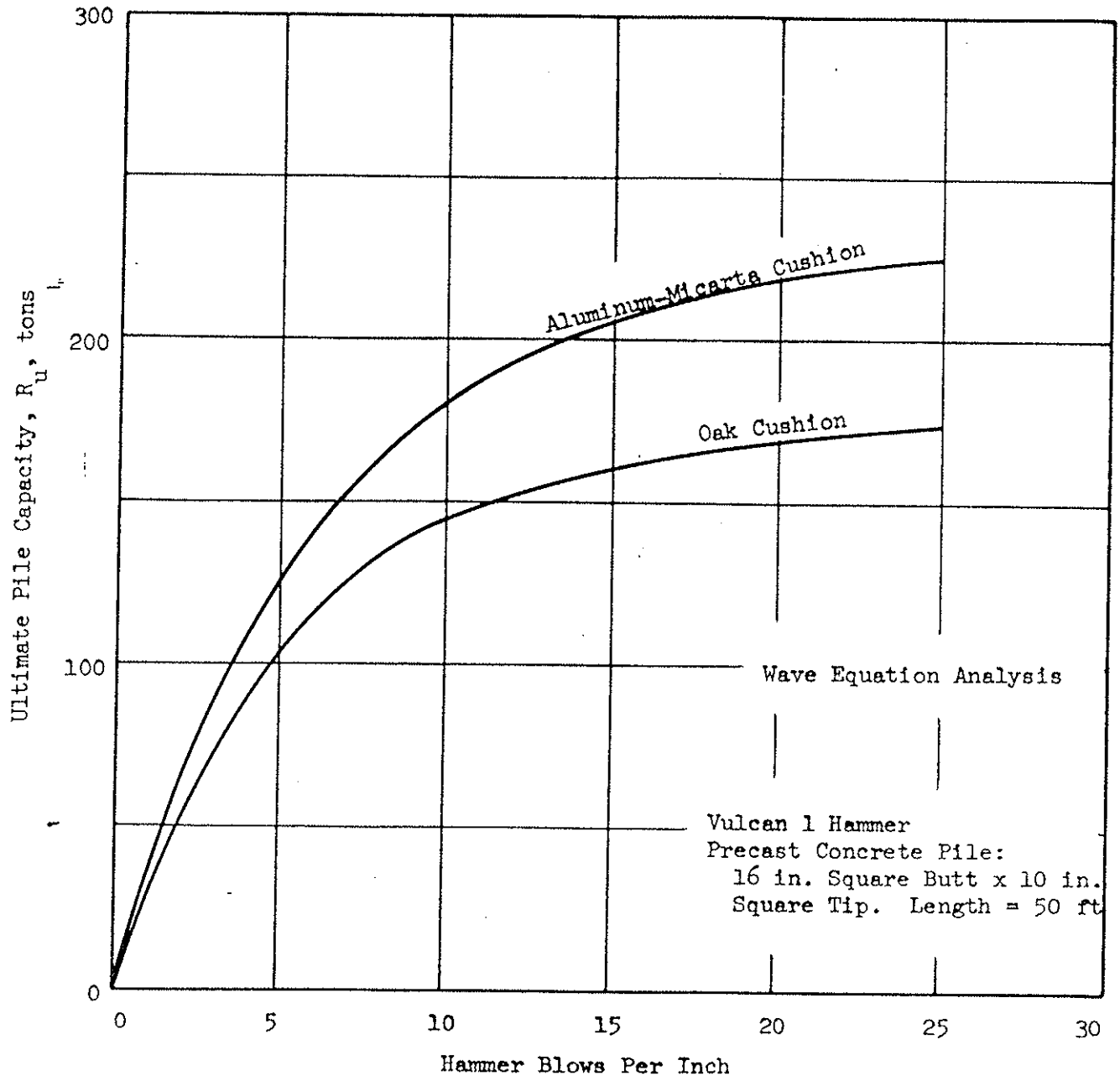

Figure 4.5, FIELD STUDY 2 - EFFECT OF HAMMER CUSHION ON PILE DRIVING

therefore, faster and easier driving is to be expected. If it is assumed that the pile has a certain ultimate capacity at 50 ft of penetration, it can be seen from Figure 4.5 that such capacity will always be obtained with fewer blows/inch with the aluminum-micarta cushion. The field driving records fully supported the analytical results; driving times with the aluminum-micarta cushion were approximately one-half that for the wood cushion.

4.3 Pile

In addition to its static load carrying function, the pile must also transmit an incident force pulse which is capable of overcoming the soil resistance. The capability of the pile to transmit the force pulse required to achieve the desired penetration is a function of pile impedance or area. Factors that influence impedance such as structural damage or a change in the pile cross-section must also be considered. Boundary conditions due to the finite length of real piles will be considered in this discussion.

Impedance or Area

The impedance match of hammer and pile for maximum energy transmission has been previously discussed and will not be repeated here; however, the effect of pile impedance on the force pulse will be evaluated. For given hammer conditions, an increase in pile impedance causes an increase in peak force (See Figure 2.10). This behavior means that a higher impedance pile is capable of transmitting a higher peak force. The limit on the peak force would be governed by the dynamic yield properties of the pile material, and pile damage would ensue if the yield

stress is exceeded. Damage can significantly alter driving characteristics; this effect will be discussed later in this section. In the following discussion it is assumed that the pile behaves elastically.

The force pulse length is inversely proportional to pile impedance, i.e. pulse length decreases with an increase in pile impedance. Long time pulses and low peak forces are associated with smaller pile impedances, whereas short pulses and high peaks prevail for larger pile impedances. This behavior suggests (Chapter 3) that the low impedance pile is more efficient (more set per blow) for driving at low soil resistance because of the longer pulse length. However, the high impedance pile is more capable of being driven to a high load capacity because of its ability to form and transmit high peak forces. The effects of pile impedance on the ability to drive to a given ultimate load capacity is shown in Figure 4.6 for the cases investigated in Chapter 3. The pile response shown in Figure 4.6 indicates the efficiency of the low impedance pile at low soil resistances, and the capability of the high impedance pile to achieve a high load capacity.

The importance of pile impedance can not be overemphasized. An optimum pile design involves a delicate balance; insufficient impedance or area prevents achieving the desired pile performance, whereas too much pile impedance or area leads to an uneconomical design. The effect of pile impedance on pile driving will be illustrated by the following field studies.

Field Study 3. The soil profile consists of 10 ft of alluvium, dense sand and gravel, underlain by a very dense sand with thin layers of silty clay. Two steel piles with different areas were driven with a Vulcan 08 hammer and a standard aluminum-micarta cushion. One pile

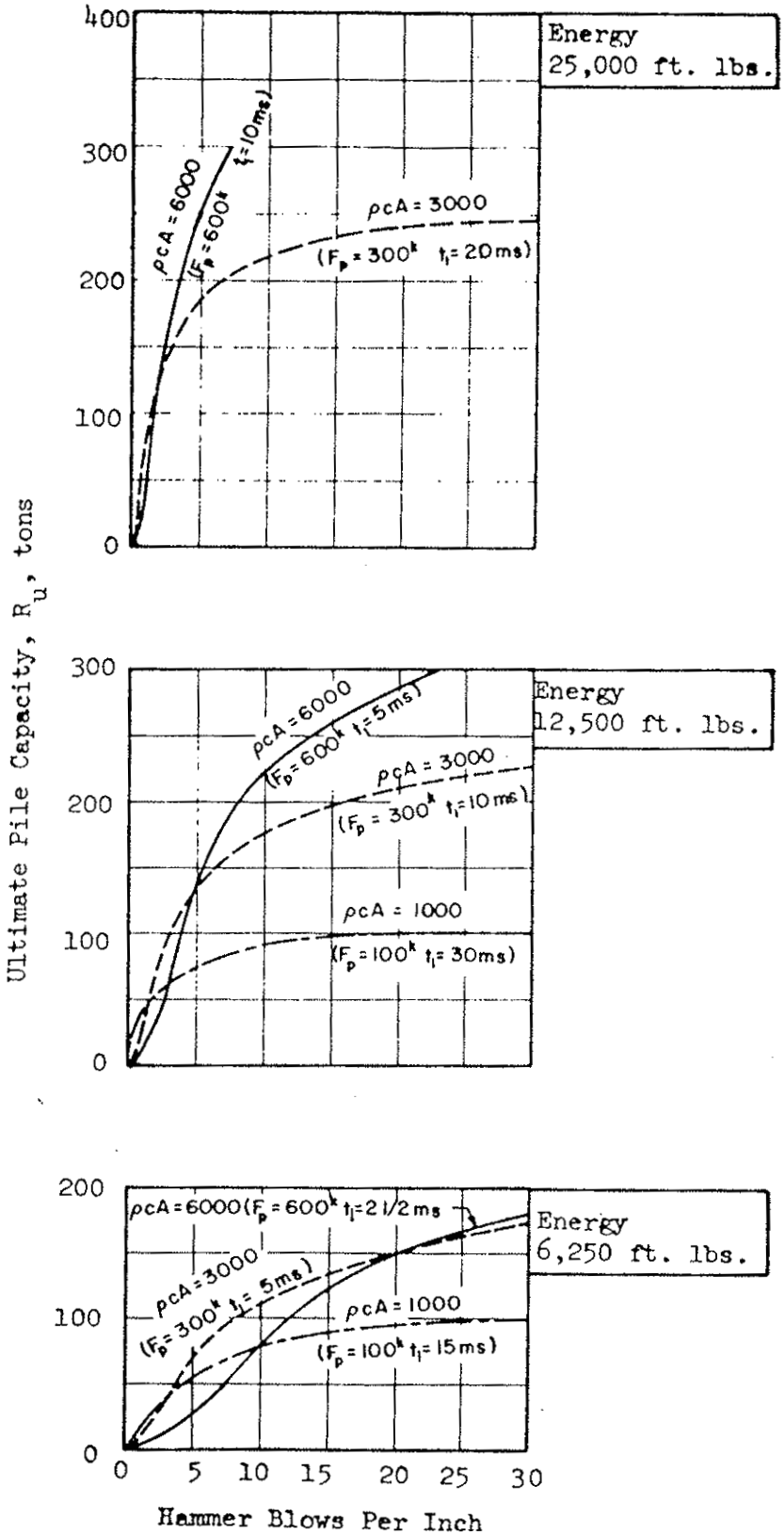

Figure 4.6 EFFECT OF PILE IMPEDANCE ON DRIVING CAPABILITY AT DIFFERENT ENERGY LEVELS

was a pipe 90 ft long of 14 in. OD by 0.375 in. wall thickness driven closed-end; the area of steel was 16.0 in.^{2}. The other pile was a 14 BP 89, 90 ft long with an area of 26.2 in.^{2}. The wave equation analysis shown in Figure 4.7 compares the behavior of the two piles. From the analysis, the pile with the greater area of steel has the ability to achieve a higher capacity and, therefore, greater depth of penetration. Driving records of these two piles, at a distance of 10 ft apart, indicate that the pipe pile achieved maximum penetration at an elevation of 224 ft and a depth of 24 ft, whereas the BP section was driven to a depth of 40 ft (Figure 4.7). The driving records and analysis are in general agreement. No load tests were performed.

Field Study 4. This field study covers two case histories that will show how an increase of pile impedance after the piles were driven made it possible to obtain the desired ultimate load capacity. In both cases, pipe piles were driven to high resistances, but were unable to obtain the desired load capacity. Greater penetration and thus higher load capacity were obtained by redriving the piles after concreting. Pile impedance is increased by concreting.

In the first case history, the soil profile consists of 107 ft of medium clay underlain by sand. Pipe piles 8 5/8 in. by 0.250 in. with closed ends, 110 ft long, were driven with a Vulcan 06 hammer and a standard wood cushion block. The piles were designed for an ultimate capacity of 100 tons, and were driven to 4.5 blows per inch. The wave equation analysis shown in Figure 4.8 predicts a capacity of 70 tons at 4.5 blows per inch, and indicates that the required 100 tons could not be achieved with the pile selected. Several load tests failed at 80 tons, or 20 tons less than required. Driving the piles deeper into

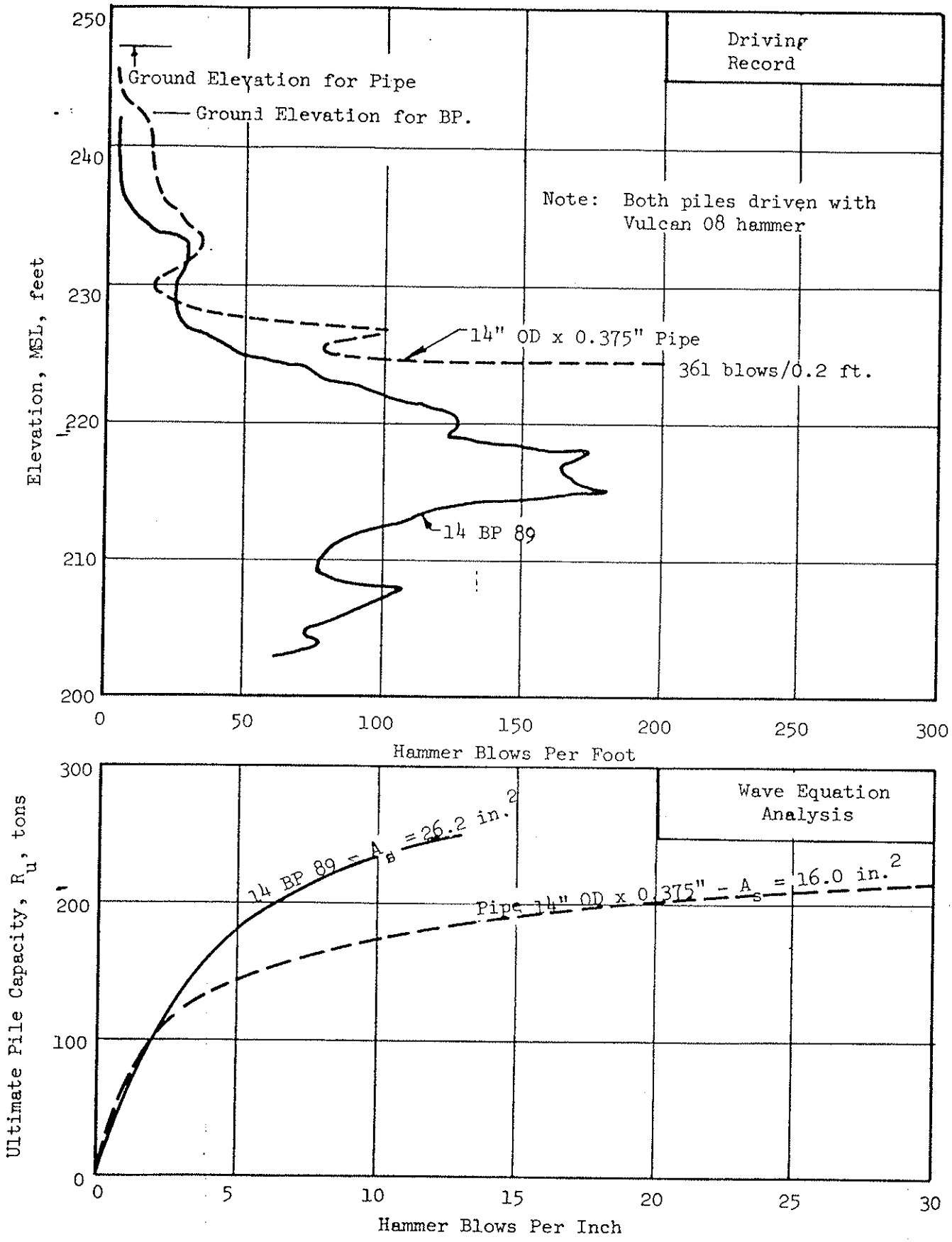

Figure 4.7 FIELD STUDY 3 - EFFECT OF PILE AREA ON DRIVING CAPABILITY

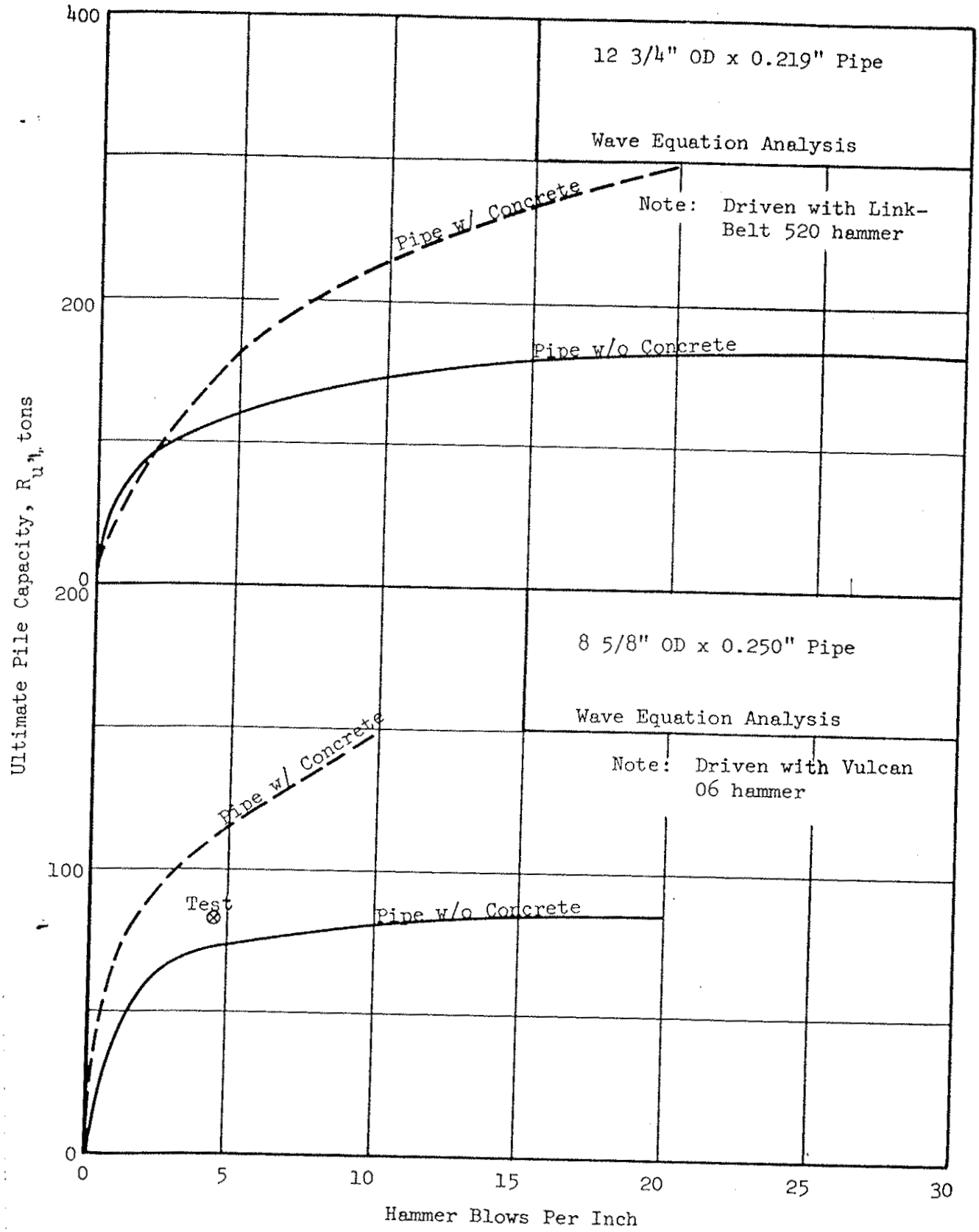

Figure 4.8 FIELD STUDY 4 – CONCRETING PIPE PILES TO IMPROVE IMPEDANCE AND ACHIEVE THE DESIRED CAPACITY

the sand was the most desirable solution. This could be accomplished by concreting to improve pile impedance before redriving. The piles were concreted and redriven with a Vulcan 06 hammer to the required depth and ultimate capacity. A comparison of the pipe pile with and without concrete as shown in Figure 4.8 clearly shows the benefit of the improved impedance.

In the other case history, the soil profile consists of 25 ft of clayey silt underlain by 60 ft of medium sand and 10 ft of dense sand and gravel overlying interbedded layers of limestone and shales with possible clay seams. The piles were pipe 105 ft long with 12 3/4 in. OD x 0.219 in. wall thickness designed for an ultimate capacity of 200 tons. All piles were driven with a Bodine Resonant Driver. The piles driven to sound bedrock satisfied the load capacity requirement; however, the desired capacity could not be achieved in the weathered bedrock zones. In order to obtain the high peak forces necessary for further penetration a Link-Belt 520 diesel hammer was chosen. Driving on the pipe pile alone produced only elastic deformation with no penetration. However, after concreting, the pipe piles were successfully driven to the desired capacity. The wave equation analysis of the pipe with and without concrete, as shown in Figure 4.8, clearly indicate the greater ability of concreted piles with respect to achieving penetration and load capacity.

Field Study 5. This field study will show how the wave equation analysis was used to explain inconsistencies in a mandrel driven pile. A mandrel driven pile consists of a thin-wall pipe or shell driven with a heavy wall pipe core; the core is commonly referred to as a mandrel. After driving, the mandrel is removed and the thin-wall pipe or shell left in the ground for concreting. Therefore, use of a mandrel is an

effective means of obtaining the impedance required during driving, whereas a minimum amount of steel (and money) can be left in the ground after driving by removing the mandrel core.

The soil profile consists of 17 ft of silt size ash underlain by 30 ft of sand and gravel grading from medium to dense. The sand and gravel are underlain by 10 ft of layered silt and clay and 45 ft of very dense sand and gravel overlying shale. Thin-wall pipe piles 12 in. OD by 0.141 in. wall thickness were driven with a 115 plf mandrel 49 ft long. The hammer was a Link Belt Model 440 with a standard aluminum-micarta cushion. The desired ultimate capacity was 180 tons, and the design load was 75 tons.

A test pile was driven to a depth of 34 ft at a resistance of 43 blows per inch. The load test was unsatisfactory; failure occurred at 125 tons. The effect of driving the pipe pile with and without the use of the mandrel was determined by using the wave equation analysis shown in Figure 4.9. The analysis clearly shows that the mandrel was not effective in transmitting the pile force; therefore, the thin-wall pipe was transmitting the pulse because the mandrel probably was not in contact with the pile tip. To be effective, it is necessary that the mandrel simultaneously engages both top and tip of the pile so that the mandrel and tip will drive together.

In order to prove whether or not the mandrel was being effectively used, comparative drives were made with and without a 3/4 inch spacer plate at the pile tip. The drive without the plate penetrated to a depth of 38 ft and a resistance of 12 blows per inch. The pile driven with the 3/4 inch plate penetrated to a depth of 46 ft at a driving resistance of 9 blows per inch. Gross set was measured during driving; a set 0.56 in.

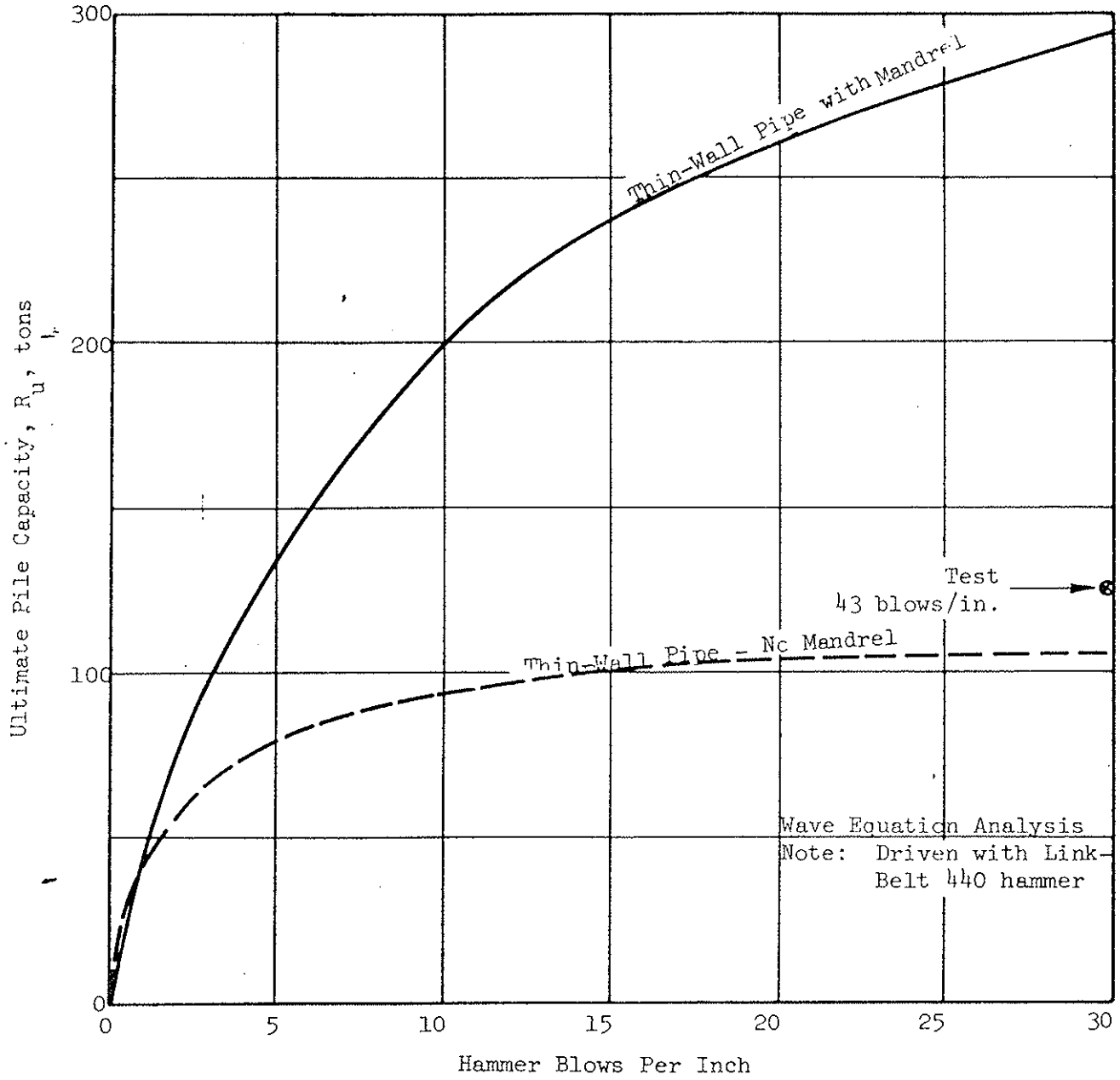

Figure 4.9 FIELD STUDY 5 - EFFECT OF MANDREL ON PILE DRIVING

was observed for the pile driven without the 3/4 inch plate, and 0.28 in. with the plate, both in accordance with predictions from the wave equation analysis. Thus, the wave equation analysis fully predicted the differences between the two driving systems. This field study and analysis also clearly shows that the capability of the pile to transmit the force pulse required to achieve the desired penetration is a function of pile impedance.

Cushioning Effect

A change in the pile cross-section will affect the pile impedance and can produce a cushioning effect. For example, compare the wave equation analysis of a 125 ft pipe pile with and without a change in the pile tip section (Figure 4.10). The pipe is 14 in. OD by 0.500 in. wall thickness and the tip section is 30 ft long of 14 in. OD by 0.188 in. wall thickness. The pile with the smaller tip cross-section has the effect of lowering the pile impedance; therefore, a cushioning effect exists. The analytical comparison clearly shows that greater penetration and higher load capacity is achieved with the higher pile impedance (without smaller cross-sectional area of tip section).

Also, pile damage caused by driving has the effect of lowering pile impedance in the damaged zone; this will be referred to herein as a cushioning effect. The damaged zone or smaller impedance section of the pile controls transmission of the force pulse. The field problem discussed herein will exemplify the cushioning effect caused by pile damage.

Field Study 6. The soil profile consists of 13 to 24 ft of fill including silt, clay, bricks, etc., underlain by stiff clay. The bedrock is at an average depth of 30 ft and consists of soft shale and lime-

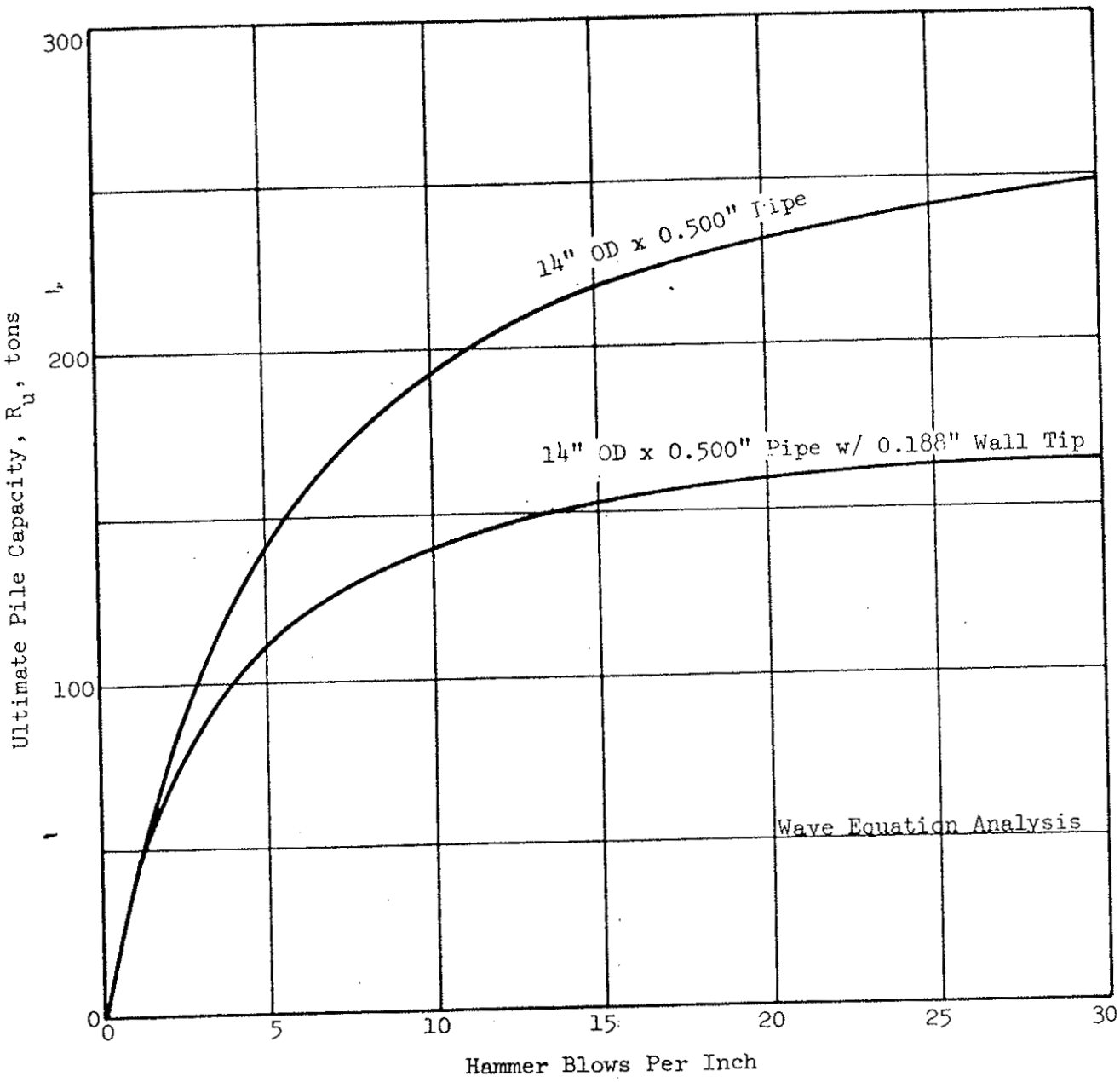

Figure 4.10 EFFECT OF DIFFERENT PILE IMPEDANCE WITHIN PILE LENGTH

stone. The piles were 10 BP 42 with a design load of 75 tons; they were driven with a Delmag D12 using a standard oak cushion. Pile load tests failed on piles driven to less than 40 blows per inch; however, the wave equation analysis indicated that the required resistance (150 tons) could be reached at 11 blows per inch (Figure 4.11).

The foregoing discrepancy between theory and test indicated that a cushioning effect could have resulted from pile damage since the tips were not reinforced and the piles were encountering bricks, etc. The effects of damage can be estimated by the wave equation analysis; for this purpose the lower pile segment was assumed to have 10 percent of its original stiffness. The comparison of predicted behavior for the damaged and the undamaged pile section clearly shows that the damaged pile could not achieve the required 150 ton ultimate load capacity (Figure 4.10). Several piles were pulled and revealed damage such as warping, bending, etc., as expected and foreseen by reference to wave propagation analysis.

Length

Pile length affects the generated force pulse shape with respect to reflections from the pile tip. Reflections can support or interfere with the incident force pulse. The pile length required for freedom from reflection interference is directly proportional to the pulse duration, which is a function of hammer weight, cushion stiffness and pile impedance. The pulse duration increases with larger ram weight and decreases with larger cushion stiffness and pile impedance. A longer pile has a better chance of transmitting a generated force pulse without interference than a short pile; however, the effect of reflections can aid or retard pile penetration depending on the relative impedance of the pile and the soil resistance.

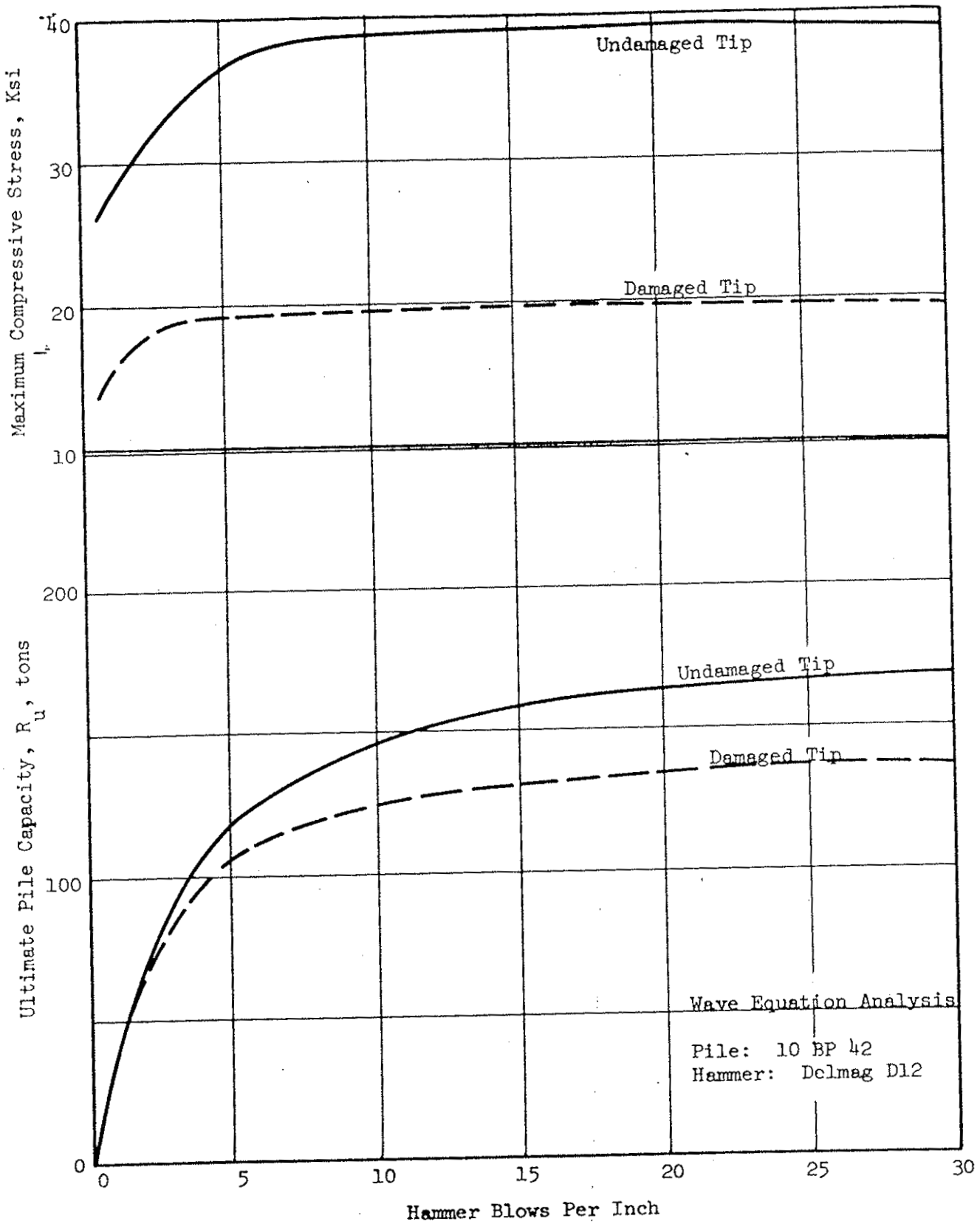

Figure 4.11 FIELD STUDY 6 - EFFECT OF DAMAGE ON PILE DRIVING

For high pile impedance, the force pulse duration is short; therefore, reflections will not significantly alter the generated force pulse even for short piles. This behavior of high pile impedance indicates the driving resistance will probably not be significantly different for a short or long pile. However, the pulse length duration is long for low pile impedances and the effect of length can aid or retard the generated force pulse. For the short pile and low pile impedance, the reflections will likely be compressive and add to the generated force pulse. For the long pile, the effect of reflections will be a separate pulse and will not add directly to the generated force pulse. This behavior of the low pile impedance indicates the short pile will probably drive more efficiently than the long pile.

The behavior of pile length for high and low pile impedances can be shown by a particular example. Consider variable steel pile areas of 5 and 40 $in.^2$ (725 and 5800 $\frac{lbs\text{-}sec}{in.}$ pile impedances, respectively), driven with a Vulcan No. 1 hammer. The pile lengths are 20 and 160 ft, and the soil resistance is considered at the pile tip only. The wave equation analysis of the combination of impedances and lengths are shown in Figure 4.12. The behavior of the piles as shown in Figure 4.12 indicates slightly more efficient driving for the longer pile than the shorter pile with high impedance; however, the difference in driving behavior between the two lengths is not significant. For the low pile impedance, the shorter pile drives much more efficiently than the longer pile.

The difference in driving efficiency of the long and short pile can be illustrated by the force-time relationship, both generated and reflected, at the head of the pile. For the high pile impedance, con-

WAVE EQUATION ANALYSIS

Job _____ Date August 1970 J _____

Location _____

Pile Steel - Low Impedance = 725 lbs-sec/in. Area 5 in.^{2} Length 20 & 160 ft

Pile Steel - High Impedance = 5800 lbs-sec/in. Area 40 in.^{2} Length 20 & 160 ft

Follower _____ Area _____ Length _____

Hammer Vulcan 1 Energy 15,000 ft-lbs e_f 70% Comb Force _____

Helmet (drive head) 1000 lbs Anvil _____

Cushion (hammer) Alum.-Micarta k 7x10^6 lbs/in. e 0.80 Q_{side} 0.10 J_{side} 0.05

Cushion (pile) _____ k _____ e _____ Q_{point} 0.10 J_{point} 0.15

Comments _____

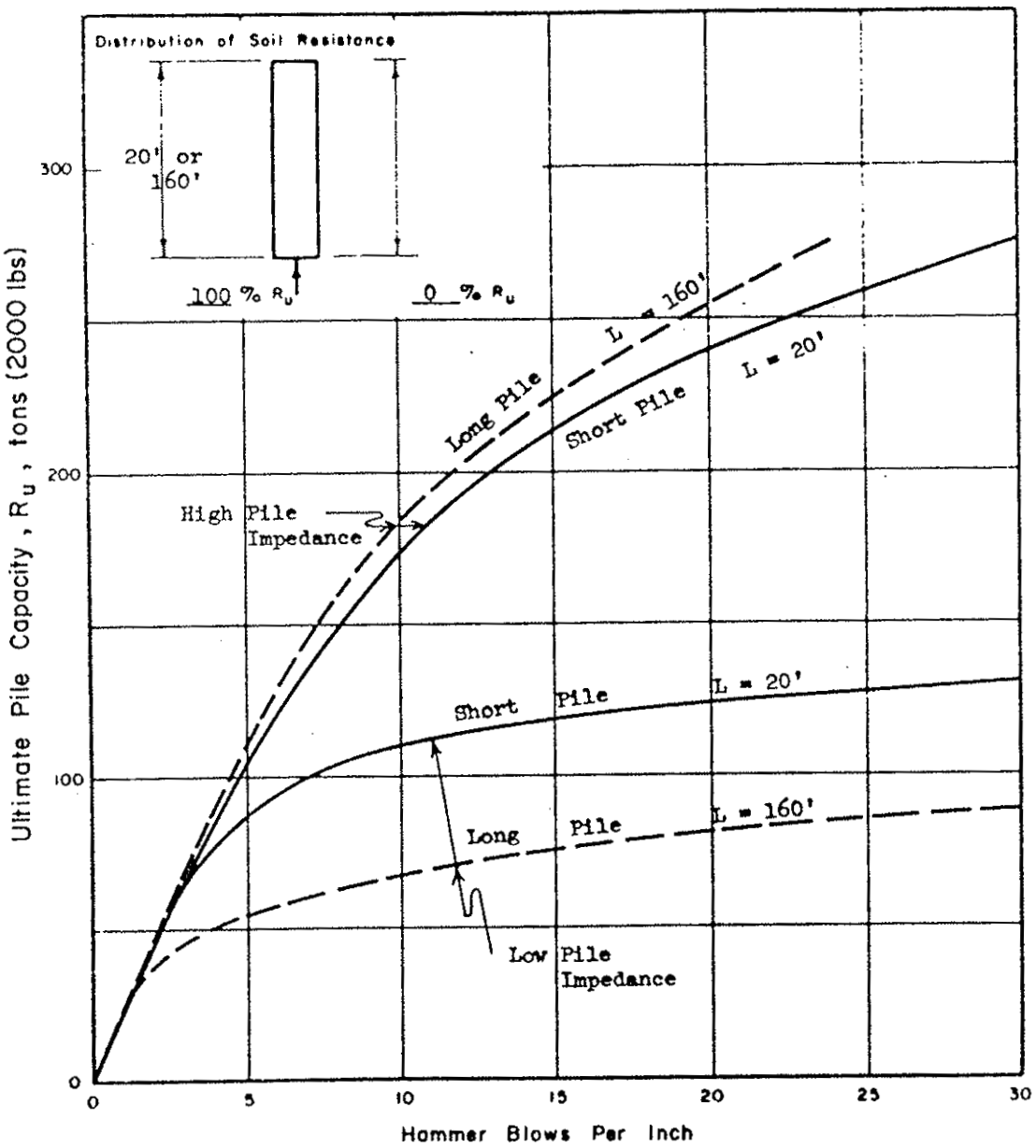

Figure 4.12 EFFECT OF PILE LENGTH ON DRIVING

sider the force pulse at the pile head for a soil spring resistance of 300 kips (Figure 4.13a). Comparison of the force pulses for the long and short pile indicate that only small differences exist when the force level is greater than the soil spring estimate resistance. However, the force pulse peak for the shorter pile was attenuated somewhat. This attenuation, as a result of tension reflection at the beginning part of the reflected pulse causes less efficient driving for the shorter pile.

For the low pile impedance and a soil spring resistance of 150 kips, the force pulse of the shorter pile has a higher peak and a long time duration above the level of the soil spring resistance (Figure 4.13b). The shorter pile has compressive reflections that add to the generated force pulse; whereas, the compressive reflections of the longer pile are separate and do not add the generated force pulse. This effect of reflections produces more efficient driving for the shorter pile than the longer pile at low impedances.

Mosley and Raamot (1970) presented wave equation analyses illustrating pile length behavior. Their results indicate a typical pattern of driving efficiency as shown in the example above; however, the difference in driving behavior was presented without explanation.

With the assumption of the same relative distribution of soil resistance along the sides and tip, irrespective of pile length, the following general conditions can be indicated: 1. For high pile impedances, driving efficiency between longer and shorter piles is not significantly different; however, longer piles will probably be slightly more efficient. 2. For low pile impedances, shorter piles will be more efficient than longer piles.

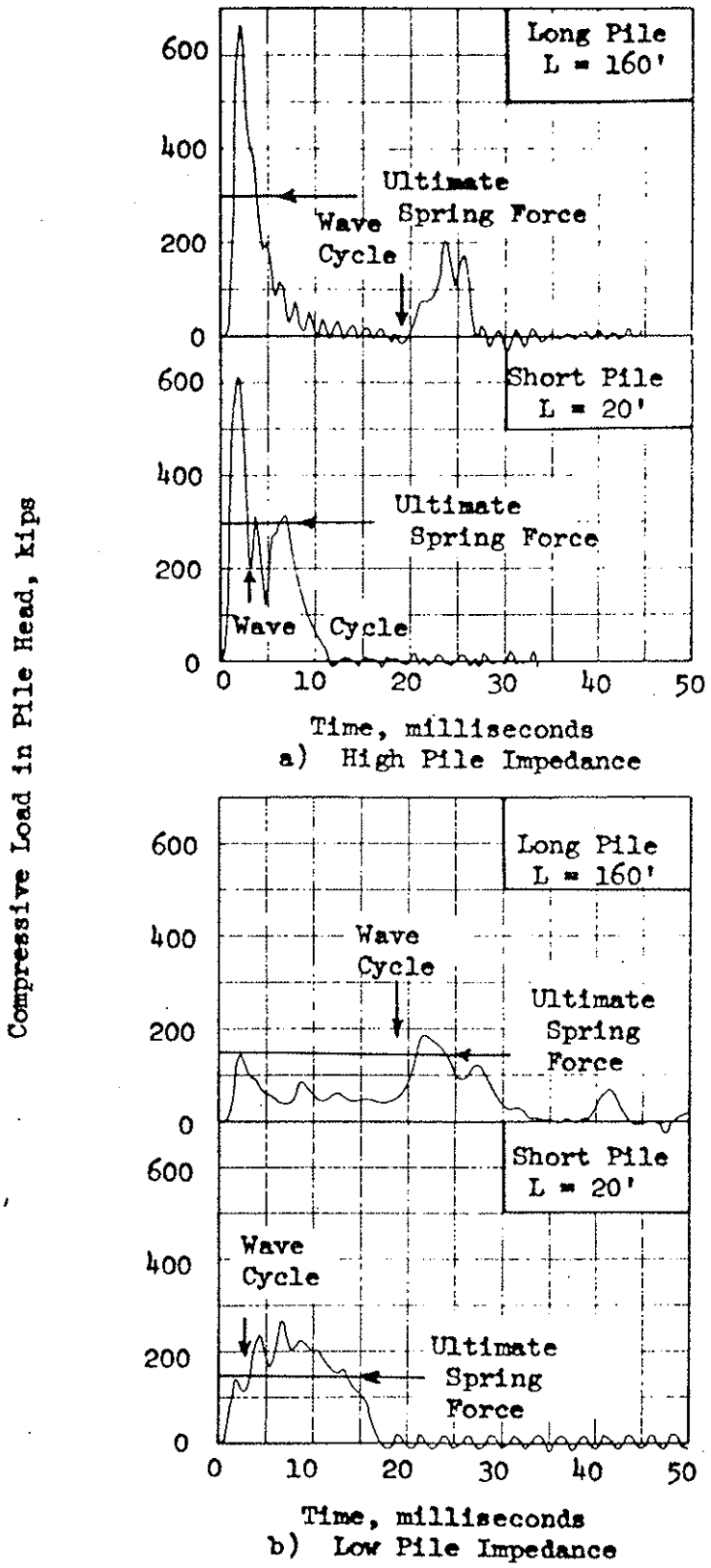

Figure 4.13 EFFECT OF PILE LENGTH ON FORCE PULSE

The behavior pattern based on pile length only is difficult because the real soil resistance distribution changes with depth. Real soil profiles are quite variable and the soil distribution as well as pile length must be considered for each individual case.

4.4 Soil Resistance

The soil provides the resistance which must be overcome by the incident force pulse in order to achieve penetration. The effect of the incident force pulse with respect to assumed resistance has been previously discussed; however, the effects of the soil characteristics in terms of the hammer-pile-soil system will be considered in this discussion. These soil characteristics include the effect of soil distribution, quake and damping, and freeze or relaxation.

Soil Resistance Distribution

Soil resistance distribution refers to the relative amounts of ultimate soil resistance at the pile tip and along the length of the pile. The soil resistance along the pile length attenuates the generated force pulse, and thereby decreases the effectiveness of the force pulse when it arrives at the pile tip. However, it should be recognized that the larger the percentage of side resistance, the smaller is the resistance at the point for a given total resistance.

For example, a friction pile derives almost all of its support from side friction; therefore, there is practically no resistance at the point and only a small pile tip force is necessary to cause penetration. By contrast, in a point bearing pile the generated force pulse is working against the total resistance at the pile point. Because of differences

in the physical mechanisms of soil failure along the pile and at the tip, the point resistance is assumed to possess higher damping than the side resistance; therefore, damping alone could cause more resistance to penetration at the pile point.

The differences in physical behavior between point bearing and skin friction can be explained very easily. If the frictional resistance acting on a given pile segment (increment of length) is examined, it is seen that the pile force pulse peak greatly exceeds the soil resistance. Thus, the force pulse can pass through many segments without serious attenuation. However, if all soil resistance is concentrated at the pile tip the large disparity between pile tip force and total soil resistance disappears, and efficiency of pile penetration diminishes (Chapter 3).

It is difficult to compare the driving resistance and load capacity in two different soil profiles, such as those wherein friction piles or point bearing piles are found; however, a field study coupled with a wave equation analysis can be presented to show the effect of driving through a soft layer to a point bearing layer.

Field Study 7. The soil profile consists of 107 ft of medium clay underlain by sand. Pipe piles 8 5/8 in. by 0.250 in. were driven closed-end with a Vulcan 06 hammer and a wood cushion. Driving resistance in the clay varied from 6 to 9 blows/ft, but final driving into the sand was at 3 to 5 blows/in. The wave equation analyses for driving in clay (10% point bearing) and into sand (70% point bearing) can be compared, as shown in Figure 4.14; 10% point bearing indicates that 10% of total soil resistance is assumed to occur at the pile tip. The comparative analysis shows the improvement of the driving efficiency for the friction pile (10% point bearing).

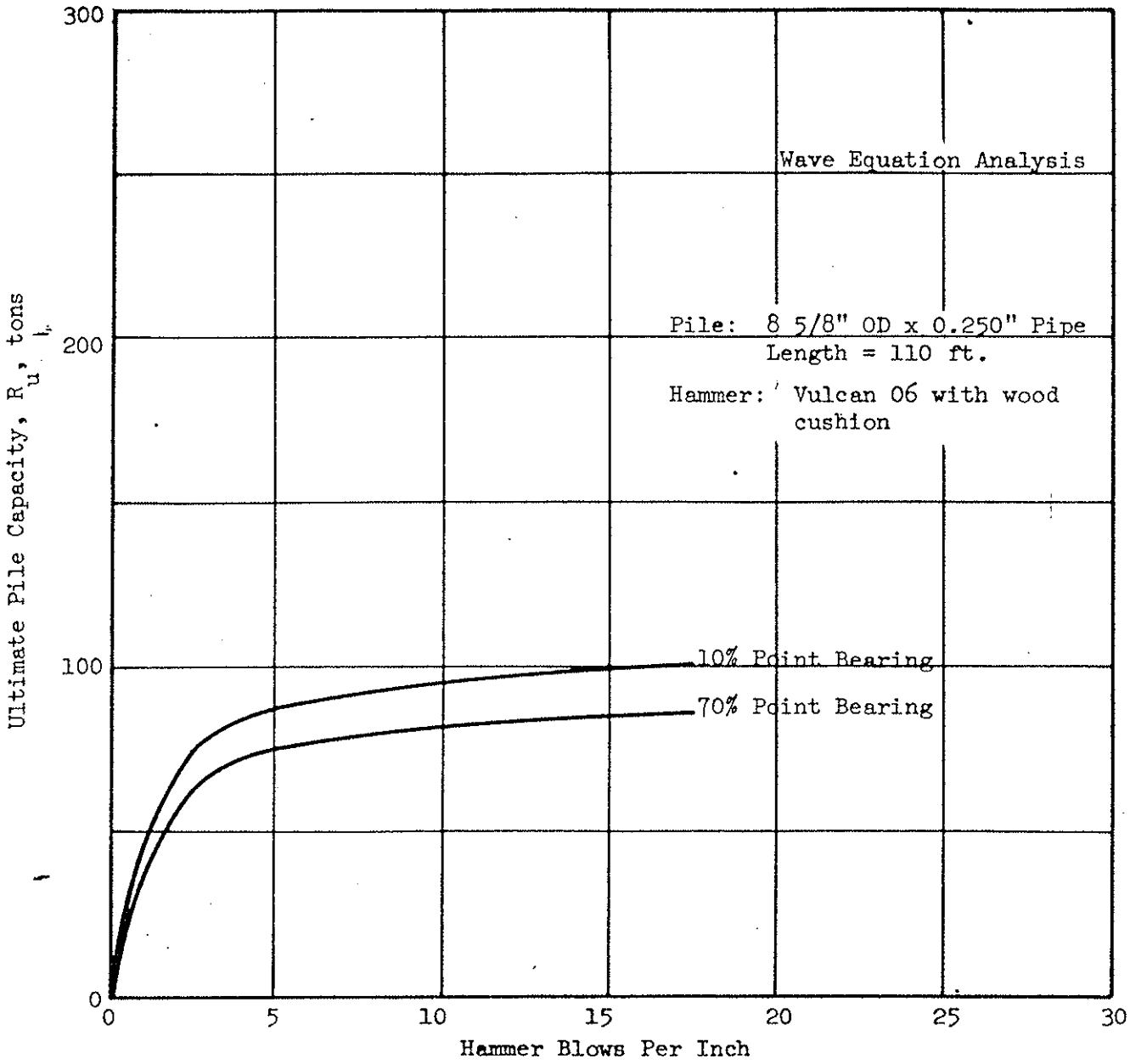

Figure 4.14 FIELD STUDY 7 - EFFECT OF THE PERCENTAGE OF POINT BEARING RESISTANCE

Also, the amount of friction can be estimated with the use of wave equation analysis. The friction amounts to 25 to 35 tons at a resistance of 6 to 9 blows/ft with an estimated total capacity of 70 tons at final driving.

Quake and Damping

An increase in both soil quake and soil damping decreases the effectiveness of a given pile force pulse. The effects of quake and damping have been discussed previously in Chapter 3; however, the effects at the pile tip will be briefly summarized herein with respect to the entire hammer-pile-soil system.

The soil quakes investigated previously with respect to an elastic-plastic soil spring cover the range of behavior for stiff and dense soils to soft or loose soils. The values of quake considered are 0.20 in., 0.10 in. and 0.05 in.; the higher quake values represent soft or loose soils, whereas the lower values represent stiff or dense soils. Several studies of field conditions indicate that a quake of 0.10 in. is a good average value. An investigation of the soil quake parameter is shown in Figure 4.15 for three different pile impedances, an input energy of 12,500 ft-lbs, and a damping constant, J_{pt}, equal to 0.15 sec/ft. Figure 4.15 clearly indicates the loss of driving capability and capacity with a corresponding increase in soil quake. Also, the effect of soil quake is more pronounced for higher pile impedances. For example, the difference in behavior with respect to quake for loose and dense soils is not significant at a pile impedance of 1000 lbs-sec/in. However, the difference is marked for a pile impedance of 6000 lbs-sec/in.

Field correlation of pile load tests with wave propagation analyses plus laboratory test results indicate that damping factors for clays

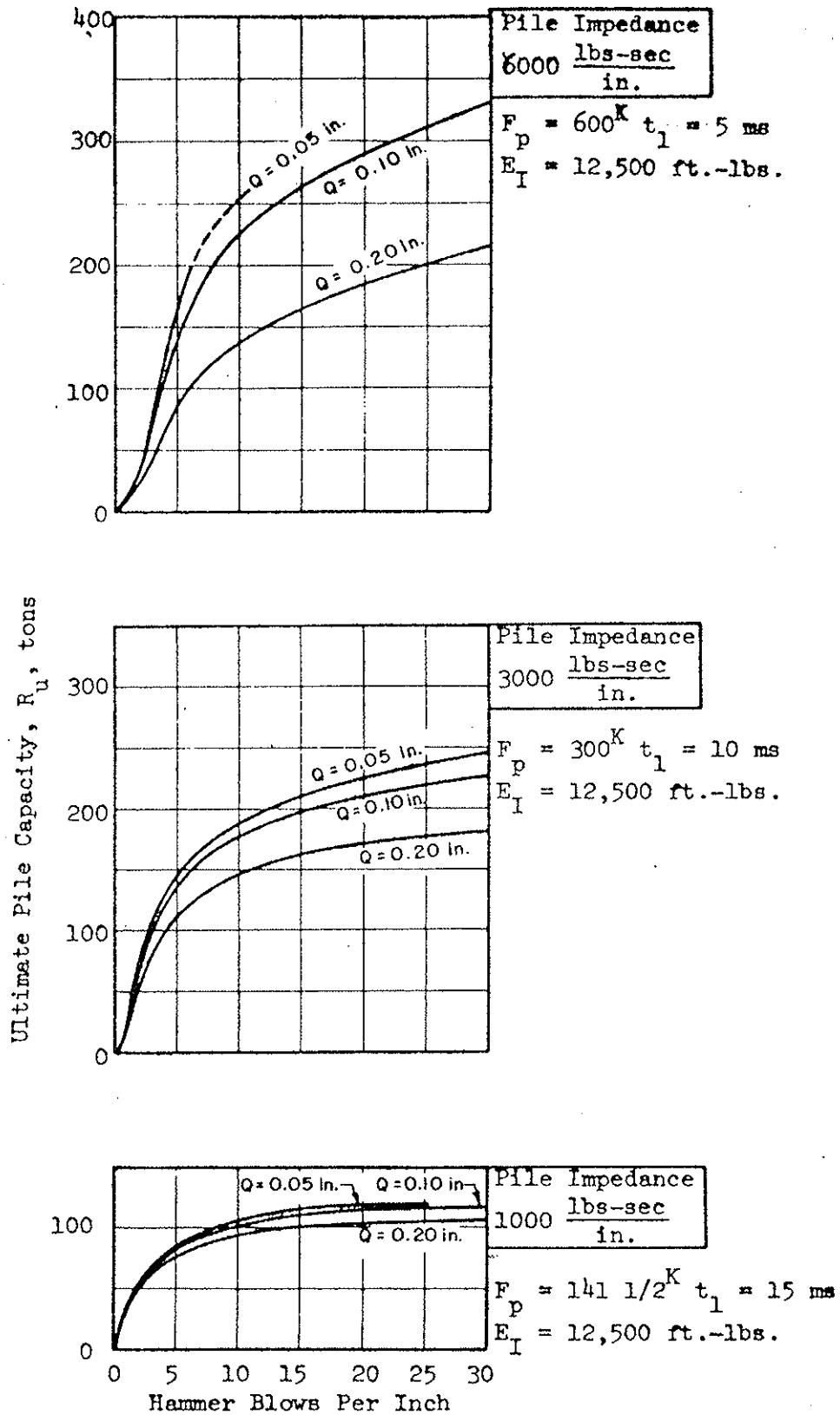

Sinusoidal Incident Force Pulse
100% Point Bearing - J_{pt} = 0.15 sec/ft

Figure 4.15 EFFECT OF SOIL QUAKE ON PILE RESPONSE

are higher than for sands. A common average damping factor, J_{pt}, for the pile tip is assumed to be 0.15 sec/ft. The investigation of damping shown in Figure 4.16 covers the range of one-half to twice the normal value. Field correlations indicate that the results for sands are in good agreement with the normally assumed value of 0.15 sec/ft; however, in clays damping values are higher, but pore pressure effects with respect to time make the analysis difficult. The effects of soil damping shown in Figure 4.16 were evaluated for three different pile impedances, an input energy of 12,500 ft-lbs, and a soil quake of 0.10 in. An increase in the damping factor decreases driving ability for all pile impedances, not just the higher impedances as is the case for soil quake.

Freeze and Relaxation

A wave propagation analysis considers the relationship between driving resistance and capacity at the time of driving; however, differences in soil properties often occur after driving and cause a discrepancy between static and dynamic pile load capacities. Increases in soil strength (set-up or freeze) occur in soils such as soft clays or loose cohesionless deposits. For soft and loose soil deposits, the gain in strength is a result of pore pressure dissipation. Thixotropic effects are prevalent in cohesive soils, whereas densification and strengthening due to adjacent pile driving can also occur in cohesionless soils. Relaxation, or loss in soil strength after driving, can possibly occur in stiff or dense deposits. In this case, dissipation of negative pore pressures or a loosening effect due to adjacent pile driving in very dense materials may cause a loss in capacity.

The engineer's ability to predict freeze or relaxation is necessary in order to achieve a technically sound and economical job. Useful

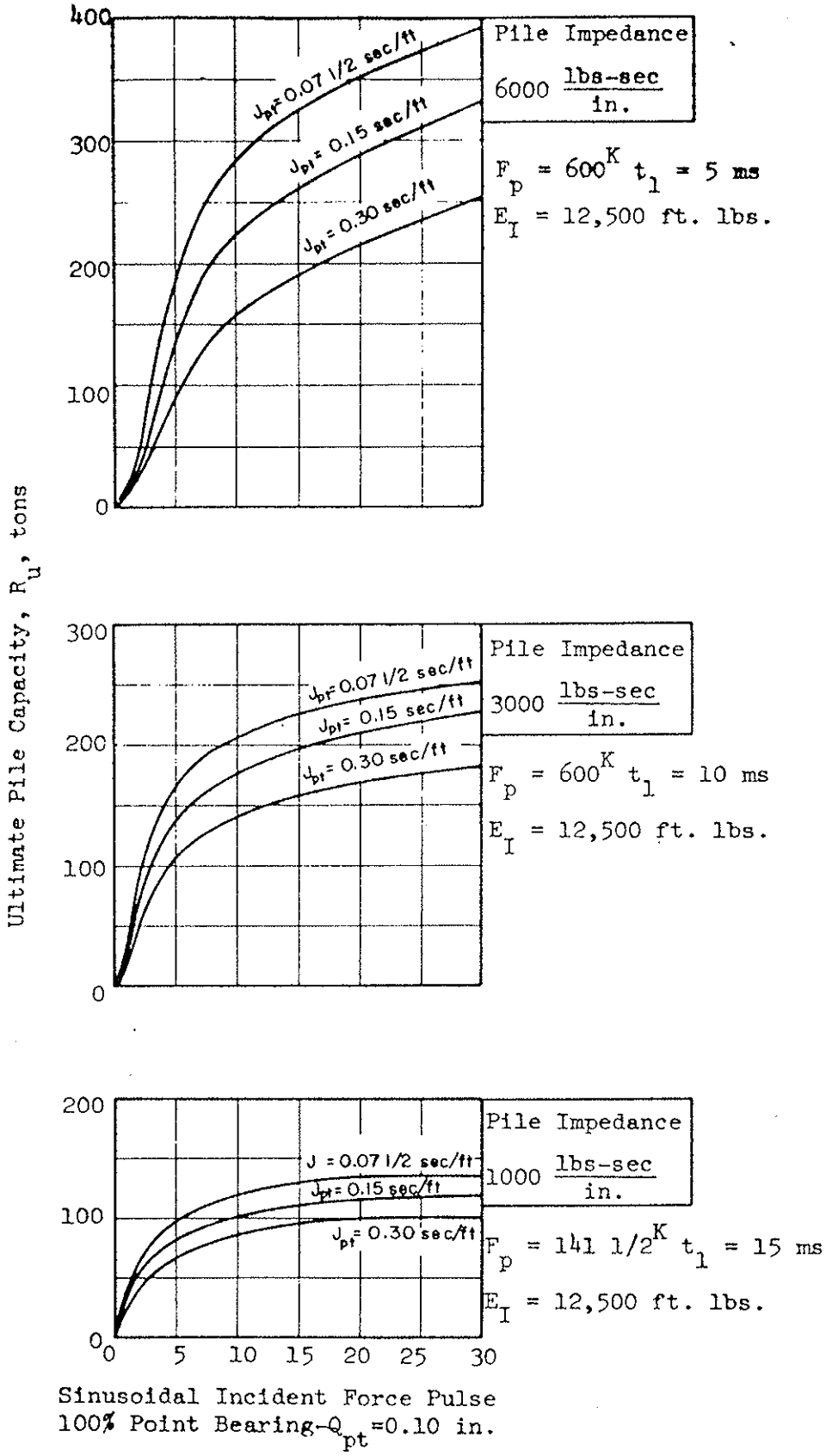

Figure 4.16 EFFECT OF SOIL DAMPING ON PILE RESPONSE

information on the magnitude of freeze or relaxation can be obtained from redriving piles. After the pile is driven and final hammer resistance in blows/in. is recorded, the pile is allowed to stand for a period of time before redriving. Redriving gives the hammer resistance in blows/in. for the first several hammer blows. This hammer resistance during redriving can be used to obtain an ultimate pile capacity from the wave equation analysis. Pile capacity as determined from redrive data can be compared with the initial driving capacity; the difference in load capacities will approximate the magnitude of relaxation or freeze. If the redriving resistance is greater than driving resistance, then freeze is exhibited. Redrive data is difficult to obtain because the first few hammer blows are critical and the hammer must be properly warmed-up in order to function at full energy during the first few hammer blows.

An accumulation of information on load tests correlated with the wave analysis as a reference framework can be achieved for various types of soils exhibiting freeze or relaxation. Freeze is a normal occurrence because of the type of soil profiles that dictate the use of piles. The following field study will show how the wave equation analysis coupled with a knowledge of freeze can be effectively used in pile foundation design.

Field Study 8. The soil profile consists of 30 ft of sand and 60 ft of soft to medium varved clay overlying hardpan. The piles are 12 3/4 in. by 0.250 in. pipe 95 ft long with closed-ends. The piles, driven with a Link-Belt 520, are designed for 110 tons working load. Analysis of this combination of pile, hammer and soil by use of the wave equation as shown in Figure 4.17 indicates that the pile can not achieve the required ultimate capacity of 220 tons (factor of safety = 2.0) without freeze. The effect of freeze was considered for the varved

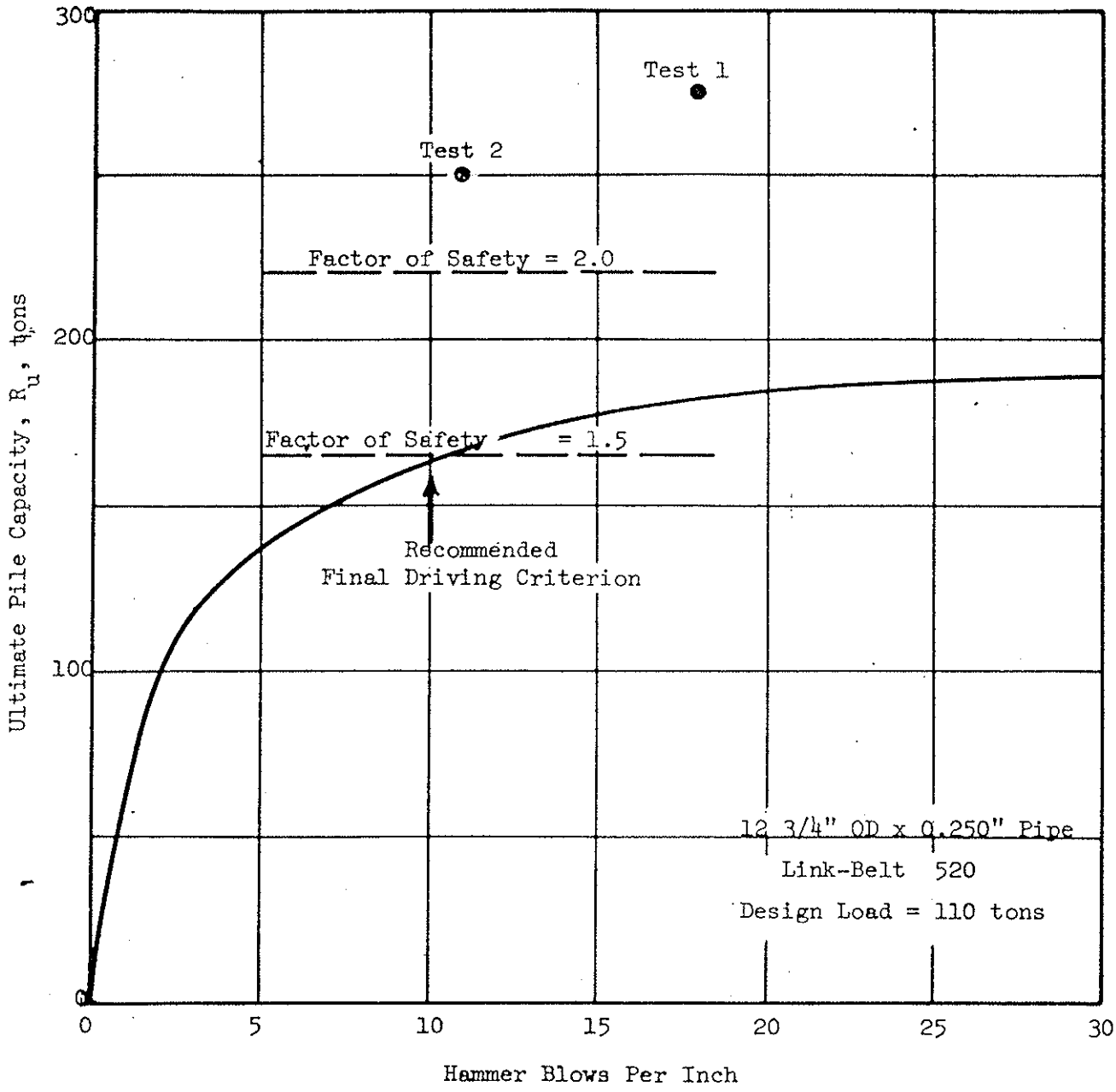

Figure 4.17 FIELD STUDY 8 - USE OF WAVE EQUATION ANALYSIS IN DESIGN FOR SOIL EXHIBITING FREEZE

clay; however, the magnitude of freeze was not known. Pile driving and redriving data from a project in the same soil deposit was analyzed with the use of the wave equation and it was found that 50 to 100 tons per pile could be attributed to freeze. The project was designed for a 165 ton ultimate (factor of safety = 1.5) at a recommended driving resistance of 10 blows/in. as shown by the wave equation analysis. The effect of freeze was expected to provide a factor of safety of 2. Two load tests were performed as shown in Figure 4.17 and the tests indicated 80 to 90 tons of freeze as expected.

4.5 Design Tool

The dynamics of driving piles with impact hammers has been amplified by independent idealized studies of the parameters controlling the generated force pulse in the head of the pile and the soil resistance parameters at the pile tip. The results of the parameter study not only indicate relative effects of the parameters controlling pile driving, but can be used as a design tool.

For example, consider a proposed 12 WF 106 pile (impedance of 4500 $\frac{\text{lbs-sec}}{\text{in.}}$) and a design load of 150 tons with a factor of safety of 2 (ultimate capacity 300 tons). The pile is 95 ft long and embedment is 45 ft. The Vulcan 010 hammer is being considered. For 70% hammer efficiency, the velocity at impact is approximately 12 ft/sec (Figure 2.11). The standard cushion size for a Vulcan 010 hammer is 13 1/2 in. in diameter and 10 in. height. The cushion material can be selected for maximum energy transmission or peak pile force; the criteria may not lead to the same cushion requirements. The cushion should be

selected such that the peak pile force exceeds the ultimate capacity of the pile; it should in addition be as efficient as possible in transmitting energy.

For maximum energy transmission, the impedance ratio relationship (Equation 2.4) can be used to calculate the desired hammer cushion. The range in calculated cushion stiffnesses is 0.6 to 2.2 x 10^6 lbs/in. The desired cushion would be a short oak wood or asbestos stack (5 in. height), or a long aluminum-micarta stack (20 in. height). An adapter would be required in order to obtain a stack height greater than 10 inches. The generated peak force with the cushion for maximum energy transmission can be obtained in Figure 2.10. The range in peak forces is 400 to 480 kips. This range can be determined by interpolation between impedances 2900 and 5800 $\frac{\text{lbs-sec}}{\text{in.}}$. For an ultimate capacity of 300 tons or 600 kips, a greater cushion stiffness than the stiffness for maximum energy transmission is desired.

In order to achieve a peak force greater than the ultimate pile capacity, a cushion stiffness of approximately 10 x 10^6 lbs/in. is selected (Figure 2.10). By interpolation, the peak force is found to be about 660 kips; therefore, the desired cushion material would be aluminum-micarta with a stack height of 7 in. The maximum driving stresses equal 22 ksi. The 7-inch cushion is stiffer than that for maximum energy transmission but is required to achieve efficient penetration.

The wave equation analysis (Smith's lumped mass-spring model) of the particular example was also performed with the results shown in Figure 4.18. The cushion selected was aluminum-micarta. As seen from Figure 4.18, the driving resistance of approximately 10 blows/in. will achieve the ultimate capacity of 300 tons. Ten hammer blows per inch is

WAVE EQUATION ANALYSIS

Job _____ Date August 1970 J _____

Location _____

Pile 12 WF 106 Area 31.2 in.^{2} Length 95 ft

Mandrel _____ Area _____ Length _____

Follower _____ Area _____ Length _____

Hammer Vulcan 010 Energy 32,500 ft-lbs e_f 70% Comb. Force --

Helmet (drive head) 1200 lbs Anvil --

Cushion (hammer) Aluminum-Micarta k 10x10^6 lbs/in. e 0.80 Q_{side} 0.20" J_{side} 0.05 sec.

Cushion (pile) -- k _____ e _____ Q_{point} 0.10" J_{point} 0.15"

Comments Design Load = 150 tons

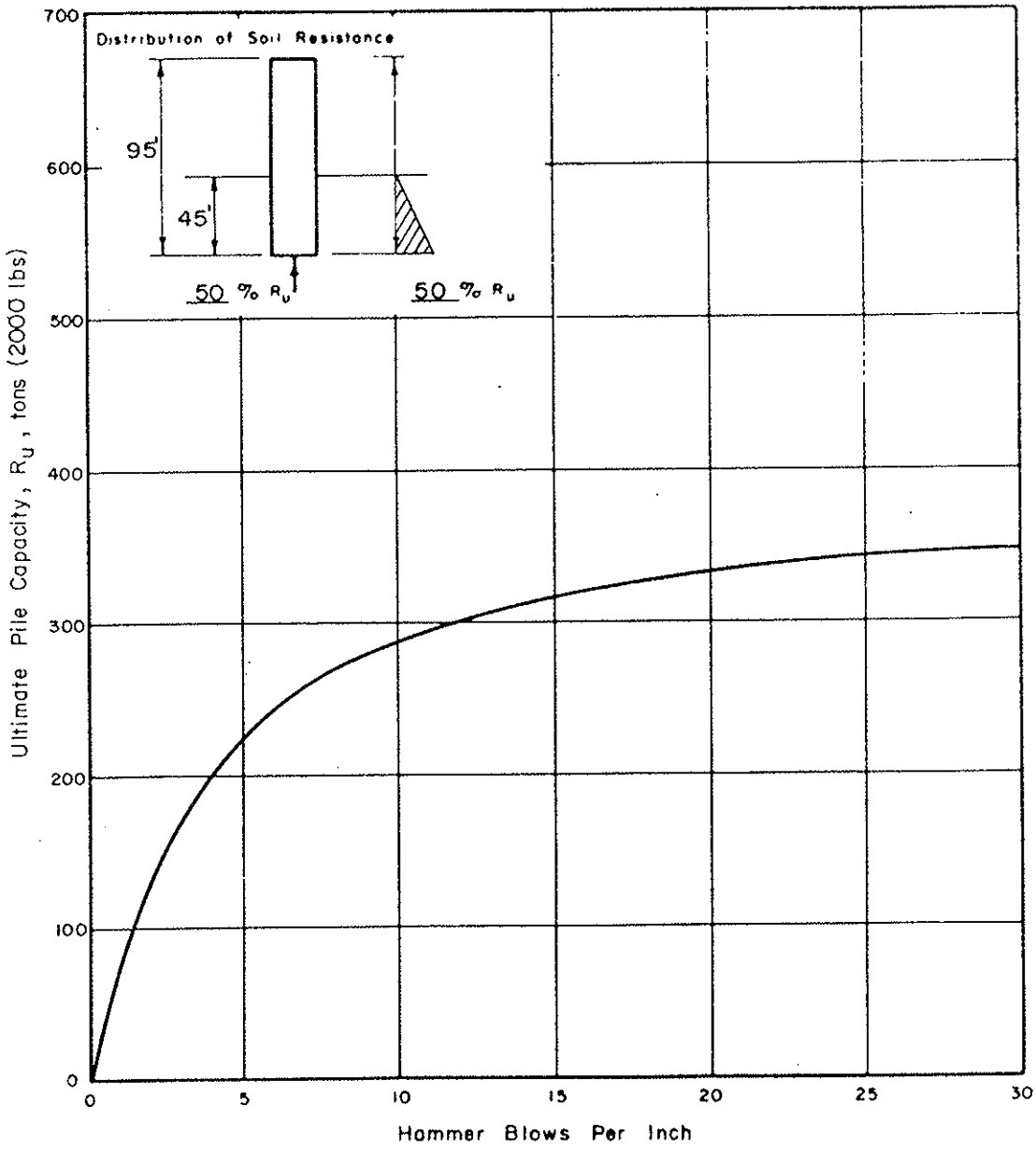

Figure 4.18 WAVE EQUATION ANALYSIS OF PROPOSED 12 WF 106 PILE

a practical limit for driving resistance. This correlation of the idealized studies of parameters and the wave equation analysis indicates that the idealized studies can be used as a preliminary design tool. The advantage of this design tool is that no computer analysis is necessary and only simple calculations along with the results incorporated herein are required.

4.6 Wave Equation Analysis Versus Energy Formulas

In the last century, energy formulas have been widely used to predict the bearing capacity and driving characteristics of an individual pile. Energy formulas are based on conservation of energy where the rated hammer energy is equated to the energy required for pile penetration plus energy losses, i.e. nonuseful energy for pile penetration.

$$E_r = R_u\, s + \text{losses} \tag{4.4}$$

where s is the net set of the pile per hammer blow. Authors of energy formulas have attempted to incorporate these losses by empiricism and/or Newtonian impact. Newtonian impact denotes the efficiency of impact of two free and massive bodies. The bodies in the pile analysis are the ram (W_1) and the pile (W_p). Also, the efficiency (e_f) of the hammer is often included to take account of losses prior to impact. Energy formulas then take the following form:

$$R_u = \frac{E_r \cdot e_f}{s + \bar{e}} \cdot \frac{W_1 + n^2 W_p}{W_1 + W_p} \tag{4.5}$$

where n is the coefficient of restitution for inelastic behavior at impact and $\bar{e}$ is a temporary set representing losses such as temporary compression, plastic deformation, etc. The $\bar{e}$ value takes many forms; it

is usually based on empiricism or simplified calculations. The expression $\frac{W_1 + n^2 W_p}{W_1 + W_p}$ accounts for the efficiency of Newtonian impact.

In reality, the pile is a distributed mass, not a concentrated mass, and is also restrained by the soil; these facts violate Newton's impact theory. These limitations and deficiencies of energy formulas are widely recognized, but no effective method was available to replace them until recently.

The impact resulting when a pile hammer strikes a pile is a practical illustration of longitudinal impact in elastic rods. The wave propagation analysis attempts to describe the force pulses generated and reflected along the pile's length. The relationship between the generated pulse and the soil resistance dictates the pile's response to driving. Correlations of wave equation analyses with field case histories illustrate the power of this analytical tool. It is a significant step forward in the art of pile foundation design.

The wave equation analysis and energy formulas are both mathematical tools used to achieve the same goal; i.e. the use of a dynamic analysis to predict driving capability and static load capacity at the time of driving. Therefore, the wave equation analysis fulfills the function of the dynamic energy formulas in a more accurate and comprehensive manner.

With the wave equation analysis established as the proper dynamic theoretical framework, the deficiencies of energy formulas can now be investigated with respect to the hammer-pile-soil system. Nineteen different and widely accepted energy formulas have been arbitrarily selected for this investigation as shown in Table A.1, Appendix A. The

variables of the hammer-pile-soil system included in the energy formulas discussed herein, are listed in Table 4.1.

Many of the energy formulas indicate that for piles driven to the same set or number of blows/in., the capacity is independent of pile area or impedance. The importance of pile impedance or area for transmitting the force pulse and developing load capacity has been exemplified by field studies and wave equation analyses (unmarked as shown in Table 4.1). Where pile impedance or other variables are taken into account in energy formulas they will be marked with an X in Table 4.1. The letter U is used to denote that the variable has been treated unsatisfactorily, whereas a blank indicates that the variable is ignored.

Some of the energy formulas attempt to account for the effect of pile impedance or area by means of pile weight; however, the energy formulation penalizes the heavier pile. For the same driving resistance, the expression $\frac{W_1 + n^2 W_p}{W_1 + W_p}$, which represents Newtonian impact efficiency, decreases with an increase in pile weight; therefore, the calculated ultimate pile capacities decrease with increase in pile weight (Equation 4.5). In reality, ultimate pile capacities increase with an increase in pile impedance (and weight) because of the improved ability to transmit force.

A closer examination of the energy formulas and the wave equation analysis shows that the two approaches are often in complete disagreement on the basis of driving resistance alone. For instance, compare a light and a heavy pile for the same soil condition, available hammer energy, pile length and embedment depth. In this problem, there is no reason to suspect any difference in the pile capacity between the light and heavy pile; however, the driving characteristics will be different. The wave

Table 4.1

COMPARISON OF WAVE EQUATION ANALYSIS AND ENERGY FORMULAS

Energy Formula	Variables						
	Pile Impedance or Area	Hammer Cushion	Pile Cushioning Effect	Soil Resistance Distribution	Hammer Energy	Ram Velocity	Drivehead Weight
1. Engineering News					X		
2. Modified Engineering News	U				X		
3. Gow	U				X		
4. Vulcan Iron Works	U				X		
5. Bureau of Yards and Docks					X		
6. Rankine	X			X	X		
7. Dutch	U				X		
8. Ritter	U				X		
9. Eytelwein	U				X		
10. Navy-McKay	U				X		
11. Sanders					X		
12. Gates					X		
13. Danish	X				X		
14. Janbu	X				X		
15. Hiley	X			X	X		
16. Redtenbacker	X			X	X		
17. Pacific Coast Uniform Building Code	X				X		
18. Canadian National Building Code	X			X	X		
19. Olson and Flaate					X		
Wave Equation Analysis	X	X	X	X	X	X	X

Legend: Blank Space - variable not accounted for
U - variable unsatisfactorily accounted for
X - variable accounted for

equation analysis clearly indicates that the heavy pile is a better transmitter of the generated force pulse; therefore, the driving resistance would be lower at a given ultimate capacity than for the light pile. Energy formulas erroneously predict a higher capacity for the higher driving resistance, i.e. for the light pile in this instance.

The hammer cushion is instrumental in shaping the generated force pulse; however, it is probably the most overlooked consideration in pile driving. The reason for this neglect can probably be attributed to the fact that most energy formulas completely ignore cushion stiffness. There are attempts to account for energy losses in a cushion, but not for the effects of stiffness.

A pile cushioning effect due to damage, or a composite section, can not be accounted for in energy formulas; however, the wave equation analysis can readily account for damage or composite section at any location along the pile's length.

Soil resistance distribution is generally not accounted for in energy formulas; however, there are attempts to account for friction versus point bearing piles in some of the formulas.

The amount of hammer energy in terms of ram weight and velocity is taken into account for all energy formulas; however, the effects of the energy components (ram velocity and ram weight) are not considered on an individual basis. As shown in the previous discussion, generated peak pile force is directly proportional to ram velocity; therefore, ram velocity is instrumental in shaping the force pulse. The force pulse shape, as shown in Chapter 3, is critical for achieving the required pile penetration and load capacity. The effect of drivehead weight on shaping the pile force pulse also is not considered in any of the energy formulas.

The aforementioned variables represent limiting factors of the hammer-pile-soil system affecting pile penetration and load capacity. However, it should be emphasized that the weak link in the hammer-pile-soil system will control driving behavior, irrespective of other variable changes. If several parameters represent equally weak links, then all such parameters would have to be changed simultaneously in order to achieve a significant change in driving capability. As discussed herein, the wave equation analysis has the ability to account for all the significant variables in the hammer-pile-soil system, whereas energy formulas possess inherent limitations.

Limitations of the energy formulas clearly revolve around the transmitting elements of the generated force pulse, i.e. pile impedance or area and hammer cushion, as well as soil considerations (See Table 4.1). These limitations do not mean that energy formulas can not be a valuable tool if they are properly used. Energy formulas are readily usable and can be a valuable tool if they are empirically adjusted for a particular driving condition, i.e. some given soil condition, pile type and driving equipment. Load tests must be used as a basis for adjusting the particular energy formula used. Although energy formulas can be useful on a job to job basis, a proper theoretical framework is necessary to consolidate and evaluate pile driving experience for the purpose of advancing the state of the art. Wave propagation analyses are the proper theoretical treatment; there is, however, a need for more refined input data for hammer, pile and soil parameters.

CHAPTER 5

CONCLUSIONS AND SUGGESTIONS FOR FUTURE RESEARCH

5.1 Conclusions

Conclusions of a general nature are presented below. Details of these conclusions have been given at the appropriate places in individual chapters.

1. In order to achieve maximum pile penetration and capacity for a given available energy, the shape of the force-time pulse is significant.
2. For a given pile, penetration and capacity increase with an increase in transmitted energy provided the generated peak force is greater than one-half the ultimate soil resistance (R_u). The effect of the increase in transmitted energy is greater for high than for low pile impedances, as measured by ρcA.
3. For a given hammer, maximum energy can be transmitted to the pile head by a proper match between pile impedance and hammer impedance; the Impedance Ratio, $\rho cA/\sqrt{m_1 k}$, should fall between 0.6 and 1.1.
4. Lost energy accomplishes no pile driving. Energy losses increase with an increase in the inelastic behavior of the cushion material (low coefficient of restitution); therefore, the ideal cushion is one that possesses a coefficient of restitution of unity (linear elastic).

5. For high pile impedances relative to hammer impedance, the generated pile force pulses are nearly sinusoidal. As the pile impedance approaches that for the best match of hammer and pile (providing maximum transmitted energy), the force pulses have a damped sinusoidal shape. Oscillatory forces are present during the unloading portion of the force pulse for low pile impedances.

6. The relationships for maximum pile penetration or maximum set per hammer blow with respect to the shape and duration of the tip force pulse are summarized below for a given energy input:

   a) For $\frac{F_{(\text{pile peak force})}}{R_{u(\text{ultimate soil spring force})}} \rightarrow \infty$, maximum pile penetration occurs with no soil resistance.

   b) For $\frac{F_{(\text{pile peak force})}}{R_{u(\text{ultimate soil spring force})}} > 1$, pile penetration increases with an increase in time duration, and is influenced relatively little by peak force.

   c) For $\frac{F_{(\text{pile peak force})}}{R_{u(\text{ultimate soil spring force})}} < 1$, and $> 1/2$, pile penetration is primarily dependent on peak force, and is influenced relatively little by duration.

   d) For $\frac{F_{(\text{pile peak force})}}{R_{u(\text{ultimate soil spring force})}} \leq 1/2$, no net pile penetration and only elastic deformations occur.

7. Peak pile force is directly proportional to ram velocity at impact provided the pile behaves elastically. Duration of the force pulse is independent of the ram velocity. The peak force data presented herein for different hammer and pile properties can be used as a guide for structural design of the pile to withstand driving.
8. Ram weight affects both peak pile force and pulse duration. If the ram weight is doubled, the peak pile force is slightly increased (less than 25%); the maximum increase occurs for high pile impedances. Pulse duration is approximately proportional to the square root of the ram weight.
9. Hammer cushion properties can be conveniently selected in order to control the shape of the force pulse as well as to match pile and hammer characteristics. The peak force generated in a pile with an aluminum-micarta cushion (stiff) is approximately double that generated with a pine plywood cushion (soft). Pulse durations for the soft cushions are larger, by a factor of 3 to 5, than the pulse length generated by stiff cushions.
10. In general, equivalent linear hammer cushions derived from appropriate secant moduli and used in analysis are in close agreement with the real behavior of nonlinear cushions.
11. Inelastic behavior of hammer cushions leads to attenuation of peak pile forces only for low pile impedances. Inelastic behavior causes attenuation of duration of the force pulse

for all pile impedances; therefore, the pulse length decreases with an increase in the degree of cushion inelasticity.

12. For given hammer conditions, generated peak pile force increases approximately in proportion to the pile impedance (or area) for low impedances. The proportion decreases for high pile impedances. Pulse duration is approximately inversely proportional to pile impedance.

13. Low impedance piles are more efficient with respect to driving (more set per blow) at low driving resistances because the force pulse is longer. However, high impedance piles are more capable of being driven to a high load capacity because of their ability to form and transmit high peak forces.

14. Greater penetration and higher load capacity can be obtained by redriving pipe piles after concreting. Pile impedance is increased by concreting.

15. A mandrel or drive core is an effective means of obtaining the impedance required for driving.

16. Pile damage caused by pile driving has the effect of lowering pile impedance in the damaged zone; therefore, the driving capability of a damaged pile is lower than for an equivalent undamaged pile.

17. Length of the pile affects interference with the generated force pulse by reflections from the pile tip. Reflections

can aid or retard pile penetration. Shorter piles are likely to be more efficient and achieve higher capacity for low pile impedances. For high pile impedances, pile length does not significantly alter either driving efficiency or load capacity.

18. Pile penetration behavior may not be particularly sensitive to soil parameters (quake and damping) along the side of piles.

19. If the frictional resistance acting on a given pile segment (increment of length) is examined, the pile peak force in general greatly exceeds the soil resistance. Thus, the force pulse can pass through many segments without serious attenuation. However, if all soil resistance is concentrated at the pile tip, the disparity between pile tip force and total resistance is not large and efficiency of pile penetration diminishes.

20. An increase in both soil quake and soil damping at the pile tip decreases the effectiveness of a given pile force pulse. The difference in behavior with respect to changes in quake are not significant for low pile impedances; however, the differences are marked for high pile impedances. An increase in the damping factor decreases driving ability for all pile impedances.

21. All dynamic analyses, including both the wave equation and energy formulae, consider the relationship between

driving resistance and load capacity at the time of driving; however, differences in soil properties often occur after driving and cause a discrepancy between static and dynamic pile load capacity. This discrepancy can be termed soil freeze or relaxation. An accumulation of information on load tests and redriving data correlated with wave equation analyses as a reference framework provides empirical data on freeze and relaxation that can be effectively used in pile foundation design.

22. With the aid of wave propagation analysis and field case histories, limiting factors to pile penetration and load capacity are summarized below in the order they are likely to be encountered in practice:

    1) Pile - Insufficient impedance or cross-sectional area.
    2) Hammer Cushion - Too soft.
    3) Pile Cushioning Effect - Pile damage or a change in pile cross-section.
    4) Soil Resistance - Too much point bearing, or soil relaxation.
    5) Hammer Energy - Insufficient.

23. It should be emphasized that the weak link in the hammer-pile-soil system will control driving behavior, irrespective of other parameters. If several parameters are equally weak, then all the weak parameters would have to be changed simultaneously in order to achieve any effective change in driving capability.

24. For pile driving, the wave equation analysis and energy formulas are mathematical tools used to achieve the same goal, namely, the use of a dynamic analysis to predict driving capability and static load capacity. However, the limitations of energy formulas include failure to take into account properly the transmitting elements (pile impedance or area, hammer cushion, drivehead) and ram velocity as they affect the generated force pulse. Energy formulas also do not account for soil considerations (distribution, yield criterion and damping), and they do not provide a stress analysis in the pile.

25. Correlations of wave equation analyses with field case histories illustrate the power of this analytical tool. It is a significant step forward in the art of pile foundation design.

5.2 Suggestions for Future Research

The ultimate goal in pile foundation design is a general understanding of both pile-soil interaction during installation, and the interaction of superstructure, piles and soil after construction. Therefore, a better understanding of pile group behavior is needed. Because of the difficulty in obtaining data on the behavior of pile groups, the following suggestions will be directed towards achieving a better understanding of single-pile behavior, which is a desirable starting point in pile foundation design.

In an effort to predict pile performance in a variable soil profile, pile drivers are placed in a rather unique dual role, namely, a contractor's driving tool and an engineer's measuring instrument. The driving resistance to pile penetration in terms of hammer blows per unit set is a measure of the pile's ability to support load. With the inherent variability of soil profiles, attainment of a prescribed driving resistance is an assurance that the desired pile capacity is achieved; therefore, dynamic analysis of single-pile behavior is of great practical importance.

Though the wave propagation analysis is quite useful, more field data must be gathered and analyzed to establish more accurately the input parameters. Better input information is required for hammer properties such as the effect of combustion in diesel hammers, impact velocity (hammer efficiency) and hammer cushion stress-strain data. More accurate soil information is needed on damping, quake, and dynamic versus static properties.

The complexity of diesel hammers as force generators is characterized by the almost simultaneous occurrences of combustion and impact forces. Information on the occurrence of the combustion with respect to impact and combustion gas forces are lacking. Hammer instrumentation is required for investigation of the interaction of ram impact and combustion in order to determine components of the generated force pulse.

More hammer input data on ram velocity at impact and cushion properties are needed. Ram velocity at impact for different hammers should be measured during field driving and correlated with hammer parameters such as speed, stroke, position etc., in order to develop

more reliable relationships with hammer efficiency. Ram velocity is important in shaping the generated force pulse. Hammer cushion data is available for common materials such as wood and aluminum-micarta; however, data is needed for other materials such as wire rope, wood chips, rope etc. Also, there is a need to find more efficient materials for hammer cushions. The capability of changing cushion behavior during driving would be desirable. For easy driving, a soft cushion is desirable, whereas a stiff cushion is needed for hard driving in order to achieve high peak forces.

Analysis of field measurements of generated pile forces should be directed towards determination of the soil resistance both at the pile tip and along the side. Quake and damping can be varied in the wave equation analysis; the analysis can be forced to match pile force measurements in order to deduce the proper soil parameters. Soil parameters should be correlated with index properties of the soil. Also, soil data must be accumulated along with load test data for development of procedures that allow the magnitude of freeze (set-up) or relaxation to be predicted.

The effects of pile length and soil distribution on soil response need investigation on a fundamental basis. Different boundary conditions of pile length cause force reflections to change the pile force pulse. The effect of reflections coupled with attenuation due to soil distribution need investigation with respect to the force pulse shape (peak and duration). The pile head and soil tip model were studied separately herein; however, future research should involve coupling the

two systems together to study the pile length and soil distribution effect. It is hoped that this will lead to approximate methods of predicting peak compressive and tensile forces in the pile without resorting to a full wave equation analysis. This in turn will allow rational structural design of the pile to resist driving.

REFERENCES

Airhart, T. P., T. J. Hirsch and H. M. Coyle, (1967), "Pile-Soil System Response in Clay as a Function of Excess Pore Water Pressure and Other Soil Properties," Texas Transportation Institute, Research Report 33-8, Texas A & M University, September.

Bender, C. H., Jr., C. G. Lyons and L. L. Lowery, Jr., (1969), "Applications of Wave-Equation Analysis to Offshore Pile Foundations," Offshore Technology Conference, Houston, Texas, May 19-21.

Bishop, A. W. and C. E. Blight, (1963), "Some Aspects of Effective Stress in Saturated and Partly Saturated Soils," Geotechnique, Vol. 13, pp. 177-197.

Casagrande, A., and W. L. Shannon, (1948), "Strength of Soils Under Dynamic Loads," Proceedings ASCE, Vol. 74, No. 4, pp. 591-608.

Chan, P. C., T. J. Hirsch and H. M. Coyle, (1967), "A Laboratory Study of Dynamic Load-Deformation and Damping Properties of Sands Concerned with a Pile-Soil System," Texas Transportation Institute, Research Report Texas A & M University, January.

Chellis, R. D., (1961), Pile Foundation, Second Edition, McGraw-Hill, New York, 704 p.

Coyle, H. M., and L. C. Reese, (1966), "Load Transfer for Axially Loaded Piles in Clay," Journal of the Soil Mechanics and Foundations Division, ASCE, Vol. 92 No. SM2, Proc. Paper 4702, pp. 1-26.

Coyle, H. M., and G. C. Gibson, (1970), "Empirical Damping Constants for Sands and Clays," Journal of the Soils Mechanics and Foundations Division, ASCE, Vol. 96, No. SM3, Proc. Paper 7296, pp. 949-965.

Cummings, A. E., (1940), "Dynamic Pile Driving Formulas," Contributions to Soil Mechanics 1925-1940, Boston Society of Civil Engineers, Boston, pp. 392-413.

Cunny, R. W. and R. C. Sloan, (1962), "Dynamic Loading Machine and Results of Preliminary Small-Scale Footing Tests," Symposium on Soil Dynamics, ASTM Special Technical Publication No. 305, pp. 65-77.

Davisson, M. T., (1969), Personal Communication.

Davisson, M. T., (1970), "Design Pile Capacity", Conference on Design and Installation of Pile Foundations and Cellular Structures, Lehigh University, April 13-15.

Davisson, M. T., and V. J. McDonald, (1969), "Energy Measurements for a Diesel Hammer," Performance of Deep Foundations, ASTM STP 444, pp. 295-337.

Donnell, L. H., (1930), "Longitudinal Wave Transmission and Impact," Transactions, ASME, Vol. 52, Paper APM-52-14.

Edwards, T. C., (1967), "Piling Analysis Wave Equation Computer Program Utilization Manual," Texas Transportation Institute, Research Report 33-11, Texas A & M University, August, 40 p.

Eiber, R. J., (1958), "A Preliminary Laboratory Investigation of the Prediction of Static Pile Resistance in Sand," Master's Thesis, Case Institute of Technology.

Feld, J., (1957), "Discussion in Session 6-Piling and Piled Foundations," Proceedings of the Fourth International Conference on Soil Mechanics and Foundation Engineering, London, Vol. 3, pp. 180-181.

Forehand, P. W. and J. L. Reese, Jr., (1963), "Pile Driving Analysis Using the Wave Equation," M.S. Thesis, Princeton University, Princeton, New Jersey.

Forehand, P. W. and J. L. Reese, Jr., (1964), "Prediction of Pile Capacity by the Wave Equation," Journal of the Soil Mechanics and Foundations Division, ASCE, Vol. 90, No. SM2, Proc. Paper 3820, March, pp. 1-25.

Fox, E. N., (1932), "Stress Phenomena Occurring in Pile Driving," Engineering, London, Vol. 134, pp. 263-265.

Gibson, G. C. and H. M. Coyle, (1968), "Soil Damping Constants Related to Common Soil Properties in Sands and Clays," Texas Transportation Institute, Research Report 125-1, Texas A & M University, September, 28 p.

Glanville, W. H., G. Grime, E. N. Fox and W. W. Davies, (1938), "An Investigation of the Stresses in Reinforced Concrete Piles during Driving," British Building Research Board Technical Paper No. 20, D. S. I. R.

Goble, G. G., R. H. Scanlan and J. J. Tomko, (1967), "Dynamic Studies on the Bearing Capacity of Piles," Presented to the Highway Research Board Annual Meeting January 18, Case Institute of Technology, 63 p.

Goble, G. G., J. J. Tomko, F. Rausche and P. M. Green, (1968), "Dynamic Studies on the Bearing Capacity of Piles," Vol. 1 and Vol. 2, Report No. 31, Case Western Reserve University, July.

Goldsmith, W., (1961), Impact, The Theory and Physical Behaviour of Colliding Soilds, Arnold LTD., London, 379 p.

Graff, C. R., (1965), "The Wave Equation and Pile Driving," Foundation Facts, Vol. 1, No. 2, p. 8.

Hagerty, D. J., (1969), "Some Heave Phenomena Associated with Pile Driving," Ph.D. Thesis, University of Illinois, Urbana, Illinois.

Healy, K. A., (1962), "The Response of Soils to Dynamic Loadings, Report 11: Triaxial Tests upon Saturated Fine Silty Sand," U. S. Army Engrs., Waterways Experiment Sta., Vicksburg, Miss.

Heising, W. P., (1955), Discussion, "Impact and Longitudinal Wave Transmission," Transactions ASME, August, pp. 971-972.

Hirsch, T. J., (1966), "Fundamental Design and Driving Considerations for Concrete Piles," Highway Research Record, Number 147, Highway Research Board, pp. 24-34.

Hirsch, T. J. and C. H. Samson, Jr., (1966), "Driving Practices for Prestressed Concrete Piles," Texas Transportation Institute, Research Report 33-3, Texas A & M University, April, 6 p.

Hirsch, T. J. and T. C. Edwards, (1966), "Impact Load-Deformation Properties of Pile Cushioning Materials," Texas Transportation Institute, Research Report 33-4, Texas A & M University, May, 12 p.

Housel, W. S., (1965), "Michigan Study of Pile Driving Hammers," Journal of the Soil Mechanics and Foundations Division, ASCE, Vol. 91, No. SM5, Proc. Paper 4483, pp. 37-64.

Ireland, H. O., (1957), "Pulling Tests on Piles in Sand," Proceedings of the Fourth International Conference on Soil Mechanics and Foundation Engineering, London, Vol. 2, pp. 43-45.

Ireland, H. O., (1966), "The Conduct and Interpretation of Pile Loading Tests," Seminar Sponsored by Foundation and Soil Mechanics Group, Metropolitan Section, ASCE, New York, April 12-13, May 10-11.

Isaacs, D. V., (1931), "Reinforced Concrete Pile Formulae," Journal of the Institution of Engineers Australia, Transactions, Vol. 12, pp. 305-323.

Johnson, C. L., (1956), Analog Computer Techniques, McGraw-Hill Book Company, Inc., New York.

Jones, R., N. W. Lister and E. N. Thrower, (1966), "The Dynamic Behavior of Soils and Foundations," Proceedings of Symposium on Vibration in Civil Engineering, Imperial College, London, pp. 121-140.

Kane, H., Davisson, M. T., R. E. Olson and G. K. Sinnamon, (1964), "A Study of the Behavior of a Clay under Rapid and Dynamic Loading in the One-Dimensional and Triaxial Tests," Report No. RTD TDR-63-3116, Air Force Weapons Lab.

Kerisel, J., (1961), "Fondations Profondes en Milieux Sableux," Proceedings of the Fifth International Conference on Soil Mechanics and Foundation Engineering, Montreal, Vol. 2, pp. 73-83.

Kerisel, J., (1964), "Deep Foundations, Basic Experimental Facts," Proceedings of North American Conference on Deep Foundations, Mexico City.

Kolsky, H., (1963), Stress Waves in Solids, Dover, New York, 213 p.

Korb, K. W. and H. M. Coyle, (1969), "Dynamic and Static Field Tests on a Small Instrumented Pile," Texas Transportation Institute, Research Report 33-12, Texas A & M University, February, 24 p.

Korn, G. A. and T. M. Korn, (1956), Electronic Analog Computers, 2nd. Ed., McGraw-Hill Company, Inc., New York.

Lee, L. L., Jr., T. C. Edwards and T. J. Hirsch, (1968), "Use of the Wave Equation to Predict Soil Resistance on a Pile During Driving," Texas Transportation Institute, Research Report 33-10, Texas A & M University, August, 32 p.

Lowery, L. L., Jr., T. J. Hirsch and C. H. Samson, Jr., (1967), "Pile Driving Analysis - Simulation of Hammers, Cushions, Piles, and Soil," Texas Transportation Institute, Research Report 33-9, Texas A & M University, August, 81 p.

Lowery, L. L., Jr., J. R. Finley, Jr. and T. J. Hirsch, (1968), "A Comparison of Dynamic Pile Driving Formulas with Wave Equation," Texas Transportation Institute, Research Report 33-12, Texas A & M University, August, 16 p.

Lowery, L. L., Jr., T. J. Hirsch, T. C. Edwards, H. M. Coyle and C. H. Samson, Jr., (1969), "Pile Driving Analysis - State of the Art," Texas Transportation Institute, Research Report 33-13, Texas A & M University, January, 79 p.

Lowery, L. L., Jr., T. C. Edwards and J. R. Finley, Jr., (1969), "Increasing the Ability to Drive Long Off-Shore Piles," Offshore Technology Conference, Houston, Texas, May 18-21.

Mansur, C. I., A. H. Hunter and M. T. Davisson, (1964), "Pile Driving and Loading Tests, Lock and Dam No. 4, Arkansas River and Tributaries," U. S. Army Engineer District, Little Rock, 82 p.

Meyerhof, G. H., (1951), "The Ultimate Bearing Capacity of Foundations," Geotechnique, Vol. 2, pp. 301-332.

Meyerhof, G. G., (1959), "Compaction of Sands and Bearing Capacity of Piles," Proceedings ASCE, Vol. 85, No. SM6, pp. 1-29.

Michigan State Highway Commission, (1965), "A Performance Investigation of Pile Driving Hammers and Piles," Research Project 61 F-60, Lansing.

Mosley, E. T., (1967), "Wave Equation Analysis," Foundation Facts, Vol. 3, No. 2, pp. 15-17.

Mosley, E. T. and T. Raamot, (1970), "Pile Driving Formulas," Paper presented at Highway Research Board Annual Meeting, January.

Nordlund, R. L., (1963), "Bearing Capacity of Piles in Cohesionless Soils," Journal of the Soil Mechanics and Foundations Division, ASCE, Vol. 89, No. SM3, Proc. Paper 3506, pp. 1-35.

Olson, R. E. and J. F. Parola, (1967), "Dynamic Shearing Properties of Compacted Clay," Proceedings of International Symposium on Wave Propagation and Dynamic Properties of Earth Materials, Albuquerque, New Mexico, pp. 173-182.

Olson, R. E. and K. S. Flaate, (1967), "Pile-Driving Formulas for Friction Piles in Sand," Journal of the Soil Mechanics and Foundations Division, ASCE, Vol. 93, No. SM6, Proc. Paper 5604, pp. 279-296.

Parsons, J. D., (1966), "Piling Difficulties in the New York Area," Journal of the Soil Mechanics and Foundations Division, ASCE, Vol. 92, No. SM1, Proc. Paper 4617, pp. 43-64.

Peck, R. B., (1958), "A Study of the Comparative Behavior of Friction Piles," Highway Research Board, Special Report 36, 72 p.

Raamot, T., (1967), "Analysis of Pile Driving by the Wave Equation," Foundation Facts, Vol. 3, No. 1, pp. 10-12.

Raamot, T. (1967), "Wave Equation Approach to Pile Driving," The Municipal Engineers Journal, Vol. 53, First Quarterly Issue, pp. 11-19.

Rakhmatulin, Kh. A. and Yu. A. Dem'yanov, (1961), Strength Under High Transient Loads, a translation of Prochnost' Pri Intensivnykh Kratkovremennykh Nagruzkakh, Israel Program for Scientific Trans-Lations, Jerusalem, 1966, 342 p.

Reeves, G. N., H. M. Coyle and T. J. Hirsch, (1967), "Investigation of Sands Subjected to Dynamic Loading," Texas Transportation Institute, Research Report 33-7A, Texas A & M University, December, 9 p.

Saint-Venant, (Before 1900), "Théorie de l'élasticité des corps solids," Clebsch. Reference referred to by Timoshenko and Goodier, (1951), Theory of Elasticity, pp. 446.

Samson, C. H., Jr., T. J. Hirsch and L. L. Lowery, Jr., (1963), "Computer Study of Dynamic Behavior of Piling," Journal of the Structural Division, ASCE, Vol. 89, No. ST4, Proc. Paper 3608, August, pp. 413-449.

Scanlan, R. H. and J. J. Tomko, (1969), "Dynamic Prediction of Pile Static Bearing Capacity," Journal of the Soil Mechanics and Foundations Division, ASCE, Vol. 95, No. SM2, Proc. Paper 6468, pp. 583-604.

Schimming, B. B., H. J. Haas and H. C. Saxe, (1966), "Study of Dynamic and Static Failure Envelopes," Journal of the Soil Mechanics and Foundations Division, ASCE, Vol. 92, No. SM3, Proc. Paper 4735, pp. 105-124.

Seed, H. B. and R. Lundgren, (1954), "Investigation of the Effect of Transient Loading on the Strength and Deformation Characteristics of Saturated Sands," Proceedings ASTM, Vol. 54, pp. 1288-1306.

Smart, J. D., (1969), "Vibratory Pile Driving," Ph.D. Thesis, University of Illinois, Urbana, Illinois.

Smith, E. A. L., (1950), "Pile Driving Impact," Industrial Computation Seminar, International Business Machines Corp., New York.

Smith, E. A. L., (1955), "Impact and Longitudinal Wave Transmission," Transactions ASME, August, pp. 963-973.

Smith, E. A. L., (1957), "The Wave Equation Applied to Pile Driving," Raymond Concrete Pile Co.

Smith, E. A. L., (1958), "Pile Calculations by the Wave Equation," Concrete and Constructional Engineer, London.

Smith, E. A. L., (1960), "Pile-Driving Analysis by the Wave Equation," Journal of Soil Mechanics and Foundations Division, ASCE, Proc. Paper 2574, August.

Smith, E. A. L., (1962), "Pile-Driving Analysis by the Wave Equation," Transactions ASCE, Vol. 127, Part I, pp. 1145-1171.

Szechy, C., (1960), "A New Pile Bearing Formula for Friction Piles in Cohesionless Sand," Symposium on Pile Foundations, International Congress of the International Association for Bridge and Structural Engineers, Stockholm, pp. 73-76.

Taylor, D. W., (1948), Fundamentals of Soil Mechanics, John Wiley and Sons, New York, 700 p.

Terzaghi, K. and R. B. Peck, (1967), Soil Mechanics in Engineering Practice, 2nd. Edition, John Wiley and Sons, New York, 729 p.

Timoshenko, S. and J. N. Goodier, (1951), Theory of Elasticity, 2nd. Edition, McGraw-Hill Co., New York, pp. 438-459.

Tomko, J. J., (1968), "Dynamic Studies on Predicting the Static Bearing Capacity of Piles," Ph.D. Thesis, Case Western Reserve University.

Tomlinson, M. J., (1957), "The Adhesion of Pile Driven in Clay Soils," Proceedings of the Fourth International Conference on Soil Mechanics and Foundation Engineering, London, Vol. 2, pp. 66-71.

Vesić, A. S., (1964), "Investigations of Bearing Capacity of Piles in Sand," Proceedings of North American Conference on Deep Foundations, Mexico City.

Vesić, A. S., (1967), "Ultimate Loads and Settlements of Deep Foundations in Sand," Proceedings of a Symposium or Bearing Capacity and Settlement of Foundations, Duke University, pp. 53-68.

Vulcan Iron Works, (1927), "Pile Driving Machinery," Catalogue No. 53, 80 p.

Whitman, R. V. (1957), "The Behavior of Soils Under Transient Loadings," Proceedings of the Fourth International Conference on Soil Mechanics and Foundation Engineering, London, Vol. 1, pp. 207-212.

Whitman, R. V. and K. A. Healy, (1962), "The Response of Soils to Dynamic Loadings, Report 9: Shearing Resistance of Sands During Rapid Loadings," U. S. Army Engrs., Waterways Experiment Sta., Vicksburg, Miss.

Whitman, R. V., A. M. Richardson, Jr. and N. M. Nasim, (1962), "The Response of Soils to Dynamic Loadings, Report 10: Strength of Saturated Fat Clay," U. S. Army Engrs., Waterways Experiment Sta., Vicksburg, Miss.

Yang, N. C., (1956), "Redriving Characteristics of Piles," Journal of the Soil Mechanics and Foundations Division, ASCE, Vol. 82, No. SM3, Proc. Paper 1026.

Yang, N. C., (1970), "Relaxation of PIles in Sand and Inorganic Silt," Journal of the Soil Mechanics and Foundations Division, ASCE, Vol. 96, No. SM2, Proc. Paper 7123, pp. 395-409.

APPENDIX A

REVIEW OF SINGLE-PILE ANALYSIS

A.1 Introduction

It is the purpose of this appendix to present the methods available for the analysis of a single pile. Current means of analyzing a single-pile may be classified either as static or dynamic. Dynamic methods of analysis include: 1) dynamic energy formulas; 2) wave equation analysis; 3) pile force and acceleration field measurements.

In order to validate design assumptions, pile load tests are generally performed. However, the interpretation of pile load test data is not unique; differences of opinion among engineers on the same test data make correlations difficult. Ireland (1966) summarized various methods of interpretation of pile load test data as well as information on procedures for pile load testing.

A.2 Static Pile Formulas

All the static pile formulas may be expressed by the following basic equation:

$$R_u = R_f + R_p \qquad (A.1)$$

where R_u is the ultimate pile capacity, R_f is the load carried by friction along the pile perimeter, and R_p is the load carried by point resistance. Variations in answers from Equation A.1 are due to the methods used to evaluate the friction and point-bearing portions of ultimate pile capacity. Driving a pile into granular soil will cause the soil in the zone around the pile to displace laterally; therefore, a change in densification and horizontal stresses is expected. In order to calculate the skin friction

resistance of a pile, the horizontal stresses acting on the pile surface as well as the coefficient of friction of the pile and soil must be evaluated. A number of investigations (Meyerhof, 1951, Ireland, 1957; Szechy, 1960; Vesic, 1964; Nordlund, 1963) have been made to determine the magnitude and distribution of the horizontal stress acting on the pile surface after driving. Experimental studies by Kerisel (1964) and Vesic (1964) help indicate the behavior of the point resistance with respect to depth. Vesic (1967) evaluated various theories of static pile capacity and concluded that no theory could be recommended to the foundation engineer without reservations. A review of various studies indicates that the state of stress around a driven pile in sand is very complex; therefore, static pile formulas for sand are still speculative.

It is commonly assumed that the capacity of a single pile in clay is due to skin friction. Several studies, such as by Tomlinson (1957) and Peck (1958), indicated that the adhesion between the pile and the clay could be related to the undisturbed strength of clay. For soft to medium clays, the adhesion is essentially equal to the undrained shear strength of the undisturbed clay. However, piles driven in stiff clay do not develop the full strength of the soil in skin friction. One possible explanation for low friction is the separation of pile and soil because of lateral pile movement. The separation can be maintained because of the clay's strength. When piles are driven in clays the soil in the vicinity of the pile is remolded; therefore, a loss in shear strength occurs. With time after driving, the soil regains strength by both consolidation and thixotropy; therefore, the relations between skin friction and time are complex and as yet are not predictable.

Limitations of static theories in sand can be summarized in two parts, namely, skin friction and tip resistance. First, the skin friction is strongly a function of pile material and construction technique, but static theory does not take into account construction technique. Second, the actual behavior of pile tips in sand is not in accord with common theories (Vesic, 1964). Static analysis does, however, give a more representative simulation of the static loading condition being investigated. Static theories take variations in the soil profile into account.

Static analysis is a useful tool in pile design; however, it should be recognized that it alone can not be relied upon. Real soil profiles are quite variable; therefore, the desired pile length or depth of penetration to achieve the required load capacity is also variable. Load capacity as measured by driving resistance (blows/inch) is a useful indicator for an individual pile that allows appropriate adjustments to be made at the time of driving.

A.3 Energy Formulas

In the last century, engineers have attempted to predict the driving characteristics and bearing capacity of piles by use of dynamic energy formulas. Dynamic energy formulas are based on the simple energy relationship:

$$\text{Energy Input} = \text{Energy Used} + \text{Energy Lost} \qquad \text{(A.2)}$$

where energy input is available hammer energy at impact, energy used is that actually used in driving the pile, and energy lost is returned to hammer (rebound) or simply lost, i.e. non-useful energy for pile penetration. Non-useful energy may include: hammer efficiency; ram rebound; plastic behavior at the contacts between the ram, cushion and pile; tempo-

rary elastic compression of the pile and soil; heat losses in the cushion block and soil; radiation losses related to soil vibrations due to generated stress waves; and friction losses due to the pile slipping with respect to the soil. A great number of pile driving formulas have been derived that incorporate these energy losses and attempt to predict the energy transmitted to the pile. These losses have been estimated by assuming that pile driving is a problem in Newtonian impact. In reality, the pile is a distributed mass, not a concentrated mass, and it is also restrained by the soil; these facts violate Newton's impact theory (Cummings, 1940). However, it should be pointed out that energy formulas are still in common use today and can be a valuable tool if they are empirically adjusted for a particular driving condition, i.e. some given soil condition, pile type and driving equipment. Load tests must be used as a basis for adjusting the particular dynamic formula used.

There are many dynamic energy formulas available today (over four-hundred according to Smith, 1960) derived from the simple energy relationship previously described; however, they can be divided into two major groups. One group is strictly empirical in which the energy losses are predicted from field data, and the other group can be classified as semi-theoretical in which the determination of losses is based on Newtonian impact. Eighteen different and widely used pile formulas plus the statistical adjustment of Gates formula by Olson and Flaate (1967) have been selected for this investigation. The energy formulas discussed are shown in Table A.1 along with a list of notation.

It is beyond the scope of this investigation to derive or discuss in detail the basis for the driving formulas in Table A.1; however, derivations and concepts can be readily found in Isaacs (1931), Cummings (1940), Taylor

Table A.1

TABULATION OF PILE ENERGY FORMULAS

1. Engineering News: $R_u = \dfrac{12\ E_r}{s + \bar{e}}$

2. Modified Engineering News: $R_u = \dfrac{12\ E_r}{s + \bar{e}} \cdot \dfrac{W_1 + n^2 W_p}{W_1 + W_p}$

3. Gow: $R_u = \dfrac{12\ e_f\ E_r}{s + \bar{e}(W_p/W_1)}$

4. Vulcan Iron Works: $R_u = \dfrac{120\ E_r}{10s + 1}$

5. Bureau of Yards and Docks: $R_u = \dfrac{12\ W_1 h}{s + 0.3}$

6. Rankine: $R_u = \dfrac{AEs}{6L}\left[\sqrt{1 + \dfrac{144\ E_r L}{s^2\ AE}} - 1\right]$

7. Dutch: $R_u = \dfrac{12\ E_r}{s} \cdot \dfrac{W_1}{W_1 + W_p}$

8. Ritter: $R_u = \dfrac{12\ E_r}{s} \cdot \dfrac{W_1}{W_1 + W_p} + W_1 + W_p$

9. Eytelwein: $R_u = \dfrac{12\ E_r}{s + 0.1\ W_p/W_1}$ Single-Acting Hammers

$R_u = \dfrac{12\ (E_r + A_p\ P)}{s + 0.1\ W_p/W_1}$ Double-Acting Hammers

10. Navy-Mckay: $R_u = \dfrac{12\ E_r}{s(1 + 0.3\ W_p/W_1)}$

11. Sanders: $R_u = \dfrac{12\ E_r}{s}$

Table A.1 (continued)

12. Gates: $R_u = 990 \sqrt{e_f E_r} \log (10/s)$

13. Danish: $$R_u = \frac{e_f E_r}{\frac{s}{12} + \sqrt{\frac{e_f E_r L}{2 AE}}}$$

14. Janbu: $$R_u = \frac{12 E_r}{k_u s}$$

$$k_u = C_d(1 + \sqrt{1 + \lambda_e / C_d})$$

$$\lambda_e = 144 E_r L / AE s^2$$

$$C_d = 0.75 + 0.15(W_p / W_1)$$

15. Hiley: $$R_u = \frac{12 e_f E_r}{s + 1/2(C_1 + C_2 + C_3)} \cdot \frac{W_1 + n^2 W_p}{W_1 + W_p}$$

16. Redtenbacker: $$R_u = \frac{AE\ s}{12\ L} \left[\sqrt{1 + \frac{288 W_r^2 h}{AE s^2 (W_1 + W_p)}} - 1 \right]$$

17. Pacific Coast Uniform Building Code:

$$R_u = \frac{AE}{24L} - s + \left[\sqrt{s^2 + \frac{576 e_f E_r L}{AE} \cdot \frac{W_1 + n^2 W_p^2}{W_1 + W_p}} \right]$$

18. Canadian National Building Code:

$$R_u = \frac{12 e_f e_1 E_r}{s + \bar{e}/2}$$

$$e_1 = \frac{W_1 + n^2 W_p}{W_1 + W_p} \quad \text{Friction Piles}$$

Table A.1 (continued)

$$e_l = \frac{W_l + 0.5n^2 W_p}{W_l + W_p} \quad \text{Point Bearing Piles}$$

$$\bar{e} = \frac{R_u}{A}\left(\frac{12\,\bar{L}}{E} + 0.0001\right)$$

19. Statistical Adjustments of Gates Formula (Olson and Flaate, 1967):

$$R_u = C_4 \sqrt{e_f E_r} \log(10/s) - C_s$$

Key:

R_u	ultimate pile capacity (lbs)
E_r	rated hammer energy (ft-lbs)
s	set (in.)
$\bar{e}$	temporary set representing losses (in.)
W_p	weight of the pile (lbs)
W_l	weight of the ram (lbs)
h	height of ram fall (ft)
A	cross-sectional area of pile ($in.^2$)
E	Young's modulus of pile (psi)
L	length of pile (ft)
$\bar{L}$	length of pile, measured from head to center of driving resistance resistance (ft)
e_f	hammer efficiency (%)
A_p	effective area of piston ($in.^2$)
p	mean pressure of steam or air (psi)

Table A.1 (continued)

n	coefficient of restitution
C_1	recoverable deformation of drivehead and pile head (in.)
C_2	recoverable deformation of pile (in.)
C_3	recoverable deformation of soil (in.)
C_4	slope of a regression line (dimensionless)
C_5	intercept of a regression line (lbs)

(1948), Chellis (1961), Terzaghi and Peck (1967), Olson and Flaate (1967) and other publications concerned with foundation engineering.

A.4 Wave Equation Analysis

Introduction

In recent years, impact and longitudinal wave transmission theory has been given considerable attention because it is a better simulation of the pile driving operation than is the theory of Newtonian impact. A comparison of the Newtonian impact model and longitudinal wave model is shown in Figure A.1.

The impact resulting when a pile hammer strikes a pile is a practical illustration of longitudinal impact in elastic rods. Wave propagation analysis attempts to describe the travel of the impulse up and down the pile as the pile is being driven. Consider qualitatively the hammer-pile-soil system shown in Figure A.2. During ram impact, the ram, drivehead and pile are assumed to deform elastically. The hammer cushion is inelastic; therefore, energy losses are inherent in the cushion.

Previous experience has shown that a hammer cushion is required in order to protect the hammer from damage. Of course, the cushion material also affects the stresses induced in the pile. A prerequisite for the cushion is that it be an expendable material; therefore, wood is commonly used whereas alternating thin discs of aluminum and micarta have become prominent in recent years. There are other types of cushion materials employed in practice today; however, aluminum-micarta and wood cushions represent the extremes in load-deformation characteristics. The aluminum-micarta assembly approaches an elastic condition whereas the wood cushion represents inelastic

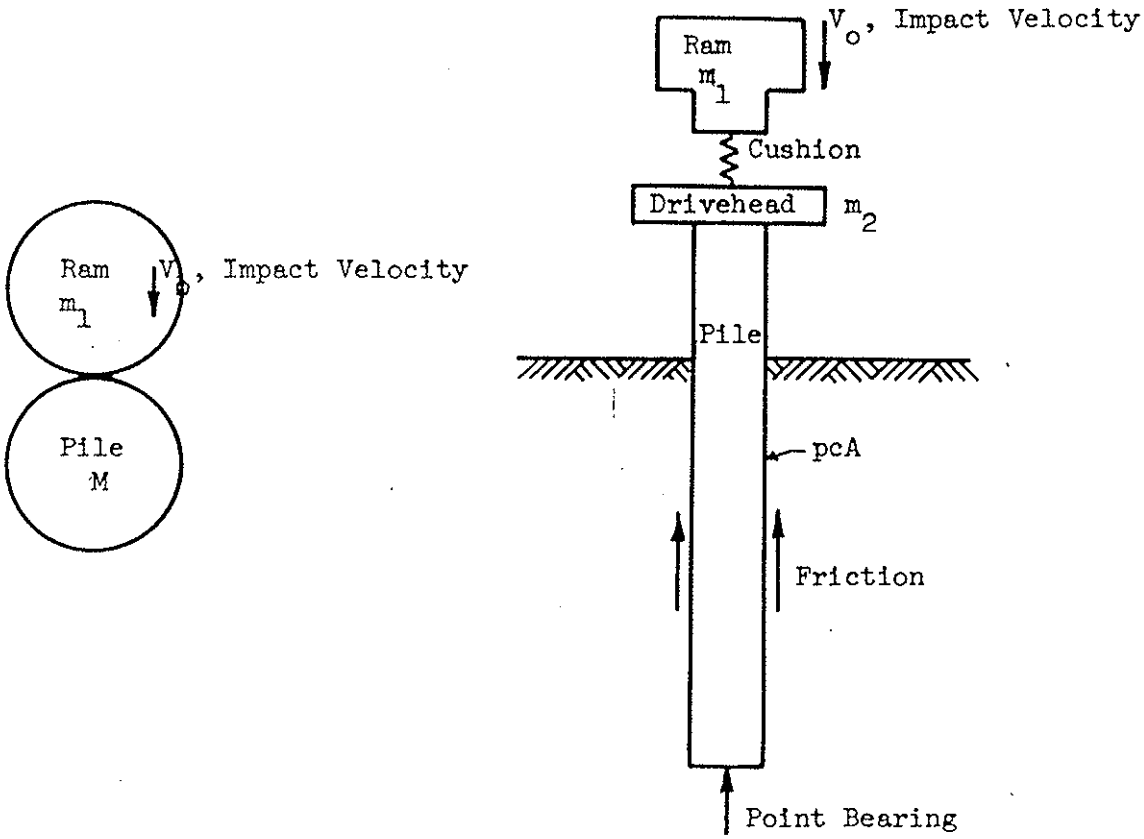

Newtonian Model

Longitudinal Wave Model

Figure A.1 IMPACT MODELS

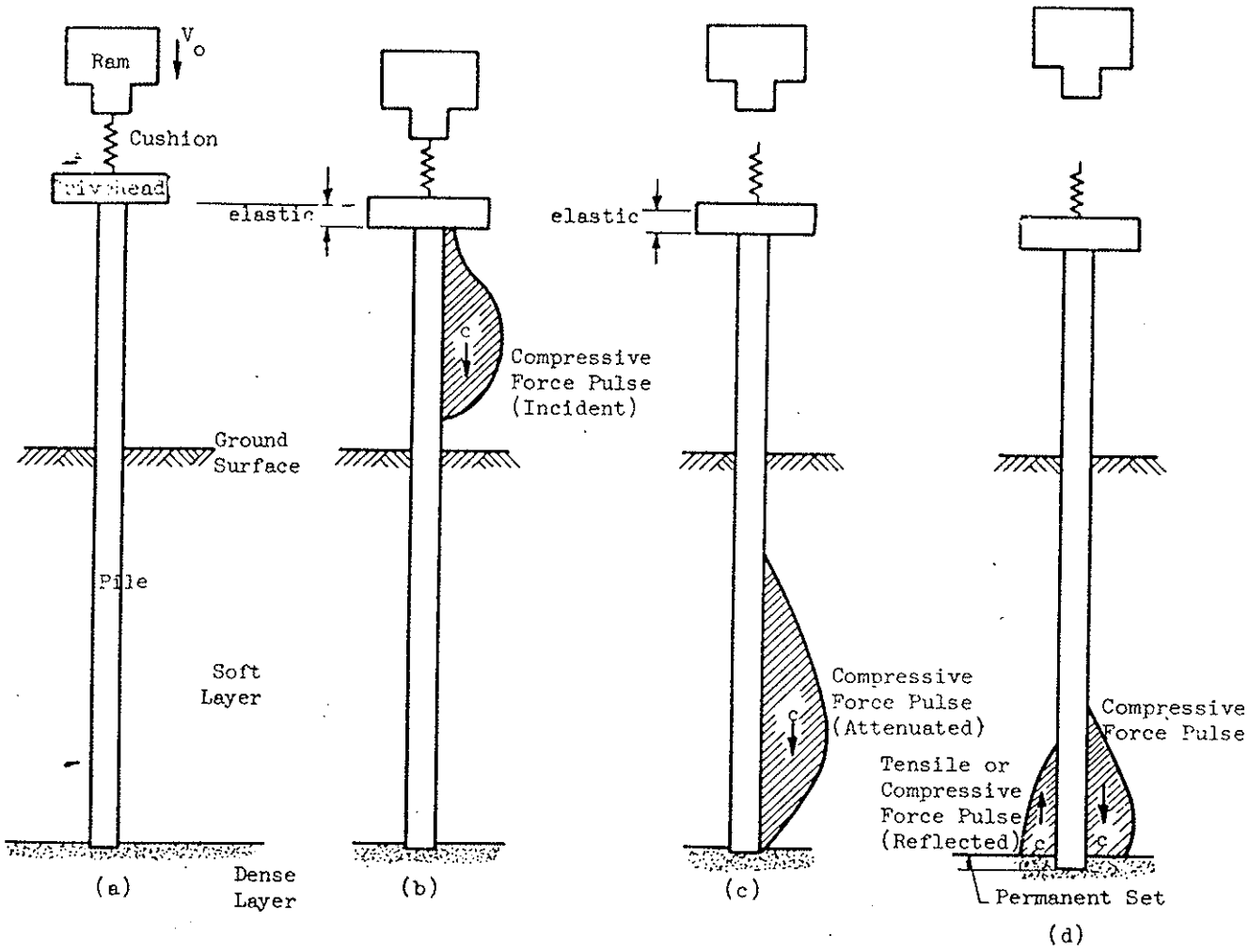

Figure A.2 HAMMER-PILE-SOIL SYSTEM

behavior. The cushion material and its effects are discussed later in detail.

The elastic compression of both the ram and drivehead may be neglected since these members are infinitely rigid. The elastic compression of the pile is appreciable, and does not occur instantaneously throughout the entire length of the pile. As ram impact occurs, a force pulse is developed in the pile that travels downward toward the pile tip at a constant velocity, c, which depends on properties of the pile material (Figure A.2b).

When the force pulse propagates within the embedded portion of the pile, it is attenuated by soil frictional resistance along the pile as shown in Figure A.2c. Until the stress wave reaches the tip, the maximum stress in the pile is independent of driving resistance. When the force pulse reaches the pile tip, a reflected force pulse, governed by the soil resistance at the tip, is generated. For the case of a pile driven to refusal, the incident compression wave is reflected as a compressive wave travelling up the pile with velocity, c, and identical in shape to the incident wave. The extreme opposite to driving refusal is a pile with a free-end. In this case, the soil offers negligible resistance to driving; therefore, the incident compressive wave is reflected as a tension wave travelling up the pile with velocity, c, and is identical in shape to the incident wave. In practice, pile driving is somewhere in between the extreme case of a fixed and a free tip condition; therefore, the reflected wave will also be a function of the soil response at the pile tip.

Some of the variables that will affect the generated force pulse shape along the pile will now be considered. Ram weight and velocity can characterize the pulse shape for a given energy input. For the same energy,

a light ram and resulting high velocity will produce high peak stresses over a short time duration, whereas a heavier ram will cause lower peak stresses with a relatively long time duration. The cushion block is very important in shaping the force pulse; therefore, special emphasis should be placed on its effects. The stiff cushion will produce high peak stresses and short time duration, whereas the soft cushion will produce a longer duration pulse with lower peak stresses. A schematic representation of the variable pulses that can be produced by a hammer with a given energy rating is shown in Figure A.3.

History

Historically, St. Venant and Boussinesq are believed to have first developed the theory of longitudinal impact of a rod struck longitudinally at one end. The development of this theory occurred within the period 1867 to 1883, and according to Timoshinko and Goodier (1951) a history of the problem can be found in the reference by St. Venant. The basis for the analysis is the classical one-dimensional wave equation

$$\frac{\partial^2 u}{\partial t^2} = c^2 \frac{\partial^2 u}{\partial x^2} \qquad \text{(A.3)}$$

in which x is the direction of the longitudinal axis; u is the longitudinal displacement of the bar in the x direction; t denotes time; c represents the velocity of propagation of stress or strain wave along the bar, $c = \sqrt{E/\rho}$; E is the modulus of elasticity of the bar; and ρ is the mass per unit volume of material. Equation (A.3) is based on the condition that lateral strains (distortion waves) are negligible so that plane trans-

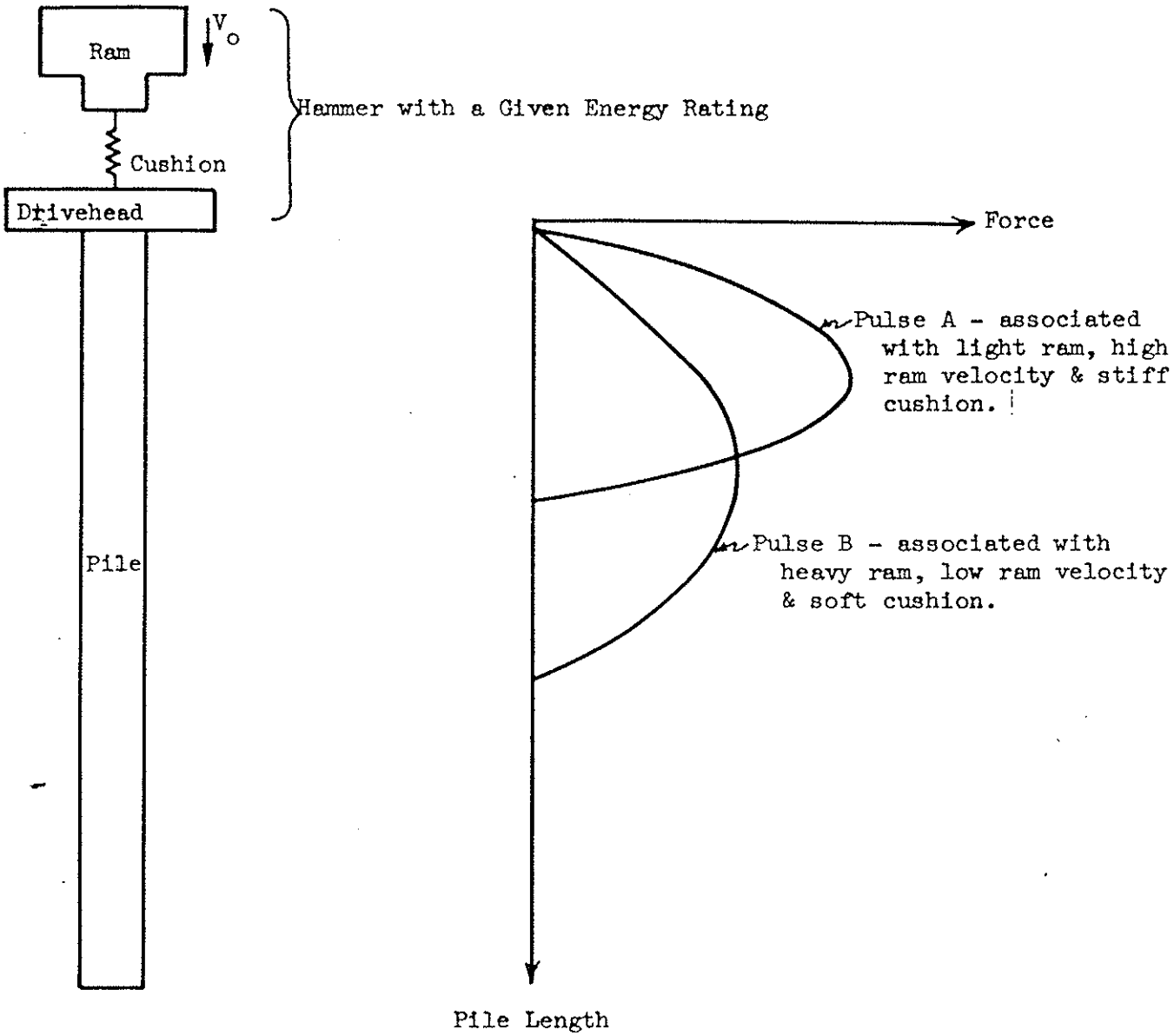

Figure A.3 VARIABLE FORCE PULSE FOR A GIVEN ENERGY INPUT

verse sections are not distorted. The assumption that plane sections remain plane is acceptable for stress pulses with lengths that are large (at least 10 times) compared to the lateral dimensions of the rod or bar (Kolsky, 1963). The general solution of Eq. (A.3) is

$$u = f\ (ct-x) + g\ (ct + x) \qquad (A.4)$$

where f and g are arbitrary functions representing waves travelling up and down the bar. The problem consists of determining the functions f and g for various time intervals after the start of impact.

The application of one-dimensional wave equation to problems of longitudinal wave transmission can be readily found in references by Kolsky (1963), Timoshinko and Goodier (1951), Donnell (1930), Rakhmatulin and Dem'yanov (1966), and Goldsmith (1960).

Isaacs (1931) is believed to be the first to apply wave analysis to pile driving. Isaacs simplified the boundary conditions by placing only an elastic spring between the hammer ram and pile. These simplified boundary conditions include zero frictional resistance along the pile, and a plastic soil resistance acting at the pile tip. Fox (1932) used the pile model proposed by Isaacs; however, Fox chose a boundary condition for the cushion that is more representative of actual cushion behavior. The cushion is represented by a visco-elastic spring throughout the range of compressive stresses.

An investigation of the stresses induced in reinforced concrete piles during driving was performed by Glanville et al. (1938). Fox's theoretical treatment was used, but it was necessary to simplify the boundary conditions in order to express the solutions in terms of quantities measurable in practice. The modified boundary conditions included elastic

cushion and soil resistance behavior. Cummings (1940) pointed out that even for these modified assumptions the complete solution involves long and complicated mathematical expressions that precludes its use for practical problems.

Considering the boundary conditions of a real pile-driving problem, i.e. soil resistance along the pile, realistic parameters for the cushion, soil, and other pile-hammer details, a rigorous solution by use of the wave equation is not known. Smith (1950) proposed a mathematical model, based on a lumped-mass and spring system, that accounts for the effects of the boundary conditions of a real pile driving problem. According to Lowery et al. (1967), Smith continued to develop his method (Smith 1955, 1957, 1958), but his method of analysis did not become popular until the paper (Smith, 1960) in which a number of parameters were recommended to account for the dynamic behavior of soil, pile and cushion. The availability of the computer made Smith's approach more attractive, and considerable effort has been done in this area, for example: Bender, et al. (1969); Davisson (1970); Graff (1965); Hirsch (1966); Korb and Coyle (1969); Lowery, et al. (1968); Lowery, et al. (1969); Mosley (1967); Raamot (1967); in addition to those mentioned elsewhere herein.

Smith's Model

Concept. Smith's mathematical model of the hammer-pile-soil system is shown in Figure A.4. The ram, hammer cushion, drivehead, pile cushion, and pile are represented by appropriate discrete weights and springs. Spring constants for the various types of cushion material can be obtained from test results, whereas those of the pile segment can be readily calculated. Soil characteristics, both along the sides and at the pile tip, are represented by a combination of elastic-plastic springs to

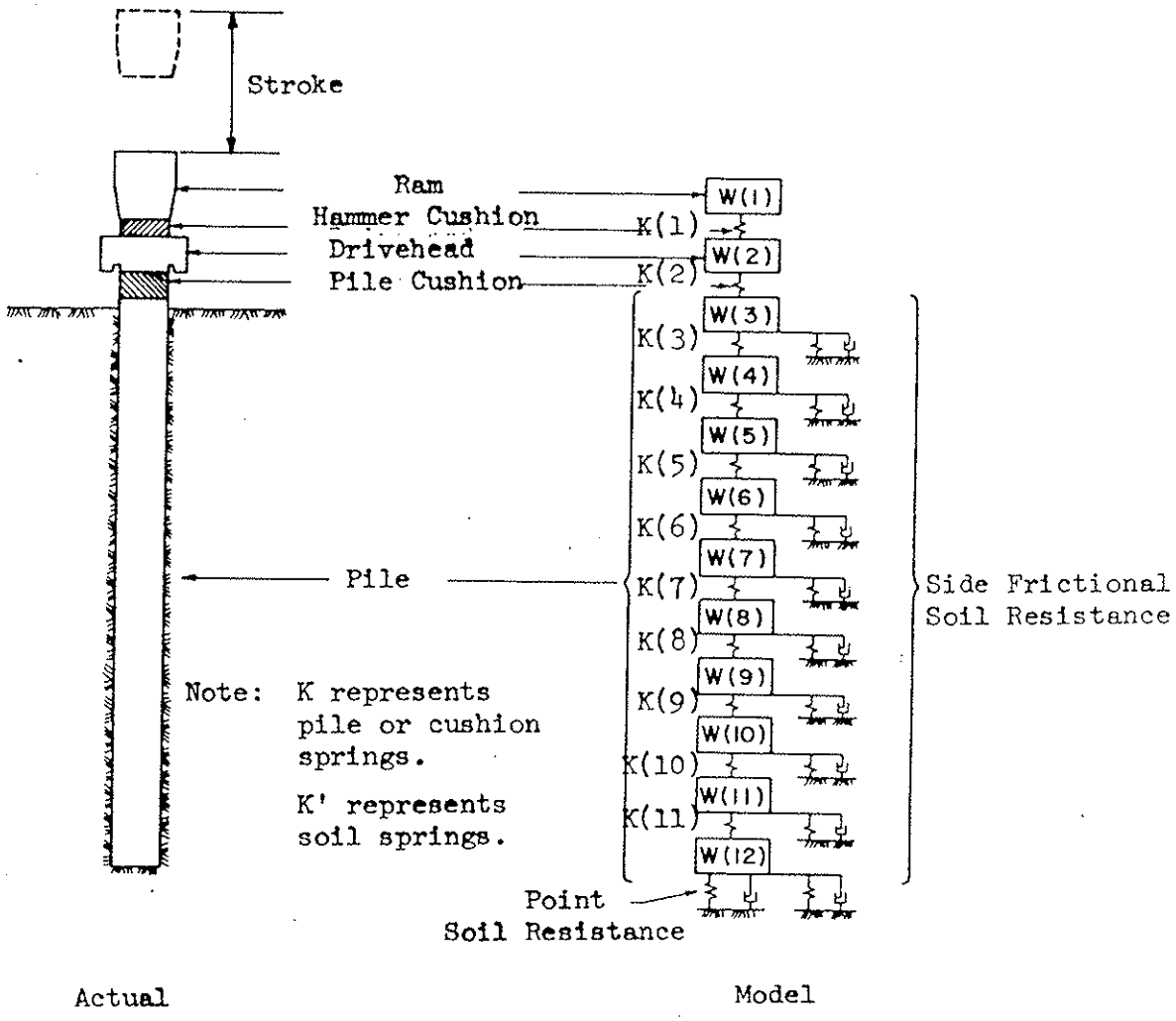

Figure A.4 SMITH'S MATHEMATICAL MODEL

simulate static resistance and dashpots to account for the dynamic response of the soil. Actual situations may deviate somewhat from those in Figure A.4. For example, a pile cushion might not be used, or an anvil may be placed between ram and hammer cushion, or a follower used; such cases are readily accommodated in Smith's analysis.

The numerical method used to describe force transmission in this mathematical model is illustrated in Figure A.5. This figure illustrates the force build-up in the pile during the initial stages of impact. The ram has an initial velocity (V_o) and acceleration that can be converted into a displacement (D_1) for a given time interval (Δt) by the equation $D_1=V_o(\Delta t)$. For this time interval ($t = t_1$), the compression of the hammer cushion can be readily determined; therefore, the force in the hammer cushion (F_1) can be calculated by the equation $F_1=K_1D_1$ as shown in Figure A.5.

The force build-up in the hammer cushion induces a drivehead acceleration which can be evaluated by the equilibrium equation $F=ma$, where m is the mass, a is acceleration, and F is the summation of forces acting on the drivehead. From this acceleration, a change in velocity can be readily calculated on the assumption that the drivehead is uniformly accelerated in rectilinear motion for the time interval (t) between times t_1 and t_2. The resulting velocity of the drivehead can be converted into a displacement. The displacement compresses the first pile spring causing a force F_2 on the first segment of the pile, K_2D_2. Also during time t_2-t_1 the ram has travelled an additional distance which can be calculated by the determination of a new velocity of the ram for the time interval. The difference in displacement between the ram and drivehead during time t_2-t_1 represents the compression of the hammer cushion, which is used to calculate a new cushion force. This procedure can be repeated for successive time intervals, and

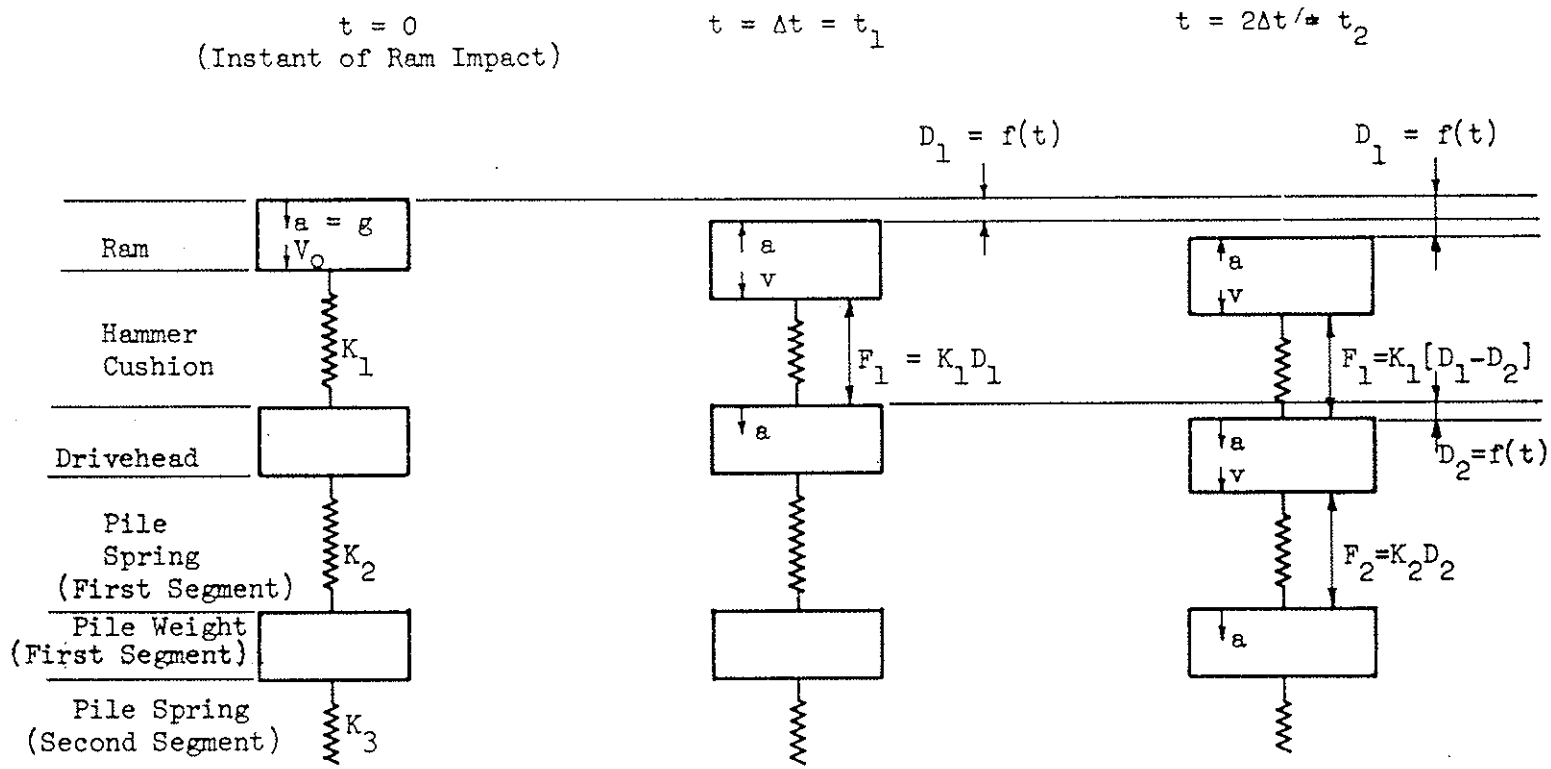

Figure A.5 FORCE TRANSMISSION IN PILE MODEL

forces in the pile system can be traced for any desired length of time. As the generated force pulse is traced along the embedded portion of the pile, the mathematical procedure has to account also for the soil resistance.

When using the lumped-mass and spring model as described above, care must be exercised in the selection of the time interval Δt. Each spring and mass unit has a "critical" time interval, which is the time required for a stress wave to traverse the particular spring and associated mass. The selected time interval for computations must never be greater than this "critical" time interval; otherwise, the numerical results will be meaningless because the calculation will not progress as fast as the actual stress wave. However, an unnecessarily small time interval involves a great deal of extra work with little or no increase in accuracy.

Basic Equations. The following equations are used for the solution of Smith's pile model:

$$D(m,t) = D(m,t-1) + 12\ \Delta t\ V(m,t-1) \tag{A.5}$$

$$C(m,t) = D(m,t) - D(m+1,t) \tag{A.6}$$

$$F(m,t) = C(m,t)\ K(m) \tag{A.7}$$

$$R(m,t) = [D(m,t)-D'(m,t)]\ K'(m)\ [1-J(m)V(m,t-1)] \tag{A.8}$$

$$V(m,t) = V(m,t-1) + [F(m-1,t)-F(m,t)-R(m,t)+W(m)]\ \frac{g\Delta t}{W(m)} \tag{A.9}$$

where m is the mass number; t denotes time interval number; Δt is the time interval, in seconds; D(m,t) is the displacement of mass m in time interval t, in inches; V(m,t) is the velocity of mass m in time interval t, in feet per second; C(m,t) represents compression of spring m during time interval t,

in inches; K(m) is the spring rate of mass m, in pounds per inch; F(m,t) is the force in internal spring m in time interval t, in pounds; R(m,t) is the total soil resistance on mass m, in pounds per inch; D'(m,t) is the plastic displacement of the soil spring m in time interval t, in inches; K'(m) is the spring constant associated with the soil spring acting on mass m, in pounds per inch; J(m) is a constant that accounts for the dynamic response of the soil acting on mass m, in seconds per feet; and g is gravitational acceleration, in feet per second^2. These basic equations can be readily programmed for solution by means of a digital computer.

Smith's Model versus Classical Wave Equation. The classical one-dimensional wave equation (Eq. A.3) can be readily converted into a difference equation for solution by successive approximation. Heising (1955) pointed out that the difference equation is an exact solution of the partial differential equation when

$$\Delta t = \frac{\Delta L}{\sqrt{E/\rho}} \qquad (A.10)$$

where ΔL is the segment length. For other values of Δt the solutions are approximate. Smith (1960) and Forehand and Reese (1963) showed that the difference equation could also be obtained by combining Smith's basic equations (Equations A.5 to A.9) into a single equation. Thus, Smith's basic equations are equivalent to the wave equation for purposes of numerical computation.

Comparison of a generated pile force pulse from the rigorous analysis of Chapter 2 and from the wave equation analysis (Smith's model) was made for a particular hammer and pile condition, as shown in Figure A.6. There was no soil resistance along the pile length and the pile was assumed long enough to avoid interference by reflection from the pile tip. The pile and

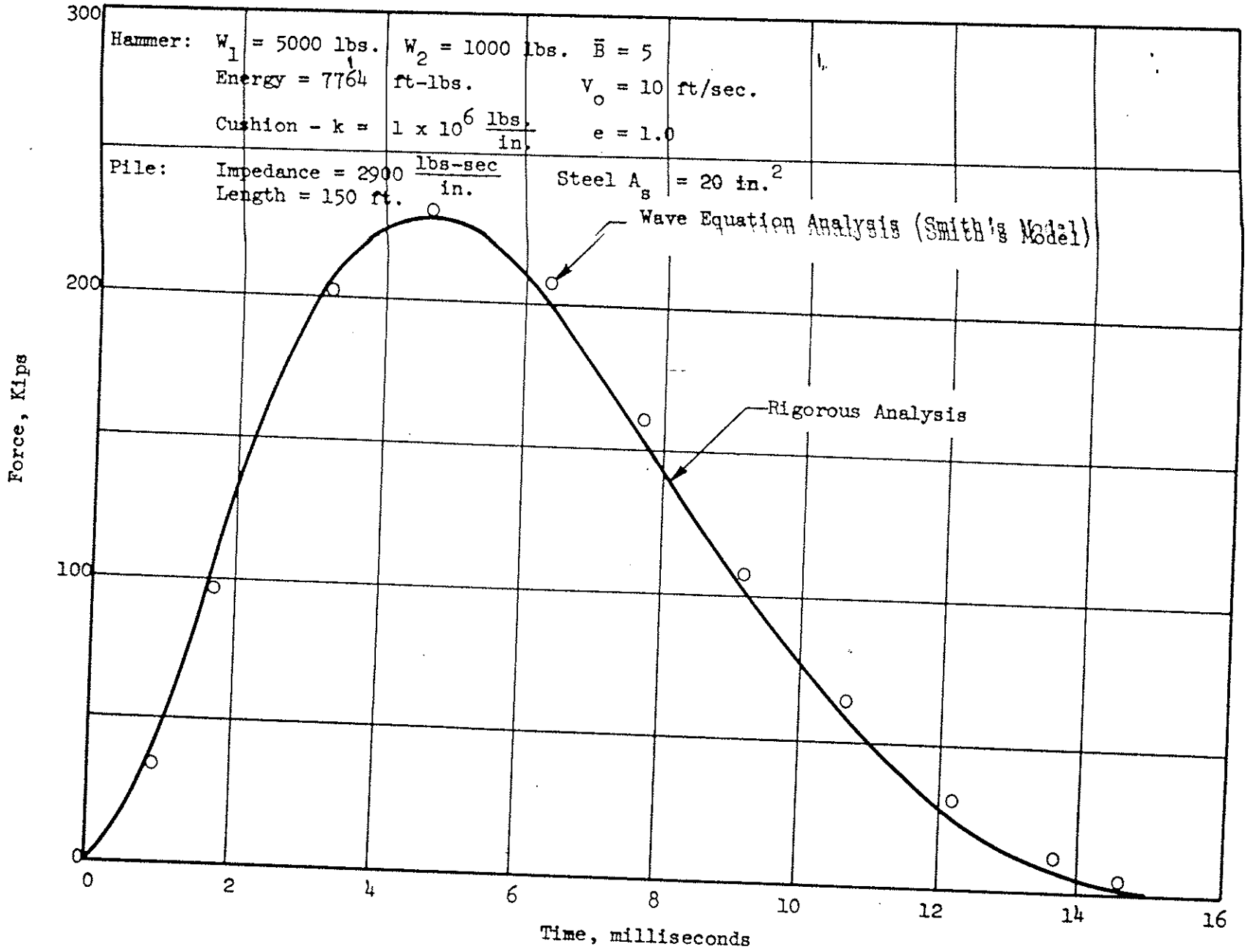

Figure A.6 COMPARISON OF GENERATED PILE FORCE PULSES

hammer characteristics are typical of current pile specifications. The induced pile forces as determined by the rigorous analysis and by the wave equation analysis are in close agreement, thus verifying Smith's model.

Input and Output. The basic equations (Equations A.5 to A.9) are programmed into a digital computer for solution. Several programs are available (lowery et al., 1967 and Edwards, 1967). The various input parameters and output data are summarized in Table A.2.

The initial condition is the impact velocity of the ram, which can be calculated from the energy of the hammer at impact, i.e. energy at impact = E_r x e_f where E_r is rated hammer energy and e_f is the hammer efficiency. Hammer efficiencies (Chapter 1) are only valid when the hammer is operating at full capacity. If the hammer is not operating properly, efficiency can be considerably less than the recommended values. Efficiency can be checked in the field by obtaining a measured ram velocity at impact and comparing this to the rated velocity as shown in the equation below:

$$e_f = \left(\frac{v_{measured}}{v_{theoretical}}\right)^2 \times 100\% \qquad (A.11)$$

The measured field velocity can be obtained by high speed photography or a radar unit; however, this type of field control is difficult and costly. Fortunately, hammer speed may be indicative of efficiency. For example, consider the relationship between hammer efficiency and hammer speed obtained with radar equipment as shown in Figure A.7 (Davisson, 1969). The operating efficiency was 70% at the rated hammer speed of 60 blows per minute. This efficiency is less than the commonly recommended value of 75 to 85% for single acting hammers. Also, efficiency drops off quite sharply with a reduction in speed, e.g. e_f = 50% at 50 blows per minute.

Table A.2

INPUT AND OUTPUT - WAVE EQUATION ANALYSIS

Input

Weight of Ram
Impact Velocity
} Energy at Impact, $E_r \cdot e_f$

Cushion Stiffness and Coefficient of Restitution
(Same for Extra Cushions)

Drive Head Weight (Anvil Also for Diesels)

Combustion Force for Diesels

Pile Length during Driving, Area, & Stiffness, Material
(Same for Mandrels)

Soil Resistance: % R_u in Friction and Its Distribution
% R_u at Tip
Quake, Q and Damping Factors, J
Analyze Borings

Follower Length, Area, & Stiffness

Joints (with or without tension)

Output

Stresses and Deflections at any Point vs. Time

Ultimate Pile Capacity, R_u, at Time of Driving vs. Blows/Inch

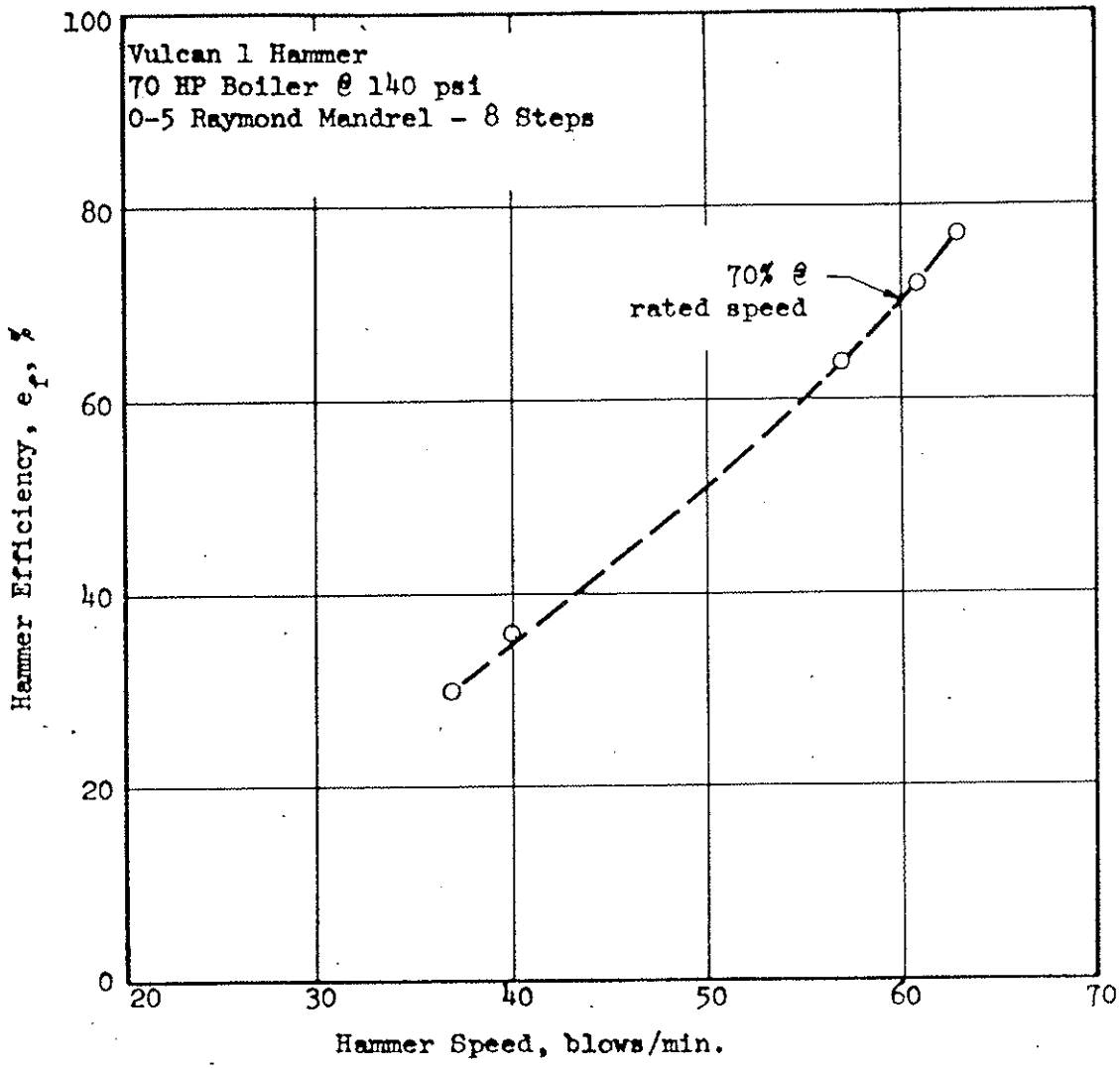

(After Davisson, 1969)

Figure A.7 RELATIONSHIP BETWEEN HAMMER EFFICIENCY AND SPEED

It is clear that more information on hammer efficiency is needed, based on actual field measurements.

The spring constants for various types of hammer cushions are obtained from test results. A typical shape of the dynamic stress-strain curve for a cushion along with the idealized shape used for the wave equation analysis is shown in Figure 2.3 (Chapter 2). According to Lowery et al (1969), it was found that the wave equation accurately predicted both the shape and magnitude of the stress wave induced in a pile when the idealized stress-strain curve is used. The idealized shape can be used as long as the loading portion is based on a secant modulus for the material, and the unloading portion of the curve is based on the actual dynamic coefficient of restitution. This coefficient of restitution accounts for the energy loss in the cushion material. Typical values of secant moduli of elasticity and coefficients of restitutions for various materials are presented below: (Lowery et al, 1969)

Cushion Material	E_c (secant) psi	e
Micarta Plastic	450,000	0.80
Oak (Green)	45,000*	0.50
Asbestos Discs	45,000	0.50
Fir Plywood	35,000*	0.40
Pine Plywood	25,000*	0.30
Gum	30,000*	0.25

* Load applied perpendicular to wood grain.

Input hammer parameters such as rated energy, hammer efficiency, ram weight, drive head weight, anvil weight, cushion properties, and combustion force for diesel hammers are summarized in Table A.3. The interaction of ram impact and combustion in a diesel hammer is not readily determinable;

Table A.3

INPUT DATA FOR DIESEL HAMMERS

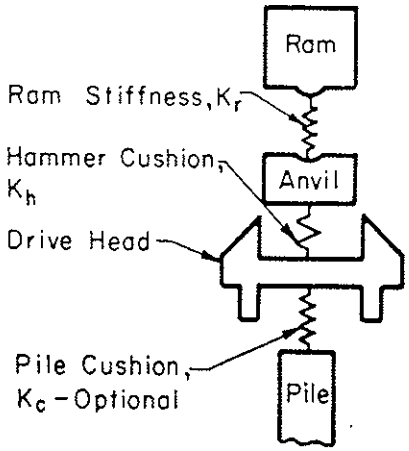

Type Hammer	Rated Energy ft-lbs.	Hammer Efficiency e_f	Ram Weight lbs.	Anvil Wt. lbs.	Drive Head Wt. lbs.	Stiffness: Ram $\frac{lbs}{in} \times 10^6$	Stiffness: Hammer Cushion $\frac{lbs}{in} \times 10^6$	Combustion Force lbs.
MKT DE-20	16,000	1.00	2000	640	Variable From 700 to 1500 lbs	--	Variable Depends on Material	46,300
MKT DE-30	22,400	"	2800	775		39		98,000
MKT DE-40	32,000	"	4000	1350		--		138,000
Delmag D5	9,040	"	1100	330		18		46,300
Delmag D12	22,600	"	2750	816		31		93,700
Delmag D22	39,800	"	4850	1576		50		158,700
Delmag D44	80,000	"	9500	4081		106		200,000
Link Belt 180	8,130	"	1724	377		44		81,000
Link Belt 312	15,000	"	3857	1188		142	15	98,000
Link Belt 440	18,200	"	4000	705		138	20	98,000
Link Belt 520	26,300	"	5070	1179		108	20	98,000

Note: 1. The hammer and pile cushion input depend on material properties

however, an idealized force-time curve can be assumed (Figure A.8). The magnitudes of explosive pressures in Table A.3 were obtained from Lowery, et al. (1969).

The complexity of the diesel hammer is best characterized by considering the details of one complete ram cycle starting with descent of the ram. As the ram descends, it passes the intake-exhaust port and traps air in the combusion chamber. With further ram descent, the ram is working against an air spring and the ram velocity is thereby decreased. Fuel injection is initiated prior to impact, and combusion occurs with peak gas force and impact force occurring almost simultaneously. During impact, the combusion force continues and eventually returns the ram to the top of its stroke. It is obvious that hammer instrumentation is required to study ram impact and velocity, and combustion forces. At present, information on the occurrence of combustion with respect to impact, combustion burn time, and peak gas forces is lacking. A study by Davisson and McDonald (1969) giving measurements of pile force of a long concrete-filled pipe pile driven with a diesel hammer indicated peak gas forces of approximately 280 kips. More research on diesel hammer input is required.

Pile input parameters include material type, length during driving cross-sectional area and modulus of elasticity. In general, piles are broken into segments not to exceed approximately 10 feet, but no fewer than five segments are used. The stiffness and weight of each pile segment can be easily calculated, and the selection of the proper time interval is included within the program to avoid instability with respect to the "critical" time interval (discussed previously). The program has provisions for handling joints in the pile-hammer system, i.e. mechanical joints which prohibit the transmission of tensile stresses or transmit tensile stresses only after a

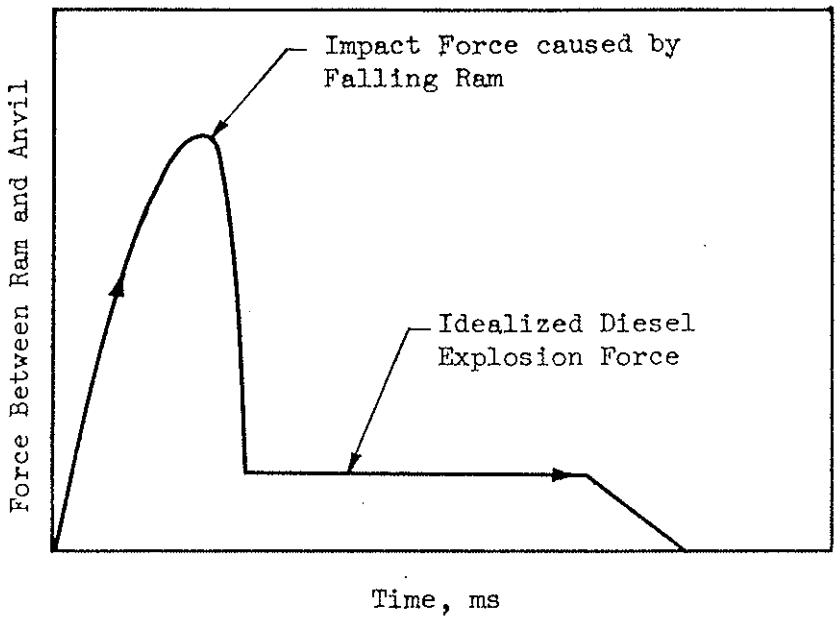

(After Lowery, et al 1969)

Figure A.8 IDEALIZED FORCE-TIME CURVE
FOR A DIESEL HAMMER

specified movement of the joint. Input properties for mandrels or followers are analogous to those for the pile.

The load-deformation characteristics assumed for soil in Smith's numerical solution are shown in Figure 3.2 (Chapter 3). The soil located along the side of the pile is assumed to resist rebound as well as downward motion. However, the soil at the tip of the pile will only resist compression. Based on a limited number of comparisons with load test data, Smith (1960) proposed the following values for the soil parameters:

$$Q_{side} = Q \text{ (along side of pile)} = 0.1 \text{ in.}$$

$$Q_{point} = Q \text{ (at pile tip)} = 0.1 \text{ in.}$$

$$J_{side} = J \text{ (along side of pile)} = 0.05 \text{ sec/ft}$$

$$J_{point} = J \text{ (at pile tip)} = 0.15 \text{ sec/ft}$$

A limited amount of work has been done on soil input data. Forehand and Reese (1964) investigated the soil parameters used in the wave equation by correlating with load test data. Correlation attempts for piles driven in sand were consistent with Smith's recommended values, whereas there was a lack of correlation for piles driven in clay. More recent investigations, Chan et al. (1967), Reeves, et al. (1967), Airhart, et al. (1967), have been directed towards obtaining better soil input data by performing laboratory dynamic and static tests on saturated sands and a full scale instrumented pile in clay. The studies showed that the soil parameters are a function of the loading velocity. Gibson and Coyle (1968) related soil damping constants with common soil properties for both sand and clay. More detailed discussion of soil response with respect to dynamic loading is considered in Chapter 3.

The soil resistance distribution must be included in the analysis. Soil resistance distribution includes the percent resistance at the

pile tip compared to the percent resistance along the sides of the pile. Also, the frictional resistance distribution must be incorporated. The soil resistance distribution can not be predicted in an exact manner, but analysis of borings can give reasonable limiting values for this distribution.

The maximum displacement of the pile tip is found during the numerical analysis of a single impact, and this displacement (set) can be converted into hammer blows per inch (reciprocal of set) for a particular ultimate resistance. With consideration of various ultimate soil resistances and the corresponding pile response, results of the wave analysis can be presented as shown in Figure A.9. The relationship between ultimate pile load capacity at the time of driving and driving resistance in blows per inch is of primary interest. Also, compressive and tensile stresses and deflections at any point with respect to time can be obtained. A tracing of the stresses can easily produce the maximum stresses that are obtained to determine whether or not the pile will be damaged during driving. For example, in Figure A.9 the maximum compressive stresses are shown versus driving resistance.

A.5 Pile Force and Acceleration Field Measurement Analysis

A method of predicting the static bearing capacity of both full-scale and reduced-scale piles from dynamic measurements taken in the field during pile driving is presented by Tomko (1968). Several other reports associated with Tomko's work also present this method of analysis (Goble et al., 1967; Goble et al., 1968; Scanlan and Tomko, 1969). The dynamic field measurements consist of force and acceleration measured as a function of time at the pile head during driving. A brief review of the proposed method will be presented.

WAVE EQUATION ANALYSIS

Job _____ Date 13 June 1969 J –

Location Boston Area

Pile 14" OD x 0.312 Pipe Area 13.44 in.^{2} Length 60 ft

Mandrel – Area – Length –

Follower – Area – Length –

Hammer Vulcan 010 Energy 32,500 ft.lbs e_f 70% Comb. Force –

Helmet (drive head) 1300 lb Anvil –

Cushion (hammer) Wood k 1×10^6 lbs/in. e 0.35 Q_{side} 0.10" J_{side} 0.05 sec/ft.

Cushion (pile) – k – e – Q_{point} 0.10" J_{point} 0.15 sec/ft.

Comments Closure is 14" ϕ x 1 1/4" Plate

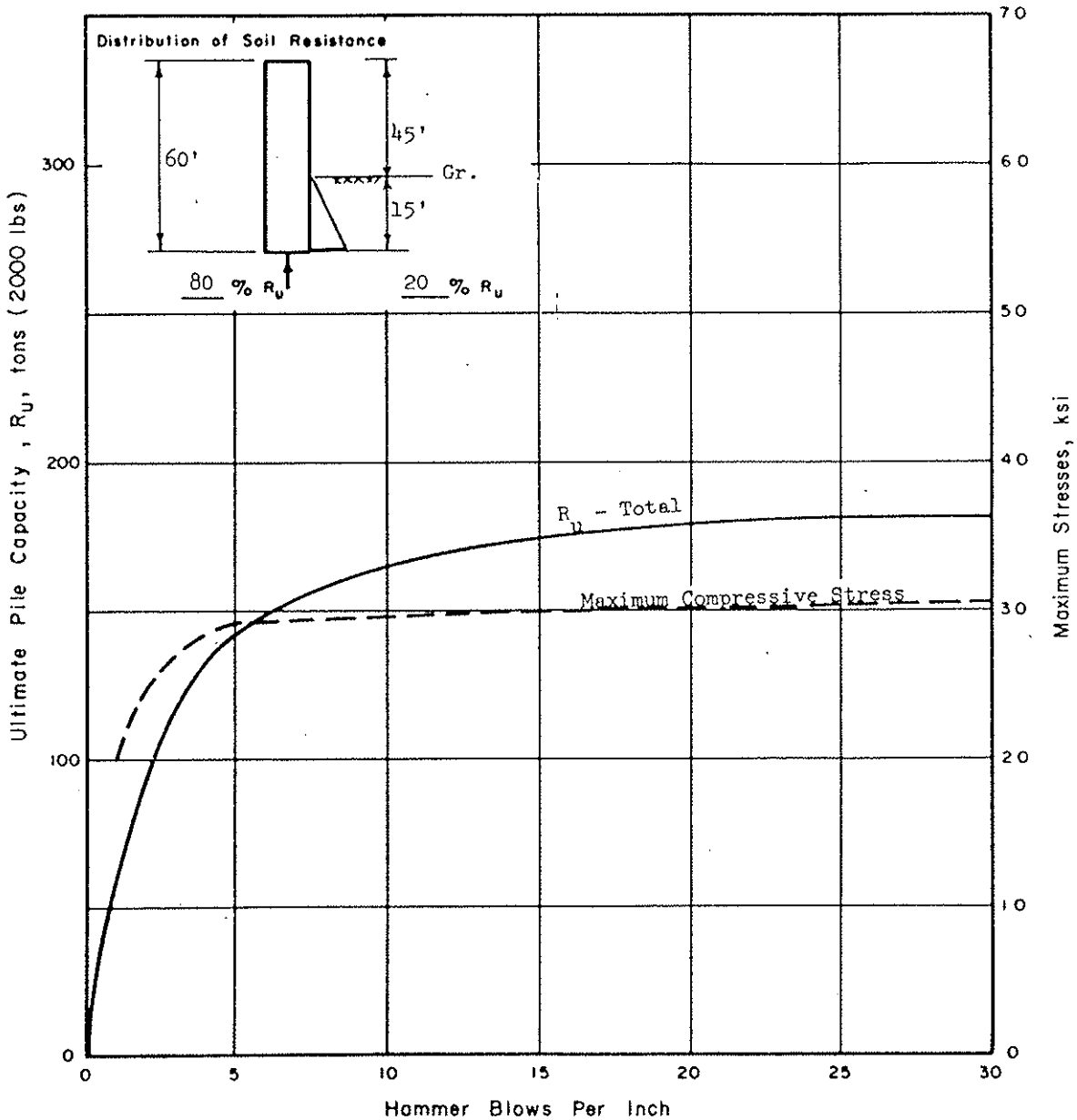

Figure A.9 TYPICAL RESULTS OF THE WAVE EQUATION ANALYSIS

The pile is assumed to be a rigid body struck by a time varying hammer force $\bar{F}(t)$ as shown in Figure A.10. Applying Newton's law to this assumed model, the following expression is obtained:

$$\bar{F}(t) - \bar{R}(t) = Ma(t) \tag{A.12}$$

where $\bar{F}(t)$ is hammer force varying with times, $\bar{R}(t)$ is the total soil resistance force with respect to time, $a(t)$ is the pile acceleration with respect to time, and M is the mass of the pile only. From this simplified theory, the predicted ultimate strength of the pile is given by

$$\bar{R}_o = \bar{F}(t_o) - Ma(t_o) \tag{A.13}$$

where $\bar{F}(t_o)$ is the force acting at the top of pile and $a(t_o)$ is the acceleration at the top of pile both measured at time t_o when the velocity of the top of the pile first reaches zero after a hammer blow. The relationship of Equation A.13 is based on the following assumed soil resistance force,

$$\bar{R}(t) = \bar{R}_o + \bar{R}_1\bar{V} + \bar{R}_2\bar{V}^2 + \bar{R}_3\bar{V}^3 + \ldots \tag{A.14}$$

where $\bar{V}$ is the velocity of the assumed rigid body pile and $\bar{R}_o$ is the static resistance. According to Tomko (1968), the general feasibility of the proposed method was determined by Eiber (1958).

Predicted static resistance (Equation A.13) can be readily obtained from force and acceleration measurements; velocity is obtained by integration of the acceleration record. The measuring and recording equipment has been set up to apply this technique in the field. Correlation between measured and predicted pile capacity shows promise; however, there are some questions about the validity of the analysis of long piles as compared to short piles.

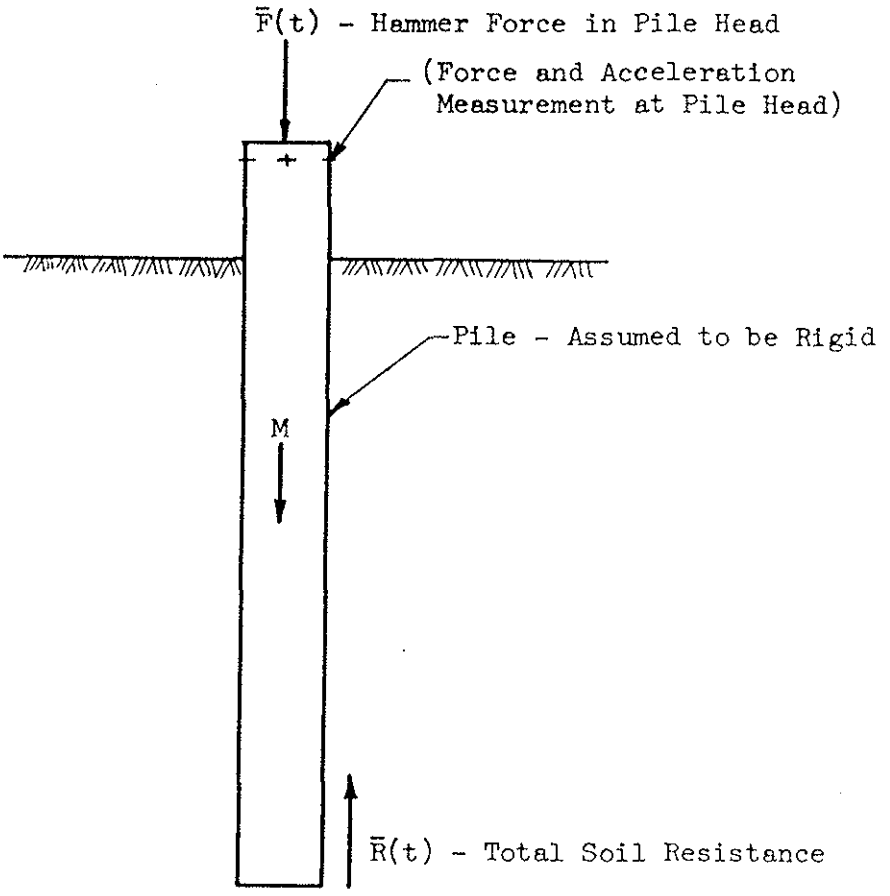

Figure A.10 SIMPLIFIED PILE MODEL

The entire length of a short pile would be influenced by the generated force pulse, thereby approaching the rigid condition. As pile length increases, the ratio of generated force pulse length to pile length decreases, making it necessary to consider wave propagation in the pile. This method for determining pile capacity has the advantage of using actual measurements on each pile; however, a disadvantage is that predetermination of driving capability is not possible.

APPENDIX B

ANALOG COMPUTER PROGRAM FOR FORCE GENERATOR

B.1 Linear and Bilinear Cushion

The analog computer program was designed to solve the differential equations in nondimensional form for the force generator model

$$\ddot{X}_1 + (X_1 - X_2) - gT^2 = 0$$

$$\ddot{X}_2 + \bar{A}\dot{X}_2 - \bar{B}\,(X_1 - X_2) = 0 \qquad \text{(B.1)}$$

in which $\dot{X} = \frac{dx}{dz}$, $X = x$, $z = t/T$, $T = \sqrt{\frac{m_1}{k}}$, $\bar{A} = \frac{\rho cA}{\sqrt{m_1 k}}$ and $\bar{B} = \frac{m_1}{m_2}$ or $\frac{W_1}{W_2}$. Details of this derivation is shown in Chapter 2. In particular, Equations B.2 were solved:

$$\ddot{X}_1 = -(X_1 - X_2) + gT^2$$

$$\ddot{X}_2 = -\bar{A}\,\dot{X}_2 + \bar{B}(X_1 - X_2) \qquad \text{(B.2)}$$

Figure B.1 illustrates the analog computer program for the general case of a force generator (pile hammer) applying a force pulse at the pile head. Integrators 1, 5, 18 and 20 and amplifiers 4, 11, 21 and 9 represent the basic circuit used in the solution. All appropriate gains are indicated on the amplifiers and integrators. The inputs to integrator 1 are the components of $\ddot{X}_1$ and inputs to amplifier 4 are the components of $\ddot{X}_2$ in Equation B.2. The term $\ddot{X}_1$ is integrated two times, through integrators 1 and 18 or 20, to produce X_1. The term $\ddot{X}_2$ is integrated two times, through integrators 5 and 18 or 20, to produce X_2.

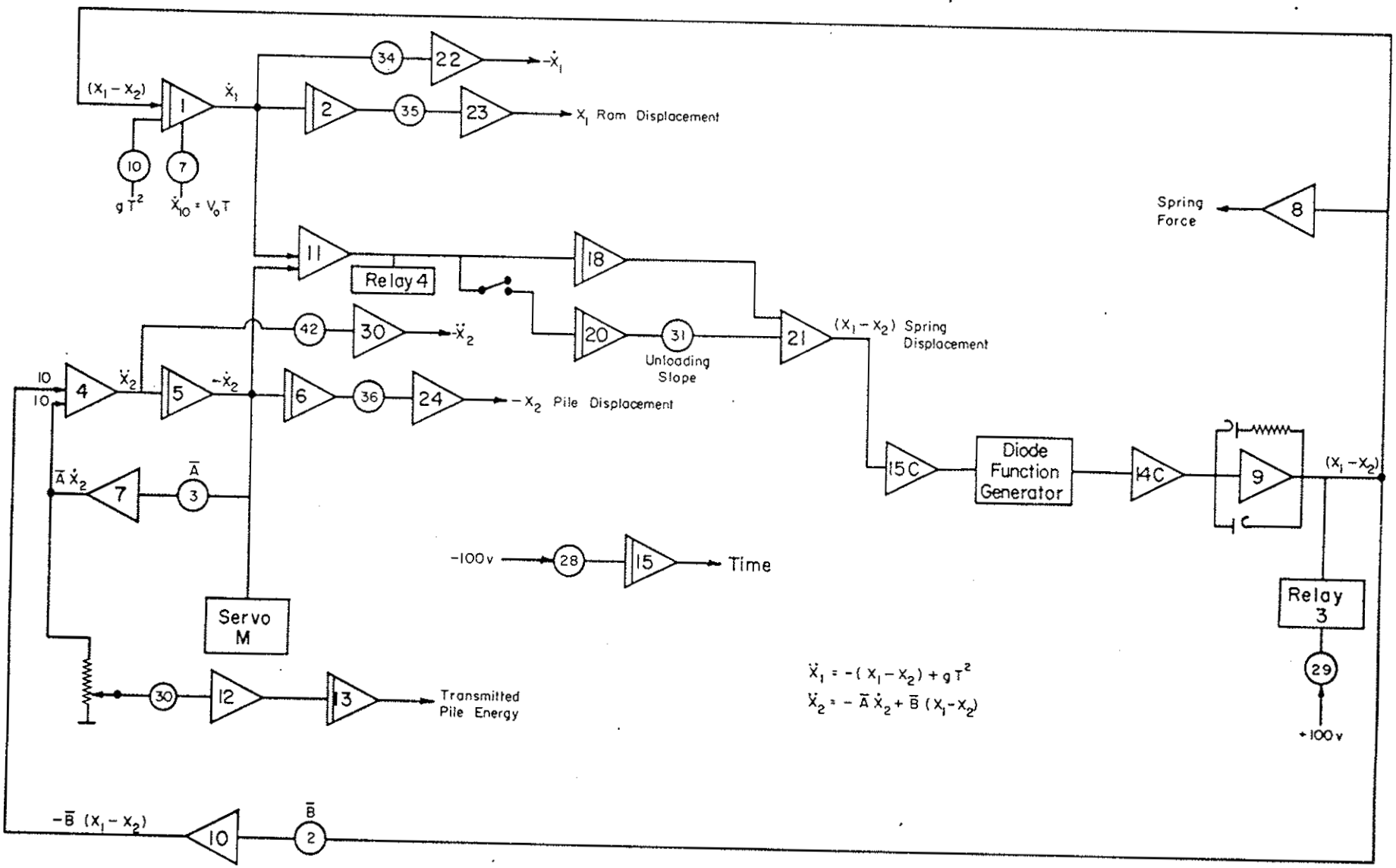

Figure B.1 ANALOG COMPUTER PROGRAM FOR FORCE GENERATOR

The loading portion of the cushion spring displacement $(X_1 - X_2)$ is controlled by integrator 18; whereas, the unloading of the cushion spring displacement is controlled by integrator 20 and potentiometer 31. Potentionmeter 31 is used to control the unloading slope of the bilinear cushion, and relay 4 is used to switch the loading to the unloading portion. The diode function generator is used for the nonlinear cushion; discussion will be reserved for the section on nonlinear cushions. For the linear and bilinear cushion, the loading slope of the spring force (amplifier 8) and deflection (amplifier 21) is set for the same output with the diode function generator. The spring force (amplifier 8) and the initial condition are fed into integrator 1 to produce $\ddot{X}$.

Initial conditions are the ram weight term gT^2 (potentiometer 10) and the ram velocity at impact V_o expressed in nondimensional terms $\dot{X}_{10} = V_o T$ (potentiometer 7). These initial conditions are fed into integrator 1. Let x_o represent the voltage for the initial condition $\dot{X}_{10} = V_o T$. The desired outputs can be readily determined from this input voltage as will be shown in the following disucssion. The input term gT^2 is usually so small compared to $V_o T$, that input of gT^2 can normally be neglected.

The pile force F, output voltage of x_7 at amplifier 7, can be determined

$$F = \frac{\rho c A}{\bar{A}} V_o [C_{F1}] \text{ or } \frac{\sqrt{m_1 k}}{\bar{B}} V_o [C_{F1}] \qquad (B.3)$$

where $C_{F1} = \frac{10\, x_7}{x_o}$. The peak pile force F_p, peak voltage output x_{7P} at amplifier 7, can be determined

$$F_p = \sqrt{m_1 k}\, V_o\, [C_{F2}] \qquad (B.4)$$

where $C_1 = 2 = \frac{10\ x_{7P}}{\bar{B}\ x_o}$.

The cushion spring force F_s, output voltage of x_8 at amplifier 8, can be determined

$$F_s = \sqrt{m_1 k}\ V_o\ [C_{FS}] \tag{B.5}$$

where $C_{FS} = \frac{x_8}{x_o}$. The spring displacement $(x_1 - x_2)$, output voltage of x_{21} at amplifier 21, can be determined

$$(x_1 - x_2) = V_o\ T\ [C_s] \tag{B.6}$$

where $C_s = \frac{x_{21}}{x_o}$.

The ram displacement (X_1) and pile head displacement (X_2) have a voltage output of x_{23} at amplifier 23 and x_{24} at amplifier 24, respectively. The displacements can be determined

$$x_1 = V_o\ T\ [C_p] \tag{B.7}$$

$$x_2 = V_o\ T\ [C_p] \tag{B.8}$$

where $C_R = x_{23}/x_o$ and $C_P = x_{24}/x_o$.

The energy transmitted to the pile can be determined by multiplying the pile force and the velocity (servo M) and the product is shown in amplifier 12. The product is integrated (integrator 13) and the results of voltage output (x_{13}) can be used to determine the energy as follows:

$$\text{Energy} = \frac{1}{2}\ m_1 V_o^2 \ .$$

It should be noted that the circuit involving the desired output of the amplifiers as previously shown could be replaced by a curve-following x-y recorder. Any amplifier's output could be plotted versus time. Time is controlled by potentiometer 28 and amplifier 15. All

possible input parameters, ram velocity and ram weight effect, may be considered as well as any combination of ram mass, hammer cushion, drivehead mass and pile impedance.

B.2 Nonlinear Cushion

For the nonlinear cushions, the nondimensional equations as shown for the linear and bilinear cushions were used to solve a particular case. A particular case includes a ram and drivehead weight, ram velocity, and cushion spring force and deformation relationship as approximated by a series of straight lines (Figure 2.15). The diode function generator is used to obtain the desired spring force and deformation relationship. The voltage output x_{21} at amplifier 21 is used for the desired deformation (Equation B.6) and voltage output x_8 at amplifier 8 is used to obtain the desired spring force (Equation B.5). The diode function generator controls the slopes and the break points of the loading curve. The hyteresis potentiometer 31 controls the slope of the unloading wave.

The desired spring force shape is set up prior to the solution with the use of an oscillatory; the diode system is cut loose from the pile system in order to set up the spring force shape efficiently.

The voltage output representing the cushion spring properties (amplifier 8 and 21) is determined by arbitrarily assuming the loading stiffness as some function of k_o. The stiffness k_o is selected within the range of upper and lower stiffnesses for a particular hammer and cushion material. For example, problem number 11 is shown in Table 2.5 (Vulcan 1 with ram velocity of 12 ft/sec and pine plywood cushion). The selected k_o for this problem was 200×10^3 lbs/in. This value of k_o

can now be used to determine $\dot{X}_{10} = V_o T$ in terms of inches; a voltage x_o represents this initial condition. All other hammer parameters (m_1, m_2, V_o, T) are now known and the pile characteristics ($\bar{A}$) can be varied to obtain a series of solutions.

After the desired cushion spring shape is set up, the analog computer program is initiated and the solution obtained. The conversion of analog output for the nonlinear cushion is identical with that shown for the linear and bilinear cushions.

APPENDIX C

ANALOG COMPUTER PROGRAM FOR PILE TIP

The analog computer program was designed to solve the differential equation for the pile tip model

$$m\ddot{x} + (c_o + \rho cA)\dot{x} + k_s x = 2\,\rho cA\,V_I \qquad (C.1)$$

In particular, Equation C.2 (machine equation) was scaled and solved:

$$\ddot{x} = g/W\left[\frac{2\rho cA}{1000}\,V_I - \frac{(c_o+\rho cA)}{1000}\,\dot{x} - \frac{k_s}{10^6}\,x\right] \qquad (C.2)$$

in which the time sealing factor is 1/1000 sec. i.e. real time = 1/1000 machine time. References by Johnson (1956) and Korn and Korn (1956) indicate analog computer techniques.

Figure C.1 illustrates the analog computer program for the general case of a force pulse applied at the pile tip. Amplifier 2, integrators 4, 7 and 13, and amplifiers 8, 14 and 9 represent the basic circuit used in the solution. All appropirate gains are indicated on the amplifiers. The inputs to amplifier 2 are the components of $\ddot{x}$ in Equation C.2. The term $\ddot{x}$ is integrated two times, through integrators 4 and 7 or 13, to produce the spring force term $\frac{k_s}{10^6}\,x$ which is fed back to amplifier 2. The loading portion of the soil spring is controlled by integrator 7 and amplifiers 8 and 11. The initial break in the soil spring is controlled by potentiometer 37 and the second slope in the soil spring is controlled by potentiometer 54. The unloading portion of the soil spring is controlled by integrator 13 and amplifier 41. Relay 1 is used to switch from the loading to unloading portion. The term $\dot{x}$ is multiplied by $\frac{c_o}{1000}$ (potentiometer 44) and by $\frac{\rho cA}{1000}$ (servo 1) before being fed back to amplifier 2 to produce $\ddot{x}$. The mass coefficient g/W (1/m) is controlled by potentiometer 43. Potentiometer 40 controls the magnitude of servo 1.

VITA

Jerry Frank Parola was born at Hillsboro, Illinois, on 7 September 1939. He attended public schools in Taylor Springs and Hillsboro, Illinois, and graduated from Hillsboro High School in 1957. He attended the University of Illinois at Urbana-Champaign and received his Bachelor of Science Degree in Civil Engineering in 1962 and the degree of Master of Science in Civil Engineering in 1963.

He has been on the staff of the Civil Engineering Department of the University of Illinois as both a teaching and a research assistant. He has been a research assistant in both structures and soil mechanics. During his education he worked as a private consultant and for private consultants in foundation engineering.

He is a member of Chi Epsilon, Phi Eta Sigma, and Sigma Xi, an Associate Member of the American Society of Civil Engineers, and a Member of the International Society of Soil Mechanics and Foundation Engineering.